FUNCTIONAL AND PROCESSABLE POLY-N-PHENYL ANILINE DERIVATIVES AND ITS COPOLYMERS: SYNTHESIS AND APPLICATIONS

Thesis

submitted to

University of Calicut

in partial fulfilment of the requirements

for the award of the Degree of

Doctor of Philosophy in

Chemistry

By

ROHINI DAS K

Under the guidance of

Dr. JINISH ANTONY M

Research & Postgraduate Department of Chemistry,

St. Thomas' College (Autonomous),

Affiliated to University of Calicut

Thrissur, Kerala, 680 001

October 2023

Research and PG Department of Chemistry
St. Thomas College (Autonomous), Thrissur, Kerala-680 001, India
(Autonomous under University of Calicut & Nationally Reaccredited at A++ Grade by NAAC –Score 3.70 in Fourth cycle)

Dr. Jinish Antony M
Research supervisor

17/05/2024

CERTIFICATE

I hereby certify that, this is the revised version of the Ph.D. thesis entitled "FUNCTIONAL AND PROCESSABLE POLY-N-PHENYL ANILINE DERIVATIVES AND ITS COPOLYMERS: SYNTHESIS AND APPLICATIONS" submitted to the University of Calicut by Ms. ROHINI DAS. K after incorporating the necessary corrections/suggestions made by the adjudicators.

Dr. JINISH ANTONY M
(Research supervisor)

Dr. JINISH ANTONY. M., Ph. D
Assistant Professor
Research & PG Department of Chemistry
St. Thomas College, Thrissur - 1

Research and PG Department of Chemistry

St. Thomas College (Autonomous), Thrissur, Kerala-680001, India

(Autonomous under University of Calicut & Nationally Reaccredited at A++ Grade by NAAC –Score 3.70 in Fourth cycle)

Date: 27 /10 /2023

CERTIFICATE

This is to certify that the thesis entitled ***"FUNCTIONAL AND PROCESSABLE POLY-N-PHENYL ANILINE DERIVATIVES AND ITS COPOLYMERS: SYNTHESIS AND APPLICATIONS"*** is an authentic record of research work carried out by **Ms. ROHINI DAS K** under my supervision in partial fulfillment of the requirements for the degree of Doctor of Philosophy in Chemistry of University of Calicut and further that no part thereof has been presented before for any other degree.

Dr. JINISH ANTONY M

(Supervising Teacher)

DECLARATION

I hereby declare that the thesis entitled ***"FUNCTIONAL AND PROCESSABLE POLY-N-PHENYL ANILINE DERIVATIVES AND ITS COPOLYMERS: SYNTHESIS AND APPLICATIONS"****, submitted to the University of Calicut in partial fulfillment of the requirement for the award of the Degree of Doctor of Philosophy in Chemistry is a bonafide research work done by me under the supervisions of* ***Dr. JINISH ANTONY M****, Assistant Professor, Research and Post graduate Department of Chemistry, St .Thomas College (Autonomous), Thrissur.*

I also declare that the material presented in this thesis is original and does not form the basis for the award of any other degree, diploma or other similar titles of any other university.

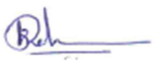

Date: 27/10/2023 **ROHINI DAS K**

Acknowledgement

I am very much obliged to my research guide, Dr. Jinish Antony M, who made it possible to accomplish my doctoral studies successfully. I remember with grace the constant support rendered by him during the difficulties that aroused during my work period. Expressing my sincere thanks to him for the thoughtful guidance, valuable support, patience, critical comments, and warm encouragement and my gratitude remains incomplete through these limited words

I express my gratitude to our Principal Dr. Martin K A for his exceptional support given in my Ph. D. period. He was always approachable and contributed a lot for the development of infrastructures in our research centre. I would like to thank our Executive Manager Rev. Fr. Biju Panengadan for providing us good research facilities and infrastructures. I thank the Head of our Chemistry Department, Dr. Paulson Mathew for his consideration and valuable support. I sincerely thank Research coordinator of St. Thomas College, Dr. Chacko V M for his valuable help and needed advices given during my research period.

I remember with thanks the former principals of St. Thomas' college Dr. Joy K L, Dr. Ignatious Antony and Dr. P O Jenson who implemented their great visions in order to develop the qualities of research. I greatly thank them for their valuable advices and support. I also extent my gratitude to the former HoDs of our Department especially Dr. Joshy C L and Dr. Joby Thomas K for their unforgettable support during my Ph. D work. I express my thanks to all other faculty members Dr. Sunil Jose T, Dr. Jency Thomas K, Dr. Reeja Johnson, Dr.Joseph Joly V L, Prof. Aji C V, and Dr. Sr.Jisha Joseph for their valuable help during my work. I sincerely thank all the non-teaching staffs of our department. They helped me a lot during my Ph. D. period. I express my gratitude to all the teaching and non-teaching staff of St. Thomas College, Thrissur for their support in one way or the other.

I further extent my sincere thanks to Dr. Shinto Varghese, Scientist-D, IACS Kolkata, who collaborated with us, arranged needed facilities and given valuable advices to complete different stages of my research work. I also remember and thank Ms. Divya, Ms. and Ms. Jisnet who aided their service in various stages of my Ph D. work.

I express my sincere thanks from the bottom of my heart to my friends, senior researchers and co-researchers namely, Dr. Swathy T S., Dr. Sini Varghese, Dr. Drishya Sashidharan, Dr.Binsi M Paulson, Dr. Ramesh Babu N, Dr. Dinoop lal S, Dr. Ragi K, Dr. Anju Rose Puthukkara P, Dr. Vidhya Thomas, Dr. Siji T B, Dr. Memsy C K, Dr. Savitha

Unnikrishnan K, Mr. Martin Francis, Ms. Raji C R, Ms. Nithya C S, Ms. Neera Rajan M, Ms. Anjana I, Mr. Rijoy K J, Ms. Nabeena C P, and Ms. Anjum Hassan C A.

I always remain thankful to various institutions which provided me the facilities for conducting my work and/or analysing my samples. These institutions include Department of Biotechnology, CUSAT, SAIF-STIC CUSAT, Kochi, CLIF Trivandrum,,CSIF- Calicut University, and various persons related to it Dr. John Naduvath and Dr. Joseph Joly V L (WXRD), Dr. Juby John (HR-MS), Dr.Ajith Vengallur (cell imaging), Dr. Abdul Jaleel K A, Ms. Deepa (MALDI-TOF), Dr. Ramanathan (FT-IR), Dr. Shibin (TGA) and Mr. Jibin (NMR). The real strength and support I enjoyed at every instance of my research career could be credited to my family members, especially my husband and my daughter. Without their unmeasurable love and support, I would not have completed my thesis.

The invisible blessings that were showered on me during all the stages of my work, by God almighty gave me the courage and wisdom in apt situations through which I could complete my Ph.D. thesis work fruitfully.

I always remember with never ending gratitude, all the personalities who helped at different stages of my work physically and/or mentally. The helping hands extended by each and every one of them are well accounted for which I always debt to remain thankful.

With heartfelt gratitude

ROHINI DAS K

Dedicated to my Family

Preface

Conjugated polymers are attractive materials due to the presence of continuous delocalization of π electrons in the polymeric backbone. They have possessed tunable molecular structure and unique properties suitable for various applications. The characteristic optical and electrical properties ensure their potential use in sensing, biological studies and electronic devices. Copolymerization of conjugated polymers allows the production of polymers in great diversities that can facilitate inherent properties of homopolymers. The controlled preparation of copolymers directs them straight into specific applications. Polyaniline have been emerged as an important conjugated polymer due to their advantageous reversible redox properties and electrical conductivities. Their applications spread across various fields including sensors, electronic devices like photovoltaic cell, solar cells, energy storage devices like supercapacitors, batteries, anti-corrosive coatings, electrochromic devices, water purification etc. Biological applications of polyaniline were limited due to their poor processability/solubility. Lack of fluorescence in polyaniline also restricted their broadened applications. Polyaniline derivatives possessed improved properties in some extents.

In this work, synthesis and characterizations of processable poly-N-phenyl aniline derivatives and their applications in sensors, cell imaging, and anticounterfeiting areas were studied. Poly-N-phenyl aniline or polydiphenylamine and their composites were effectively used in electrochemical sensors and other applications based on their electrochemical and physicochemical properties. The studies on light absorption and fluorescence emission in poly-N-phenyl aniline or their derivatives were rare. The functional applications utilizing the optical properties of poly-N-phenylaniline derivatives were also not explored. The synthesis of highly fluorescent, conjugated and redox active poly-N-phenyl anthranilic acid and sensing of oxidizing analytes through fluorescence quenching were discussed in chapter 2. The redox sensitive fluorescence of the polymer was used to determine the micromolar quantities of ferrous ion by microscale redox titrations, which was described in chapter 3. In addition, an experiment was designed for the students of undergraduate courses to make them aware of benefits of microscale titrations using fluorometric indication method.

The synthesis of poly-N-phenyl-o-phenylenediamine, which is a poly-N-phenyl aniline derivative, and their structural characterizations were given in chapter 4. A colorimetric acid content sensor was developed based on the pH dependent color changes exhibited by the aqueous polymer solution. The state of charge in lead-acid batteries were also determined by utilizing the linear variation of absorbance of polymer with acid content. A copolymerization strategy using o-phenylenediamine was adopted to study the changes in the fluorescence emission and redox properties of poly-N-phenyl anthranilic acid. Prior to the copolymerization, homopolymer of poly-o-phenylenediamine, which is a polyaniline derivative, was synthesized and their fluorescence properties were studied in chapter 5. The oxidative fluorescence turn-off in poly-o-phenylenediamine was used for the silver ion sensing. The oxidative power selective fluorescence tuning in copolymers of N-phenyl anthranilic acid and o-phenylenediamine were described in chapter 6. Also, an emission tuning strategy was developed based on the variations in the reactivity of monomers towards copolymerization and pH dependent emission changes in homopolymers.

The strong fluorescence emission of conjugated polymers in aqueous acidic medium was useful to impart fluorescence to non-fluorescent hydrophilic substrates. Chapter 7 describes the utilization of hydrophilic poly-N-phenyl anthranilic acid as a fluorescent dye to produce fluorescence in hydrophilic substrates by simple mixing of solutions and as an invisible ink. In addition, a comparative study on the nuclear targeting ability of polymer and monomer in cancer cells and normal cells were also carried out.

Abbreviations

PANI	Polyaniline
NPA	N-phenyl anthranilic acid
PNPA	Poly-N-phenyl anthranilic acid
NMR	Nuclear magnetic resonance
FT-IR	Fourier transform infrared
ATR	Attenuated total reflectance
XRD	X-ray diffraction
TGA	Thermogravimetric analysis
MALDI-TOF	Matrix assisted laser desorption ionization- time of flight
CV	Cyclic voltammetry
UV	Ultraviolet
LOD	Limit of detection
AA	Ascorbic acid
PPOPD	Poly-N-phenyl-o-phenylenediamine
SoC	State of charge
OCV	Open circuit voltage
OPD	o-phenylenediamine
POPD	Poly-o-phenylenediamine
FE-SEM	Field emission scanning electron microscopy
P(NPA-co-OPD)	Poly-N-phenyl anthranilic acid-poly-o-phenylenediamine copolymer
PNPA-blend-POPD	Poly-N-phenyl anthranilic acid-poly-o-phenylenediamine blend
PVA	Polyvinyl alcohol
TLC	Thin layer chromatography
MTT	3-(4,5-dimethylthiazol-2-yl)-2,5-diphenyltetrazolium bromide
DAPI	3.5 μM 4’, 6 - diamidino-2-phenylindole

Abstract

Polyaniline and their derivative are highly demanded conjugated polymers in opto-electronic, biomedical, and physico-chemico-mechanical fields due to their peculiar properties. In this work, poly-N-phenyl aniline derivatives were synthesized and their optical properties and some of their applications were studied. Fluorescent and colorimetric sensors based on poly-N-phenyl aniline derivatives working in water media were also developed.

The main objectives of our work are as follows: - (1) synthesis, characterization, and applications of poly-N-phenyl anthranilic acid, (2) synthesis, characterization, and applications of poly-N-phenyl-o-phenylenediamine, (3) synthesis, characterization, and applications of poly-o-phenylenediamine, and (4) synthesis, characterization, and applications of copolymers of N-phenyl anthranilic acid and o-phenylenediamine. Synthesis of poly-N-phenyl anthranilic acid, poly-N-phenyl-o-phenylenediamine, and poly-o-phenylenediamine was carried out with chemical oxidative polymerizations using $FeCl_3$ as oxidizing agent in ethanol medium. Copolymers of N-phenyl anthranilic acid and o-phenylenediamine was also synthesized by chemical oxidative polymerization using $FeCl_3$ as oxidizing agent in ethanol medium and their properties were compared with physical blends of homopolymers. General characterizations of polymers with proton nuclear magnetic resonance spectroscopy, Fourier transform infrared spectroscopy, powder x-ray diffractometry, and MALDI-TOF analysis were carried out. Thermal stability studies were done using thermogravimetry. Morphological studies of homopolymers, copolymer, and physical blend were carried out using field emission scanning electron microscopy. Fluorescence properties of poly-N-phenyl anthranilic acid and poly-o-phenylenediamine were studied and the relationship between electrochemical redox states in polymer and fluorescence behavior were established. Fluorescent sensors for oxidizing analytes were developed using poly-N-phenyl anthranilic acid, poly-o-phenylenediamine, and their copolymer. A colorimetric acid content sensor useful for state of charge determination in lead-acid batteries was developed based on poly-N-phenyl-o-phenylenediamine. The fluorescent turn-off in poly-N-phenyl anthranilic acid and N-phenyl anthranilic acid with oxidizing agents were utilized for the quantitative estimations using microscale redox titrations with fluorometric

indication. The studies on invisible dye like characteristics and cell imaging promised poly-N-phenyl anthranilic acid as an efficient material in anti-counterfeiting and biological fields.

സംഗ്രഹം

പോളിഅനിലിനും അതിന്റെ ഉത്പന്നങ്ങളും അവയുടെ പ്രത്യേക സ്വഭാവ സവിശേഷതകൾ മൂലം വിവിധ മേഖലകളിൽ ഉപയോഗപ്പെടുത്തിയിരിക്കുന്നു. പോളി-എൻ-ഫിനൈൽ അനിലിന്റെ ഉലപന്നങ്ങൾ നിർമിക്കുകയും അവയുടെ പ്രത്യേകതകൾ പഠിക്കുകയും ചെയ്തു. പോളി-എൻ-ഫിനൈൽ ആന്ത്രനീലിക് ആസിഡ്, പോളി-എൻ-ഫിനൈൽ -ഓർത്തോ ഫിനൈലിൻഡൈഅമിൻ, പോളി-ഓർത്തോ ഫിനൈലിൻഡൈഅമിൻ തുടങ്ങിയ പോളിമെറുകൾ കെമിക്കൽ ഓക്സിഡേറ്റീവ് പോളിമറൈസേഷൻ വഴി ഫെറിക് ക്ലോറൈഡ് ഓക്സീകാരിയായി ഉപയോഗിച്ച എഥനോൾ ലായകത്തിൽ നിർമിച്ചു. എൻ-ഫിനൈൽ ആന്ത്രനീലിക് ആസിഡിന്റെയും ഓർത്തോ ഫിനൈലിൻ ഡൈഅമിന്റെയും കോപോളിമേഴ്സും കെമിക്കൽ ഓക്സിഡേറ്റീവ് പോളിമെറൈസേഷൻ വഴി നിർമിച്ചു. പോളി-എൻ-ഫിനൈൽ ആന്ത്രനീലിക് ആസിഡ്, പോളി-ഓർത്തോ ഫിനൈലിൻ ഡൈഅമിൻ തുടങ്ങിയ പോളിമെറുകളുടെയും അവയുടെ കോപോളിമെറുകളുടെയും ഫ്ലൂറസെന്റ് സവിശേഷതകൾ ഉപയോഗപ്പെടുത്തി സെൻസറുകൾ നിർമിച്ചു. പോളി-എൻ-ഫിനൈൽ ഓർത്തോ ഫിനൈലിൻ ഡൈഅമിന്റെ പിഎച്ച് നു അനുസരിച്ചുള്ള നിറവ്യത്യാസം ഉപയോഗപ്പെടുത്തി ആസിഡ് സെൻസർ നിർമിക്കുകയും അത് ഉപയോഗപ്പെടുത്തി ലെഡ് ആസിഡ് ബാറ്ററിയുടെ സ്റ്റേറ്റ് ഓഫ് ചാർജ് കണ്ടെത്തുകയും ചെയ്തു. പോളി-എൻ-ഫിനൈൽ ആന്ത്രനീലിക് ആസിഡിനെ മൈക്രോ സ്കെയിൽ റെഡോക്സ് ടൈട്രേഷനിൽ ഫ്ലൂറോസെന്റ് ടേൺ ഓഫ് ഇൻഡിക്കേറ്റർ ആയും സെൽ ഇമേജിങ്നും ആന്റി കൗണ്ടർഫെയ്റ്റിംഗ്നും അനുയോജ്യമായ ഉല്പന്നമായി ഉപയോഗപ്പെടുത്തുകയും ചെയ്തു.

TABLE OF CONTENTS

Contents		Page No.
List of Figures		**vii-xvi**
List of Tables		**xvii-xix**
Chapter 1 Introduction and Literature Review		**1-28**
1.1.	*Introduction to conjugated polymers*	3
1.2.	*Types of conjugated polymers*	4
1.2.1.	*Conducting polymers*	6
1.2.2.	*Fluorescent conjugated polymers*	7
1.2.3.	*Electrochromic conjugated polymers*	8
1.2.4.	*Redox active conjugated polymers*	9
1.3.	*Synthetic methods of conjugated polymers*	10
1.3.1	*Chemical oxidative polymerization*	10
1.3.2.	*Electrochemical polymerization*	11
1.3.3.	*Transition metal catalyzed cross-coupling reactions*	11
1.4.	*Copolymerization method for conjugated polymers*	12
1.5.	*Applications of conjugated polymers*	13
1.5.1.	*Sensors*	13
1.5.2.	*Biological applications*	15
1.5.3.	*Electrical and electronic applications*	15
1.5.4.	*Photocatalysis*	16
1.5.5.	*Anticorrosion applications*	16
1.5.6.	*Anticounterfeiting applications*	17
1.6.	*Poly-N-phenyl aniline derivatives*	18
	Reference	19
Chapter 2 Synthesis, Characterization and Analytical Sensing of Redox and Conjugated Poly-N-phenyl anthranilic acid		**29-62**
2.1.	*Introduction*	31
2.2.	*Experimental*	37
2.2.1.	*Materials and Reagents*	37
2.2.2.	*Measurements and Instruments*	37
2.2.3.	*Synthesis of Poly N-phenyl anthranilic acid (PNPA)*	38

TABLE OF CONTENTS

2.2.4.	*Preparation of PNPA-H solution (1×10^{-5} M)*	39
2.2.5.	*Electrochemical studies*	39
2.3.	*Results and Discussion*	39
2.3.1.	*Synthesis of Poly-N-phenyl anthranilic acid*	39
2.3.2.	*Structural characterization of PNPA*	40
2.3.3.	*Fluorescence studies of PNPA-H*	46
2.3.4.	*Fluorescence sensing of oxidizing analytes*	47
2.3.5.	*Application of PNPA-H in titrations*	55
2.4.	*Conclusion*	56
	Reference	58
Chapter 3 Microscale Redox Titrations Using Poly-N-Phenyl Anthranilic Acid Fluorescent Turn-Off Indicator		**63-100**
3.1.	*Introduction*	65
3.2.	*Experimental*	69
3.2.1.	*Materials and Reagents*	69
3.2.2.	*Measurements and Instruments*	70
3.2.3.	*Preparation of indicators*	70
3.2.3.A.	*Preparation of fluorescent indicator (PNPA-H)*	70
3.2.3.B.	*Preparation of fluorescent indicator (NPA-H)*	70
3.2.3.C.	*Preparation of NPA-Na (conventional N-phenyl anthranilic acid indicator)*	70
3.2.4.	*Titrations in micro molar concentrations*	70
3.2.4.A.	*Preparation of standard Mohr's salt solution*	70
3.2.4.B.	*Standardization of oxidizing titrants*	71
3.2.4.C.	*Estimation of ferrous ion*	71
3.2.5.	*Titrations in Semi-Micro Volume Scale*	72
3.2.5.A.	*Preparation of standard Mohr's salt solution*	72
3.2.5.B.	*Standardization of oxidising titrant*	72
3.2.5.C.	*Estimation of ferrous ion*	72
3.2.6.	*Procedure for estimation using semi-micro volume in micro molar titrations (1×10^{-4} M)*	72
3.3.	*Results and Discussion*	73
3.3.1.	*Preparation of fluorescent indicators*	73

TABLE OF CONTENTS

3.3.2.	*Application of fluorescent PNPA-H and NPA-H in microscale redox titrations*	74
3.3.3.	*Application of fluorescent indicator PNPA-H in semi-micro volume redox titrations*	80
3.3.4.	*Mechanism of fluorescent indicators*	81
3.3.5.	*Method validation*	83
3.3.6.	*Experiment overview*	88
3.3.7.	*Experiment design*	88
3.3.8.	*Experiment evaluation*	90
3.4.	*Conclusion*	96
	Reference	97
Chapter 4 Acid Content Sensing and State of Charge Determination of Lead-acid Battery using Poly-N-phenyl-o-phenylenediamine		**101-136**
4.1.	*Introduction*	103
4.2.	*Experimental*	107
4.2.1.	*Materials and Reagents*	107
4.2.2.	*Measurements and Instruments*	107
4.2.3.	*Synthesis of poly-N-phenyl-o-phenylenediamine (PPOPD)*	107
4.2.4.	*Preparation of poly-N-phenyl-o-Phenylenediamine solution (7.5×10^{-5} M)*	108
4.2.5.	*The pH-dependent absorption studies*	108
4.2.6.	*Electrochemical studies*	108
4.2.7.	*Calibration plot of PPOPD solution with different known concentrations of acids*	108
4.2.8.	*Determination of battery acid content*	108
4.2.9.	*Determination of the state of charge of lead-acid batteries from absorbance*	109
4.2.10.	*Determination of State of Charge of Lead-acid batteries from open circuit voltage*	109
4.2.11.	*Determination of specific gravity from density measurement*	109
4.3.	*Results and Discussion*	110
4.3.1.	*Synthesis of Poly-N-phenyl-o-phenylenediamine*	110
4.3.2.	*Structural characterisation of PPOPD*	110

TABLE OF CONTENTS

4.3.3.	*The pH-dependent absorption studies of PPOPD*	114
4.3.4.	*Electrochemical studies*	117
4.3.5.	*State of charge determination in Lead-acid batteries using PPOPD*	123
4.4.	*Conclusion*	131
	Reference	132
Chapter 5 Redox Type Poly-o-phenylenediamine for Reversible Fluorescence Sensing of Silver ion		**137-168**
5.1.	*Introduction*	139
5.2.	*Experimental*	144
5.2.1.	*Materials and Reagents*	144
5.2.2.	*Measurements and Instruments*	144
5.2.3.	*Synthesis of poly-o-phenylenediamine (POPD)*	144
5.2.4.	*Fluorescence turn-off in POPD solution using silver nitrate*	145
5.2.5.	*Electrochemical studies*	145
5.3.	*Results and Discussion*	145
5.3.1.	*Synthesis of Poly-o-phenylenediamine*	145
5.3.2.	*Structural characterisation of POPD*	146
5.3.3.	*Fluorescence sensing of $AgNO_3$*	152
5.3.4.	*Fluorescence reversibility of oxidised POPD*	155
5.3.5.	*Mechanism of fluorescence sensing*	159
5.3.6.	*Electrochemical activities of POPD*	161
5.4.	*Conclusion*	162
	Reference	163
Chapter 6 Random Block Type Copolymers of Poly-N-phenyl anthranilic acid-co-Poly-o-phenylenediamine for Oxidizing Analyte Selective Fluorescence Sensing		**169-214**
6.1.	*Introduction*	171
6.2.	*Experimental*	176
6.2.1.	*Materials and Reagents*	176
6.2.2.	*Measurements and Instruments*	176
6.2.3.	*Synthesis of homopolymers*	177
6.2.4.	*Synthesis of copolymers of NPA and OPD*	177

TABLE OF CONTENTS

6.2.4.A.	*Synthesis of copolymer P(NPA-co-OPD) 10:90*	177
6.2.4.B.	*Synthesis of copolymer P(NPA-co-OPD) 25:75*	177
6.2.5.	*Synthesis of physical blends of PNPA and POPD*	178
6.2.5.A.	*Synthesis of PNPA-blend-POPD 10:90*	178
6.2.5.B.	*Synthesis of PNPA-blend-POPD 25:75*	178
6.2.6.	*Preparation of $AgNO_3$ and acidified $KMnO_4$ solutions as oxidizing analytes*	178
6.2.7.	*The pH-dependent studies of homopolymers, copolymers, and blends*	179
6.2.8.	*Analyte selective oxidation in P(NPA-co-OPD) 10:90 with $AgNO_3$ and $KMnO_4$*	179
6.3.	*Results and Discussion*	179
6.3.1.	*Synthesis of homopolymers, copolymers and physical blends*	179
6.3.2.	*Structural characterization of copolymers and physical blends*	181
6.3.3.	*pH dependent emission tuning in copolymers and blends*	197
6.3.4.	*Fluorescent sensing of oxidizing analytes*	202
6.4.	*Conclusion*	208
	Reference	209
Chapter 7 Poly-N-Phenyl Anthranilic Acid Fluorescent Polymer Dye for Cell Imaging and Secret Writing Applications		**215-244**
7.1.	*Introduction*	217
7.2.	*Experimental*	224
7.2.1.	*Materials and Reagents*	224
7.2.2.	*Measurements and Instruments*	224
7.2.3.	*Preparation of PNPA-H solution*	224
7.2.4.	*Preparation of fluorescent polyvinyl alcohol hydrogels and films*	224
7.2.5.	*Preparation of NPA-H and PNPA-H solutions for cell imaging and cytotoxicity studies*	225
7.2.6.	*Procedure for incorporating fluorescent PNPA-H into different hydrophilic substrates like filter paper, water gel balls, glass fiber, and silica gel*	225

TABLE OF CONTENTS

7.2.7.	*Procedure for cell culture and cytotoxicity Experiment*	225
7.2.8.	*Procedure for Immunocytochemistry analysis*	226
7.3.	*Results and Discussion*	227
7.3.1.	*Synthesis of PNPA-H as fluorescent dye*	227
7.3.2.	*UV-Visible absorption studies*	228
7.3.3.	*Fluorescence stability studies of PNPA-H*	229
7.3.4.	*Application of PNPA-H on hydrophilic substrates*	230
7.3.5.	*Secret writing using PNPA-H*	232
7.3.6.	*Cytotoxicity and cell imaging using NPA-H and PNPA-H*	233
7.4.	*Conclusion*	237
	Reference	238
Chapter 8 Summary and Conclusions		**245**
Publications and Conference presentations		**251**

List of Figures

Figure No.	Figure caption	Page No.
Chapter 1 Introduction and Literature Review		
1.1.	*Structures of parent conjugated polymers and some derivatives of polyaniline.*	3
1.2.	*Types of conjugated polymers.*	4
1.3.	*Different redox structures of PANI in doped and undoped states.*	6
1.4.	*A) Photothermal image and confocal fluorescent image of MEH-PPV for simultaneous absorption and emission measurement. B) Reaction scheme for synthesizing polyfluorene derivatives and photographs of their emission.*	7
1.5.	*A) Cyclic voltammogram of polypyrrole film and B) redox reversible states in polypyrrole.*	9
1.6.	*Basic oxidative polymerization mechanism for thiophene and pyrrole.*	11
1.7.	*a) Cyclic voltammogram of polyaniline-co-polycarbazole demonstrating excellent cyclic stability, b) UV-visible absorption spectra of copolymers on applying potentials c) redox reversible colour changes shown by copolymer films and d) redox reversible states in copolymer.*	12
1.8.	*Schematic representation of fluorescence turn-on in polyphenylenebutadiynylene in the presence of anions.*	13
1.9.	*PANI-based colorimetric sensor for detecting Hg^{2+} ions.*	14
1.10.	*A) Cis-trans isomerization of conjugated polymer containing azobenzene and fluorene units. B) Thermostability and C) photostability of dual patterns conjugated polymer with azobenzene and fluorene units.*	17
1.11.	*A) Polymerization mechanism for the formation of polydiphenylamine and B) structure of oxidised and reduced forms of polydiphenylamine.*	18
Chapter 2 Synthesis, Characterization and Analytical Sensing of Redox and Conjugated Poly-N-phenyl anthranilic acid		
2.1.	*Schematic representation of different types of fluorescent materials available as sensors.*	31
2.2.	*Schematic representation of possible mechanisms in fluorescent sensors.*	32
2.3.	*Mechanisms and detection modes involved in fluorescent conjugated polymer-based sensor.*	33
2.4.	*Conjugated polymer-based fluorescent turn-off sensors for the*	

List of figures

	detection of analytes. A) pyrazole and benzothiadiazole-based conjugated porous polymers for sensing of amines B) Polyfluorenes and amidoxime groups containing fluorescent polymer for the sensing of uranyl ion ($UO2^{2+}$).	34
2.5.	*A) Reversible fluorescence turn-off in fluorescent conjugated polymer with Cu^{2+} ions and turn-on with PMDTA. B) Reversible fluorescence turn-on in conjugated polymer probe with Al^{3+} ions and turn-off with EDTA.*	36
2.6.	*Schematic representation of the synthesis of PNPA using chemical oxidative polymerisation using $FeCl_3$, along with photographs of PNPA in acid and basic media.*	40
2.7.	*^1H NMR spectra of NPA and PNPA in $CDCl_3$.*	41
2.8.	*A) FT-IR spectra of NPA and PNPA and B) MALDI-TOF spectra of PNPA.*	42
2.9.	*A) Powder XRD diffractogram and B) TGA thermogram of NPA and PNPA.*	43
2.10.	*UV-visible absorption spectra of A) PNPA and B) NPA in sodium hydroxide (2 M) with photographs in the inset.*	44
2.11.	*A) UV-visible absorption spectra of A) NPA-H and PNPA-H having different concentrations in sulphuric acid and B) NPA and PNPA in chloroform.*	45
2.12.	*Cyclic voltammogram of A) NPA-H and B) PNPA-H.*	46
2.13.	*Fluorescence images of dissolved PNPA and NPA in chloroform, PNPA-Na and NPA-Na in NaOH, and different concentrations of PNPA-H and NPA-H in H_2SO_4.*	47
2.14.	*Fluorescence quenching studies of PNPA-H with different concentrations of analytes like Ce^{4+}, $KMnO_4$ and $K_2Cr_2O_7$ by colorimetric detection.*	48
2.15.	*UV-Visible absorption spectra of A) Polymer + MnO_4^- ions in solution, B) Polymer + Ce^{4+} ions in solution and C)) Polymer + $Cr_2O_7^{2-}$ in solution, respectively.*	49
2.16.	*Emission spectra of A) Polymer + MnO_4^- ions in solution, B) Polymer + Ce^{4+} ions and C) Polymer + $Cr_2O_7^{2-}$ in solution.*	51
2.17.	*Mole ratio plots of A) Polymer + MnO_4^- ions, B) Polymer + Ce^{4+} ions and C) Polymer + $Cr_2O_7^{2-}$ ions in solution with linear calibration on the quenching concentrations.*	52
2.18.	*Plot of (I_0/I) Vs. concentration of analytes.*	53
2.19	*Mechanism of fluorescence quenching and reappearance of PNPA-H on adding oxidising and reducing analytes with its photographs.*	54
2.20	*A) UV-visible absorption spectra of polymer-analyte solutions on adding ascorbic acid solutions. B) Photographs of PNPA-H under UV light on multiple oxidations and reductions for*	55

	reversibility studies.	
2.21	*A & B) Potentiometric titration curve ((ΔE/ΔV) Vs. volume of analyte) of PNPA-H with different analytes and C) photographs of fluorometric titrations in which 1×10^{-5} M PNPA-H solutions was titrated against 1×10^{-5} M $KMnO_4$ solutions in UV light and visible light.*	56
Chapter 3 Microscale Redox Titrations Using Poly-N-Phenyl Anthranilic Acid Fluorescent Turn-Off Indicator		
3.1.	*Microscale titration apparatus used in the laboratories. A) Experimental setup for automatic titration. B) Microscale acid-base titration unit.*	66
3.2.	*A) Fluorescent organic molecules used in acid-base and redox titrations. B) Quantum dot-based fluorescent indicator for pH sensing and redox titration for Fe^{2+} and Cr^{3+}. C) Structural and fluorescence changes associated with Benzimidazole- BODIPY with pH.*	67
3.3.	*Synthesis of **PNPA** from **NPA** and its fluorescence quenching action with oxidizing agents in acid media.*	74
3.4.	*Photographs of endpoint detection in permanaganometry at different concentrations of ferrous ions using **PNPA-H** as a fluorescent indicator. From top row to bottom a) 1×10^{-2} M in UV light, b) 1×10^{-2} M in visible light, c) 1×10^{-3} M in UV light d) 1×10^{-3} M in visible light, e) 1×10^{-5} M in UV light and f) 5×10^{-6} M in UV light.*	75
3.5.	*Photographs showing endpoint detection in cerimetry at different concentrations of ferrous ions using **PNPA-H** as a fluorescent indicator.*	76
3.6.	*Photographs showing endpoint detection in dichrometry at different concentrations of ferrous ions using **PNPA-H** as a fluorescent indicator.*	76
3.7.	*Photographs showing endpoint detection in permanaganometry at different concentrations of ferrous ions using **NPA-H** as a fluorescent indicator.*	79
3.8.	*Photographs showing endpoint detection in cerimetry at different concentrations of ferrous ions using **NPA-H** as a fluorescent indicator.*	79
3.9.	*Photographs showing endpoint detection in dichrometry at different concentrations of ferrous ions using **NPA-H** as a fluorescent indicator.*	80
3.10.	*Photographs show semi-micro volume titrations of ferrous ions with endpoint detection using fluorescence indicator **PNPA-H.***	81
3.11.	*UV-visible absorption spectra of titrating mixture with fluorescence indicators **PNPA-H** (A) and **NPA-H** (B) before and*	

	at the endpoint in molar concentrations. The inset shows the titrating mixture in UV light (top row) and visible light (bottom row).	82
3.12.	*Mechanism of fluorometric indicating action of **PNPA-H** and **NPA-H** in the redox titrations.*	83
3.13.	*A) Mean masses of ferrous ion estimated using conventional and fluorometric indicating methods for 10^{-2} M concentration. The standard distribution curves of mass were obtained from B) permanganometry, C) cerimetry and D) dichrometry for 10^{-2} M analyte concentrations.*	85
3.14.	*Bar diagram showing the comparison of $t_{critical}$, $t_{calculated}$, $F_{critical,}$ and $F_{calculatd}$ values for a fluorometric indicating method of **PNPA-H** (A and C) and **NPA-H** (B and D).*	86
3.15.	*Linear regression of estimated mass of Fe^{2+} ions using fluorometric indicating methods at different concentrations via dilution A) permanganometry, B) cerimetry, and C) dichrometry.*	87
3.16.	*A) Schematic representation and B) photograph of home-built semi-micro volume titrating setup for fluorometric indicating method.*	89
Chapter 4 Acid Content Sensing and State of Charge Determination of Lead-acid Battery using Poly-N-phenyl-o-phenylenediamine		
4.1.	*A) pH sensing using polyaniline-coated polysulfone membrane and B) UV-visible absorption spectra of the polymer at different pH with photographs.*	103
4.2.	*A) Plot showing dependence of the state of charge on open circuit voltage in the lead-acid battery. B) Plot showing the sulphuric acid specific gravity change measured by developed sensor and hydrometer in the lead acid battery during discharging.*	106
4.3.	*Schematic representation of the synthesis of **PPOPD** using oxidative chemical polymerization and photographs of the aqueous solution of **PPOPD** in basic, neutral, and acidic pH.*	110
4.4.	*^{1}H NMR Spectra of the monomer **POPD** and polymer **PPOPD** in d_6-DMSO.*	111
4.5.	*A) FT-IR spectra of **POPD** and **PPOPD** and B) Powder WXRD diffractogram of **POPD** and **PPOPD.***	112
4.6.	*A) MALDI-TOF spectra of **PPOPD**. B) Possible mechanism of formation of **PPOPD.***	113
4.7.	*A) pH-dependent UV-visible absorption spectra of 7.5×10^{-5} M **PPOPD** and photographs of aqueous solutions of **PPOPD** at different pH and B) Plot of absorbance maxima at 518, 485, and 455 nm versus increasing pH.*	115
4.8.	*A) UV-visible absorption spectra of different concentrations of*	

	PPOPD *in water and B) Determination of molar extinction coefficient of* ***PPOPD****.*	116
4.9.	*UV-visible absorption spectra of* ***PPOPD*** *solution in different acids having acid strength 1M and photographs of* ***PPOPD*** *in different acids.*	117
4.10.	*Cyclic voltammogram of PPOPD in A) water and B) 1% and 4% H_2SO_4 solutions.*	118
4.11.	*A) UV-visible absorption spectra of* ***PPOPD*** *(7.5×10^{-5} M) and their photographs in solutions having different H_2SO_4 percentages ranging from 0.5 % to 4% and B) Calibration plot (absorbance at 518 nm vs. acid percentage) for the determination of unknown acid content.*	119
4.12.	*A) Absorbance of* ***PPOPD s****olution duplicated four times from the same solution at 518 nm in known acid percentage. B) Absorbance of* ***PPOPD****, prepared in bulk quantity C) Absorbance of* ***PPOPD s****olution having concentrations (2×10^{-4} M, 1×10^{-4} M and 7.5×10^{-5} M) at 518 nm produced in known acid solutions and D) corresponding photographs of* ***PPOPD*** *solutions.*	121
4.13.	*UV-Visible absorption spectra of* ***PPOPD*** *solutions having A) 1% acid, B) 4% acid prepared from bulk solution of* ***PPOPD*** *and C) 1% acid, D) 4% acid prepared from three different batches of synthesized* ***PPOPD*** *samples.*	122
4.14.	*Calibration plot of specific gravity of standard acid solutions from density measurements at 27°C with error bars (N=3).*	123
4.15.	*The color change of* ***PPOPD*** *in battery acids and the chemical reaction in a battery during charging and discharging.*	125
4.16.	*A) UV-Visible absorption spectra of battery acids with* ***PPOPD*** *at different open circuit voltages on discharging conditions and B) Determination of battery acid content taken during discharging via extrapolating absorbance of* ***PPOPD*** *with the linear calibration plot.*	126
4.17.	*A) UV-Visible absorption spectra of battery acids with* ***PPOPD s****olution at different open circuit voltages on charging conditions and B) Determination of battery acid content taken during charging via extrapolating absorbance of* ***PPOPD*** *with the linear calibration plot.*	127
4.18.	*State of charge vs. absorbance of* ***PPOPD*** *solution in battery acid at 518 nm and state of charge vs. open circuit voltage on discharging condition.*	129
Chapter 5 Redox Type Poly-o-phenylenediamine for Reversible Fluorescence Sensing of Silver ion		
5.1.	*Acid-doped and undoped forms of poly-o-phenylenediamine and*	

	corresponding changes in the UV-visible absorption spectra of POPD.	140
5.2.	*A) Heteroatom-doped fluorescence tuning in POPD and B) fluorescent turn-off sensing of Cu^{2+} ions using POPD. C) Morphology-controlled fabrication of poly-o-phenyelendiamine and development of POPD-based fluorescent pH sensor.*	141
5.3.	*Schematic representations of A) fluorescence sensing of analytes based on the oxidation of o-phenylenediamine and B) fluorescence development during the oxidation of o-phenylenediamine for Ag^{+} ion detection.*	143
5.4.	*Schematic representation of the synthesis of POPD from OPD by chemical oxidative polymerization and photographs showing pH-dependent color changes of POPD.*	146
5.5.	*^{1}H NMR spectra of OPD, semi-oxidized POPD and oxidized POPD in DMSO d_6.*	147
5.6.	*A) FT-IR spectra of OPD and POPD and B) Powder X-ray diffractogram of OPD and POPD.*	148
5.7.	*FE-SEM images of POPD with different magnifications A) 2µm and B) 1 µm.*	149
5.8.	*A) MALDI-TOF spectra of POPD and B) Thermograms of OPD and POPD.*	150
5.9.	*A) UV-visible absorption spectra of POPD at different concentrations in neutral pH. (Inset: Photographs of POPD having different concentrations in visible light) and B) The plot of absorbance at 419 nm vs. concentration of POPD for the determination of the molar extinction coefficient of POPD.*	151
5.10.	*Photographs of POPD solution in A) UV light at different concentrations from 4.6×10^{-4} M to 5×10^{-5} M. Photographs of POPD solution in B) visible and C) UV light on adding different concentrations of $AgNO_3$ solution to 1×10^{-4} M POPD.*	152
5.11.	*A) UV-visible absorption spectra and B) Fluorescence spectra of POPD with different concentrations of $AgNO_3$.*	153
5.12.	*A) Fluorescence intensity of POPD at 550 nm plotted vs. concentration of $AgNO_3$. Stern-Volmer plot with non-linear curve fitting was shown in the inset, and B) absorbance of POPD at 419 nm plotted vs concentration of $AgNO_3$.*	154
5.13.	*Photographs under UV light of different concentrations of POPD (5×10^{-5} M, 1×10^{-5} M, 5×10^{-6} M) with $AgNO_3$ at a mole ratio of $[AgNO_3]/[POPD]$ as 10 respectively.*	155
5.14.	*A) Photographs of Ox-POPD solution at different concentrations from 1.0×10^{-4} M to 1×10^{-6} M, A) in visible light, B) in UV light and on adding different concentrations of $NaBH_4$ solution to 1×10^{-4} M Ox. POPD C) in visible light, and D) in UV*	

	light.	156
5.15.	*A) UV-visible absorption spectra and B) Fluorescence spectra of oxidized POPD having concentration 1×10^{-4} M on adding different concentrations of $NaBH_4$.*	157
5.16.	*A) Fluorescence spectra of POPD on multiple oxidation and reduction for reversibility studies and corresponding photographs under UV light in the inset. B) UV-visible absorption spectra of POPD solution with 5×10^{-3} M $AgNO_3$ taken at different time intervals 0.25 hrs, 24 hrs, and 48 hrs.*	158
5.17	*A) Possible mechanism of oxidation and reduction in POPD B) Photographs of POPD solution (1×10^{-4} M) with different metal ion analytes having concentration 1×10^{-3} M under UV light and C) Photographs of POPD under UV light in the presence of silver discarded electroplating solution.*	159
5.18.	*The cyclic voltammograms of POPD in A) water and B) 0.1 M H_2SO_4.*	161
5.19.	*Possible redox states in poly-o-phenylenediamine.*	162
Chapter 6 Random Block Type Copolymers of Poly-N-phenyl anthranilic acid-co-Poly-o-phenylenediamine for Oxidizing Analyte Selective Fluorescence Sensing		
6.1.	*Schematic representation of different types of copolymers and physical blends.*	172
6.2.	*A) Emission tuning in polymer blend composed of poly-2-methoxy-5-(2-ethylhexyloxy)-1,4-phenylene vinylene (MEH-PPV) and a nonconjugated polymer – poly(methyl methacrylate) (PMMA) and B) photos of polymer blend films with various MEH-PPV concentrations in visible light and UV light.*	172
6.3.	*A) Photoinduced electron transfer in poly-o-phenylenediamine and rhodamine B copolymer dot and nitrite detection. Fluorescent cell imaging of HeLa cells using B) polyluminol (PLU) C) poly-o-phenylenediamine (POPD) and C) PLU-POPD copolymer.*	175
6.4.	*Schematic representation of the synthesis of copolymers from co-monomers OPD and NPA by oxidative chemical polymerization and physical blending of homopolymers POPD and PNPA.*	180
6.5.	*Photographs of homopolymers POPD, PNPA, copolymer and blend at acidic, neutral and basic pH in visible light.*	181
6.6.	*^1H NMR spectra of homopolymers POPD, PNPA, copolymers P(NPA-co-OPD) 10:90, P(NPA-co-OPD) 25:75,P(NPA-co-OPD) 50:50, and physical blend PNPA-blend-POPD 25:75 in d_6-DMSO solvent.*	183

6.7.	*^{13}C NMR spectra of homopolymers POPD, PNPA copolymer P(NPA-co-OPD) 10:90, P(NPA-co-OPD) 25:75, and P(NPA-co-OPD) 50:50 in d_6-DMSO solvent.*	184
6.8.	*FT-IR spectra of A) homopolymers POPD, PNPA, and copolymers P(NPA-co-OPD) 10:90, P(NPA-co-OPD) 25:75, and P(NPA-co-OPD) 50:50 and B) homopolymers POPD, PNPA, and blend PNPA-blend-POPD 10:90, PNPA-blend-POPD 25:75, and PNPA-blend-POPD 50:50.*	185
6.9.	*FT-IR absorbance percentage of quinoid C=N stretch vs. weight percentage ratio NPA: OPD or PNPA: POPD.*	188
6.10.	*Fineman-Ross plot of $F(f-1)/f$ vs. F^2/f to determine A) monomer reactivity ratio in copolymers and B) reactivity ratio of homopolymers in blends.*	190
6.11.	*Powder WXRD pattern of A) PNPA, P(NPA-co-OPD) 75:25, P(NPA-co-OPD) 50:50, P(NPA-co-OPD) 25:75 P(NPA-co-OPD) 10:90 and POPD B) PNPA, PNPA-blend-POPD 75:25, PNPA-blend-POPD 50:50, PNPA-blend-POPD 25:75, PNPA-blend-POPD 10:90 and POPD.*	192
6.12.	*A) MALDI-TOF spectra copolymer P(NPA-co-OPD) 25:75 and B) Thermogram of PNPA, POPD, copolymer P(NPA-co-OPD) 25:75 and blend PNPA-blend-POPD 25:75.*	193
6.13.	*FE-SEM images of homopolymers PNPA, POPD, and copolymers P(NPA-co-OPD) 25:75 and blend PNPA-blend-POPD 25:75.*	194
6.14.	*DSC thermograms of homopolymers PNPA, POPD, and copolymers P(NPA-co-OPD) 25:75, P(NPA-co-OPD) 50:50, P(NPA-co-OPD) 75:25 and blend PNPA-blend-POPD 25:75.*	195
6.15.	*Possible mechanism of copolymer P(NPA-co-OPD) 25:75 formation.*	196
6.16.	*UV-visible absorption spectra of A) PNPA, B) POPD, and fluorescence spectra of C) PNPA and D) POPD at different pH.*	198
6.17.	*UV-Visible absorption spectra of A) copolymer P(NPA-co-OPD) 25:75 and B) blend PNPA-blend-POPD 25:75 at different pH.*	199
6.18.	*A) The photographs of P(NPA-co-OPD) 25:75 and PNPA-blend-POPD 25:75 solutions in UV light at different pH and B) fluorescence spectra of blend PNPA-blend-POPD 25:75.*	200
6.19.	*Photographs of copolymer solutions P(NPA-co-OPD) 10:90, P(NPA-co-OPD) 50:50 and blend solutions PNPA-blend-POPD 10:90, PNPA-blend-POPD 50:50 at different pH in UV light.*	201
6.20.	*UV-Visible absorption spectra of POPD on adding different $KMnO_4$ concentrations (1×10^{-5} M, 1×10^{-4} M, 2.5×10^{-4} M, and 5.0×10^{-4} M). The plot of absorbance at 420 nm of POPD vs concentrations of $KMnO_4$ in the inset.*	202

6.21.	*Photographs showing changes in A) the emission in UV light and B) colour in visible light of P(NPA-co-OPD) 10:90 on adding $AgNO_3$ followed by acidified $KMnO_4$.*	203
6.22.	*A) UV-visible absorption spectra of copolymer P(NPA-co-OPD) 10:90 and B) fluorescence spectra of copolymer P(NPA-co-OPD) 10:90 on adding different concentrations of $AgNO_3$ at neutral pH. (Inset: photographs of copolymer solution on adding $AgNO_3$ in visible light and UV light).*	204
6.23.	*A) Plot of fluorescence intensity at 445 nm and B) plot of fluorescence intensity at 550 nm in copolymer P(NPA-co-OPD) 10:90 on adding different concentrations of $AgNO_3$.*	205
6.24.	*A) UV-visible absorption spectra of copolymer P(NPA-co-OPD) 10:90 and B) fluorescence spectra of copolymer P(NPA-co-OPD) 10:90 on adding different concentrations of $AgNO_3$ and fixed concentration of 5×10^{-4} M acidified $KMnO_4$ (Inset: photographs of copolymer solution on adding $AgNO_3$ followed by 5×10^{-4} M acidified $KMnO_4$ in visible light and UV light).*	206
6.25.	*Fluorescence spectra of A) copolymer P(NPA-co-OPD) 10:90 and B) PNPA on adding acidified $KMnO_4$ having concentrations 2.5×10^{-4} M and 5.0×10^{-4} M.*	207
Chapter 7 Poly-N-Phenyl Anthranilic Acid Fluorescent Polymer Dye for Cell Imaging and Secret Writing Applications		
7.1.	*Structure of fluorescent organic dyes.*	217
7.2.	*Schematic representation for preparing polyfluorene derivative and its application in water-based invisible ink.*	218
7.3.	*Fluorescence images of A) BALB/C3T3 cells incubated sequentially with poly (p-phenylene ethynylene nanoparticles (green) and Hoechst dye (blue) and B) Live BALB/C3T3 cells incubated with poly (p-phenylene ethynylene nanoparticles. C) Differential interference contrast images and D) fluorescence images of macrophage cell J774 incubated with poly (p-phenylene ethylene). E) Phase contrast images and F) fluorescence images of A549 cells incubated with polythiophene derivative.*	219
7.4.	*Fluorescence microscopy images of A) H522 cells and B) A549 cells incubated with DAPI (a&b), Hoechst 33258 (c&d), Acridine orange-ethidium bromide (e&f) and Dichlorodihydrofluorecein diacetate (g&h).*	221
7.5.	*The schematic representation of protonation in poly-N-phenyl anthranilic acid (PNPA-H) and the photographs of protonated PNPA-H in concentrated H_2SO_4 under UV light and visible light.*	227

7.6.	*Photographs of 1 mg PNPA dissolved in different volumes in concentrated H_2SO_4 under UV light and visible light before and after dilution with deionised water (10 mL).*	228
7.7.	*UV-Visible absorption spectra of PNPA-H with concentrations 1.58×10^{-4} M, 1.18×10^{-4} M, and 9.45×10^{-5} M A) before neutralisation and B) after neutralisation. Photographs of PNPA-H under visible light and UV light before and after neutralisation is given in the inset.*	229
7.8.	*Photographs of PNPA-H with different concentrations like 2.36×10^{-4} M, 1.58×10^{-4} M, 1.18×10^{-4} M, and 9.45×10^{-5} M at pH 3.0, 5.0 and 7.0 under UV light in day 1, day 3, day 5, and day 10.*	230
7.9.	*Photographs of different hydrophilic substrates blended with PNPA-H and irradiated under UV light (365 nm). A) Silica TLC plate in the absence and presence of PNPA-H, B) Filter paper coated with PNPA-H, C) PVA film containing PNPA-H, D) Glass fiber in the presence and absence of PNPA-H, E) PVA hydrogel containing PNPA-H and D) PNPA-H incorporated water gel beads.*	231
7.10.	*Photographs of letters written using PNPA-H A) in visible light and B) in UV light. C) Removing letter using ce(IV) solution and rewriting letter using PNPA-H under UV light.*	232
7.11.	*The plot of cell viability percentage of normal cell L929 vs. concentration of A) NPA-H and B) PNPA-H and that of cancer cell MDA-T32 vs. concentration of C) NPA-H and D) PNPA-H, respectively.*	234
7.12.	*Fluorescence microscopic images of normal cell L929 incubated with control and different concentrations of NPA-H in A) dark field and B) merged dark and bright field Cancer cell MDA-T32 incubated with DAPI and different concentrations of NPA-H in C) dark field and D) merged dark and bright field under 365 nm excitation.*	235
7.13.	*Fluorescence microscopic images of normal cell L929 incubated with DAPI and different concentrations of PNPA-H in A) dark field and B) merged dark and bright field. Cancer cells MDA-T32 incubated with control and different concentrations of PNPA-H in C) dark field and D) merged dark and bright field under 365 nm excitation.*	236

List of Tables

Table No.	Table heading	Page No.
Chapter 1 Introduction and Literature Review		
1.1.	*Examples of different types of conjugated polymers.*	5
Chapter 2 Synthesis, Characterization and Analytical Sensing of Redox and Conjugated Poly-N-phenyl anthranilic acid		
2.1.	*Conjugated polymer-based reversible fluorescent sensors for detecting analytes, the limit of detection, mechanism and sensing mode reported in the literature.*	34
Chapter 3 Microscale Redox Titrations Using Poly-N-Phenyl Anthranilic Acid Fluorescent Turn-Off Indicator		
3.1.	*Fluorescent indicator, titrant used, estimated analyte and estimated concentration of analytes previously reported in the literature.*	68
3.2.	*Details of analyte, titrant, and indicator concentrations, times of dilution fluorescent indicator from bulk, titrant/ indicator molar ratio, and volume of PNPA-H required for different concentrations.*	77
3.3.	*Comparative mass values of ferrous ions estimated by conventional titrations and semi micro-volume redox titration using fluorescent indicators.*	81
3.4.	*Comparative mean mass values of ferrous ions obtained experimentally using conventional indicating method and fluorometric indicating methods in permanganometry.*	84
3.5.	*Comparative mass values of ferrous ions estimated by cerimetry using conventional and fluorescent indicators for different molarity range.*	84
3.6.	*Comparative mass values of ferrous ions estimated by dichrometry using conventional and fluorescent indicators for different molarity range.*	85
3.7.	*comparative results of statistical f test and student's t-test taken for redox titrations using fluorescent and conventional indicators.*	87
3.8.	*Comparative estimated mass values of ferrous ions from molar concentration, micromolar concentration, and semimicro volume using different indicating methods and analyte concentrations.*	92
3.9.	*Pre-lab survey and post-lab survey questions provided to the students.*	93

3.10.	*Comparison of post lab survey results for student evaluation of the microscale titrations.*	95
Chapter 4 Acid Content Sensing and State of Charge Determination of Lead-acid Battery using Poly-N-phenyl-o-phenylenediamine		
4.1.	*Different parameters used to determine the state of charge in batteries, along with advantages and limitations available in the literature.*	104
4.2.	*Acid content (%), absorbance of **PPOPD** at 518 nm having known acid content, and specific gravity determined from direct density and hydrometer.*	124
4.3.	*Specific gravity of battery acid on discharging intervals, open circuit voltage (V) of lead acid battery on discharging intervals, the absorbance of **PPOPD** in battery acid at 518 nm, battery acid content (%) determined from absorbance, and state of charge (%) calculated from open circuit voltage and absorbance of **PPOPD** in battery acid.*	130
4.4.	*Specific gravity of battery acid on discharging intervals, open circuit voltage (V) of lead acid battery on charging intervals, the absorbance of **PPOPD** in battery acid at 518 nm, battery acid content (%) determined from absorbance, and state of charge (%) calculated from open circuit voltage and absorbance of **PPOPD** in battery acid.*	130
Chapter 5 Redox Type Poly-o-phenylenediamine for Reversible Fluorescence Sensing of Silver ion		
5.1.	*POPD-based sensors reported in the literature.*	142
Chapter 6 Random Block Type Copolymers of Poly-N-phenyl anthranilic acid-co-Poly-o-phenylenediamine for Oxidizing Analyte Selective Fluorescence Sensing		
6.1.	*Co-monomers used to copolymerize with o-phenylenediamine via chemical oxidative polymerization, the structure of copolymer, and improved properties/applications via copolymerization reported in the literature.*	173
6.2.	*The mass of co-monomers NPA and OPD taken for copolymer synthesis, the mass of PNPA and POPD taken for blending, the weight ratio of NPA: OPD or PNPA: POPD, the mole ratio of NPA/OPD or PNPA/POPD, and corresponding yields of copolymers and blends.*	181
6.3.	*FT-IR spectral data of homopolymers, copolymers and physical blends.*	186
6.4.	*Monomer/ homopolymer feed ratio, copolymer/homopolymer composition from FT-IR analysis,*	

	monomer/homopolymer ratio in the copolymer/blend, and Fineman-Ross parameters for copolymers/blends having different weight percentages of monomers/homopolymers.	189
Chapter 7 Poly-N-Phenyl Anthranilic Acid Fluorescent Polymer Dye for Cell Imaging and Secret Writing Applications		
7.1.	*Fluorescent materials reported for cell imaging and other applications with cell viability, concentrations of fluorophore used for staining, and stained part of cell adapted from literature.*	222

List of tables

CHAPTER 1

Introduction and Literature Review

Chapter 1

1.1. Introduction to conjugated polymers

Conjugated polymers have emerged as unique polymeric materials with various applications like sensing, anti-corrosive coating, energy storage, electronic devices, and biomedical diagnosis. They possess advantage over ordinary insulating plastic materials in optoelectronic and conducting properties [1]. The presence of π conjugation in the polymeric skeleton made them distinctively different from other polymeric materials. Conjugated polymers also possess attractive features like light-weight, thermal/mechanical stability, flexibility and low cost of production. The popularity of conjugated polymers began in 1977 with the discovery of the conductivity in polyacetylene film via doping. Alan J. Heeger, Alan G. MacDiarmid, and Hideki Shirakawa have bagged the Nobel Prize in 2000 for developing electrical conductivity in polymers [2]. The studies on the synthesis and properties of conjugated polymers have opened a new dimension to create new devices and find novel applications.

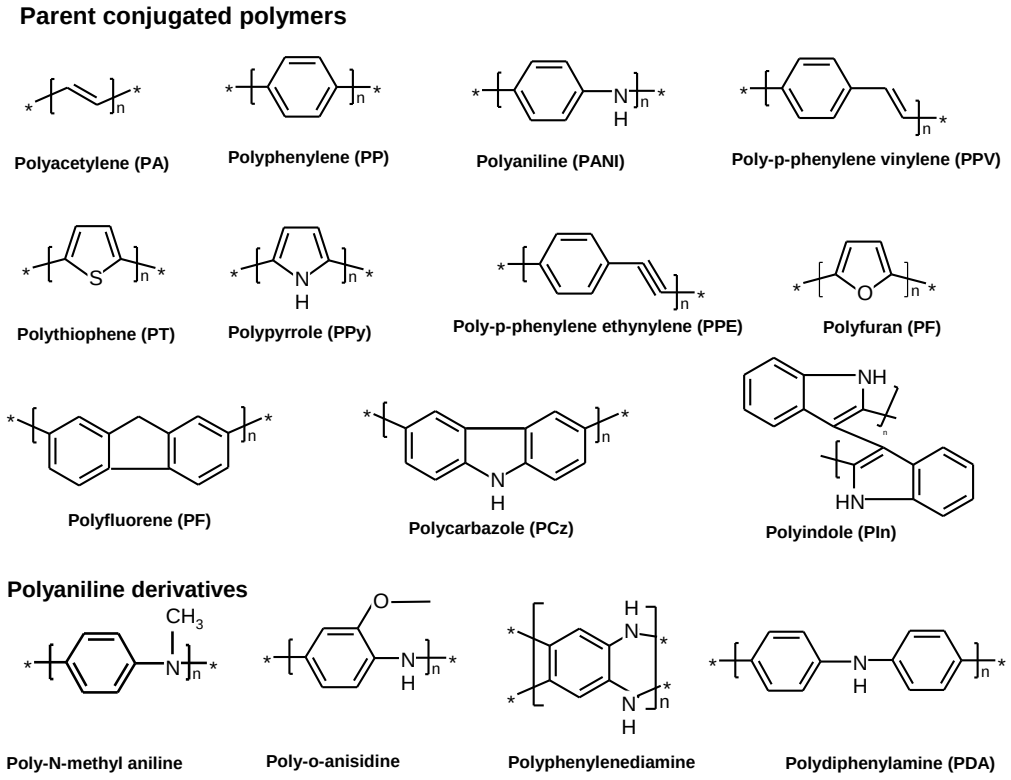

Figure 1.1. *Structures of parent conjugated polymers and some derivatives of polyaniline.*

The structural diversities in the backbone of conjugated polymers make them suitable for specific applications. Conjugated polymers with different structures have been synthesized. Important conjugated polymers are polyaniline (PANI), polyacetylene (PA),

polyphenylene (PP), polythiophene (PT), polyphenylenevinylene (PPV) and polypyrrole (PPy). The combination of electronic and optical properties has given them considerable attention in various technological areas. Their derivatives also gained research interest due to their enhanced properties compared to the parent compounds (See **Figure 1.1.**) Among the conjugated polymers, polyaniline and its derivatives have received much attention due to their conducting nature, electrochemical activities, and optical properties. They have been well-studied and employed in various fields [3, 4].

1.2. Types of conjugated polymers

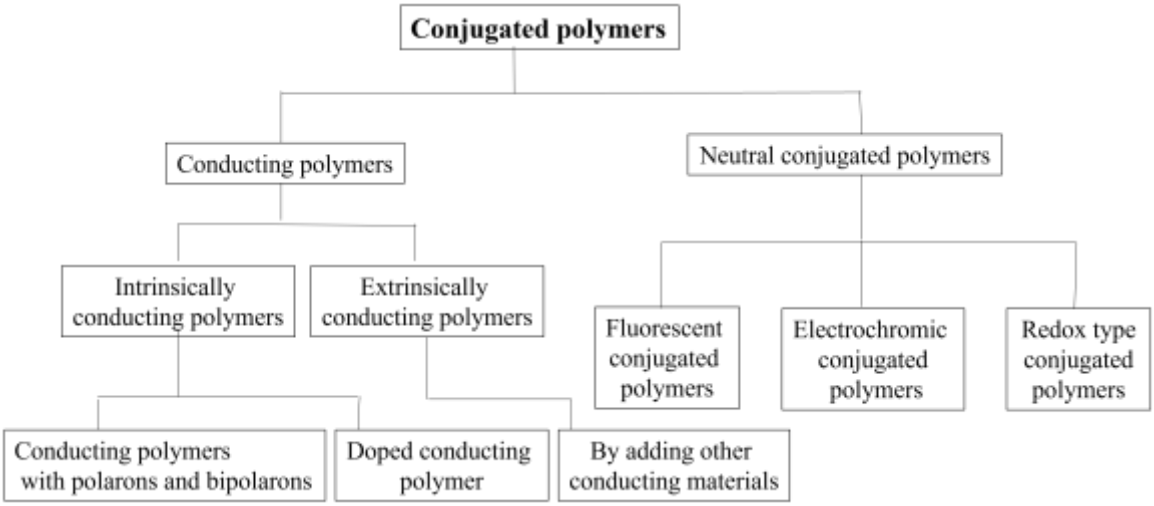

Figure 1.2. *Types of conjugated polymers.*

Conjugated polymers are of two types: conducting polymers and neutral conjugated polymers [5] (see **Figure 1.2.**). Conducting polymers can be further classified into intrinsically and extrinsically conducting polymers [6]. Intrinsically conducting polymers contain either delocalized charge carriers inherently or by doping of chemical reagents for electrical conductivity. In extrinsically conducting polymers, conductivity arises by introducing other conducting materials into the polymer. Neutral conjugated polymers mainly exist in non-conducting at neutral state and exhibiting attractive optical and electrical properties on doping, oxidation, or reduction. Neutral conjugated polymers can be grouped into different types based on their characteristic properties and applications: i) fluorescent conjugated polymers, ii) electrochromic conjugated polymers and iii) redox-type conjugated polymers [7]. Examples of some of the parent conjugated polymers and their derivatives falling under different categories were given in **Table 1.1.**

Table 1.1. *Examples of different types of conjugated polymers.*

Intrinsically conducting polymers		**Neutral conjugated polymers**				
Doped conducting polymers		**Fluorescent conjugated polymer**		**Electrochromic conjugated polymers**	**Redox-type conjugated polymer**	
Polymer	**Conductivity range on doping (S/cm)**	**Polymer**	**Quantum yield (ϕ)**		**polymer**	**Oxidation Potential (V)**
Polyacetylene	10^2 - 10^3 [8]	Poly-p-phenylene vinylene	0.14-0.30 [15]	Polypyrrole [23]	Polyindole	0.85 [22]
Polyaniline	2 - 45 [19]	Polyfluorene	0.30[16]			
Polythiophene	5.9 - 200 [10]	Poly-o-phenylenediamine	0.18 [17]	Polythiophene [24]	MEH-PPV	-0.65 [27]
Poly-p-phenylene vinylene	10^{-4} – 10^{-3} [11]	Poly-N-vinylcarbazole	0.11[18]	Polyindole [25]	Polypyrrole	+0.2 [28]
Poly-p-phenylene	10^{-10} - 10^{2} [12]	Poly-p-phenylene ethynylene	0.35-0.40 [19]		Polyacetylene	+0.65[29]
Poly-o-phenylenediamine	10^{-7} - 10^{-4} [13]	Polyindole [22]	10^{-3} [21]		Poly-3,4-ethylenedioxy-thiophene (PEDOT)	-0.6 [30]
Poly-o-anisidine	10^{-4} -10^{-1} [14]	Poly-2-methoxy-5-(2'-ethylhexyloxy)-1,4-phenylene vinylene (MEH-PPV)	0.20 [20]			

1.2.1. Conducting polymers

Most of the conjugated polymers are semiconducting in their pristine form. Their conductivity can be enhanced through doping by adding p-type or n-type dopants via the degree of doping. Conducting polymers were widely used in electrochemical sensing, batteries, supercapacitors and solar cells [31]. Polyaniline is one of the important conducting polymer, which exists in three different structures. In 1997, MacDiarmid suggested the existence of a fully reduced leucoemaraldine form, semi-oxidized emaraldine form and fully oxidized pernigraniline form of polyaniline [26, 32,33] (see **Figure 1.3.**). Polyaniline is conducting only in the doped emaraldine form, and all other forms are insulating. The conductivity of polyaniline can be enhanced from 10^{-10} S/cm (in basic emaraldine form) to 10 S/cm (in doped emaraldine form) through acid doping [34]. Gupta et al. synthesized polypyrrole films and enhanced the conductivity of polypyrrole films via doping with an organic dye acriflavin hydrochloride [35]. The enhanced conductivity in other conjugated polymers by doping with suitable dopants was also reported [36,37].

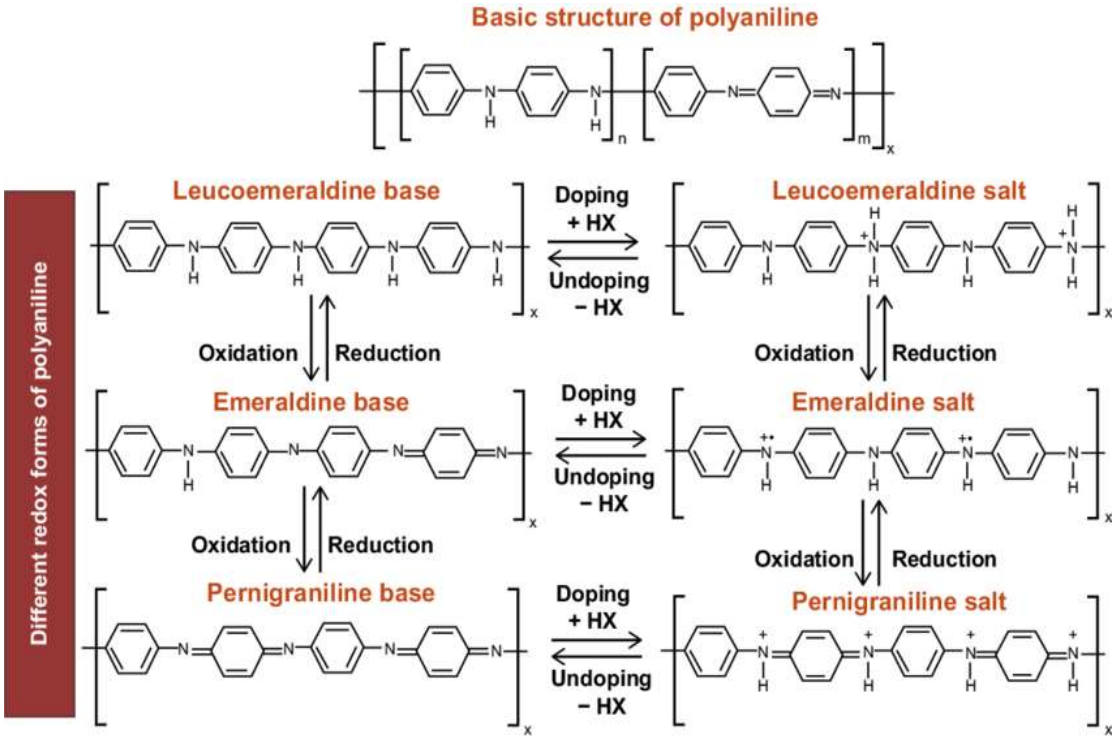

Figure 1.3. *Different redox structures of PANI in doped and undoped states (Adapted from Malhotra et al. 2015).*

1.2.2. Fluorescent conjugated polymers

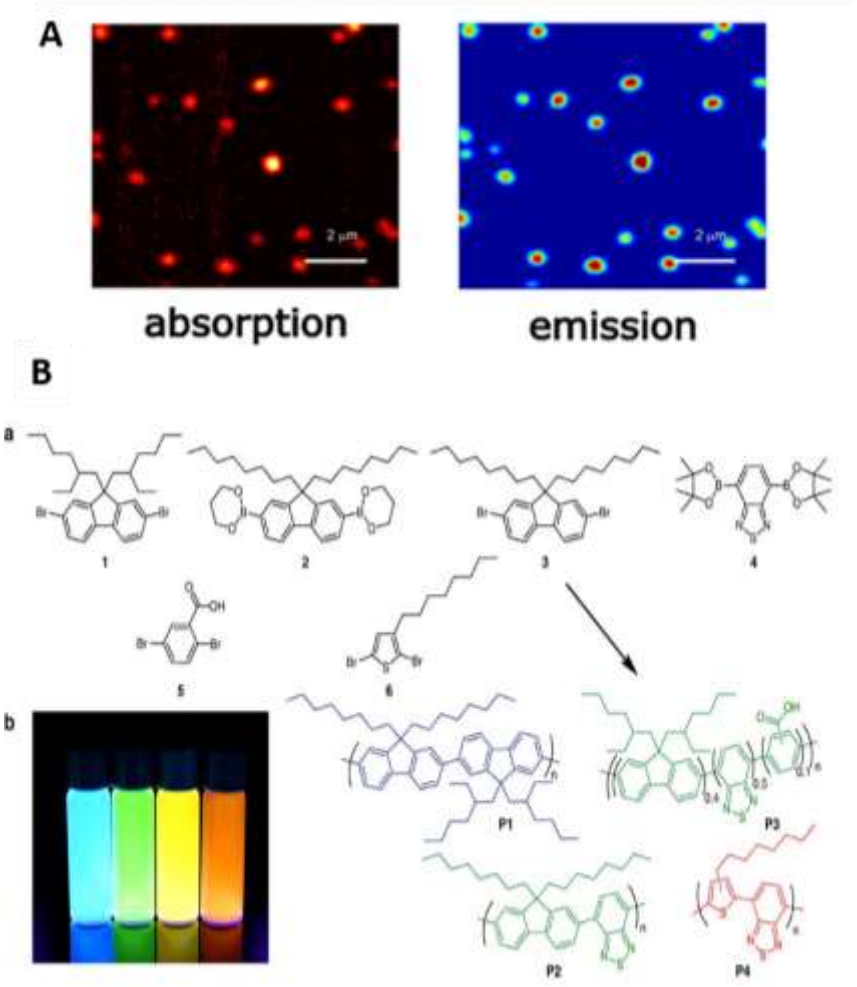

Figure 1.4. *A) Photothermal image and confocal fluorescent image of MEH PPV for simultaneous absorption and emission measurement (Adapted from Hou et al. 2016). B) Reaction scheme for synthesizing polyfluorene derivatives and photographs of their emission (Adapted from Kuehne et al. 2012).*

The conjugated polymers with fluorescence properties have advantages like tunable emission and photoluminescent efficiencies. Strong fluorescence, high quantum yield, and high photostability are some of the characteristic properties of fluorescent conjugated polymers [38]. They have potential sensing applications for pollutants and metal ions, bio-imaging, photodynamic treatments, light-emitting diodes, electronic displays and anticounterfeiting devices. The extended conjugation in the polymeric backbone provides narrow band gap, in which the light absorption results in the radiative energy transfer. The fluorescence efficiency of conjugated polymers is very much related to the extent of delocalization and polarizations of the polymer backbone and conformational changes

associated with polymers [39]. Thus, fluorescence efficiency in conjugated polymers can be easily tuned to the desired extent by controlling their conjugation and conformations. Bazan et al. studied the effect of polymer chain length and interchain contacts on the fluorescence quantum yield of poly-p-phenylene [40]. Kim et al. reported that fluorescent conjugated polymers with poly-p-phenylene backbone showing blue, green, and red emissions pointing to their applications in white illumination [41]. Huang et al. synthesized water-soluble fluorene-containing polyarylene ethynylens and studied the effect of water solubility on aggregation and photoluminescent efficiency [42]. Hou et al. measured the absorption and emission of poly-2-methoxy-5-(2-ethyl hexyloxy)-1,4-phenylene vinylene (MEH-PPV) simultaneously, which could provide information regarding radiative and non-radiative decays in the conjugated polymer (see **Figure 1.4.**) [43]. Kuehne et al. synthesized several monodispersive polyfluorene derivatives and studied the fluorescence behavior of such polymers [44]. Thus, studies on the fluorescence properties of conjugated polymers were effective in modifying existing technologies and designing novel applications.

1.2.3. Electrochromic conjugated polymers

Electrochromic conjugated polymers have shown a reversible colour change in response to the electrochemical redox process, resulting from changes in the conjugated π electrons. The band gap in conjugated polymers can be controlled by doping-dedoping process so that their electrochromic behavior can also be altered. Electrochromic conjugated polymers have applications in multifunctional smart windows, optical filters & displays, electronic paper, and ophthalmic lenses [45, 46]. Watanabe et al. investigated electrochromism in polyaniline films which showed multiple colour changes from yellow to green and to blue upon electrochemical oxidation [47]. Qin et al. synthesized polyaniline, and its electrochromic property was enhanced by copper doping [48]. Nie et al. synthesized poly-5-formylindole film and studied its electrochromic properties. The polymer showed yellow colour on electrochemical reduction and green colour on electrochemical oxidation and was effective in developing electrochromic devices [49]. Nicho et al. reported the electrochromic properties of polythiophene derivatives, which showed a blue colour on electrochemical reduction and red colour on electrochemical oxidation [24]. Girotto et al. synthesized dodecyl sulfate doped polypyrrole, which showed high colouration efficiency and optical contrast suitable for ideal electrochromic material [50]. Similarly, the electrochromic properties of other conjugated polymers and their derivatives were also efficiently used in electrochromic devices.

1.2.4. Redox active conjugated polymers

Redox-active conjugated polymer undergoes redox reaction on doping and de-doping. They have been considered an important organic energy storage material and have been used for sensing various analytes. The presence of active redox states in conjugated polymers has been studied using a cyclic voltammogram. Huang et al. studied the electrochemical activity of polyaniline and confirmed the redox states in emaraldine form with the presence of two oxidation and two reduction peaks in the CV [51, 52]. Nie et al. determined the presence of reversible redox states in polypyrrole films (See **Figure 1.5.)** [53]. Qu et al. synthesized polyaniline containing quinone moiety and showed the existence of quasi-reversible redox states [54]. Vacca et al. prepared PEDOT: PSS thin film electrode and determined the presence of two redox peaks in cyclic voltammogram and its high capacitive behavior [55]. The electrochemical redox activities in other conjugated polymers have also been used for various applications.

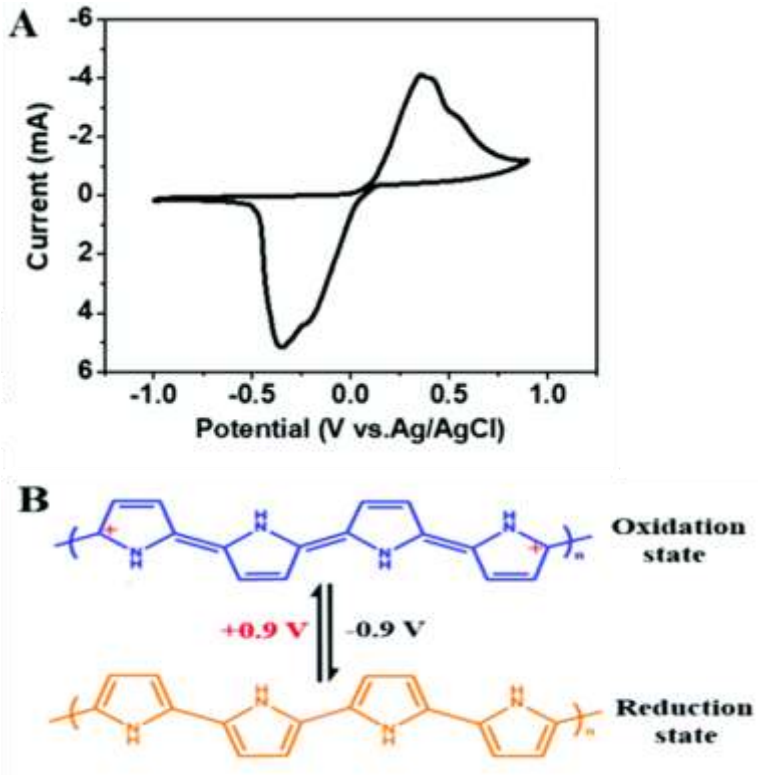

Figure 1.5*. A) Cyclic voltammogram of polypyrrole film and B) redox reversible states in polypyrrole (Adapted from Nie et al. 2019).*

1.3. Synthetic methods of conjugated polymers

Conjugated polymers can be synthesized using various methods. Important synthetic methods involve chemical oxidative polymerization, electrochemical polymerization, and transition metal-catalyzed cross-coupling reactions.

1.3.1. Chemical oxidative polymerization

Most of the conjugated polymers like polyaniline, polypyrrole, polythiophene, polyphenylene and polyphenylenediamines have been synthesized by chemical oxidative polymerization in the presence of oxidizing agents. In this method, the oxidizing agent initiates the polymerization process through the formation of radical cations and these radical cations further react with other monomers to form polymers [34] (see **Figure 1.6.**). Commonly used oxidizing agents are ferric chloride ($FeCl_3$), ammonium persulfate (APS), silver nitrate ($AgNO_3$), hydrogen peroxide (H_2O_2), and copper chloride ($CuCl_2$). Chemical oxidative polymerization can be effectively used for the bulk production of polymers at a reasonable cost with good mechanical properties [56]. Conjugated polymers with different morphologies can be produced using chemical oxidative polymerization by simply varying the reaction conditions. Abu-Thabit et al. synthesized polyaniline via chemical oxidative polymerization using ammonium persulfate as an oxidizing agent for electronic textile applications [57]. Tang et al. investigated the effect of variation in the mole ratios of monomer, oxidizing agent, and acid required for the chemical oxidative polymerization of aniline [58]. Nanosheets and nanofibres of polyaniline were obtained by varying the mole ratios. Yussuf et al. synthesized polypyrrole by chemical oxidative polymerization using different oxidizing agents like $FeCl_3$ and APS and investigated the effect of oxidizing agents on the conductivity and morphology of polypyrrole [59]. Durgaryan et al. synthesized poly-p-phenylenediamine by chemical oxidative polymerization using potassium persulfate in HCl medium and reported the formation of pernigraniline form similar to polyaniline [60]. Synthesis of conjugated polymers like polyindole, PEDOT, polycarbazole etc., have also been reported using chemical oxidative polymerization [61-63].

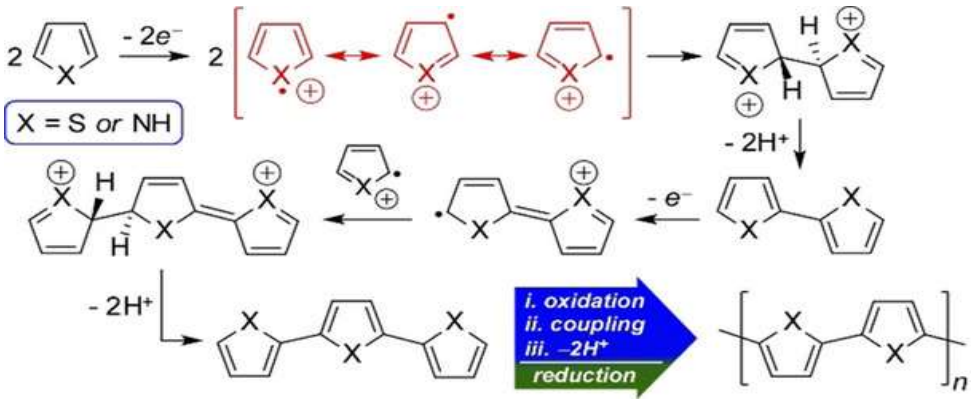

Figure 1.6. *Basic oxidative polymerization mechanism for thiophene and pyrrole (Adapted from Rasmussen et al. 2020).*

1.3.2. Electrochemical polymerization

Electrochemical polymerization of conjugated polymers can be performed either potentiostatically or potentiodynamically. The synthesis required a three-electrode set-up in which the electrochemical oxidation of monomers was carried out on a suitable anode. Radical cations of monomers were initially formed at the electrode by applying potential and then polymerization proceeds through radical coupling [64]. Electrochemical polymerization was effective for producing high molecular weight polymer films with short time periods, but low productivity and yield were the major disadvantages [57]. Electrochemical polymerization was adopted to synthesize polyaniline, polypyrrole, polythiophene, polyfuran, and poly-p-phenylene in polymer films with controllable thickness and morphology [65-69].

1.3.3. Transition metal catalyzed cross-coupling reactions

Transition metal-catalyzed cross-coupling reactions involve the coupling reaction between an aryl di-halogen monomer and another monomer in the presence of transition metal catalysts. The most common transition metal catalysts are organometallic complexes of nickel or palladium ions. Stille, Suzuki, Heck, Sonogashira, and Kumada coupling are transition metal-catalyzed reactions that produce conjugated polymers [64]. The synthesis involves three reaction steps: i) transition metal catalyzed oxidative addition reaction to carbon-halogen bond of monomer, ii) Transmetalation with organometallic nucleophile, and iii) reductive elimination leading to the product formation via carbon-carbon bond formation and regeneration of catalyst [70]. Conjugated polymers with high purity, high molecular weight, and controllable structures were obtained using transition metal-

catalyzed cross-coupling reactions [64]. Synthesis of poly-p-phenylenevinylene, polyfluorene derivatives, polycarbozole derivatives and polythiophenes using transition metal catalysed cross-coupling reactions have been reported [71-74].

1.4. Copolymerization method for conjugated polymers

Copolymerization methods have been widely adopted to design conjugated copolymers with specific chemical structures and compositions with controllable physical and chemical properties. Thus, copolymerization can be considered as an effective method for polymer engineering at the molecular level [75]. Most conjugated copolymers have been synthesized by chemical oxidative copolymerization, electrochemical copolymerization, or free radical copolymerization. Spectroscopic characterization methods like fourier-transform infrared spectroscopy (FT-IR), nuclear magnetic resonance spectroscopy (NMR), and elemental analysis can be used to determine the reactivity ratios of the copolymers so that the copolymer formation can be established [76-78]. Copolymers have been synthesized by varying monomer mole ratios to get desired properties suitable for specific applications.

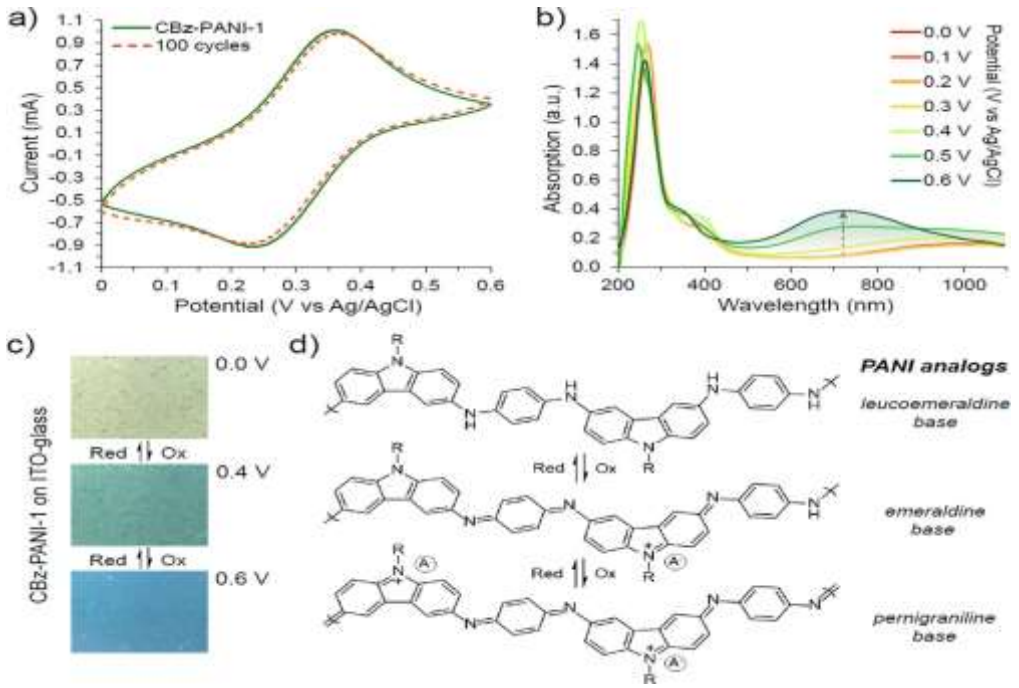

Figure 1.7. *a) Cyclic voltammogram of polyaniline-co-polycarbazole demonstrating excellent cyclic stability, b) UV-visible absorption spectra of copolymers on applying potentials c) redox reversible colour changes shown by copolymer films and d) redox reversible states in copolymer (Adapted from Almitri et al. 2022).*

Almitri et al. synthesized a copolymer of polyaniline derivative with carbazole unit and 2,5-dimethyl-p-phenylenediamine, and resultant copolymers were used to fabricate electrodes for supercapacitor devices (see **Figure 1.7.**) [79]. Xu et al. synthesized copolymers of fluorene and thiophene and determined efficient charge transfer properties suitable for developing photovoltaic materials [80]. Gidron et al. synthesized copolymers of furan and thiophene and determined the high fluorescence, enhanced solubility, and formation of stable radical for copolymerization. Their suitability in optoelectronic applications were also studied [81]. Different chemical, electrochemical, and fluorescent sensors have also been developed based on copolymers. Hosseini et al. synthesized copolymer films of 3-methoxyethoxy thiophene with aniline, thiophene and pyrrole, and fabricated a gas sensor to detect gases like hydrogen halide, halogens, hydrogen cyanide by measuring mass and conductivity of copolymers [82]. Dominguez-Aragon et al. developed a colorimetric sensor based on poly-o-phenylenendiamine-co-aniline copolymer for measuring freshness of tilapia fish. The pH-responsive colour change of copolymer was effectively used for sensing volatile amines produced during fish spoilage [83].

1.5. Applications of conjugated polymers

1.5.1. Sensors

Sensors can easily detect the presence of analytes or changes in the surrounding environment without interference. Conjugated polymers offer collective properties, which could be easily used to monitor slight perturbations. Conjugated polymers have gained much demand in developing various types of sensors like fluorescent, colorimetric, and electrochemical sensors. The properties of the conjugated polymers resulting from the delocalised electrons can be easily altered concerning intramolecular aggregation, energy transfer, conformational changes, and redox reactions induced by the analytes. Such changes could be easily utilized for developing sensors.

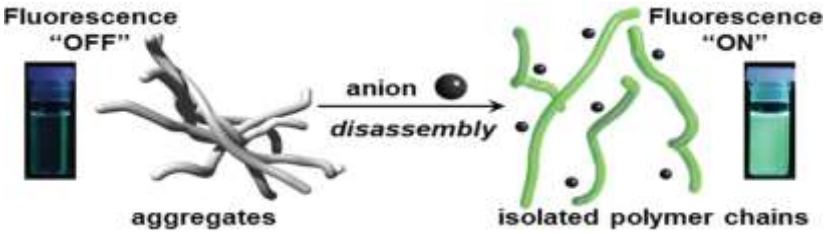

Figure 1.8. *Schematic representation of fluorescence turn-on in polyphenylenebutadiynylene in the presence of anions (Adapted from Sakai et al.2016).*

Fluorescent sensors are one of the important chemical sensors in which the fluorescence emission detects the presence of an analyte. Fluorescent sensors contain receptors and fluorophores in which receptor moieties interact with analyte and fluorophores provide responses for this interaction [84]. Sensitive fluorescence properties and signal amplification make conjugated polymer-based fluorescent sensors advantageous over other sensors. Swager et al. demonstrated the amplification of fluorescence quenching in poly-p-phenyleneethynylene derivative with paraquat by energy migration [85]. Various conjugated polymers like poly-p-phenylenevinylenes, poly-p-phenyleneethynylenes, polyphenylenebutadiynylenes, polythiophenes, polyfluorenes were used to develop fluorescent sensors for detecting various metal ions, explosives, and pollutants. (see **Figure 1.8.**). [86-88]

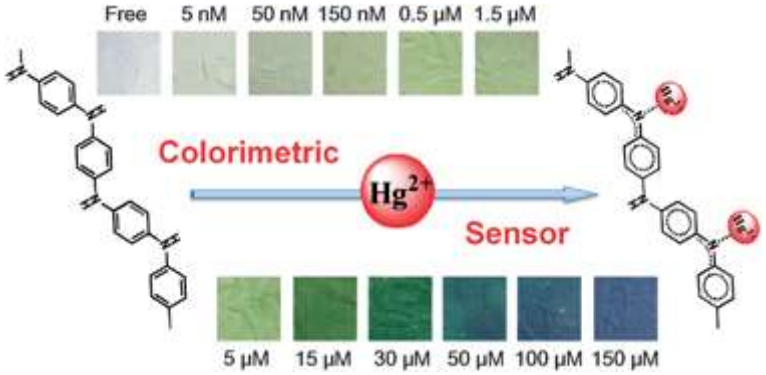

Figure 1.9. *PANI-based colorimetric sensor for detecting Hg^{2+} ions (Adapted from Si et al. 2016).*

Colorimetric sensors show changes in the light absorption properties of materials by the interation with the analyte. Colorimetric biosensors based on polythiophenes and polydiacetylenes have been developed to sense biological molecules, DNA, and proteins based on conformational changes [89]. Si et al. developed a polyaniline-based immobilized sensor for Hg^{2+} ions, which exhibits a colorimetric response for doping of Hg^{2+} ions in polyaniline (See **Figure 1.9.**) [90]. Chen et al. used poly-3, 4-propylenedioxythiophene as a colorimetric sensor to detect Fe^{3+} ions in water by disassembling inter-chain aggregates and conformational changes in polymer by Fe^{3+} ions [91].

Electrochemical sensors recognize the interaction between analytes and receptors by changing the electrical properties like conductivity, resistivity, and potential. Voltammetry, amperometry, potentiometry, impedimetry, and conductometry are the commonly used electrochemical techniques for analyte detection [92]. The redox-active

nature of polypyrrole and its derivatives were effectively used to develop potentiometric sensors, voltammetric sensors, and conductometric sensors of various heavy metal ions, neutral molecules, biomolecules, organic vapours etc [93]. Similarly, polythiophene derivatives and composites, polyaniline derivatives and composites, and polyindole incorporated composites have been utilized for developing electrochemical and biosensors [94-96].

1.5.2. Biological applications

Water-soluble conjugated polymers have been widely used in biological and biomedical applications due to their biocompatibility, good optical properties, high photostability, high quantum yield, and ease of surface modification [97]. Polydiacetylenes and polythiophenes were used as biomarkers to diagnose microbial infections and tumors [98]. Fluorescent conjugated polymers like polyphenyleneethynylene derivatives, polyphenylenevinylene derivatives, and polyfluorene derivatives with or without specific targeting elements have been used effectively in vitro and in vivo cell imaging [99]. The hydrophobic backbones of conjugated polymers were suitable for encapsulating drugs, so they have been used for drug delivery. Photothermal conjugated polymers containing thiophene, cyclopentadithiophenes, benzodithiophenes as electron donors and bezodiathiazole, diketopyrrolopyrrole were used as electron acceptors in photothermal therapies [100].

1.5.3. Electrical and electronic applications

Conjugated polymers possessing good electrochemical properties, good conductivity and significant energy density are suitable for electrical applications like batteries and supercapacitors [34]. Polyaniline is an important candidate in supercapacitors due to its stable electrochemical redox properties and high specific capacitance [101]. Energy conversion and energy storage in conjugated polymers were due to their electrochemical redox activities and high conductivities make them suitable as electrodes in batteries. Polyaniline nanocomposites, sulfonated polyaniline, polypyrrole, and polythiophene were reported as suitable charge storage materials [102]. The ability of conjugated polymers to tune their electronic properties like charge transfer mobility, optical absorption, and tunable band gap allowed them to find suitable applications in organic photovoltaics, organic light-emitting diodes, and field effect transistors [7]. Poly-3-substituted thiophenes have been designed with solution processability and structural regularity to provide high field effect

mobility suitable for organic field effect transistors [103]. Nanowires of polyaniline and polypyrrole based polymers were also effectively used in field effect transistors because of the higher carrier mobilities due to their ordered packing structures [104, 105]. Dialkyloxy substituted poly-p-phenylenevinylene and poly-3-hexyl thiophenes with strong light absorption and high photo conversion efficiencies were employed in photovoltaic cells [106, 107]. Highly luminescent conjugated polymers like polyfluorene and its derivatives like MEH-PPV were used in organic light-emitting diodes [108].

1.5.4. Photocatalysis

The conjugated conducting polymers with semiconducting band gaps were applied as a photocatalyst due to their metal-free nature, robustness, and visible and near-infrared light activities [109]. Muktha et al. used poly-3-hexyl thiophene and MEH-PPV to degrade textile dyes like alizarine and orange G [110]. Linear conjugated polymers like poly-p-phenylene, and polypyrrole, nano-conjugated polymers, conjugated polymers with microporous structures, hybrids of conjugated polymers with metal oxides like polyaniline-titanium dioxide, polypyrrole-titanium dioxide, poly-3-hexyl thiophene-titanium dioxide and hybrids of conjugated polymer with graphene have been developed as an efficient photocatalyst for dye degradation [109].

1.5.5. Anticorrosion applications

Conjugated polymers have exhibited good anticorrosion efficiency in their conducting state and can store charges on the metal surface as a passive coating [111]. Conducting conjugated polymers like polyaniline, and their composites were used as a protective coating on iron, steel, and aluminium alloys for corrosion protection [112]. Polypyrrole and their derivatives with intrinsic corrosion properties have shown enhanced anticorrosion properties through anodic protection, cathodic protection, corrosion resistance and barrier effect [113]. Leon et al. used superhydrophobic and conductive polythiophene coatings to protect steel substrates by preventing water attack and inhibiting corrosion by shifting anodic corrosion potential [114]. Anticorrosion efficiencies of polyphenylenesulfide, polyphenylenediamines, and polyindole nanocomposites have been used as protective coatings [115-117].

1.5.6. Anticounterfeiting applications

Conjugated polymers with fluorescence or stimuli-responsive colour changes have been used in anticounterfeiting fields due to their high stability. Liu et al. synthesized a conjugated polymer containing fluorene and azobenzene units in which the combination of photo-switchable azobenzene and thermally stable fluorene units developed photo-responsive and thermally stable anticounterfeiting material (see **Figure 1.10.**). [118]. Thermochromic materials like polydiacetylenes and polythiophenes, which showed colour change with temperature, and thermo fluorochromic materials like poly-p-phenylenevinylene, which showed fluorescence change with temperature, were suitable as anticounterfeiting materials. The optical changes of these materials were associated with variations in conformations, aggregations and degree of conjugations [20]. Duan et al. synthesized an alternate copolymer of p-phenyelene ethynylene and thienylene ethynylene containing spiropyran units. Reversible fluorescent emission changes in the polymer under UV and visible light via the foster resonance energy transfer mechanism were effective in anticounterfeiting applications [119]. Thermofluorochromic MEH-PPV and thermochromic polydiacetynes have also emerged as suitable anticounterfeiting materials [7,20].

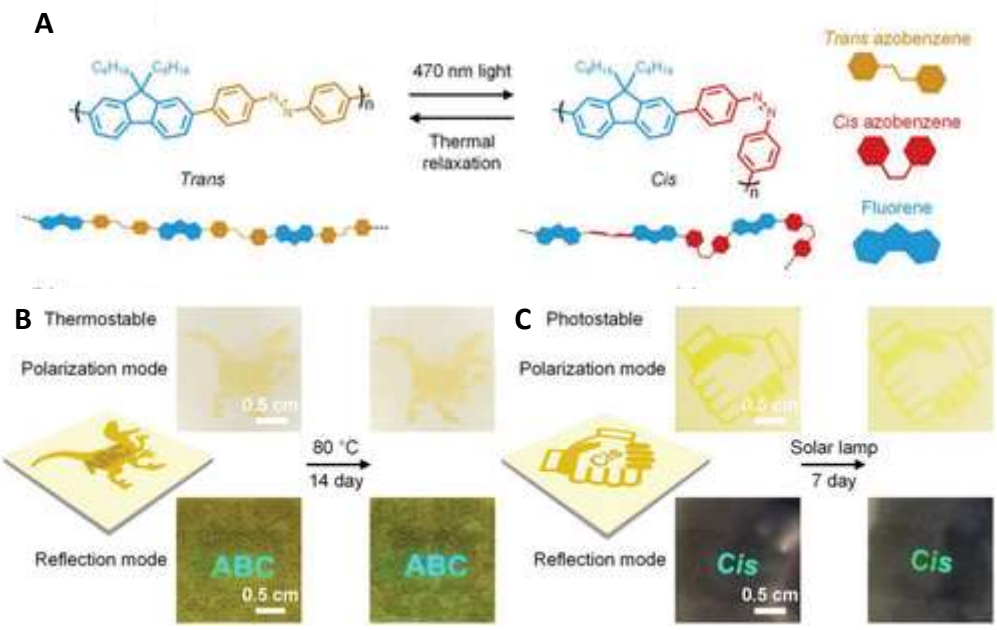

Figure 1.10. *A) Cis-trans isomerization of conjugated polymer containing azobenzene and fluorene units. B) Thermostability and C) photostability of dual patterns of conjugated polymer with azobenzene and fluorene units (Adapted from Liu et al. 2023).*

1.6. Poly-N-phenyl aniline derivatives

Polyaniline is one of the exclusively studied and well-employed conducting polymers due to its strong electrochemical redox properties. The major drawbacks associated with polyaniline were its low processability, poor mechanical strength, and weak emission [120]. Copolymerization of aniline with other monomers, use of polyaniline derivatives and doping of polyaniline with long alkyl chain organic acids were adopted to overcome these limitations [121]. The structure, properties and applications of poly-N-phenyl aniline or polydiphenylamine were reported. Chang et al. studied the formation mechanism and electrochemical redox properties of polydiphenylamine [122]. (See **Figure 1.11.**). Wen et al. reported the electrochemical synthesis of methane sulfonic acid doped polydiphenylamine with improved solubility [123]. Obrezkov determined the high energy density of polydiphenylamine and proposed its application in dual-ion batteries as a positive electrode [124].

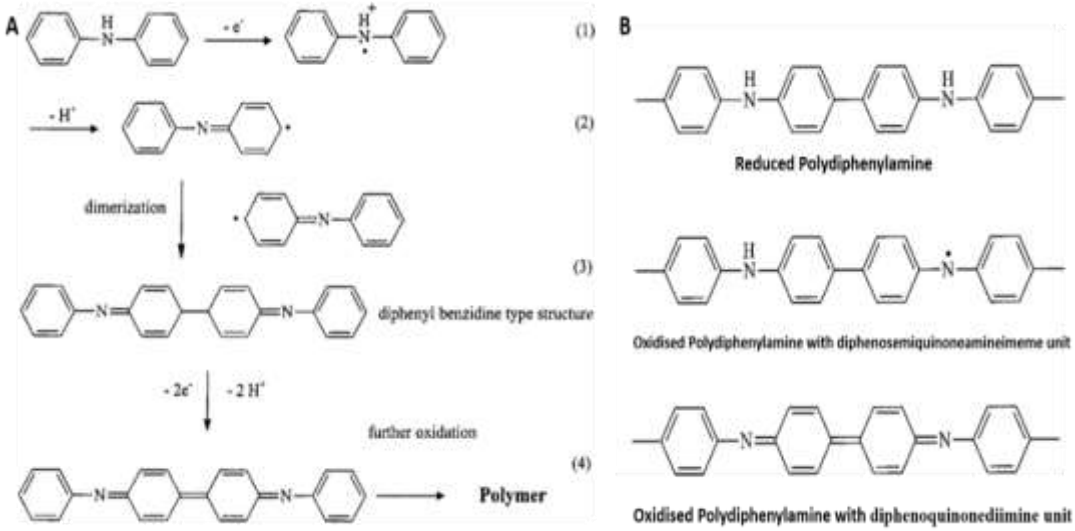

Figure 1.11. *A) Polymerization mechanism for the formation of polydiphenylamine and B) structure of oxidized and reduced forms of polydiphenylamine (Adapted from Chen et al. 2002).*

A few literature reports were available on the studies related to poly-N-phenyl aniline derivatives. The synthesis of poly-N-phenyl anthranilic acid by chemical oxidative polymerization and studies on their thermal stability and electroactivity were reported by Ozkan et al. [125, 126]. Abalyaeva et al. studied the electrochemical properties of poly-N-phenyl anthranilic acid and proposed their applications for designing electrodes for

supercapacitors [127]. The electrochemical synthesis of poly-N-phenyl-o-phenylenediamine was reported by Coteralo et al. and Ojani et al. [128-129]. The optical and analytical properties of poly-N-phenylaniline derivatives and their functional applications were not explored. In this thesis, we have focused on the synthesis, properties, and applications of poly-N-phenyl aniline derivatives like poly-N-phenyl anthranilic acid, Poly-N-phenyl-o-phenylenediamine, and copolymers of poly-N-phenyl anthranilic acid and poly-o-phenylenediamine.

Reference

1. Rasmussen, S. C. (2020). Conjugated and conducting organic polymers: The First 150 Years. *ChemPlusChem*, *85*(7), 1412–1429. https://doi.org/10.1002/cplu.202000325.
2. Press Release. NobelPrize.org. Nobel Media AB 2020. https://www.nobelprize.org/prizes/chemistry/2000/press-release (accessed september 27, 2023).
3. Giri, H., J. Dowell, T., Almtiri, M., & N. Scott, C. (2023). Polyaniline Derivatives and Their Applications. In *Polyaniline - From Synthesis to Practical*. IntechOpen. https://doi.org/10.5772/intechopen.1001940.
4. Ahmad, M. N., Nadeem, S., Soltane, R., Javed, M., Iqbal, S., Kanwal, Z., Farid, M. F., Rabea, S., Elkaeed, E. B., Aljazzar, S. O., Alrbyawi, H., & Elkhatib, W. F. (2022). Synthesis, Characterization, and Antibacterial Potential of Poly(o-anisidine)/BaSO4 Nanocomposites with Enhanced Electrical Conductivity. *Processes*, *10*(9), 1878. https://doi.org/10.3390/pr10091878.
5. Yongfang Li, J. H. (2016). Major Classes of Conjugated Polymers and Synthetic Strategies. In *Introduction to Organic Electronic and Optoelectronic Materials and Devices* (second). CRC Press.
6. E K, F., & C, B. (2021). Corrosion protection by conducting polymers: A review. *SSRN Electronic Journal*. https://doi.org/10.2139/ssrn.4017865.
7. Lu, H., Li, X., & Lei, Q. (2021). Conjugated Conductive Polymer Materials and its Applications: A Mini-Review. *Frontiers in Chemistry*, *9*. https://doi.org/10.3389/fchem.2021.732132.
8. Basescu, N., Liu, Z.-X., Moses, D., Heeger, A. J., Naarmann, H., & Theophilou, N. (1987). High electrical conductivity in doped polyacetylene. *Nature*, *327*(6121), 403–405. https://doi.org/10.1038/327403a0.
9. Stejskal, J., Riede, A., Hlavatá, D., Prokeš, J., Helmstedt, M., & Holler, P. (1998). The effect of polymerization temperature on molecular weight, crystallinity, and electrical conductivity of polyaniline. *Synthetic Metals*, *96*(1), 55–61. https://doi.org/10.1016/S0379-6779(98)00064-2.
10. Akimoto, M., Furukawa, Y., Takeuchi, H., Harada, I., Soma, Y., & Soma, M. (1986). Correlation between vibrational spectra and electrical conductivity of polythiophene. *Synthetic Metals*, *15*(4), 353–360. https://doi.org/10.1016/0379-6779(86)90084-6.
11. Hörhold, H.-H., & Helbig, M. (1987). Poly(phenylenevinylene)s - synthesis and redox chemistry of electroactive polymers. *Makromolekulare Chemie. Macromolecular Symposia*, *12*(1), 229–258. https://doi.org/10.1002/masy.19870120112.
12. Yoshino, K., Ueno, H., Uesugi, F., & Satoh, M. (1987). Enhancement of electrical conductivity of poly(*p*-phenylene) and polynaphthylene films by heat treatment. *Journal of Applied Physics*, *61*(4), 1493–1496. https://doi.org/10.1063/1.338081.
13. Samanta, S., Roy, P., & Kar, P. (2016). Structure and properties of conducting poly(o-phenylenediamine) synthesized in different inorganic acid medium. *Macromolecular Research*, *24*(4), 342–349. https://doi.org/10.1007/s13233-016-4054-0.

14. Neetika, M., Rajni, J., Singh, P. K., Bhattacharya, B., Singh, V., & Tomar, S. (2017). Synthesis and properties of polyaniline, poly(o -anisidine), and poly[aniline-co-(*o* -anisidine)] using potassium iodate oxidizing agent. *High Performance Polymers*, *29*(3), 266–271. https://doi.org/10.1177/0954008316639366.
15. Rodrigues, A. C. B., Geisler, I. S., Klein, P., Pina, J., Neuhaus, F. J. H., Dreher, E., Lehmann, C. W., Scherf, U., & Seixas de Melo, J. S. (2020). Designing highly fluorescent, arylated poly(phenylene vinylene)s of intrinsic microporosity. *Journal of Materials Chemistry C*, *8*(7), 2248–2257. https://doi.org/10.1039/C9TC06028F.
16. Monkman, A., Rothe, C., King, S., & Dias, F. Polyfluorene Photophysics. *Polyfluorenes* (pp. 187–225). Springer Berlin Heidelberg. https://doi.org/10.1007/12_2008_147.
17. Liao, F., Yang, S., Li, X., Yang, L., Xie, Z., Hu, C., Yan, S., Ren, T., & Liu, Z. (2014). Preparation of heteroatom doped poly(o-phenylenediamine) fluorescent nanospheres: Tunable fluorescent spectrum and sensing performance. *Synthetic Metals*, *189*, 126–134. https://doi.org/10.1016/j.synthmet.2014.01.008.
18. Chemek, M., Khlaifia, D., Massuyeau, F., Duvail, J. L., Faulques, E., Wéry, J., & Alimi, K. (2014). A copolymer of PVK and P3HT and its nanocomposite with single-walled carbon nanotubes. *Synthetic Metals*, *197*, 246–251. https://doi.org/10.1016/j.synthmet.2014.09.004.
19. Swager, T. M., Gil, C. J., & Wrighton, M. S. (1995). Fluorescence Studies of Poly(p-phenyleneethynylene)s: The Effect of Anthracene Substitution. *The Journal of Physical Chemistry*, *99*(14), 4886–4893. https://doi.org/10.1021/j100014a003.
20. Gettinger, C. L., Heeger, A. J., Drake, J. M., & Pine, D. J. (1994). A photoluminescence study of poly(phenylene vinylene) derivatives: The effect of intrinsic persistence length. *The Journal of Chemical Physics*, *101*(2), 1673–1678. https://doi.org/10.1063/1.468438.
21. Salikhov, R. B., Mustafin, A. G., Mullagaliev, I. N., Salikhov, T. R., Andriianova, A. N., Latypova, L. R., & Sharafullin, I. F. (2021). Photoconductivity of Thin Films Obtained from a New Type of Polyindole. *Materials*, *15*(1), 228. https://doi.org/10.3390/ma15010228.
22. Mozaffari, S., Behdani, J., & Ghorashi, S. M. B. (2022). Synthesis of polyindole nanoparticles and its copolymers via emulsion polymerization for the application as counter electrode for dye-sensitized solar cells. *Polymer Bulletin*, *79*(8), 6777–6796. https://doi.org/10.1007/s00289-021-03833-4.
23. Camurlu, P., & Toppare, L. (2015). Electrochromic Polymers. In *Encyclopedia of Polymeric Nanomaterials* (pp. 666–676). Springer Berlin Heidelberg. https://doi.org/10.1007/978-3-642-29648-2_32.
24. Nicho, M. (2004). Synthesis of derivatives of polythiophene and their application in an electrochromic device. *Solar Energy Materials and Solar Cells*, *82*(1–2), 105–118. https://doi.org/10.1016/j.solmat.2004.01.009.
25. Maarouf, E. B., Billaud, D., & Hannecart, E. (1994). Electrochemical cycling and electrochromic properties of polyindole. *Materials Research Bulletin*, *29*(6), 637–643. https://doi.org/10.1016/0025-5408(94)90119-8.
26. Pruneanu, S., Veress, E., Marian, I., & Oniciu, L. (1999). Characterization of polyaniline by cyclic voltammetry and UV-Vis absorption spectroscopy. *Journal of Materials Science*, *34*(11), 2733–2739. https://doi.org/10.1023/A:1004641908718.
27. Ding, H., Bertoncello, P., Kumar Ram, M., & Nicolini, C. (2002). Electrochemical investigation on MEH-PPV/C60 nanocomposite Langmuir–Schaefer films. *Electrochemistry Communications*, *4*(6), 503–505. https://doi.org/10.1016/S1388-2481(02)00359-4.
28. Grzeszczuk, M., & Ozsakarya, R. (2014). Surface morphology and corresponding electrochemistry of polypyrrole films electrodeposited using a water miscible ionic liquid. *RSC Adv.*, *4*(42), 22214–22223. https://doi.org/10.1039/C4RA03497J.
29. Chiang, C. K., Blubaugh, E. A., & Yap, W. T. (1984). Electrochemical studies on doping of polyacetylene. *Polymer*, *25*(8), 1112–1116. https://doi.org/10.1016/0032-3861(84)90348-3.

30. Wang, D., Lu, C., Zhao, J., Han, S., Wu, M., & Chen, W. (2017). High energy conversion efficiency conducting polymer actuators based on PEDOT:PSS/MWCNTs composite electrode. *RSC Advances*, *7*(50), 31264–31271. https://doi.org/10.1039/C7RA05469F.
31. Tajik, S., Beitollahi, H., Nejad, F. G., Shoaie, I. S., Khalilzadeh, M. A., Asl, M. S., van Le, Q., Zhang, K., Jang, H. W., & Shokouhimehr, M. (2020). Recent developments in conducting polymers: applications for electrochemistry. *RSC Advances*, *10*(62), 37834–37856. https://doi.org/10.1039/D0RA06160C.
32. Malhotra, B., Dhand, C., Lakshminarayanan, R., Dwivedi, N., Mishra, S., Solanki, P., Venkatesh, M., Beuerman, R. W., & Ramakrishna, S. (2015). Polyaniline-based biosensors. *Nanobiosensors in Disease Diagnosis*, 25. https://doi.org/10.2147/NDD.S64841.
33. MacDiarmid, A. G. (1997). Polyaniline and polypyrrole: Where are we headed? *Synthetic Metals*, *84*(1–3), 27–34. https://doi.org/10.1016/S0379-6779(97)80658-3.
34. Majeed, A. H., Mohammed, L. A., Hammoodi, O. G., Sehgal, S., Alheety, M. A., Saxena, K. K., Dadoosh, S. A., Mohammed, I. K., Jasim, M. M., & Salmaan, N. U. (2022). A Review on Polyaniline: Synthesis, Properties, Nanocomposites, and Electrochemical Applications. *International Journal of Polymer Science*, *2022*, 1–19. https://doi.org/10.1155/2022/9047554.
35. Gupta, S., Acharya, U., Pištěková, H., Taboubi, O., Morávková, Z., Kašparová, M., Humpolíček, P., & Bober, P. (2021). Tuning the Conductivity, Morphology, and Capacitance with Enhanced Antibacterial Properties of Polypyrrole by Acriflavine Hydrochloride. *ACS Applied Polymer Materials*, *3*(12), 6063–6069. https://doi.org/10.1021/acsapm.1c00775.
36. Li, H., DeCoster, M. E., Ming, C., Wang, M., Chen, Y., Hopkins, P. E., Chen, L., & Katz, H. E. (2019). Enhanced Molecular Doping for High Conductivity in Polymers with Volume Freed for Dopants. *Macromolecules*, *52*(24), 9804–9812. https://doi.org/10.1021/acs.macromol.9b02048.
37. Kim, J., Guo, J., Sini, G., Sørensen, M. K., Andreasen, J. W., Woon, K. L., Coropceanu, V., Paleti, S. H. K., Wei, H., Peralta, S., Mallouki, M., Müller, C., Hu, Y., Bui, T.-T., & Wang, S. (2023). Remarkable conductivity enhancement in P-doped polythiophenes via rational engineering of polymer-dopant interactions. *Materials Today Advances*, *18*, 100360. https://doi.org/10.1016/j.mtadv.2023.100360.
38. Ahumada, G., & Borkowska, M. (2022). Fluorescent Polymers Conspectus. *Polymers*, *14*(6), 1118. https://doi.org/10.3390/polym14061118.
39. McQuade, D. T., Pullen, A. E., & Swager, T. M. (2000). Conjugated Polymer-Based Chemical Sensors. *Chemical Reviews*, *100*(7), 2537–2574. https://doi.org/10.1021/cr9801014.
40. Bazan, G. C., Miao, Y.-J., Renak, M. L., & Sun, B. J. (1996). Fluorescence Quantum Yield of Poly(*p* -phenylenevinylene) Prepared via the Paracyclophene Route: Effect of Chain Length and Interchain Contacts. *Journal of the American Chemical Society*, *118*(11), 2618–2624. https://doi.org/10.1021/ja953716g.
41. Kim, C., Gwon, Y. J., Kim, J., & Lee, T. S. (2018). Synthesis of fluorescent conjugated polymer nanoparticles and their immobilization on a substrate for white light emission. *Polymer Chemistry*, *9*(48), 5671–5679. https://doi.org/10.1039/C8PY01314D.
42. Huang, Y.-Q., Fan, Q.-L., Lu, X.-M., Fang, C., Liu, S.-J., Yu-Wen, L.-H., Wang, L.-H., & Huang, W. (2006). Cationic, water-soluble, fluorene-containing poly(arylene ethynylene)s: Effects of water solubility on aggregation, photoluminescence efficiency, and amplified fluorescence quenching in aqueous solutions. *Journal of Polymer Science Part A: Polymer Chemistry*, *44*(19), 5778–5794. https://doi.org/10.1002/pola.21628.
43. Hou, L., Adhikari, S., Tian, Y., Scheblykin, I. G., & Orrit, M. (2017). Absorption and Quantum Yield of Single Conjugated Polymer Poly[2-methoxy-5-(2-ethylhexyloxy)-1,4-phenylenevinylene] (MEH-PPV) Molecules. *Nano Letters*, *17*(3), 1575–1581. https://doi.org/10.1021/acs.nanolett.6b04726.

44. Kuehne, A. J. C., Gather, M. C., & Sprakel, J. (2012). Monodisperse conjugated polymer particles by Suzuki–Miyaura dispersion polymerization. *Nature Communications*, *3*(1), 1088. https://doi.org/10.1038/ncomms2085.
45. Kim, J., Rémond, M., Kim, D., Jang, H., & Kim, E. (2020). Electrochromic Conjugated Polymers for Multifunctional Smart Windows with Integrative Functionalities. *Advanced Materials Technologies*, *5*(6). https://doi.org/10.1002/admt.201900890.
46. Beverina, L., Pagani, G. A., & Sassi, M. (2014). Multichromophoric electrochromic polymers: colour tuning of conjugated polymers through the side chain functionalization approach. *Chem. Commun.*, *50*(41), 5413–5430. https://doi.org/10.1039/C4CC00163J.
47. Watanabe, A., Mori, K., Iwasaki, Y., Nakamura, Y., & Niizuma, S. (1987). Electrochromism of polyaniline film prepared by electrochemical polymerization. *Macromolecules*, *20*(8), 1793–1796. https://doi.org/10.1021/ma00174a015.
48. Qin, T., Deng, L., Zhang, P., Tang, M., Li, C., Xie, H., Huang, S., & Gao, X. (2022). Enhancement of Electrochromic Properties of Polyaniline Induced by Copper Ions. *Nanoscale Research Letters*, *17*(1), 51. https://doi.org/10.1186/s11671-022-03689-1.
49. Nie, G., Zhou, L., & Yang, H. (2011). Electrosynthesis of a new polyindole derivative obtained from 5-formylindole and its electrochromic properties. *Journal of Materials Chemistry*, *21*(36), 13873. https://doi.org/10.1039/c1jm11723h.
50. Girotto, E. M., & Paoli, M.-A. de. (1998). Polypyrrole color modulation and electrochromic contrast enhancement by doping with a dye. *Advanced Materials*, *10*(10), 790–793. https://doi.org/10.1002/(SICI)1521-4095(199807)10:10<790::AID-ADMA790>3.0.CO;2-R.
51. Huang, W.-S., Humphrey, B. D., & MacDiarmid, A. G. (1986). Polyaniline, a novel conducting polymer. Morphology and chemistry of its oxidation and reduction in aqueous electrolytes. *Journal of the Chemical Society, Faraday Transactions 1: Physical Chemistry in Condensed Phases*, *82*(8), 2385. https://doi.org/10.1039/f19868202385.
52. Song, E., & Choi, J.-W. (2013). Conducting Polyaniline Nanowire and Its Applications in Chemiresistive Sensing. *Nanomaterials*, *3*(3), 498–523. https://doi.org/10.3390/nano3030498.
53. Nie, X., Xiao, T., & Liu, Z. (2019). A redox-generated biomimetic membrane potential across polypyrrole films. *Chemical Communications*, *55*(67), 10023–10026. https://doi.org/10.1039/C9CC04021H.
54. Qu, K., Fang, M., Zhang, S., Liu, H., & Zeng, X. (2018). A Redox Conjugated Polymer-Based All-Solid-State Reference Electrode. *Polymers*, *10*(11), 1191. https://doi.org/10.3390/polym10111191.
55. Vacca, A., Mascia, M., Rizzardini, S., Corgiolu, S., Palmas, S., Demelas, M., Bonfiglio, A., & Ricci, P. C. (2015). Preparation and characterisation of transparent and flexible PEDOT:PSS/PANI electrodes by ink-jet printing and electropolymerisation. *RSC Advances*, *5*(97), 79600–79606. https://doi.org/10.1039/C5RA15295J.
56. Li, X.-G., Huang, M.-R., Duan, W., & Yang, Y.-L. (2002). Novel Multifunctional Polymers from Aromatic Diamines by Oxidative Polymerizations. *Chemical Reviews*, *102*(9), 2925–3030. https://doi.org/10.1021/cr010423z.
57. Abu-Thabit, N. Y. (2016). Chemical Oxidative Polymerization of Polyaniline: A Practical Approach for Preparation of Smart Conductive Textiles. *Journal of Chemical Education*, *93*(9), 1606–1611. https://doi.org/10.1021/acs.jchemed.6b00060.
58. Tang, S.-J., Wang, A.-T., Lin, S.-Y., Huang, K.-Y., Yang, C.-C., Yeh, J.-M., & Chiu, K.-C. (2011). Polymerization of aniline under various concentrations of APS and HCl. *Polymer Journal*, *43*(8), 667–675. https://doi.org/10.1038/pj.2011.43.
59. Yussuf, A., Al-Saleh, M., Al-Enezi, S., & Abraham, G. (2018). Synthesis and Characterization of Conductive Polypyrrole: The Influence of the Oxidants and Monomer on the Electrical, Thermal, and Morphological Properties. *International Journal of Polymer Science*, *2018*, 1–8. https://doi.org/10.1155/2018/4191747.
60. Durgaryan, A. A., Arakelyan, R. A., & Durgaryan, N. A. (2014). Oxidative polymerization of p-phenylenediamine. *Russian Journal of General Chemistry*, *84*(6), 1095–1100. https://doi.org/10.1134/S1070363214060073.

61. Billaud, D., Maarouf, E. B., & Hannecart, E. (1995). Chemical oxidation and polymerization of indole. *Synthetic Metals*, *69*(1–3), 571–572. https://doi.org/10.1016/0379-6779(94)02573-H.
62. Ghafourisaleh, S., Popov, G., Leskelä, M., Putkonen, M., & Ritala, M. (2021). Oxidative MLD of Conductive PEDOT Thin Films with EDOT and $ReCl_5$ as Precursors. *ACS Omega*, *6*(27), 17545–17554. https://doi.org/10.1021/acsomega.1c02029.
63. Siove, A., & Adès, D. (2004). Synthesis by oxidative polymerization with FeCl3 of a fully aromatic twisted poly(3,6-carbazole) with a blue-violet luminescence. *Polymer*, *45*(12), 4045–4049. https://doi.org/10.1016/j.polymer.2004.03.048.
64. Liu, J., Baek, J.-B., & Dai, L. (2014). Conjugated Polymer Synthesis. In *Encyclopedia of Polymeric Nanomaterials* (pp. 1–7). Springer Berlin Heidelberg. https://doi.org/10.1007/978-3-642-36199-9_273-1.
65. Kaneda, C., Sueyasu, Y., Tanaka, E., & Atobe, M. (2020). Electrochemical synthesis of microporous polyaniline films using foam templates prepared by ultrasonication. *Ultrasonics Sonochemistry*, *64*, 104991. https://doi.org/10.1016/j.ultsonch.2020.104991.
66. Gvozdenovic, M., Jugovic, B., Stevanovic, J., & Grgur, B. (2014). Electrochemical synthesis of electroconducting polymers. *Hemijska Industrija*, *68*(6), 673–684. https://doi.org/10.2298/HEMIND131122008G.
67. Wei, Y., Chan, C. C., Tian, J., Jang, G. W., & Hsueh, K. F. (1991). Electrochemical polymerization of thiophenes in the presence of bithiophene or terthiophene: kinetics and mechanism of the polymerization. *Chemistry of Materials*, *3*(5), 888–897. https://doi.org/10.1021/cm00017a026.
68. Wan, X., Yan, F., Jin, S., Liu, X., & Xue, G. (1999). Low Potential Electrochemical Synthesis of Polyfuran and Characterization of the Obtained Free-Standing Film. *Chemistry of Materials*, *11*(9), 2400–2407. https://doi.org/10.1021/cm9900453.
69. Kobayashi, K., Yang, T. X., Maruyama, K., Shimomura, M., & Miyauchi, S. (1995). Electrochemical polymerization of poly(para-phenylene) and its electrical properties. *Synthetic Metals*, *69*(1–3), 475–476. https://doi.org/10.1016/0379-6779(94)02532-4.
70. Cheng, Y.-J., Yang, S.-H., & Hsu, C.-S. (2009). Synthesis of Conjugated Polymers for Organic Solar Cell Applications. *Chemical Reviews*, *109*(11), 5868–5923. https://doi.org/10.1021/cr900182s.
71. Nojima, M., Saito, R., Ohta, Y., & Yokozawa, T. (2015). Investigation of Mizoroki-Heck coupling polymerization as a catalyst-transfer condensation polymerization for synthesis of poly(*p* -phenylenevinylene). *Journal of Polymer Science Part A: Polymer Chemistry*, *53*(4), 543–551. https://doi.org/10.1002/pola.27472.
72. Liu, B., Yu, W.-L., Lai, Y.-H., & Huang, W. (2003). Synthesis of polyfluorene derivatives through polymer reaction. *Optical Materials*, *21*(1–3), 125–133. https://doi.org/10.1016/S0925-3467(02)00124-6.
73. Li, G., Qin, L., Yao, C., & Xu, Y. (2017). Controlled synthesis of conjugated polycarbazole polymers via structure tuning for gas storage and separation applications. *Scientific Reports*, *7*(1), 15394. https://doi.org/10.1038/s41598-017-10372-4.
74. Tierney, S., Heeney, M., & McCulloch, I. (2005). Microwave-assisted synthesis of polythiophenes via the Stille coupling. *Synthetic Metals*, *148*(2), 195–198. https://doi.org/10.1016/j.synthmet.2004.09.015.
75. Waware, U. S., Hamouda, A. M. S., & Majumdar, D. (2020). Synthesis, characterization and physicochemical studies of copolymers of aniline and 3-nitroaniline. *Polymer Bulletin*, *77*(9), 4469–4488. https://doi.org/10.1007/s00289-019-02957-y.
76. Al-Deyab, S. S., Al-Hazmi, A. M., & El-Newehy, M. H. (2010). Synthesis and Characterization of Organotin Containing Copolymers: Reactivity Ratio Studies. *Molecules*, *15*(3), 1784–1797. https://doi.org/10.3390/molecules15031784.
77. Fineman, M., & Ross, S. D. (1950). Linear method for determining monomer reactivity ratios in copolymerization. *Journal of Polymer Science*, *5*(2), 259–262. https://doi.org/10.1002/pol.1950.120050210.
78. Erol, I., Sen, O., Dedelioglu, A., & Cifci, C. (2009). Synthesis and characterization of novel fluorine-containing methacrylate copolymers: Reactivity ratios, thermal properties, and

antimicrobial activity. *Journal of Applied Polymer Science*, *114*(6), 3351–3359. https://doi.org/10.1002/app.30835.
79. Almtiri, M., Dowell, T. J., Giri, H., Wipf, D. O., & Scott, C. N. (2022). Electrochemically Stable Carbazole-Derived Polyaniline for Pseudocapacitors. *ACS Applied Polymer Materials*, *4*(5), 3088–3097. https://doi.org/10.1021/acsapm.1c01616.
80. Xu, X., Chen, H., Cai, X. R., Li, Y., & Jiang, Q. (2007). Synthesis and properties of polyfluorene copolymers bearing thiophene and porphyrin. *Chinese Chemical Letters*, *18*(7), 879–882. https://doi.org/10.1016/j.cclet.2007.05.040.
81. Gidron, O., Varsano, N., Shimon, L. J. W., Leitus, G., & Bendikov, M. (2013). Study of a bifuran vs. bithiophene unit for the rational design of π-conjugated systems. What have we learned? *Chemical Communications*, *49*(56), 6256. https://doi.org/10.1039/c3cc41795f.
82. Hosseini, S. H., & Entezami, A. A. (2001). Chemical and electrochemical synthesis of homopolymer and copolymers of 3-methoxyethoxythiophene with aniline, thiophene and pyrrole for studies of their gas and vapour sensing. *Polymers for Advanced Technologies*, *12*(9), 524–534. https://doi.org/10.1002/pat.122.
83. Domínguez-Aragón, A., Olmedo-Martínez, J. A., & Zaragoza-Contreras, E. A. (2018). Colorimetric sensor based on a poly(ortho-phenylenediamine-co-aniline) copolymer for the monitoring of tilapia (Orechromis niloticus) freshness. *Sensors and Actuators B: Chemical*, *259*, 170–176. https://doi.org/10.1016/j.snb.2017.12.020.
84. Wang, T., Zhang, N., Bai, W., & Bao, Y. (2020). Fluorescent chemosensors based on conjugated polymers with N-heterocyclic moieties: two decades of progress. *Polymer Chemistry*, *11*(18), 3095–3114. https://doi.org/10.1039/D0PY00336K.
85. Zhou, Q., & Swager, T. M. (1995). Method for enhancing the sensitivity of fluorescent chemosensors: energy migration in conjugated polymers. *Journal of the American Chemical Society*, *117*(26), 7017–7018. https://doi.org/10.1021/ja00131a031.
86. Thomas, S. W., Joly, G. D., & Swager, T. M. (2007). Chemical Sensors Based on Amplifying Fluorescent Conjugated Polymers. *Chemical Reviews*, *107*(4), 1339–1386. https://doi.org/10.1021/cr0501339.
87. Pak, Y. L., Wang, Y., & Xu, Q. (2021). Conjugated polymer based fluorescent probes for metal ions. *Coordination Chemistry Reviews*, *433*, 213745. https://doi.org/10.1016/j.ccr.2020.213745.
88. Sakai, R. (2016). Conjugated polymers applicable to colorimetric and fluorescent anion detection. *Polymer Journal*, *48*(1), 59–65. https://doi.org/10.1038/pj.2015.72.
89. Lee, K., Povlich, L. K., & Kim, J. (2010). Recent advances in fluorescent and colorimetric conjugated polymer-based biosensors. *The Analyst*, *135*(9), 2179. https://doi.org/10.1039/c0an00239a.
90. Si, Y., Wang, X., Li, Y., Chen, K., Wang, J., Yu, J., Wang, H., & Ding, B. (2014). Optimized colorimetric sensor strip for mercury(II) assay using hierarchical nanostructured conjugated polymers. *J. Mater. Chem. A*, *2*(3), 645–652. https://doi.org/10.1039/C3TA13867D.
91. Chen, X., Zhao, Q., Zou, W., Qu, Q., & Wang, F. (2017). A colorimetric Fe^{3+} sensor based on an anionic poly(3,4-propylenedioxythiophene) derivative. *Sensors and Actuators B: Chemical*, *244*, 891–896. https://doi.org/10.1016/j.snb.2017.01.027
92. Rahman, Md., Kumar, P., Park, D.-S., & Shim, Y.-B. (2008). Electrochemical Sensors Based on Organic Conjugated Polymers. *Sensors*, *8*(1), 118–141. https://doi.org/10.3390/s8010118.
93. Maksymiuk, K. (2006). Chemical Reactivity of Polypyrrole and Its Relevance to Polypyrrole Based Electrochemical Sensors. *Electroanalysis*, *18*(16), 1537–1551. https://doi.org/10.1002/elan.200603573.
94. AL-Refai, H. H., Ganash, A. A., & Hussein, M. A. (2021). Polythiophene and its derivatives –Based nanocomposites in electrochemical sensing: A mini review. *Materials Today Communications*, *26*, 101935. https://doi.org/10.1016/j.mtcomm.2020.101935.
95. Shoaie, N., Daneshpour, M., Azimzadeh, M., Mahshid, S., Khoshfetrat, S. M., Jahanpeyma, F., Gholaminejad, A., Omidfar, K., & Foruzandeh, M. (2019). Electrochemical sensors and

biosensors based on the use of polyaniline and its nanocomposites: a review on recent advances. *Microchimica Acta*, *186*(7), 465. https://doi.org/10.1007/s00604-019-3588-1.

96. Sharma, S., Joshi, P., Mehtab, S., Zaidi, Md. G. H., Singhal, K., & Siddiqi, T. I. (2020). Development of Non-enzymatic Cholesterol Electrochemical Sensor Based on Polyindole/Tungsten Carbide Nanocomposite. *Journal of Analysis and Testing*, *4*(1), 13–22. https://doi.org/10.1007/s41664-020-00117-0.
97. Lin, H., Bai, H., Yang, Z., Shen, Q., Li, M., Huang, Y., Lv, F., & Wang, S. (2022). Conjugated polymers for biomedical applications. *Chemical Communications*, *58*(52), 7232–7244. https://doi.org/10.1039/D2CC02177C.
98. Hao, Y.-J., & Zhu, G.-M. (2020). Advances in Fabrication of Polydiacetylene Vesicles and Their Applications in Medical Detection. *Chinese Journal of Analytical Chemistry*, *48*(2), 164–173. https://doi.org/10.1016/S1872-2040(19)61213-2.
99. Zhu, C., Liu, L., Yang, Q., Lv, F., & Wang, S. (2012). Water-Soluble Conjugated Polymers for Imaging, Diagnosis, and Therapy. *Chemical Reviews*, *112*(8), 4687–4735. https://doi.org/10.1021/cr200263w.
100. Wang, Y., Zhang, H., Wang, Z., & Feng, L. (2020). Photothermal Conjugated Polymers and Their Biological Applications in Imaging and Therapy. *ACS Applied Polymer Materials*, *2*(10), 4222–4240. https://doi.org/10.1021/acsapm.0c00672
101. Eftekhari, A., Li, L., & Yang, Y. (2017). Polyaniline supercapacitors. *Journal of Power Sources*, *347*, 86–107. https://doi.org/10.1016/j.jpowsour.2017.02.054.
102. Holze, R. (2022). Conjugated Molecules and Polymers in Secondary Batteries: A Perspective. *Molecules*, *27*(2), 546. https://doi.org/10.3390/molecules27020546.
103. Facchetti, A. (2011). π-Conjugated Polymers for Organic Electronics and Photovoltaic Cell Applications. *Chemistry of Materials*, *23*(3), 733–758. https://doi.org/10.1021/cm102419z.
104. Wanekaya, A. K., Bangar, M. A., Yun, M., Chen, W., Myung, N. v., & Mulchandani, A. (2007). Field-Effect Transistors Based on Single Nanowires of Conducting Polymers. *The Journal of Physical Chemistry C*, *111*(13), 5218–5221. https://doi.org/10.1021/jp067213g.
105. Lee, S.-Y., Choi, G.-R., Lim, H., Lee, K.-M., & Lee, S.-K. (2009). Electronic transport characteristics of electrolyte-gated conducting polyaniline nanowire field-effect transistors. *Applied Physics Letters*, *95*(1). https://doi.org/10.1063/1.3176444.
106. Chen, L., Hong, Z., Li, G., & Yang, Y. (2009). Recent Progress in Polymer Solar Cells: Manipulation of Polymer:Fullerene Morphology and the Formation of Efficient Inverted Polymer Solar Cells. *Advanced Materials*, *21*(14–15), 1434–1449. https://doi.org/10.1002/adma.200802854.
107. Wang, L., Liu, Y., Jiang, X., Qin, D., & Cao, Y. (2007). Enhancement of Photovoltaic Characteristics Using a Suitable Solvent in Hybrid Polymer/Multiarmed CdS Nanorods Solar Cells. *The Journal of Physical Chemistry C*, *111*(26), 9538–9542. https://doi.org/10.1021/jp0715777.
108. Yahiaoui, I., Khennous, E., & Khenata, R. (2016). *Electronic and optical properties of polymer MEH-PPV and their applications in hybrid optoelectronic devices*. 85–88. https://doi.org/10.21741/9781945291197-21.
109. Park, J. (2017). Visible and near infrared light active photocatalysis based on conjugated polymers. *Journal of Industrial and Engineering Chemistry*, *51*, 27–43. https://doi.org/10.1016/j.jiec.2017.03.022.
110. Muktha, B., Madras, G., Guru Row, T. N., Scherf, U., & Patil, S. (2007). Conjugated Polymers for Photocatalysis. *The Journal of Physical Chemistry B*, *111*(28), 7994–7998. https://doi.org/10.1021/jp071096n.
111. de Riccardis, M. F. (2015). Anticorrosion Coatings Based on Conjugated Polymers. In *Fundamentals of Conjugated Polymer Blends, Copolymers and Composites* (pp. 519–579). Wiley. https://doi.org/10.1002/9781119137160.ch10.
112. Mirmohseni, A., & Oladegaragoze, A. (2000). Anti-corrosive properties of polyaniline coating on iron. *Synthetic Metals*, *114*(2), 105–108. https://doi.org/10.1016/S0379-6779(99)00298-2.

113. Zadeh, M. K., Yeganeh, M., Shoushtari, M. T., & Esmaeilkhanian, A. (2021). Corrosion performance of polypyrrole-coated metals: A review of perspectives and recent advances. *Synthetic Metals*, *274*, 116723. https://doi.org/10.1016/j.synthmet.2021.116723.
114. de Leon, A. C. C., Pernites, R. B., & Advincula, R. C. (2012). Superhydrophobic Colloidally Textured Polythiophene Film as Superior Anticorrosion Coating. *ACS Applied Materials & Interfaces*, *4*(6), 3169–3176. https://doi.org/10.1021/am300513e.
115. Nayak, S. R., Mohana, K. N. S., Hegde, M. B., Rajitha, K., Madhusudhana, A. M., & Naik, S. R. (2021). Functionalized multi-walled carbon nanotube/polyindole incorporated epoxy: An effective anticorrosion coating material for mild steel. *Journal of Alloys and Compounds*, *856*, 158057. https://doi.org/10.1016/j.jallcom.2020.158057.
116. Kohl, M., & Kalendová, A. (2015). Anticorrosion properties of organic coatings containing polyphenylenediamine phosphate. *Advances in Science and Technology Research Journal*, *9*(28), 47–50. https://doi.org/10.12913/22998624/60782.
117. Zheng, H., Liu, W., He, S., Wang, R., Zhu, J., Guo, X., Liu, N., Guo, R., & Mo, Z. (2022). A superhydrophobic polyphenylene sulfide composite coating with anticorrosion and self-cleaning properties for metal protection. *Colloids and Surfaces A: Physicochemical and Engineering Aspects*, *648*, 129152. https://doi.org/10.1016/j.colsurfa.2022.129152.
118. Liu, C., Steppert, A., Liu, Y., Weis, P., Hu, J., Nie, C., Xu, W., Kuehne, A. J. C., & Wu, S. (2023). A Photopatternable Conjugated Polymer with Thermal-Annealing-Promoted Interchain Stacking for Highly Stable Anticounterfeiting Materials. *Advanced Materials*, *35*(36). https://doi.org/10.1002/adma.202303120.
119. Duan, H., Zhang, J., Weng, Y., Fan, Z., & Fan, L.-J. (2022). Dynamic Fluorescent Anticounterfeiting Labels Based on Conjugated Polymers Confined in Submicron Fibrous Membranes. *ACS Applied Materials & Interfaces*, *14*(28), 32510–32521. https://doi.org/10.1021/acsami.2c06965.
120. Marcasuzaa, P., Reynaud, S., Ehrenfeld, F., Khoukh, A., & Desbrieres, J. (2010). Chitosan- *graft* -Polyaniline-Based Hydrogels: Elaboration and Properties. *Biomacromolecules*, *11*(6), 1684–1691. https://doi.org/10.1021/bm100379z.
121. Farrokhzad, H., van Gerven, T., & van der Bruggen, B. (2013). Preparation and characterization of a conductive polyaniline/polysulfone film and evaluation of the effect of co-solvent. *European Polymer Journal*, *49*(10), 3234–3243. https://doi.org/10.1016/j.eurpolymj.2013.06.027.
122. Chang, C.-F., Chen, W.-C., Wen, T.-C., & Gopalan, A. (2002). Electrochemical and Spectroelectrochemical Studies on Copolymerization of Diphenylamine with 2,5-Diaminobenzenesulfonic Acid. *Journal of The Electrochemical Society*, *149*(8), E298. https://doi.org/10.1149/1.1491984.
123. Wen, T.-C., Chen, J.-B., & Gopalan, A. (2002). Soluble and methane sulfonic acid doped poly(diphenylamine)—synthesis and characterization. *Materials Letters*, *57*(2), 280–290. https://doi.org/10.1016/S0167-577X(02)00779-6.
124. Obrezkov, F. A., Shestakov, A. F., Vasil'ev, S. G., Stevenson, K. J., & Troshin, P. A. (2021). Polydiphenylamine as a promising high-energy cathode material for dual-ion batteries. *Journal of Materials Chemistry A*, *9*(5), 2864–2871. https://doi.org/10.1039/D0TA09427G.
125. Ozkan, S. Zh., Eremeev, I. S., Karpacheva, G. P., Prudskova, T. N., Veselova, E. v., Bondarenko, G. N., & Shandryuk, G. A. (2013). Polymers of diphenylamine-2-carboxylic acid: Synthesis, structure, and properties. *Polymer Science Series B*, *55*(3–4), 107–115. https://doi.org/10.1134/S1560090413030032.
126. Ozkan, S. Zh., Bondarenko, G. N., & Karpacheva, G. P. (2010). Oxidative polymerization of diphenylamine-2-carboxylic acid: Synthesis, structure, and properties of polymers. *Polymer Science Series B*, *52*(5–6), 263–269. https://doi.org/10.1134/S1560090410050015.
127. Abalyaeva, V. v., Dremova, N. N., Kabachkov, E. N., Efimov, O. N., Baskakova, Yu. v., & Karpacheva, G. P. (2021). Electrochemical Polymerization of Diphenylamine-2-

Carboxylic Acid on Glassy Carbon and Activated Graphite Foil. *Polymer Science, Series B*, *63*(4), 392–403. https://doi.org/10.1134/S1560090421040011.

128. Cotarelo, M. A., Huerta, F., Mallavia, R., Morallón, E., & Vázquez, J. L. (2006). On the polymerization of 2-aminodiphenylamine. *Synthetic Metals*, *156*(1), 51–57. https://doi.org/10.1016/j.synthmet.2005.10.007

129. Ojani, R., Raoof, J.-B., & Ahmady-Khanghah, Y. (2011). Copper-poly(2-aminodiphenylamine) as a novel and low cost electrocatalyst for electrocatalytic oxidation of methanol in alkaline solution. *Electrochimica Acta*, *56*(9), 3380–3386. https://doi.org/10.1016/j.electacta.2010.12.082.

CHAPTER 2

Synthesis, Characterization and Analytical Sensing of Redox and Conjugated Poly-N-phenyl anthranilic acid

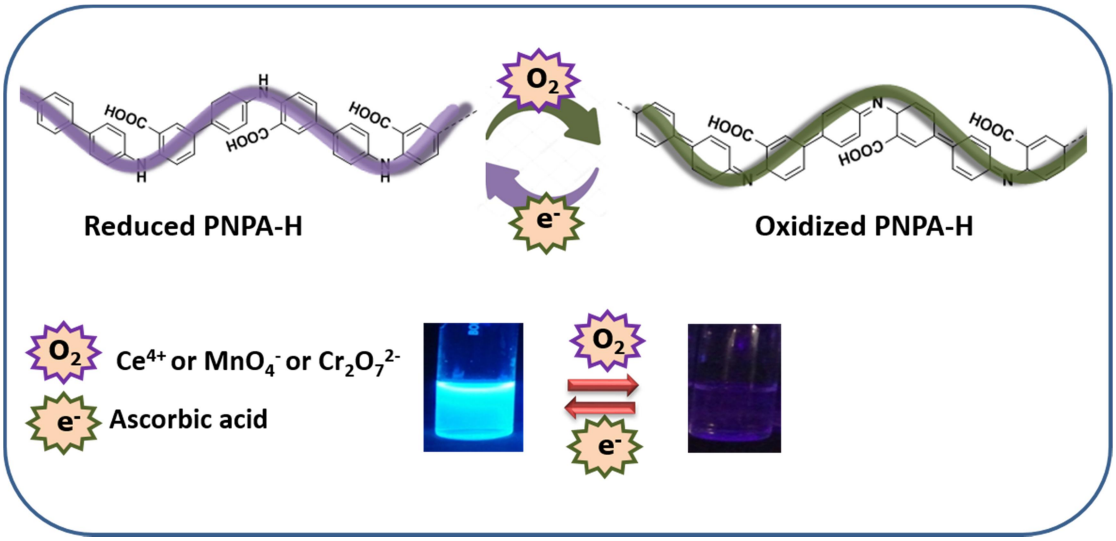

2.1. Introduction

Fluorescent molecules have gathered great attention in the past few decades, mainly due to their various applications in chemical and biochemical sensing, cell imaging, drug delivery, light-emitting diodes, medical diagnostics, and fluorescence technologies [1-4]. Fluorescence is described as a light emission phenomenon resulting from UV or visible light absorption. Sir Fredrick William Herschel et al. reported the fluorescence from quinine solution in 1845 [5]. Some materials have inherent fluorescence in their natural form, like chlorophyll, vitamin A, fluorite, calcite minerals, and gemstones like rubies and emeralds. Most organic materials were made fluorescent by chemical preparation/treatment [6-8]. Fluorescence emission is highly dependent on the environment of fluorophores, so they are highly sensitive to various physical and chemical conditions like pH, pressure, temperature, electrochemical potential, hydrogen bonding, and the presence of specific molecules [9-11].

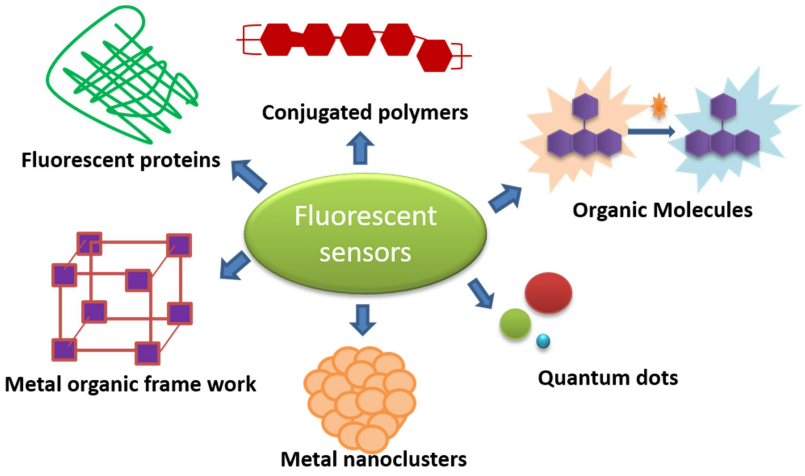

Figure 2.1. *Schematic representation of different types of fluorescent materials available as sensors.*

Fluorescent materials like inorganic quantum dots, metal nanoclusters, proteins, carbon quantum dots, dye-modified silica nanoparticles, conjugated polymers, and metal-organic frameworks have been effectively utilized for the development of fluorescent sensors due to their high sensitivity (see **Figure 2.1.**)[12-16]. Due to their high demand in these fields, an enormous amount of work was dedicated to these fluorescent nanomaterials [9, 10]. The response or mode for analyte sensing in fluorescence-based sensors involves fluorescence turn-on (enhancement), fluorescence turn-off (quenching)

and shift in fluorescence emission wavelength. Fluorescence sensing may involve any one of the mechanisms like foster resonance energy transfer (FRET), intramolecular charge transfer (ICT), photoinduced electron transfer (PET), and aggregation-induced emission (AIE) [17, 18] (see **Figure 2.2.**). Fluorescence turn-off can be either due to static or dynamic quenching or a combination of static and dynamic quenching mechanisms. Mechanistic approaches of analyte sensing are relevant for further development of fluorescent sensors. The limitations like water insolubility of fluorescent organic molecules, heavy metal toxicity of quantum dots, weak signal due to external interferences in fluorescent metal-organic frameworks (MOF), low selectivity and low photoluminescent efficiencies were some of the significant obstacles in the development of fluorescence-based sensors [19-21].

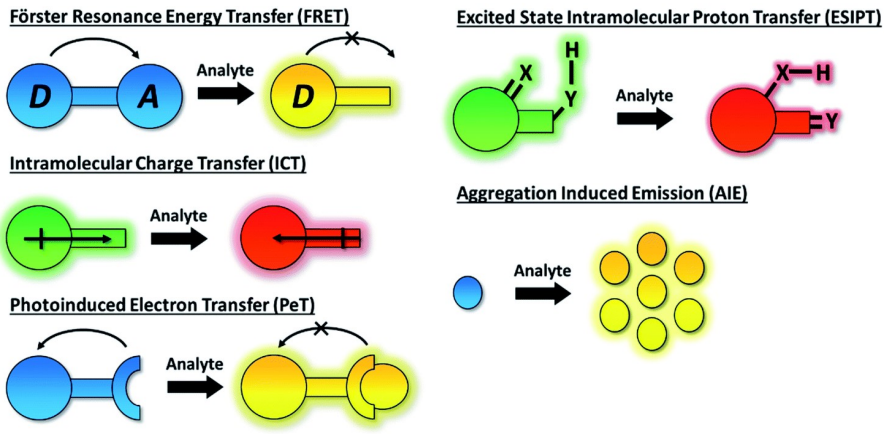

Figure 2.2. *Schematic representation of possible mechanisms in fluorescent sensors. (Adapted from Tian et al. 2021).*

The fluorescent conjugated polymers possess advantages over small fluorescent molecules in mechanical/thermal stability and resistance to colour or fluorescence bleaching due to many repeated monomer units [22]. Synthetic strategies of fluorescent conjugated polymers include the polymerization of fluorescent monomers or non-fluorescent monomers via metal-catalyzed polymerization reactions, oxidative chemical polymerization reactions and electrochemical polymerization reactions or the use of fluorescent initiator or chain transfer agents [23-25]. The introduction of fluorophores as side chains into the polymer backbone was also reported for the development of fluorescent conjugated polymers [26].

Fluorescent-conjugated polymers function as a signal-amplified smart material due to the perfect combination of fluorescence and other characteristic properties.

Therefore, they have been employed to develop bio-sensors, chemo-sensors, environmental sensors, optoelectronic devices and solar energy systems [27]. Sensors based on fluorescent conjugated polymers have great potential due to their high detection sensitivity, high selectivity, quick response and real-time detection. The fluorescence of particular conjugated polymers may depend on the synthesis method, reaction conditions, and surrounding environment. The changes in the electronic energy levels or electron transport associated with the interaction between fluorescent conjugated polymer and analyte could also affect the fluorescence. [28] The modes of sensing actions available in conjugated fluorescent polymers were fluorescent turn-off via quenching of fluorescence and fluorescence turn-on via suppression of fluorescence quenching and fluorescence colour change in the presence of analyte molecules, which are similar to the other fluorescent systems (see **Figure 2.3.**). Mechanisms like photo electron transfer (PET), intramolecular charge transfers (ICT) and electronic energy transfer have been reported for the development of efficient conjugated polymer-based fluorescence sensors [29].

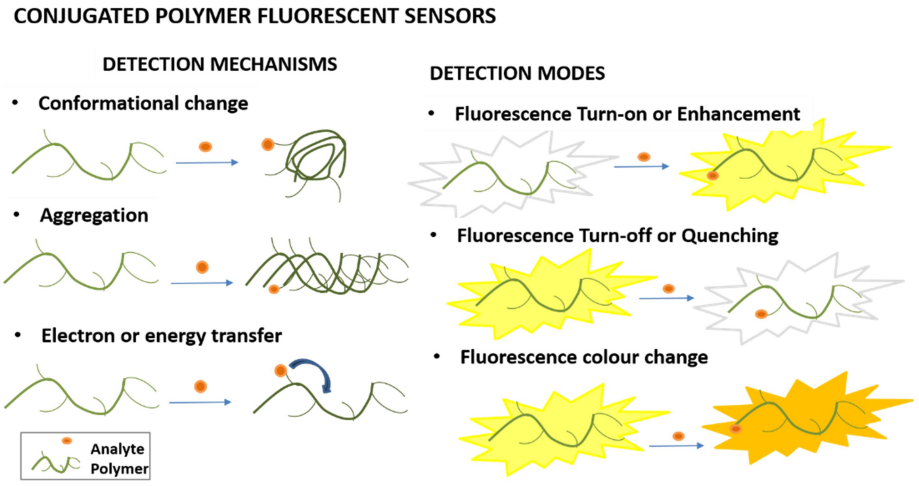

Figure 2.3. *Mechanisms and detection modes involved in fluorescent conjugated polymer-based sensor.*

The first fluorescent conjugated polymer sensor was developed by Zhuo et al. using poly para-phenylenethylenes for the detection of paraquat (methyl viologen) by introducing the concept of enhanced sensitivity through amplified fluorescence in conjugated polymers [30]. Various fluorescent conjugated polymers have been used to develop fluorescent turn-off sensors of different analytes with low limit of detection (LOD). Yu et al. used pyrazole and benzothiadiazole-based conjugated porous polymers

for the sensing of amines with turn-off behavior (see **Figure 2.4.A**) [12]. Hu et al. developed a fluorescent turn-off sensor of uranyl ion ($UO2^{2+}$) based on amidoxime groups and polyfluorenes (see **Figure 2.4.B**) [32]. Reversible fluorescence sensors have received more attention due to their enhanced selectivity and multiple analyte detection ability. The conjugated polymers like polyfluorenes, polythiophenes, and poly phenyleneethynylenes, which have intrinsic fluorescence emission, were used to develop reversible fluorescence sensors for multi-analyte detections (see **Table 2.1** and **Figure 2.5**).

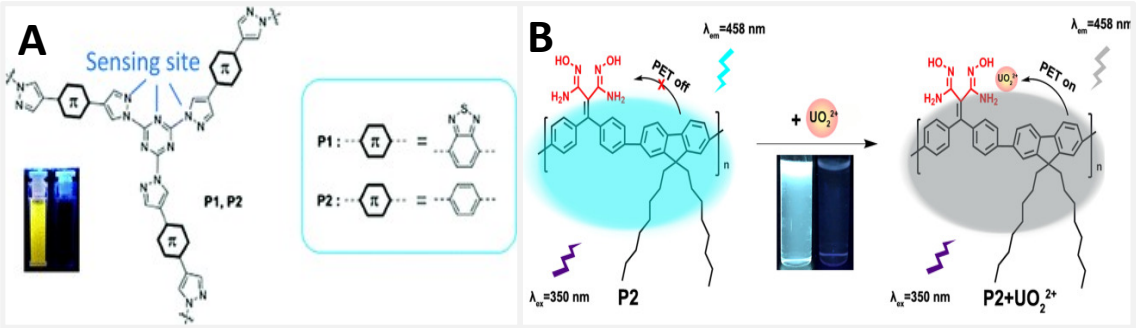

Figure 2.4. *Conjugated polymer-based fluorescent turn-off sensors for the detection of analytes. A) pyrazole and benzothiadiazole-based conjugated porous polymers for sensing amines (Adapted from Yu et al. 2020). B) Polyfluorenes and amidoxime groups containing fluorescent polymer for the sensing of uranyl ion (UO_2^{2+})(Adapted from Hu et al. 2021).*

Table 2.1. *Conjugated polymer-based reversible fluorescent sensors for detecting analytes, the limit of detection, mechanism and sensing mode reported in the literature.*

Sl. No.	Fluorescent conjugated polymer	Analyte	LOD	Mechanism	Mode of sensing	Ref
1	Polyfluorene bearing sulfate functional group	Cu^{2+} & CN^-	2.5 & 6 µM	-	Reversible Turn-off with Cu^{2+} and turn-on with CN^-	33
2	Poly phenylene vinylene with sulfonated side chain	Methyl viologen & Avidin	10^{-9} M & 1.2×10^{-8} M	Aggregation	Reversible turn-off with methyl viologen & turn-on with avidine	34
3	Polyfluorene with sulfonated side	Ascorbic acid	50 nM	Scavenging mechanism	Reversible turn-off with cationic	35

	chain				nitroxide radical and turn-on with ascorbic acid.	
4	Polyquinolines	Ag^{+}	-	Inter-polymer aggregation	Reversible turn-off with Ag^{+} and turn-on with aqueous ammonia.	36
5	Polythiophene contain thymine moiety	Hg^{2+}	30 µM	Inter-polymer aggregation	Reversible turn-off with Hg^{2+} and turn-on with Cl^{-}.	37
6	Polyfluorene derivative with aldehyde and trifluoroacetyl units	Aromatic amines	0.52 ppb	Photoinduced electron transfer	Reversible turn-off with aromatic amines and turn-on with primary aliphatic amines	38
7	2-Methyl-acrylic acid 10-(4-{2-[2,5-dimethyloxy-4-(2-pyridine-4-yl-vinyl)-phenyl]-vinyl}-phenoxy)-decyl ester	Cu^{2+}	-	Static quenching	Reversible turn-off with Cu^{2+} and turn-on with 1,1,4,7,7-pentamethyldiethylenetriamine	39
8	Polyfluorene derivative	Cu^{2+}	5 µM	Electron or energy transfer	Reversible turn-off with Cu^{2+} and turn-on with EDTA	40
9	Polyfluorene derivative	Fe^{3+} & F^{-}	5.3µM, & 6.78 µM	Metal to ligand charge transfer (MLCT)	Reversible turn-off with Fe^{3+} and turn-on with F^{-}	41
10	Poly-phenylene ethynylene	TNT	10 µM	Static quenching	Reversible turn-off with TNT and turn-on with Ethanol/water	42
11	Poly ethylene glycol-salicylidine Schiff base	Al^{3+}	4.05×10^{-9} M	Photoelectron transfer	Redox reversible Turn-off with Al^{3+} and turn-on with EDTA	43

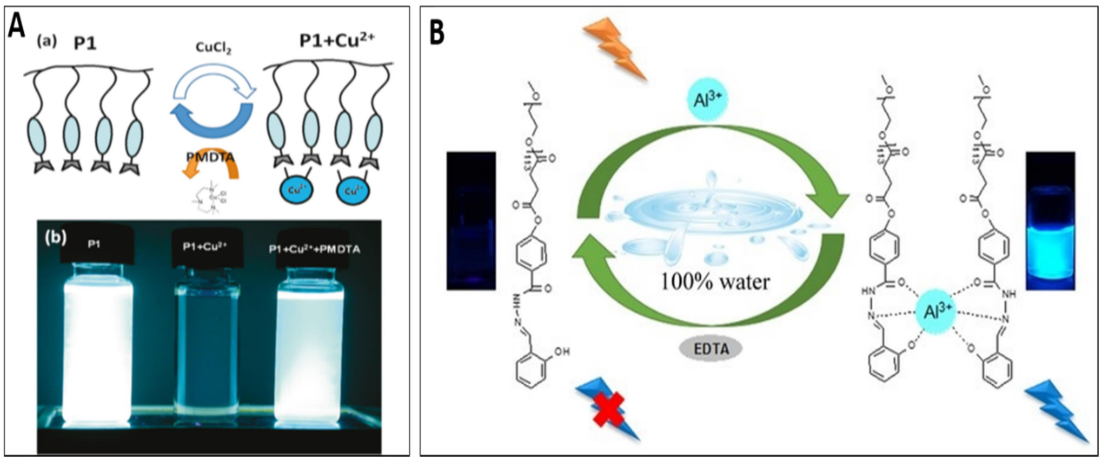

Figure 2.5. *A) Reversible fluorescence turn-off in fluorescent conjugated polymer with* Cu^{2+} *ions and turn-on with PMDTA (Adapted from Chu et al. 2011). B) Reversible fluorescence turn-on in conjugated polymer probe with* Al^{3+} *ions and turn-off with EDTA (Adapted from Bai et al. 2019).*

Redox states of the conjugated polymers were used for sensor applications due to their different optical, electrical, mechanical or chemical properties produced in redox-susceptible conditions. The redox-active fluorescent conjugated polymers were more effective in optical sensors, as the redox reaction with redox analytes can easily switch their fluorescence. Zhao et al. developed a fluorescent turn-off antioxidant sensor based on conjugated polymer dots, in which the reversible surface redox process in polymer with antioxidants was responsible for the fluorescence quenching. [44]. Li et al. developed six luminescent conjugated polymers which showed reversible redox reactions in the presence of Fe^{3+} and H_2O. The reversible colour and fluorescence modulation, resulting from redox reactions, was used for multi-colour and multi-fluorescence printing. [45]

In this chapter, we have developed a fluorescent poly-N-phenyl anthranilic acid (PNPA) polymer with redox properties to sense various oxidizing agents in an aqueous acidic medium. Chemical or biochemical colorimetric sensors working in aqueous media have the added advantage of a non-toxic and universal solvent system for analytical applications. We have synthesized a poly-N-phenyl anthranilic acid (PNPA) homopolymer via chemical oxidative polymerisation using ferric chloride as oxidizing agent in ethanol solvent. The structural characterization of monomer and polymer has been carried out by nuclear magnetic resonance spectroscopy (^{1}H-NMR) and fourier transform infrared spectroscopy (FT-IR). The powder X-ray diffraction studies have revealed intense crystalline peaks corresponding to monomer (NPA) and broad low-intensity peaks corresponding to the amorphous domain of polymer (PNPA).

Thermogravimetric analysis revealed that polymer (PNPA) has more thermal stability than monomer (NPA), especially for higher temperatures. The good solubility of monomer and polymer in sulphuric acid and sodium hydroxide solutions enabled us to study absorption and emission properties in aqueous solutions. Analytes like Ce^{4+}, MnO_4^- and $Cr_2O_7^{2-}$ ions were studied by fluorescence quenching of PNPA with a naked-eye fluorescence detection, UV-visible absorption spectra and spectrofluorometry. The redox reaction between the reduced form of poly-N-phenyl anthranilic acid (PNPA-H) and oxidizing analytes have been contributed for the fluorescence quenching action. The non-fluorescent oxidized PNPA-H was reduced back to fluorescent PNPA-H with reducing biomolecules like ascorbic acid, indicating the system's redox reversibility. In short, we have synthesized and characterized efficient redox-active, fluorescent poly-N-phenyl anthranilic acid conjugated polymer and successfully demonstrated its use in quantitative sensing of analytes via fluorescent quenching.

2.2. Experimental

2.2.1. Materials and Reagents: N-Phenyl anthranilic acid (97%) was purchased from LOBA chemicals and purified by double recrystallization using acetone as solvent. Anhydrous ferric chloride ($FeCl_3$) was purchased from Sigma Aldrich. Ammonium cerium (IV) sulphate dihydrate GR, potassium permanganate, potassium dichromate GR, acetone and concentrated H_2SO_4 (98%) were purchased from Merck Chemicals, India. Double distilled ethanol and deionised water were used to synthesize and purify polymer.

2.2.2. Measurements and Instruments: Proton nuclear magnetic resonance (PNMR) spectra of the samples were recorded using a 400 MHz Bruker Avance III NMR Spectrophotometer in $CDCl_3$ solvent using TMS as an internal standard. The FT-IR spectra of the samples were recorded by Shimadzu FT-IR spectrometer using KBr pellet method. The elemental analysis (CHN) of the samples were recorded by elementar vario EL III. Thermogravimetric analysis (TGA) of the samples was measured by Perkin Elmer, Diamond TG/DTA in an inert atmosphere of nitrogen gas at a heating rate of 10 °C per minute. Powder wide-angle X-ray diffraction of the samples was measured using Anton Paar, TTK 450 diffractometer in the range of 2θ values between 3 to 80°. UV-Visible spectra of the samples were recorded by Shimadzu UV-Visible spectrometer 1800 series in the 200-800 nm range with deionised water. Fluorescence emission of the polymer samples was checked using long wave UV light (λ =365 nm) in a Rotek UV

inspection cabinet of 230 Volts. The polymer-specific viscosity (η_{sp}) was measured using Ostwald's U-tube viscometer by taking ~ 0.25 w/w % of samples in ethanol. Polymer molecular weight determination of the PNPA samples has been carried out using Ultraflextreme MALDI-TOF/TOF from Bruker Daltonics using 2, 5-dihydroxy benzoic acid (DHB) matrix. Cyclic voltammetric studies of polymer were performed using Ivium compactStat electrochemical interface consisting of a three-electrode electrochemical cell in which Ag/AgCl is used as the reference electrode, small platinum wire is used as the counter electrode, and glassy carbon is used as the working electrode. Potentiometric titrations were performed using a digital potentiometer of model DP001. Electrical conductivity of the sample was measured using DFP-RM-200 with constant current source Model CCS-01 and DC microvoltmeter. Fluorescence emission spectra of the samples were recorded in FluoroMax-4. The fluorescence quantum yield (Φ_f) was determined by a relative method by using quinine sulfate (Φ_f = 0.53) as a reference in 0.1M H_2SO_4. The optical density of the solutions was kept below 0.1 absorbance and excited at 366nm. The quantum yield was calculated by using the following equation.

$$Q = Q_R \frac{I}{I_R} \frac{OD_R}{OD} \frac{\eta}{\eta^2_R}$$

Where Q, I, η and O.D represent fluorescence quantum yield, integrated intensity, refractive index of the solvent, absorbance of the solution and subscript 'R' denotes the reference fluorophore.

2.2.3. Synthesis of Poly N-phenyl anthranilic acid (PNPA): The recrystallized monomer N-phenyl anthranilic acid (0.5 g, 2.34 mmol) was dissolved in 15 ml double distilled ethanol. Anhydrous $FeCl_3$ (0.57 g, 3.52 mmol) dissolved in 5 ml ethanol was added to monomer solution dropwise at 30^oC, and the polymerization was allowed to proceed for 2 hours without any disturbance. The blue polymer solution was precipitated into deionised water, filtered, and washed first with water and then many times with a water-acetone mixture until the filtrate became colourless. The dark blue powder was dried in a vacuum oven at 60^oC for 3h. Yield = 0.382 g (76.4 %). ^1H NMR (400 MHz, $CDCl_3$) δ: 7.47 (m, 6H, Ar-H), 6.32 (m, 8H, Ar-H). FT-IR (KBr, cm^{-1}): 3347, 3038, 1601, 1582, 1504, 1451, 1393, 1272, 1153, 753 and 503 cm^{-1}. Element analysis (anal., wt %): C, 63.42; H, 4.27; N, 5.79.

2.2.4. Preparation of PNPA-H solution (1×10^{-5} M): Poly N-phenyl anthranilic acid (9.70 mg, 0.046 mmol) was dissolved in 10 ml of conc. H_2SO_4 (18 M) using a sonicator. A dark blue-colored solution of PNPA-H was obtained. The above prepared PNPA-H solution (0.3 ml) was added to a 100 ml standard flask and then made up to 100 ml using deionised water.

2.2.5. Electrochemical studies: PNPA (9.70 mg, 0.046 mmol) was dissolved in 10 ml of conc. H_2SO_4 (18 M) using a sonicator to obtain 4.6×10^{-3} M PNPA-H solution. The above solution (5.0 mL) was added to a 10 mL standard flask and then made up to 10 mL using deionised water to obtain a 2.3×10^{-3} M PNPA-H solution. Similarly, 2.3×10^{-3} M NPA-H solution was prepared by dissolving 9.79 g NPA in 10 ml of conc. H_2SO_4, followed by the dilution of 5 mL of the above solution to 10 mL using deionised water. The cyclic voltammogram of 2.3×10^{-3} M PNPA-H solution and NPA-H solution was recorded using three electrodes electrochemical cell set up in which PNPA-H and NPA-H solution were used as electrolyte.

2.3. Results and Discussion

2.3.1. Synthesis of Poly-N-phenyl anthranilic acid

Poly-N-phenyl anthranilic acid has been synthesized via oxidative chemical polymerisation of N-phenyl anthranilic acid using anhydrous ferric chloride as oxidizing agent in ethanol solvent (see **Figure 2.6.**). The dark blue polymer powder obtained was soluble in organic solvents like acetone, ether, chloroform and ethanol. Although monomer and polymer were insoluble in water, they are soluble in basic sodium hydroxide (~1 to 5 M) and sulphuric acid medium at moderate and high concentrations (~ 9 to 18 M). Poly-N-phenyl anthranilic acid contains an ionisable carboxylic acid group, which loses its protons at basic pH to become carboxylate anionic side groups. On the other hand, the polymer becomes partially protonated in acidic pH on the secondary amine group contained in the polymer backbone.

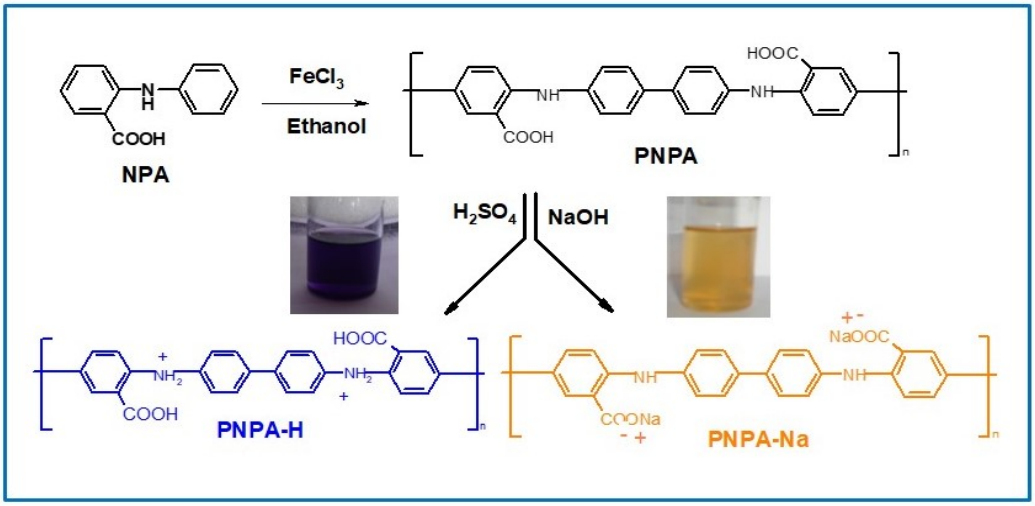

Figure 2.6. *Schematic representation of the synthesis of PNPA using chemical oxidative polymerisation using $FeCl_3$, and the photographs of PNPA in acid and basic media.*

2.3.2. Structural characterization of PNPA

The good solubility of the polymer in basic and acidic solution was due to the electrostatic attractive forces between polymer and solvent that overcome the repulsive forces [46]. The proton NMR spectra of NPA and PNPA were recorded in $CDCl_3$ have shown in **Figure 2.7.** The doublet present at 8.03 - 8.06 ppm was assigned to aromatic proton H_a. The downfield shift of this aromatic proton may be due to the presence of an electron-withdrawing group at its ortho position. The H_c proton and two H_f protons are overlapped and formed as a multiplet with a chemical shift in the range 7.28-7.33 ppm. The multiplet in the range 7.20-7.25 ppm was assigned due to two H_e protons. The H_d proton shows doublet in the range 7.21-7.23 ppm. Both H_b and H_g protons form a triplet due to the coupling of two neighbouring protons in the region 7.11-7.15 ppm and 6.74-6.77 ppm, respectively.[47] The peak at 9.29 ppm of the monomer was assigned to the N-H proton [48]. In the case of polymer, H_1, H_2 and H_3 protons present in substituted benzene have shown multiplet in the region 7.47 - 8.01ppm in addition to solvent peak at 7.26 ppm. The benzenoid protons H_4, H_5 and H_6 also showed multiplet in the region 6.32-6.59 ppm due to the coupling of neighbouring protons and the overlapping of peaks.

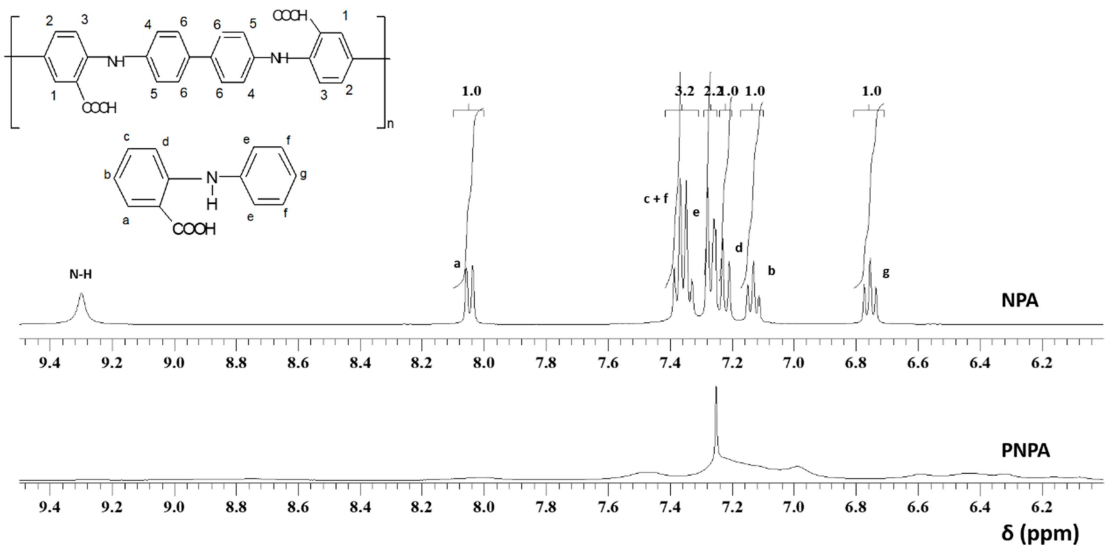

Figure 2.7. *^{1}H NMR spectra of NPA and PNPA in $CDCl_3$.*

The monomer (NPA) and polymer (PNPA) were characterized by FT-IR spectroscopy by making thin pellets of samples with KBr powder (see **Figure 2.8.A**.). The monomer showed characteristic strong peaks at 1665, 1576, 1503, 1438, 1324, 1255 and 1156 cm^{-1} corresponding to C=O stretching, aromatic ring stretching, C=C stretching, carboxylic-OH bending, C-N stretching, C-O stretching and C-H stretching respectively.[47-48] The peaks at 745 and 694 cm^{-1} were due to aromatic C-H out-of-plane bending vibrations, characteristic bands of substituted phenyl rings.[49, 50] The polymer PNPA has also shown characteristic peaks at 1601, 1582, 1504, 1451, 1393, 1272, 1153, 753 and 503 cm^{-1} corresponding to C=O stretching, aromatic ring stretching, C=C stretching, carboxylic-OH bending, C-N stretching, C-O stretching, C-H in-plane bending in benzenoid rings, C-H out of plane bending and N-H out of plane bending respectively.[47, 51-55] The structural difference between monomer and polymer was clearly evident from the C-N stretching, C-O stretching and carboxylic-OH bending which have different peak positions (see **Figure 2.8.A**). The polymer and monomer have shown characteristic peaks of N-H asymmetric stretching and broad O-H stretching of carboxylic acid at 3347 cm^{-1} and 3038 $cm^{-1,}$ respectively. [47, 53] Specific viscosity of monomer and polymer (PNPA) in ethanol solvent was measured using Ostwald's U-tube viscometer, and its value was found to be 0.01 and 0.08 (± 0.005), respectively, at 28°C. The specific viscosity of the polymer indicates the formation of a low molecular weight polymer rather than a very high molecular weight polymer. MALDI-TOF analysis of the PNPA has been carried out using a 2,5-dihydroxy benzoic acid matrix to find the number of repeating units and confirm

polymer formation (see **Figure 2.8.B**). The polymer molecular ions peaks of PNPA have been repeated at regular intervals of m/Z equal to 211 for molecular formula $(C_{13}H_9NO_2)_n$ and on an average 6-7 repeating units (mass in the range 832 -1870 amu) were present. The other repeating peaks of equal mass difference corresponding to polymer adducts and fragmented peaks were also observed. The molecular weight of polymers of aromatic amines synthesised via chemical oxidative polymerisation were depending on the reaction conditions. The molecular weight of polymers was increasing upon increase in the production of monomer radical cations and decrease in the monomer to oxidising agent mole ratio due to the generation of primary chain aggregates. Also, strong oxidising agents have a tendency to form hight molecular weight polymers [80]. Here, the adopted reaction conditions produced low molecular weight polymer. They are sufficient for the sensing studies in aqueous acidic medium due to the ease of processability. Also, quantitative sensing studies are more efficient with low molecular weight polymers. The synthesized PNPA existed as a non-conducting conjugate polymer. However, the dried PNPA polymer, after dipping in concentrated sulphuric acid, has shown electrical conductivity of 4.8×10^{-5} S/cm.

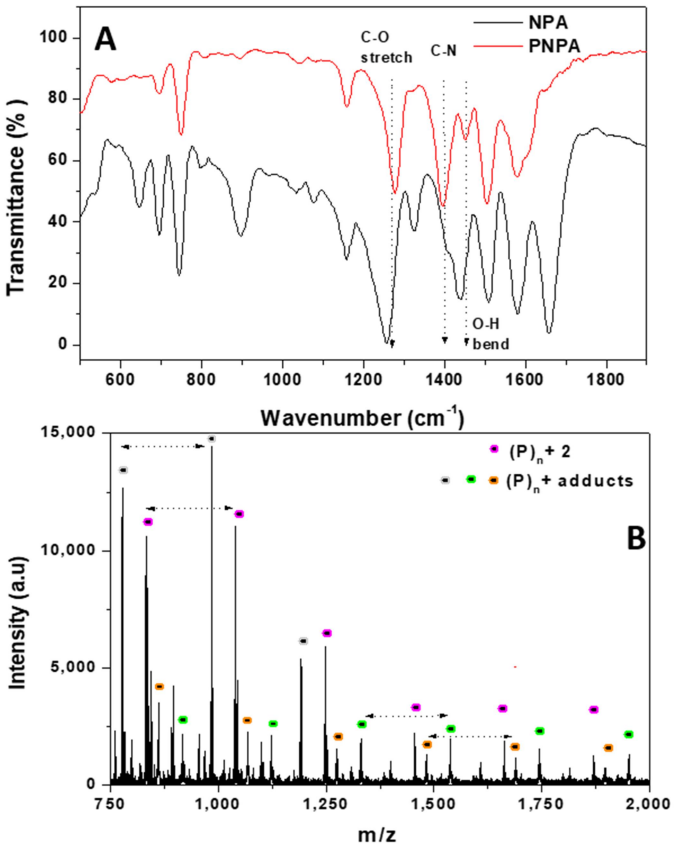

Figure 2.8.*A) FT-IR spectra of NPA and PNPA and B) MALDI-TOF spectra of PNPA.*

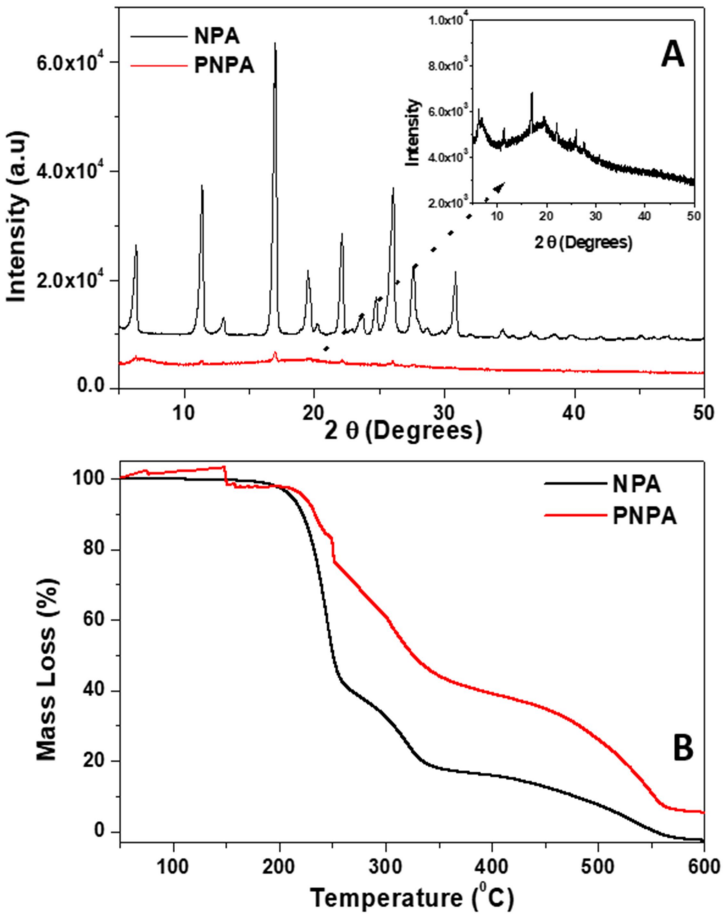

Figure 2.9. *A) Powder XRD diffractogram and B) TGA thermogram of NPA and PNPA.*

The powder X-ray diffraction studies provide information regarding the amorphous, crystalline or semicrystalline nature of the samples. X-ray diffraction patterns of monomer N-phenyl anthranilic acid (NPA) and poly-N-phenyl anthranilic acid (PNPA) were shown in **Figure 2.9.A**. The recrystallized monomer N-phenyl anthranilic acid has shown sharp crystalline peaks at 2θ values 6.5, 11.4, 17.13, 19.5, 22, 26, 27 and 30°. Poly-N-phenyl anthranilic acid (PNPA) samples do not have sharp crystalline peaks; instead, they show less intense peaks from broader regions (see inset for expanded diffractogram of PNPA). The polymer has shown a lower angle peak centered at 2θ = 6.10, corresponding to the organized polymer domains. The presence of a less intense peak, as well as broad nature in the 2θ range 17 to 30°, showed the weak interchain interactions and amorphous nature of the polymer similar to the parallel and perpendicular periodicity of polymer chain in polydiphenylamine and polyaniline. [54, 56-60] The thermal stability of monomer and polymer was recorded by thermogravimetric analysis by heating the samples in a nitrogen atmosphere up to 700°C. The monomer showed 10% weight loss at 218 °C and then a sudden weight loss of 50% was observed

on increasing temperature to 250 °C (see **Figure 2.9.B**). The polymer has shown 10 % weight loss at 230 °C and then slowly loses 55 % weight on increasing temperature to 360°C. The thermal stability of the polymer was higher than that of the monomer, especially for higher temperatures. [61, 52-55].

The good solubility of the monomer and polymer in sodium hydroxide solution enabled us to record the UV-visible absorption spectra of samples in the basic aqueous medium. The absorption spectra of polymer and monomer at different concentrations have been recorded in sodium hydroxide denoted by PNPA-Na and NPA-Na, respectively (see **Figure 2.10.A.** and **2.10.B.**). Dark blue-coloured PNPA changes to a yellowish-brown solution upon adding sodium hydroxide, whereas colourless NPA does not change its colour. Two peaks were observed for both NPA and PNPA at 288 nm and 339 nm, corresponding to benzenoid (π-π*) and extended π-π* transition of conjugated phenyl rings in reduced amine. [62, 63]

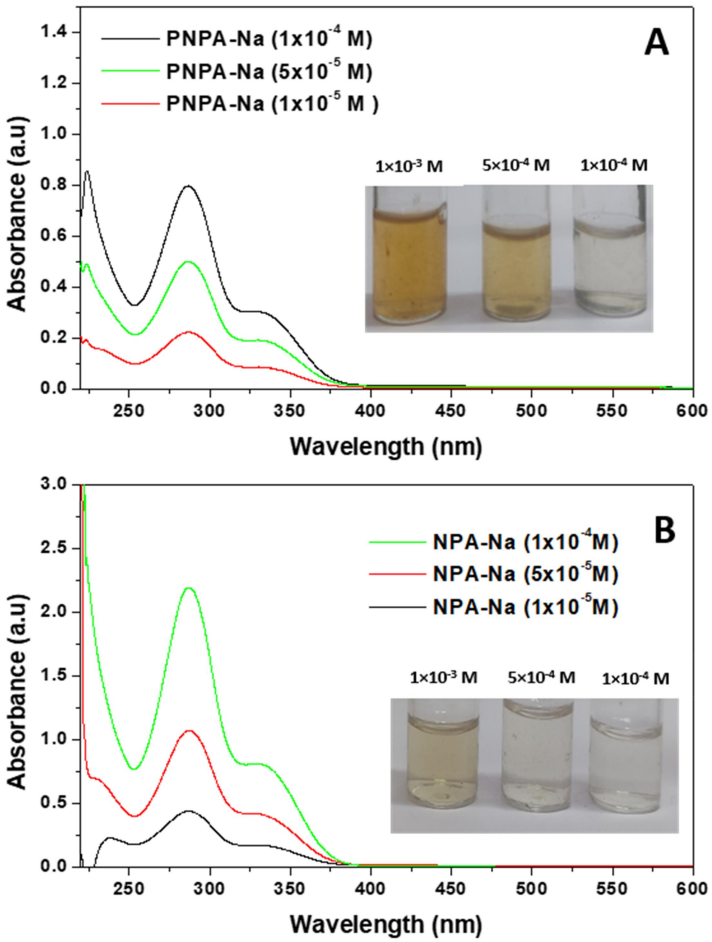

***Figure 2.10**. UV-visible absorption spectra of A) PNPA and B) NPA in sodium hydroxide (2 M) with photographs in the insect.*

Concentration-dependent absorption spectra of polymer PNPA-H in sulphuric acid have been recorded for different concentrations of polymer by varying its concentrations from 1.0×10^{-4} to 4.6×10^{-6} M (see **Figure 2.11.A.**). The UV-visible absorption spectra of PNPA in sulphuric acid was denoted as PNPA-H, have shown a sharp benzenoid peak at 254 nm and a broad absorption band with vibronic peaks at 363, 387 and 404 nm corresponding to protonated conjugated polymer structure (see **Figure 2.11.A.**) [49]. The PNPA-H has not shown any shift in peak position with a change in concentration. The UV-visible absorption spectra of NPA-H in sulphuric acid have also shown two absorptions, one at 254 nm corresponding to benzenoid transition and a broad vibronic peak at 404 nm corresponding to extended π -π^* transition. The absorption spectra of NPA and PNPA in organic solvents like chloroform have shown two absorption maxima at 290 nm and 358 nm corresponding to benzenoid and extended π -π^* transition, respectively (see **Figure 2.11.B**) [64]. The absorption corresponding to the oxidized quinoid unit (above 620 nm) was absent in the polymer structure, indicating the neutral reduced state of the polymer [52, 65]. It was interesting to see a blue shift of 20 nm in basic conditions and red shift of 50 nm in acidic conditions with respect to absorption obtained for 358 nm peak in chloroform.

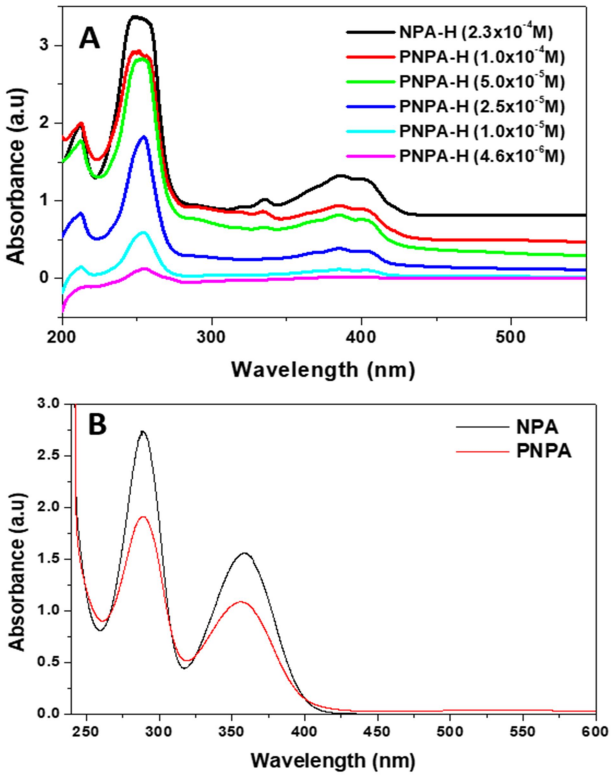

***Figure 2.11**. A) UV-visible absorption spectra of A) NPA-H and PNPA-H having different concentrations in sulphuric acid and B) NPA and PNPA in chloroform.*

The electrochemical activities of NPA-H and PNPA-H were studied by recording the cyclic voltammogram of NPA-H and PNPA-H solutions using a glassy carbon working electrode (see **Figure 2.12.**). The NPA-H solution has shown an anodic peak at +1.24 V corresponding to the oxidation of dimerised NPA having diphenyl benzidine dicarboxylic acid unit to oxidized NPA having diphenyl diquinoid dicarboxylic acid [74,76]. On a reverse sweep, the cathodic peak at -0.42 V corresponds to the reduction of dimerised NPA units. The PNPA-H solution has shown two redox peaks in the positive potential sweep, which arose due to coupled proton and electron transfer within the polymer structure. The anodic peaks at +0.60 V and +0.84 V were due to the oxidation of PNPA from diphenyl benzidine dicarboxylic acid units to diphenyl diquinoid dicarboxylic acid units similar to NPA. In the cathodic sweep, two reduction peaks at +0.74 V and -0.32 V were obtained, corresponding to the reduction of oxidized PNPA-H. Redox reversible peaks in the cyclic voltammogram of NPA-H and PNPA-H confirmed the existence of electroactive states. The less anodic peak potential of PNPA-H than the NPA-H indicated more feasibility towards oxidation.

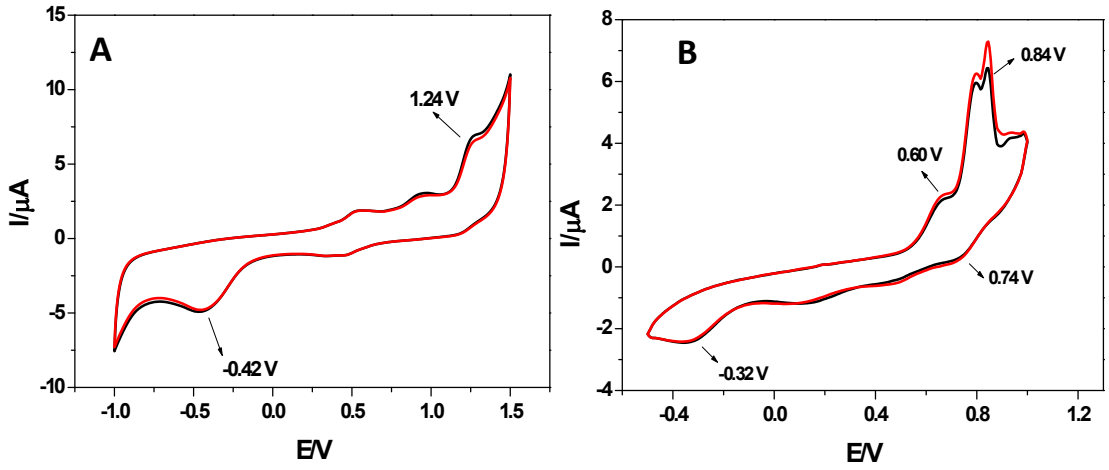

***Figure 2.12**. Cyclic voltammogram of A) NPA-H and B) PNPA-H.*

2.3.3. Fluorescence studies of PNPA-H

The fluorescence emission of monomer (NPA-H) and blue-coloured polymer (PNPA-H) at different concentrations have been checked in dilute sulphuric acid by irradiating solutions under UV light (λ = 365 nm) in a dark chamber. The polymer solutions have intense bluish-white fluorescence and the intensity of the bluish-white fluorescence of the polymer samples decrease with decrease in concentration (see photographs in **Figure 2.13.**). In an acidic environment, PNPA is partially protonated,

and the polymer structure becomes more rigid because of the repulsion of charges and extended conjugation, resulting in the stronger fluorescence intensity. The UV-visible spectroscopy shows that the onset of the extended π- π*conjugated peak of PNPA-H in acid medium, PNPA-Na in basic medium and PNPA in chloroform were at 440 nm, 375 nm and 410 nm, respectively, which indicate the change in conjugation. The fluorescence quantum yield (Φ_f) of the polymer solution has been quantified as 0.38 ± 5% by a comparative method using quinine sulphate as a reference at an excitation wavelength of 365 nm. Monomer (NPA) has shown weak green fluorescence in chloroform, bluish-white fluorescence in sulphuric acid and no fluorescence in sodium hydroxide solution. The polymer (PNPA) has intense bluish-white fluorescence in sulphuric acid and no visible emission in chloroform and sodium hydroxide solution.

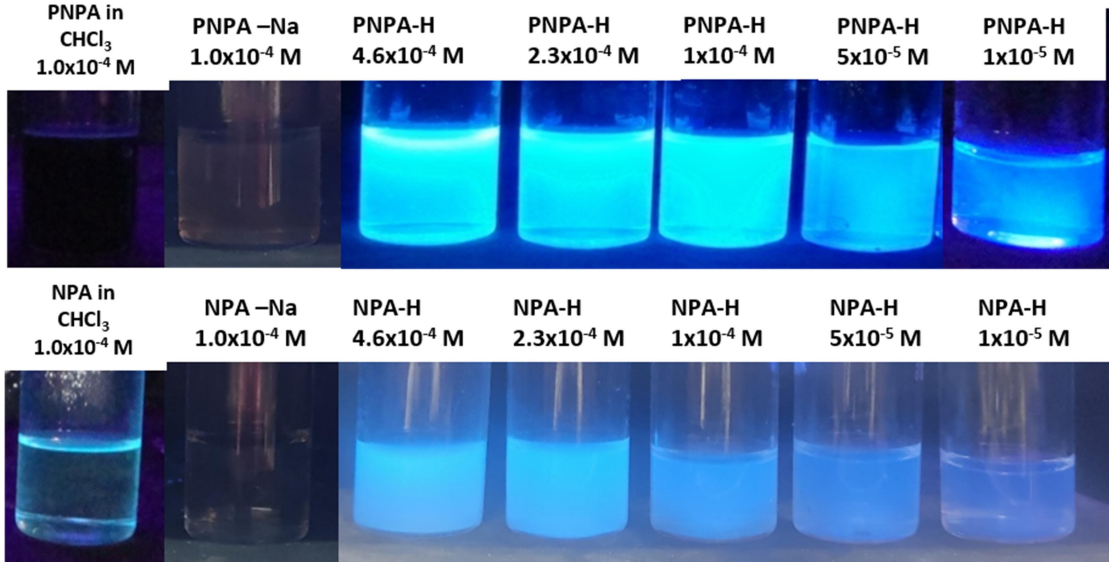

Figure 2.13. *Fluorescence images of dissolved PNPA and NPA in chloroform, PNPA-Na and NPA-Na in NaOH, and different concentrations of PNPA-H and NPA-H in H_2SO_4.*

2.3.4. Fluorescence sensing of oxidizing analytes

The light emission of polymer solutions is very sensitive and detection of specific ions, atoms or small molecules in a trace level is possible by fluorescent intensity change or fluorometric colour sensing [66-67]. Different anions and cations such as Ce^{4+}, MnO_4^-, $Cr_2O_7^{2-}$, Cu^{2+}, Co^{2+}, Hg^{2+} and molecules such as glucose, urea, ascorbic acid were randomly added to the bluish-white light-emitting polymer solution of PNPA-H to check any change in fluorescence signal. Strong oxidizing agents such as cerium ammonium sulphate dihydrate, potassium permanganate and potassium dichromate solutions instantly

quenched the bluish-white fluorescence of the polymer. Systematic concentration-dependent studies have been carried out to find the actual concentration at which fluorescence quenching was observed by adding the solution of analytes. For this purpose, the concentration of aqueous salt solutions of Ce^{4+}, MnO_4^- and $Cr_2O_7^{2-}$ ions were systematically varied in the concentration range from 1×10^{-2} M to 1×10^{-5} M and the polymer concentration was fixed as 1×10^{-5} M (see **Figure 2.14.**). Naked eye fluorescence quenching was observed on and above 5×10^{-5} M, 7.5×10^{-5} M and 2.5×10^{-3} M for Ce^{4+}, MnO_4^- and $Cr_2O_7^{2-}$ respectively. The [analyte]/ [polymer] mole ratio for which fluorescence quenching was obtained for [Ce^{4+}]/ [PNPA-H], [MnO_4^-]/ [PNPA-H] and [$Cr_2O_7^{2-}$]/ [PNPA-H] were 5, 7.5 and 250 respectively. The limit of detection (LOD) of analytes for simple naked eye fluorescence detection has been found to be 0.5 μM, 0.75 μM and 25 μM for Ce^{4+}, MnO_4^- and $Cr_2O_7^{2-}$ ions, respectively, by taking the lowest naked eye emissive polymer concentration as 1×10^{-7} M.

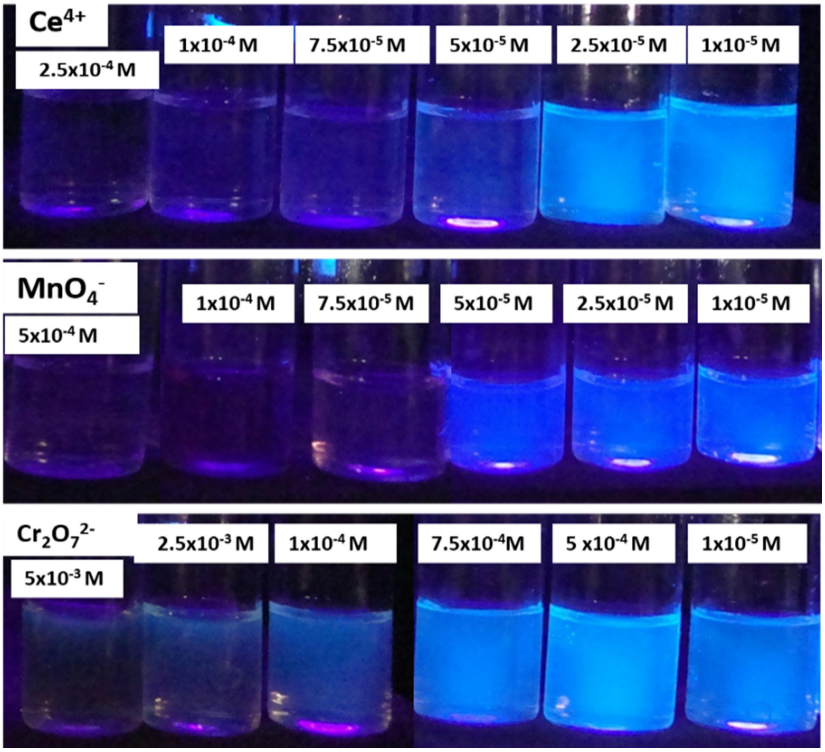

Figure 2.14. *Fluorescence quenching studies of PNPA-H with different concentrations of analytes like* Ce^{4+}, $KMnO_4$ *and* $K_2Cr_2O_7$ *by colorimetric detection.*

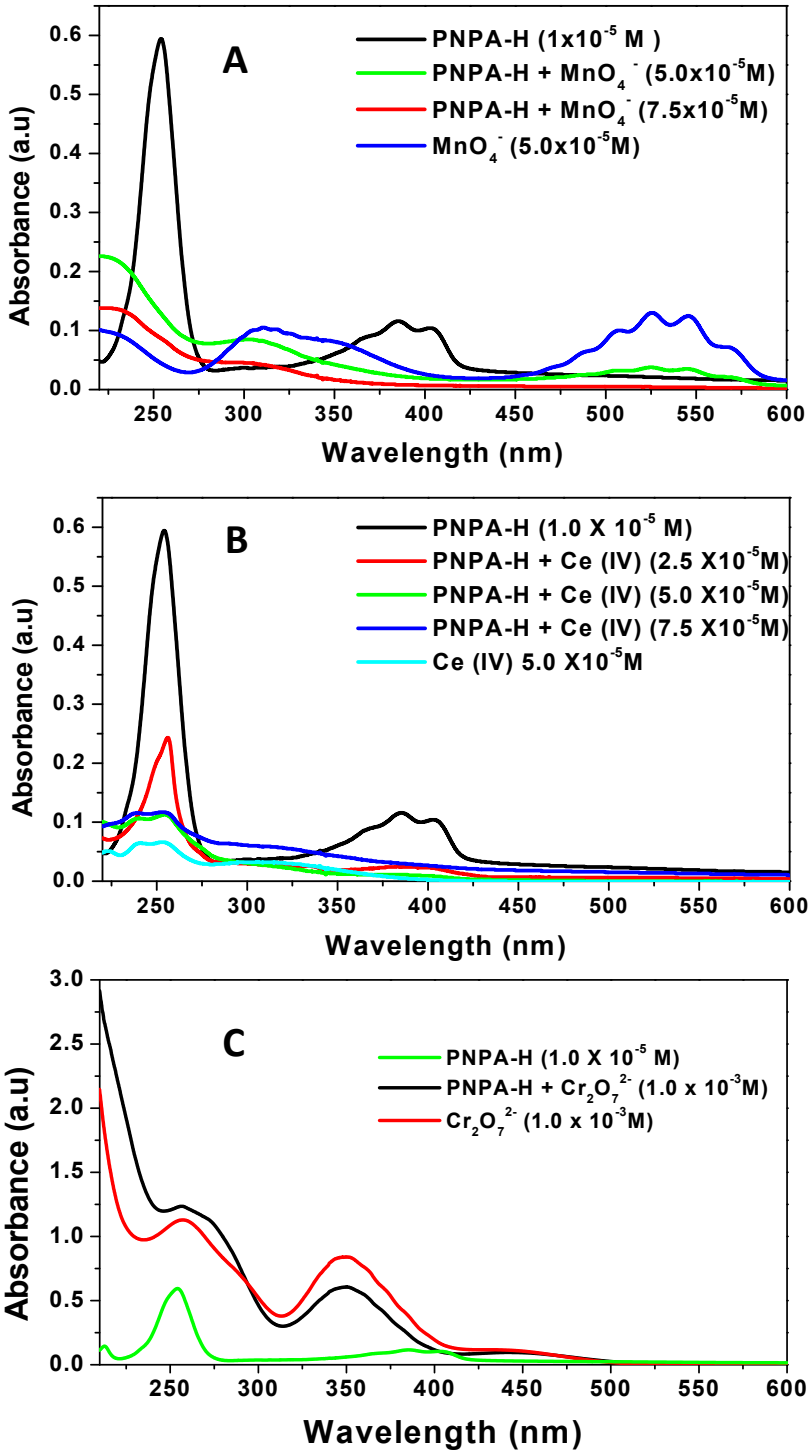

Figure 2.15. *UV-Visible absorption spectra of A) Polymer + MnO_4^- ions in solution, B) Polymer + Ce^{4+} ions in solution and C)) Polymer + $Cr_2O_7^{2-}$ ions in solution, respectively.*

The UV-visible absorption spectra of polymer and polymer + analyte solutions were recorded to find any changes in the absorption spectra of PNPA-H by adding

analytes. The absorption spectra of the polymer were taken at the same concentration limit where naked-eye fluorescence quenching was observed (1×10^{-5} M) (see **Figure 2.15.**). In the case of analytes like Ce^{4+} and MnO_4^{2-} ions, absorption at 388 nm vanished entirely upon increasing analyte concentration to 5×10^{-5} M and 7.5×10^{-5} M, respectively. In addition to that, the absorbance of the benzenoid peak present at 280 nm was suppressed considerably, indicating the changes in the benzenoid structure. In the case of UV-visible absorption spectra of dichromate + polymer mixture, strong light absorption of potassium dichromate at 380 nm region hampered our efforts to note changes in absorbance (see **Figure 2.15.C.**).

Emission spectra of polymer and polymer + analytes have been recorded using a spectrofluorometer to get the quenching concentration from the changes in fluorescence intensity. The range of polymer and analyte concentrations selected for spectrofluorometric studies was the same as that used for naked-eye fluorescence detection and UV-visible absorption studies. The quenching of fluorescence of PNPA-H obtained from spectrofluorimetry for Ce^{4+} and MnO_4^- ions were at concentrations equal to 1×10^{-4} M and 7.5×10^{-5} M and 2.5×10^{-3} M, respectively (see **Figure 2.16.A** and **2.16.B.**). The emission spectra of dichromate + polymer mixture has shown fluorescence quenching of PNPA-H at concentration of 2.5×10^{-3} M $Cr_2O_7^{2-}$ ions (see **Figure 2.16.C.**).

Fluorescence intensity changes of the polymer obtained after the addition of different analyte concentrations have been plotted against the [analyte]/ [polymer] mole ratio (see **Figure 2.17.**). The analyte/polymer mole ratio for Ce^{4+} / PNPA-H, MnO_4^-/ PNPA-H and $Cr_2O_7^{2-}$/ PNPA-H for quenching action were obtained 8, 4.5 and 100, respectively, via extrapolating the straight line to x-axis. The accuracy of sensing action in naked-eye fluorescence detection and UV-visible absorption spectra would be slightly variable, especially at very low concentrations due to the difficulty in judging the visibility of fluorescence and low absorbance, respectively. On the other hand, a spectrofluorometer is a highly sensitive instrument that can measure fluorescence signals even at very low concentrations (up to nanomolar concentration) of polymer + analyte mixture. The calibration curve shows that the linear range of response was fairly straight with a higher coefficient of determination (r^2) and low p-value (< 0.05), which suggests that the model was fairly fitted with good precision. Moreover, the three independent techniques provided reasonably in good agreement for the fluorescence quenching action of analytes within the experimental limit.

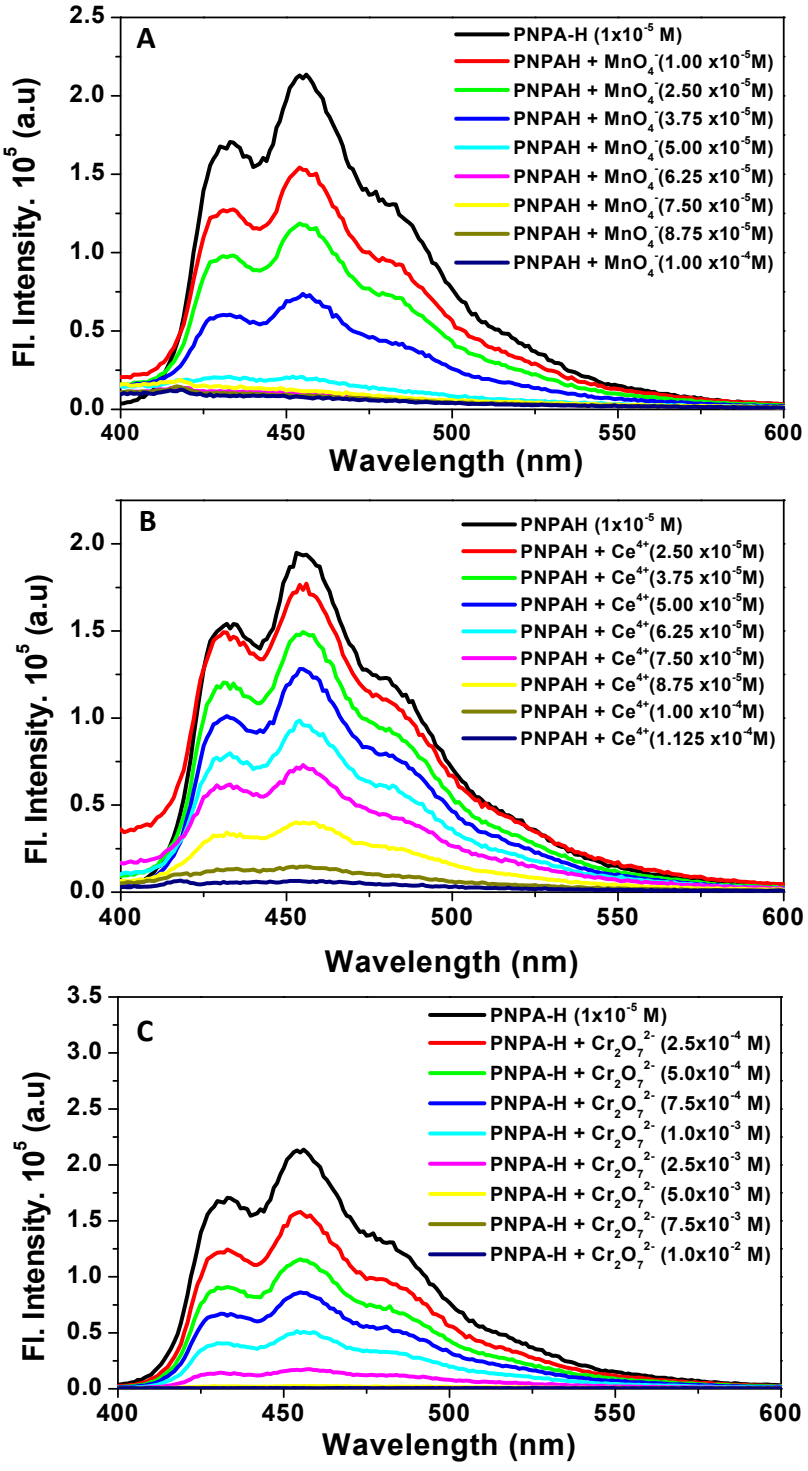

Figure 2.16. *Emission spectra of A) Polymer + MnO_4^- ions in solution, B) Polymer + Ce^{4+} ions and C) Polymer + $Cr_2O_7^{2-}$ in solution.*

The fluorescence intensity ratio (I_0/I) plotted against the concentration of the analyte was shown in **Figure 2.18.**, where I_0 and I are the intensity of transmitted light in the absence and presence of the analyte. The plots have shown a curve with a positive

deviation from the straight line, which indicates static quenching. It may be because of a non-fluorescent complex formation for a higher [analyte]/[polymer] mole ratio. One of the requirements for Stern-Volmer theory is that the donor concentration should be low, so that the donor molecules do not influence each other.[77-78] We have calculated the slope of the curve from linear range manually using the equation, slope = $\Delta Y/\Delta X$ by taking two concentrations from the curve and the slope of the curve for MnO_4^-, Ce^{4+} and $Cr_2O_7^{2-}$ ions were 3.73 $\times 10^5$, 9.41 $\times 10^4$ and 5.00$\times 10^3$ M^{-1} and the sensitivity of different analytes follow the order $MnO_4^- > Ce^{4+} > Cr_2O_7^{2}$.

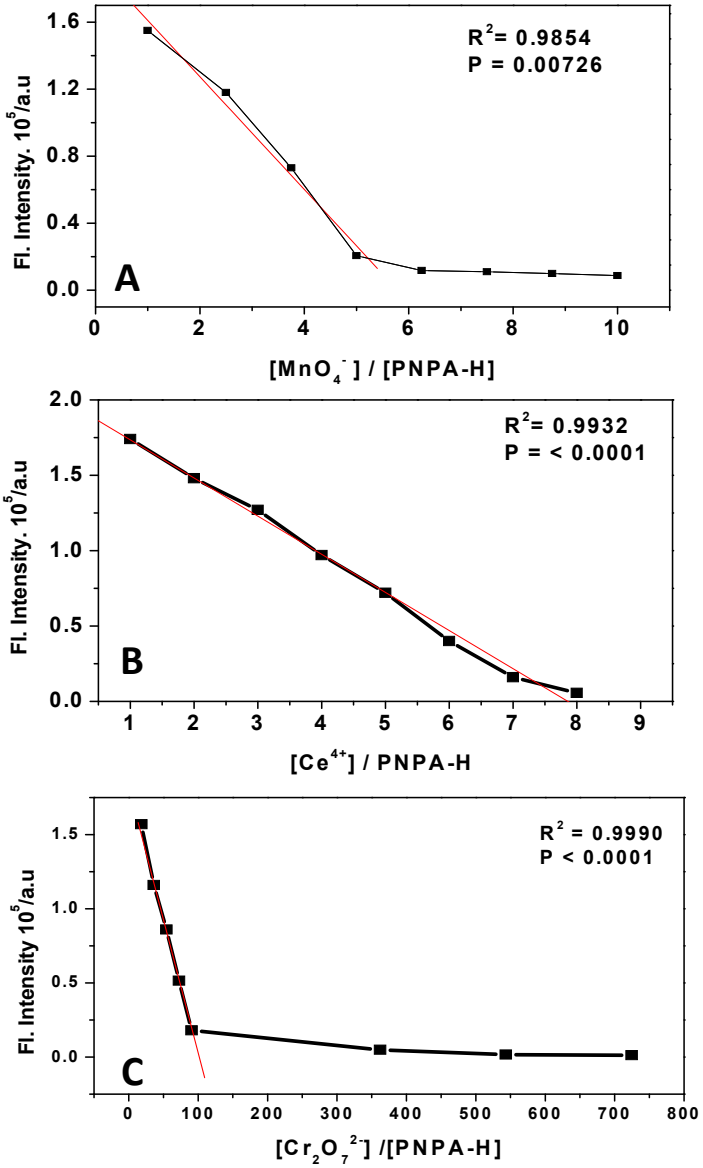

Figure 2.17. *Mole ratio plots of A) Polymer + MnO_4^- ions, B) Polymer + Ce^{4+} ions and C) Polymer + $Cr_2O_7^{2-}$ ions in solution with linear calibration on the quenching concentrations.*

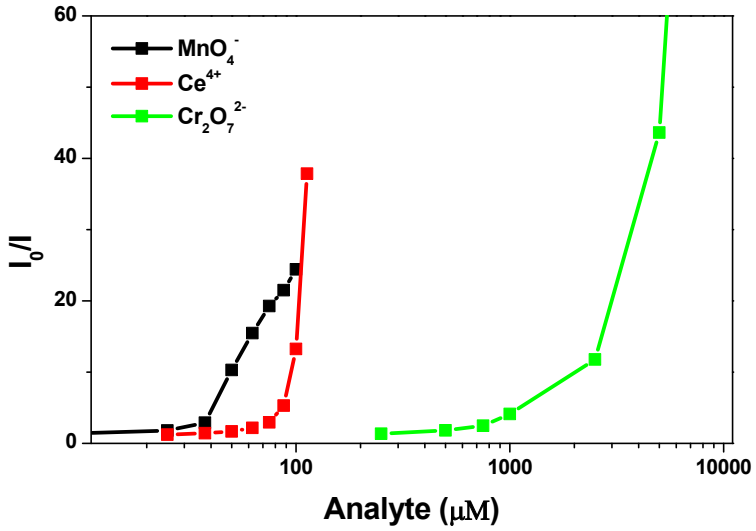

Figure 2.18. *(I_0/I) Vs. Concentration of analytes.*

The fluorescence quenching mechanism was proposed based on the oxidizing action of analytes on PNPA-H in reduced form (see **Figure 2.19.**). The oxidizing power of analytes in the solution can be obtained from the standard reduction potential (E°) of Ce^{4+}/Ce^{3+} (+1.44 V), MnO_4^-/Mn^{2+} (+1.51V), and $Cr_2O_7^{2-}/Cr^{3+}$ (1.36 V) in acid medium. [68-70]. The first step of the oxidation of N-phenyl anthranilic acid in redox titration is an irreversible step that results in the formation of colourless diphenyl benzidine dicarboxylic acid (reduced), which upon oxidation forms violet-red diphenyl diquinone dicarboxylic acid (oxidized) [71-75]. The standard redox potential for reduced (colourless) and oxidized forms (violet-red) of N-phenyl anthranilic acid dimer was found to be 1.08 V [72, 76]. The blue coloured polymer (PNPA-H) synthesized for the present studies also contain diphenyl benzidine dicarboxylic acid repeating units in the reduced form, however, which upon further oxidation becomes a non-fluorescent diquinone structure (see **Figure 2.19.**). The [analyte]/[polymer] mole ratio at which fluorescence quenching was observed was lowest for MnO_4^- ions (7.5) and highest for $Cr_2O_7^{2-}$solutions (250) from spectrofluorimetry. The high [$Cr_2O_7^{2-}$]/ [PNPA-H] mole ratio reveals that potassium dichromate was a weak oxidizing analyte (E° = + 1.36 V) for PNPA-H in comparison to other analytes. The other two analytes ($MnO_4^-/Mn^{2+}$and Ce^{4+}/Ce^{3+}) have more positive standard reduction potential than $Cr_2O_7^{2-}/Cr^{3+}$ and thus, they reacted with PNPA-H at low analyte / PNPA-H mole ratio.

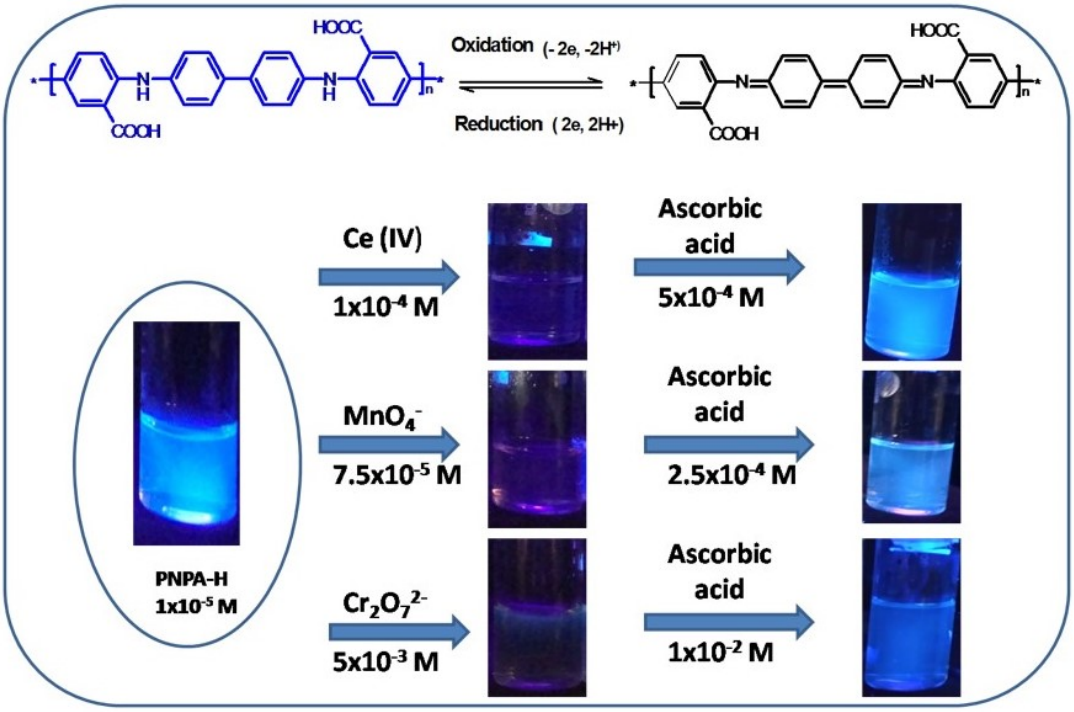

Figure 2.19. *Mechanism of fluorescence quenching and reappearance of PNPA-H on adding oxidizing and reducing analytes with its photographs.*

Reversibility and the redox behaviour of PNPA-H have been checked by adding reducing biomolecules like ascorbic acid to the oxidized non-fluorescent form of polymer in solution. The standard reduction potential (E°) value for dehydroascorbic acid (DHA)/ascorbic acid (AsA) was reported to be -0.066 V. [79] Ascorbic acid was added to the polymer at the concentration in which fluorescence was just quenched by analytes (1×10^{-4} M for Ce^{4+}, 7.5×10^{-5} M for MnO_4^-, and 2.5×10^{-3} M for $Cr_2O_7^{2-}$). The fluorescence reappeared on adding ascorbic acid at concentrations 5×10^{-4} M, 2.5×10^{-4} M and 1×10^{-2} M, respectively for Ce^{4+}, MnO_4^- and $Cr_2O_7^{2-}$ solutions (see **Figure 2.19.**). Although the system was reversible, a slight excess of reductant or oxidant concentration was required to reappear or quench the fluorescence, possibly due to the polymeric structure in which variable levels of reduction or oxidation can occur. The intensity of fluorescence of solutions from naked eye detection indicated the complete recovery of original polymer. The changes in the UV-visible absorption spectra of polymer + analyte mixtures by adding ascorbic acid were also checked (see **Figure 2.20.A.**). Polymer + analyte + ascorbic acid mixture absorbs at 265 nm, indicating the reformation of benzenoid structure in PNPA-H. However, a peak that was responsible for blue light emission at 388 nm was not visible due to the broad absorption of other reduced ions of analytes, slight

excess ascorbic acid and low concentration PNPA-H in the final mixture. Fluorescence reversibility in PNPA-H was studied by another oxidizing reagent like $KMnO_4$ (1×10^{-4} M) and then reduced back using ascorbic acid (1×10^{-1} M). The fluorescence quenching of PNPA-H by MnO_4^- and fluorescence reappearance using ascorbic acid for two oxidation-reduction cycles have been carried out. Although the dilution effect decreases the fluorescence intensity on reduction, the fluorescence turns-off and turn-on was clear (see **Figure 2.20.B.**).

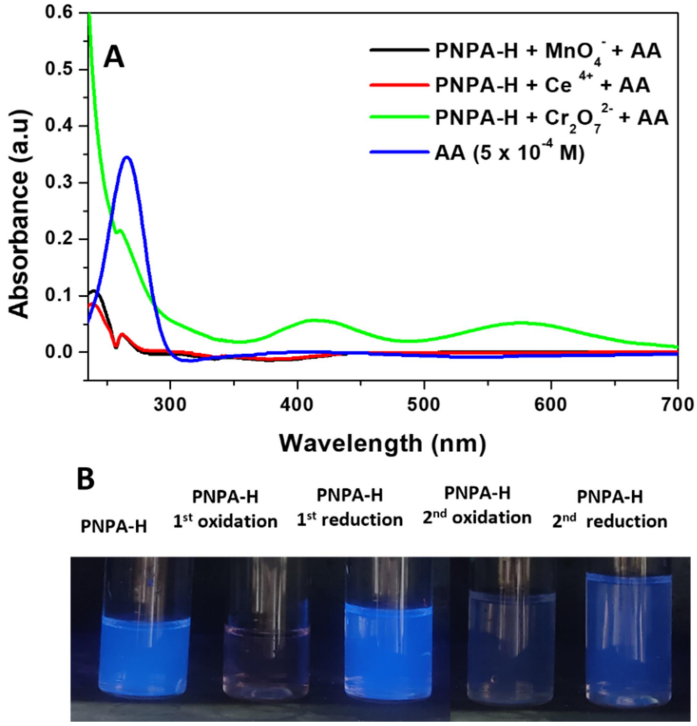

Figure 2.20. *A) UV-visible absorption spectra of polymer-analyte solutions on adding ascorbic acid solutions. B) Photographs of PNPA-H under UV light on multiple oxidations and reductions for reversibility studies.*

2.3.5. Application of PNPA-H in titrations

The potentiometric titrations of the polymer (PNPA-H) against the analytes (for a fixed concentration of for polymer (1×10^{-5} M) and analyte (1×10^{-5} M)) have been carried out. The change of potential with respect to volume ($\Delta E/\Delta V$) was plotted against the volume of the analyte to obtain a potentiometric redox titration curve (see **Figure 2.21.A. and B.**). The analyte concentration calculated from the first derivative plot of potentiometric titration was relatively in agreement with the quenching concentration of the analyte obtained from other methods.

A naked-eye fluorometric titration of analytes has been carried out using PNPA-H solution to demonstrate its potential application as fluorescent indicators, especially at very low concentrations of analytes (see **Figure 2.21.C.**). The concentrations of polymer and analytes taken were comparable (1×10^{-5} M) for fluorometric titration and the [analyte] / [polymer] mole ratio at which fluorescence quenching was observed was found to be relatively in good agreement with other methods. Ordinary or conventional titrations could not perform the endpoint of titrations with very low concentrations of analytes. Here, the endpoint of titrations with low concentration of analyte (1×10^{-5} M) was effectively determined with fluorescence quenching of PNPA-H. We have also studied the effect of interfering analytes, especially mild oxidizing agents like $FeCl_3$, $CuSO_4$, $NaWO_4$ and $Pb(NO_3)_2$, on the fluorescence intensity of PNPA-H using a naked-eye detection test. It has been found that these analytes have no effect on the fluorescence of PNPA-H. We have also checked the combined effect of these analytes separately with Ce^{4+}, MnO_4^- and $Cr_2O_7^{2}$ and it has been noted that $FeCl_3$, $CuSO_4$, $NaWO_4$ and $Pb(NO_3)_2$ do not interfere with the polymer-analyte reaction. This also indicated the highly sensitive nature of poly-N-phenyl anthranilic acid towards strong oxidizing agents like Ce^{4+}, MnO_4^- and $Cr_2O_7^{2-}$. The redox reaction between conjugated fluorescent PNPA-H and analytes, which leads to quenching of bright bluish-white fluorescence, has been used for sensing applications.

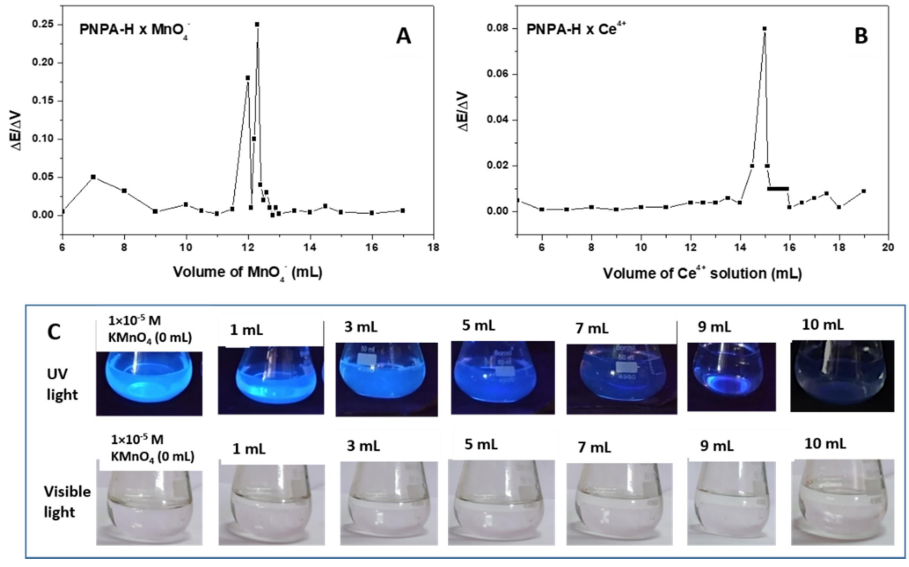

Figure 2.21. *A & B) Potentiometric titration curve ((ΔE/ΔV) Vs. volume of analyte) of PNPA-H with different analytes and C) Photographs of fluorometric titrations in which 1×10^{-5} M PNPA-H solutions was titrated against 1×10^{-5} M $KMnO_4$ solutions in UV light and visible light.*

2.4. Conclusion

Chemical oxidative polymerization of N-Phenyl anthranilic acid was successfully synthesized using anhydrous ferric chloride as an oxidizing agent in ethanol solvent to produce an efficient bluish-white light emitting poly-N-phenyl anthranilic acid (PNPA-H), which was utilized for the sensing of analytes like Ce^{4+}, MnO_4^- and $Cr_2O_7^{2-}$ solutions. Polymer (PNPA) formation was confirmed by ^1H NMR, FT-IR, and MALDI-TOF mass spectroscopy. Powder X-ray diffraction studies have revealed the highly crystalline nature of monomer and the amorphous nature of polymers. The thermal stability of the polymer was found to be much higher than that of the monomer. UV-visible absorption spectra of polymer in sodium hydroxide solution (PNPA-Na) and in sulphuric acid solution (PNPA-H) have shown marked differences in absorption spectra. The polymer has shown broad band with vibronic peaks at 363, 387 and 404 nm in sulphuric acid medium, which was mainly responsible for bluish-white light emission. The bluish-white emission of PNPA-H was quenched by oxidizing analytes like Ce^{4+}, MnO_4^- and $Cr_2O_7^{2-}$ ions, which were quantified by three independent methods like colorimetric sensing, UV-Vis absorption spectra and fluorescence emission spectroscopy. The analytes like Ce^{4+}, MnO_4^- and $Cr_2O_7^{2-}$ have shown different [analyte]/[polymer] mole ratios for fluorescence quenching, which was correlated with different redox potential. The redox reaction between reduced diphenyl benzidine units to oxidized diquinoid units of polymer by oxidizing analytes was responsible for fluorescence quenching. The reversibility of the redox reaction was confirmed by the reappearance of fluorescence by the addition of reducing biomolecules like ascorbic acid. The limit of detection obtained for naked eye fluorescence detection of PNPA-H was for Ce^{4+}, MnO_4^-, and $Cr_2O_7^{2-}$ ions were 0.5 µM, 0.75 µM and 25 µM respectively and sensitivity was obtained highest for MnO_4^- ions and lowest for $Cr_2O_7^{2-}$ ions. The cyclic voltammogram of PNPA-H confirmed the presence of electrochemical reversible redox states. In short, we have developed a novel method for the detection of oxidizing analytes like potassium dichromate, potassium permanganate and cerium ammonium sulphate by the utilization of poly N-phenyl anthranilic acid (PNPA-H) as a redox fluoroprobe.

Reference

1. Ettinger, A., & Wittmann, T. (2014). *Fluorescence live cell imaging* (pp. 77–94). https://doi.org/10.1016/B978-0-12-420138-5.00005-7.
2. Bugaj, A., Sieroń, Kawczyk-Krupka, Dariusz Straszak, Sebastian Kwiatek, Wojciech Latos, & Sieron-Stoltny, K. (2013). The role of fluorescence diagnosis in clinical practice. *OncoTargets and Therapy*, 977. https://doi.org/10.2147/OTT.S42074.
3. Georgiev, N. I., Bakov, V. v., Anichina, K. K., & Bojinov, V. B. (2023). Fluorescent Probes as a Tool in Diagnostic and Drug Delivery Systems. *Pharmaceuticals*, *16*(3), 381. https://doi.org/10.3390/ph16030381.
4. Irie, M., Fukaminato, T., Sasaki, T., Tamai, N., & Kawai, T. (2002). A digital fluorescent molecular photoswitch. *Nature*, *420*(6917), 759–760. https://doi.org/10.1038/420759a.
5. IV. ’Αμόρφωγa, no. I.— on a case of superficial colour presented by a homogeneous liquid internally colourless. (1845). *Philosophical Transactions of the Royal Society of London*, *135*, 143–145. https://doi.org/10.1098/rstl.1845.0004.
6. Modreski, P. J. (1987). Ultraviolet fluorescence of minerals--Examples from New Mexico. *New Mexico Geology*, *9*(2), 25–30. https://doi.org/10.58799/NMG-v9n2.25.
7. Dai, Y., Shen, Z., Liu, Y., Wang, L., Hannaway, D., & Lu, H. (2009). Effects of shade treatments on the photosynthetic capacity, chlorophyll fluorescence, and chlorophyll content of Tetrastigma hemsleyanum Diels et Gilg. *Environmental and Experimental Botany*, *65*(2–3), 177–182. https://doi.org/10.1016/j.envexpbot.2008.12.008.
8. Tsai, T.-H., & D’Haenens-Johansson, U. F. S. (2019). Gemstone Screening and Identification Using Fluorescence Spectroscopy. *Frontiers in Optics + Laser Science APS/DLS*, JTu3A.109. https://doi.org/10.1364/FIO.2019.JTu3A.109.
9. Vibhute, A.; Patil, T.; Gambhir, R.; Tiwari, A. P. (2022). Fluorescent Carbon Quantum Dots: Synthesis Methods, Functionalization and Biomedical Applications. *Appl. Surf. Sci. Adv. 11*. https://doi.org/10.1016/j.apsadv.2022.100311.
10. Mader, H.; Li, X., Saleh, S., Link, M., Kele, P., Wolfbeis, O. S. (2008). Fluorescent Silica Nanoparticles. *Ann. N. Y. Acad. Sci.*, *1130*, 218–223. https://doi.org/10.1196/annals.1430.053.
11. Chandra, A., Prasad, S., Gigli, G., & del Mercato, L. L. (2020). *Fluorescent nanoparticles for sensing* (pp. 117–149). https://doi.org/10.1016/B978-0-08-102828-5.00006-1.
12. Li, J., Yuan, S., Qin, J., Pang, J., Zhang, P., Zhang, Y., Huang, Y., Drake, H. F., Liu, W. R., & Zhou, H. (2020). Stepwise Assembly of Turn-on Fluorescence Sensors in Multicomponent Metal–Organic Frameworks for in Vitro Cyanide Detection. *Angewandte Chemie International Edition*, *59*(24), 9319–9323. https://doi.org/10.1002/anie.202000702.
13. Zhang, L., & Wang, E. (2014). Metal nanoclusters: New fluorescent probes for sensors and bioimaging. *Nano Today*, *9*(1), 132–157. https://doi.org/10.1016/j.nantod.2014.02.010.
14. Sun, X., & Lei, Y. (2017). Fluorescent carbon dots and their sensing applications. *TrAC Trends in Analytical Chemistry*, *89*, 163–180. https://doi.org/10.1016/j.trac.2017.02.001.
15. Alvarez, A., Costa-Fernández, J. M., Pereiro, R., Sanz-Medel, A., & Salinas-Castillo, A. (2011). Fluorescent conjugated polymers for chemical and biochemical sensing. *TrAC Trends in Analytical Chemistry*, *30*(9), 1513–1525. https://doi.org/10.1016/j.trac.2011.04.017.
16. Wang, M., Da, Y., & Tian, Y. (2023). Fluorescent proteins and genetically encoded biosensors. *Chemical Society Reviews*, *52*(4), 1189–1214. https://doi.org/10.1039/D2CS00419D.
17. The Huy, B., Thangadurai, D. T., Sharipov, M., Ngoc Nghia, N., van Cuong, N., & Lee, Y.-I. (2022). Recent advances in turn off-on fluorescence sensing strategies for sensitive biochemical analysis - A mechanistic approach. *Microchemical Journal*, *179*, 107511. https://doi.org/10.1016/j.microc.2022.107511.

18. Tian, X., Murfin, L. C., Wu, L., Lewis, S. E., & James, T. D. (2021). Fluorescent small organic probes for biosensing. *Chemical Science*, *12*(10), 3406–3426. https://doi.org/10.1039/D0SC06928K.
19. Zuliani, A., Khiar, N., & Carrillo-Carrión, C. (2023). Recent progress of metal–organic frameworks as sensors in (bio)analytical fields: towards real-world applications. *Analytical and Bioanalytical Chemistry*, *415*(11), 2005–2023. https://doi.org/10.1007/s00216-022-04493-7.
20. Xiao, D., Qi, H., Teng, Y., Pierre, D., Kutoka, P. T., & Liu, D. (2021). Advances and Challenges of Fluorescent Nanomaterials for Synthesis and Biomedical Applications. *Nanoscale Research Letters*, *16*(1), 167. https://doi.org/10.1186/s11671-021-03613-z.
21. Huang, X., & Tang, M. (2021). Research advance on cell imaging and cytotoxicity of different types of quantum Dots. *Journal of Applied Toxicology*, *41*(3), 342–361. https://doi.org/10.1002/jat.4083.
22. Ahumada, G., Borkowska, M. (2022). Fluorescent Polymers Conspectus. *Polymers (Basel).*, *14* (6). https://doi.org/10.3390/polym14061118.
23. Yuan, J., Wang, S., Shan, J., Peng, J., Wei, L., Xu, X. (2010). Formation and Photoluminescence of Fluorescent Polymers. *Int. J. Polym. Sci.*, *2010*. https://doi.org/10.1155/2010/526348.
24. Liu, J.; Baek, J.-B.; Dai, L. (2014). Conjugated Polymer Synthesis. *Encycl. Polym. Nanomater.*, 1–7. https://doi.org/10.1007/978-3-642-36199-9_273-1.
25. Zou, L., Wen, Y., Zhang, H., Chai, J., Duan, X., Shen, L., Zhang, G., Xu, J. (2018). Highly Sensitive Fluorescent Sensor Based on Electrosynthesized Poly(Fmoc-L-Serine) Enables Ultra-Trace Analysis of $Cr_2O_7^{2-}$ in Water and Agro-Product Samples. *Sensors Actuators, B Chem.*, *277*, 394–400. https://doi.org/10.1016/j.snb.2018.09.046.
26. De Silva, A. P., Gunaratne, H. Q. N., Gunnlaugsson, T., Huxley, A. J. M., McCoy, C. P.;,Rademacher, J. T., Rice, T. E. (1997). Signaling Recognition Events with Fluorescent Sensors and Switches. *Chem. Rev.*, *97* (5), 1515–1566. https://doi.org/10.1021/cr960386p.
27. Chen, X., Hussain, S., Hao, Y., Tian, X., Gao, R. (2021). Review—Recent Advances of Signal Amplified Smart Conjugated Polymers for Optical Detection on Solid Support. *ECS J. Solid State Sci. Technol.*, *10* (3), 037006. https://doi.org/10.1149/2162-8777/abeed1.
28. Huy, B., Thangadurai, D. T., Sharipov, M., Ngoc Nghia, N., Van Cuong, N., Lee, Y. I. (2022). Recent Advances in Turn Off-on Fluorescence Sensing Strategies for Sensitive Biochemical Analysis - A Mechanistic Approach. *Microchem. J.*, *179*. https://doi.org/10.1016/j.microc.2022.107511.
29. Lee, K., Povlich, L. K., Kim, J. (2010). Recent Advances in Fluorescent and Colorimetric Conjugated Polymer-Based Biosensors. *Analyst*, *135* (9), 2179–2189. https://doi.org/10.1039/c0an00239a.
30. Zhou, Q., Swager, T. M. (1995). Methodology for Enhancing the Sensitivity of Fluorescent Chemosensors: Energy Migration in Conjugated Polymers. *J. Am. Chem. Soc.*, *117* (26), 7017–7018. https://doi.org/10.1021/ja00131a031.
31. Yu, J., & Zhang, C. (2020). Fluorescent sensing for amines with a low detection limit based on conjugated porous polymers. *Journal of Materials Chemistry C*, *8*(46), 16463–16469. https://doi.org/10.1039/D0TC02592E.
32. Hu, Q., Zhang, W., Yin, Q., Wang, Y., & Wang, H. (2021). A conjugated fluorescent polymer sensor with amidoxime and polyfluorene entities for effective detection of uranyl ion in real samples. *Spectrochimica Acta Part A: Molecular and Biomolecular Spectroscopy*, *244*, 118864. https://doi.org/10.1016/j.saa.2020.118864.
33. Chakraborty, C., Singh, P., Maji, S. K., Malik, S. (2013). Conjugated Polyfluorene-Based Reversible Fluorescent Sensor for Cu(II) and Cyanide Ions in Aqueous Medium. *Chem. Lett.*, *42* (11), 1355–1357. https://doi.org/10.1246/cl.130630.
34. Chen, L., McBranch, D. W., Wang, H. L., Helgeson, R., Wudl, F., Whitten, D. G. (1999). Highly Sensitive Biological and Chemical Sensors Based on Reversible Fluorescence

Quenching in a Conjugated Polymer. *Proc. Natl. Acad. Sci. U. S. A.*, *96* (22), 12287–12292. https://doi.org/10.1073/pnas.96.22.12287.

35. Tang, Y., He, F., Yu, M., Wang, S., Li, Y. (2006). Radical Scavenging Mediating Reversible Fluorescence Quenching of an Anionic Conjugated Polymer: Highly Sensitive Probe for Antioxidants. *Chem. Mater.*, *18*, 3605–3610. https://doi.org/10.1021/cm060062+.
36. Tong, H., Wang, L., Jing, X., Wang, F. (2002). Highly Selective Fluorescent Chemosensor for Silver(I) Ion Based on Amplified Fluorescence Quenching of Conjugated Polyquinoline. *Macromolecules*, *35* (19), 7169–7171. https://doi.org/10.1021/ma025540q.
37. Tang, Y., He, F., Yu, M., Feng, F., An, L., Sun, H., Wang, S., Li, Y., Zhu, D. (2006). A Reversible and Highly Selective Fluorescent Sensor for Mercury(II) Using Poly(Thiophene)s That Contain Thymine Moietiesa. *Macromol. Rapid Commun.*, *27* (6), 389–392. https://doi.org/10.1002/marc.200500837.
38. Fu, Y., Yao, J., Xu, W., Fan, T., He, Q., Zhu, D., Cao, H., Cheng, J. (2015). Reversible and "Fingerprint" Fluorescence Differentiation of Organic Amine Vapours Using a Single Conjugated Polymer Probe. *Polym. Chem.*, *6* (12), 2179–2182. https://doi.org/10.1039/c4py01793e.
39. Chu, H. C., Lee, Y. H., Hsu, S. J., Yang, P. J., Yabushita, A., Lin, H. C. (2011). Novel Reversible Chemosensory Material Based on Conjugated Side-Chain Polymer Containing Fluorescent Pyridyl Receptor Pendants. *J. Phys. Chem. B*, *115* (28), 8845–8852. https://doi.org/10.1021/jp201586c.
40. Lv, F., Feng, X., Tang, H., Liu, L., Yang, Q., Wang, S. (2011). Development of Film Sensors Based on Conjugated Polymers for Copper (II) Ion Detection. *Adv. Funct. Mater.*, *21* (5), 845–850. https://doi.org/10.1002/adfm.201001738.
41. Ding, W., Xu, J., Wen, Y., Zhang, J., Liu, H., Zhang, Z. (2017). Highly Selective "Turn-on" Fluorescent Sensing of Fluoride Ion Based on a Conjugated Polymer Thin Film-Fe^{3+} Complex. *Anal. Chim. Acta*, *967*, 78–84. https://doi.org/10.1016/j.aca.2017.02.027.
42. He, G., Yan, N., Yang, J., Wang, H., Ding, L., Yin, S., Fang, Y. (2011). Pyrene-Containing Conjugated Polymer-Based Fluorescent Films for Highly Sensitive and Selective Sensing of TNT in Aqueous Medium. *Macromolecules*, *44* (12), 4759–4766. https://doi.org/10.1021/ma200953s.
43. Bai, L., Xu, Y., Li, G., Tian, S., Li, L., Tao, F., Deng, A., Wang, S., & Wang, L. (2019). A Highly Selective Turn-on and Reversible Fluorescent Chemosensor for Al^{3+} Detection Based on Novel Salicylidene Schiff Base-Terminated PEG in Pure Aqueous Solution. *Polymers*, *11*(4), 573. https://doi.org/10.3390/polym11040573.
44. Zhao, W., Xiang, Y., Xu, J., He, X., & Zhao, P. (2020). The reversible surface redox of polymer dots for the assay of total antioxidant capacity in food samples. *Microchemical Journal*, *156*, 104805. https://doi.org/10.1016/j.microc.2020.104805.
45. Li, W., Yin, M., Liu, J., Fu, H., Shao, X., Dong, Y., Song, Q., Zhang, C., Wong, W. Y. (2022). Reversible Color Modulation of Luminescent Conjugated Polymers Based on a Chemical Redox Mechanism and Applications in Rewritable Paper and Multiple Information Encryption. *Mater. Horizons*, *9* (8), 2198–2206. https://doi.org/10.1039/d2mh00566b.
46. Kocak, G., Tuncer, C., & Bütün, V. (2017). pH-Responsive polymers. *Polymer Chemistry*, *8*(1), 144–176. https://doi.org/10.1039/C6PY01872F.
47. Miltojevic, A., & Radulovic, N. (2015). Complete assignment of 1H- and 13C-NMR spectra of anthranilic acid and its hydroxy derivatives and salicylic acid and its amino derivatives. *Facta Universitatis - Series: Physics, Chemistry and Technology*, *13*(2), 121–132. https://doi.org/10.2298/FUPCT1502121M.
48. Rajendiran, N., & Balasubramanian, T. (2007). Dual fluorescence of N-phenylanthranilic acid: Effect of solvents, pH and β-cyclodextrin. *Spectrochimica Acta Part A: Molecular and Biomolecular Spectroscopy*, *68*(3), 867–876. https://doi.org/10.1016/j.saa.2006.12.072.

49. Ozkan, S. Zh., Eremeev, I. S., Karpacheva, G. P., Prudskova, T. N., Veselova, E. v., Bondarenko, G. N., & Shandryuk, G. A. (2013). Polymers of diphenylamine-2-carboxylic acid: Synthesis, structure, and properties. *Polymer Science Series B*, *55*(3–4), 107–115. https://doi.org/10.1134/S1560090413030032.
50. Einholm, E. J. (1996). Introduction to Spectroscopy. *Journal of Magnetic Resonance, Series A*, *121*(1), 93–94. https://doi.org/10.1006/jmra.1996.0145.
51. Sivakumar, C., Vasudevan, T., Gopalan, A., & Wen, T.-C. (2001). Chemical Oxidative Polymerization and in situ Spectroelectrochemical Studies of a Sulfonated Aniline Derivative by UV−Visible Spectroscopy. *Industrial & Engineering Chemistry Research*, *40*(1), 40–51. https://doi.org/10.1021/ie0005607.
52. Sophia, I. A., Gopu, G., & Vedhi, C. (2012). Synthesis and Characterization of Poly Anthranilic Acid Metal Nanocomposites. *Open Journal of Synthesis Theory and Applications*, *01*(01), 1–8. https://doi.org/10.4236/ojsta.2012.11001.
53. Chabukswar, V., Horne, A., Bhavsar, S., & Mohite, K. (2012). Studies on Synthesis and Effect of Dopants on Conductivity and Morphology of Organically Soluble Poly(o-anisidine). *Journal of Macromolecular Science, Part A*, *49*(11), 926–930. https://doi.org/10.1080/10601325.2012.722850.
54. Antony, M. J., & Jayakannan, M. (2011). Polyaniline Nanoscaffolds for Colorimetric Sensing of Biomolecules via Electron Transfer Process. *Langmuir*, *27*(10), 6268–6278. https://doi.org/10.1021/la200047t.
55. Ozkan, S. Zh., Eremeev, I. S., Karpacheva, G. P., & Bondarenko, G. N. (2013). Oxidative Polymerization of N-Phenylanthranilic Acid in the Heterophase System. *Open Journal of Polymer Chemistry*, *03*(03), 63–69. https://doi.org/10.4236/ojpchem.2013.33012.
56. Showkat, A. M., Cao, X. T., Kim, D. W., Islam, M. R., & Lim, K. T. (2015). Characterization of poly(diphenylamine)-gold nanocomposites obtained by self-assembly. *IOP Conference Series: Materials Science and Engineering*, *77*, 012007. https://doi.org/10.1088/1757-899X/77/1/012007.
57. Zaragoza-Contreras, E. A., Hernández-Escobar, C. A., Estrada-Monje, A., & Kobayashi, T. (2016). Synthesis of diphenylamine-co-aniline copolymers in emulsified systems using a reactive surfactant as the emulsifying agent and aniline monomer. *Synthetic Metals*, *214*, 5–13. https://doi.org/10.1016/j.synthmet.2016.01.007.
58. Zhang, L., Wan, M., & Wei, Y. (2006). Nanoscaled Polyaniline Fibers Prepared by Ferric Chloride as an Oxidant. *Macromolecular Rapid Communications*, *27*(5), 366–371. https://doi.org/10.1002/marc.200500760.
59. Rohini Das, K., & Jinish Antony, M. (2016). Synthesis and characterization of water dispersible copolymer submicron spheres of poly-(phenylenediamine-co-N-sulfopropyl aniline) via random copolymerisation. *Polymer*, *87*, 215–225. https://doi.org/10.1016/j.polymer.2016.01.078.
60. Pouget, J. P., Jozefowicz, M. E., Epstein, A. J., Tang, X., & MacDiarmid, A. G. (1991). X-ray structure of polyaniline. *Macromolecules*, *24*(3), 779–789. https://doi.org/10.1021/ma00003a022.
61. Athawale, A. A., Deore, B. A., & Chabukswar, V. V. (1999). Studies on poly(diphenylamine) synthesized electrochemically in nonaqueous media. *Materials Chemistry and Physics*, *58*(1), 94–100. https://doi.org/10.1016/S0254-0584(98)00258-2.
62. Ozkan, S. Zh., Bondarenko, G. N., & Karpacheva, G. P. (2010). Oxidative polymerization of diphenylamine-2-carboxylic acid: Synthesis, structure, and properties of polymers. *Polymer Science Series B*, *52*(5–6), 263–269. https://doi.org/10.1134/S1560090410050015.
63. Chan, H. S. O., Ng, S. C., Sim, W. S., Tan, K. L., & Tan, B. T. G. (1992). Preparation and characterization of electrically conducting copolymers of aniline and anthranilic acid: evidence for self-doping by x-ray photoelectron spectroscopy. *Macromolecules*, *25*(22), 6029–6034. https://doi.org/10.1021/ma00048a026.
64. Liu, M., Yin, C., Chen, P., Zhang, M., Parkin, S., Zhou, P., Li, T., Yu, F., & Long, S. (2017). sp_2 CH···Cl hydrogen bond in the conformational polymorphism of 4-chloro-

phenylanthranilic acid. *CrystEngComm*, *19*(30), 4345–4354. https://doi.org/10.1039/C7CE00772H.

65. Orlov, A. v., Ozkan, S. Zh., Bondarenko, G. N., & Karpacheva, G. P. (2006). Oxidative polymerization of diphenylamine: Synthesis and structure of polymers. *Polymer Science Series B*, *48*(1), 5–10. https://doi.org/10.1134/S1560090406010027.
66. Balamurugan, A., Reddy, M. L. P., & Jayakannan, M. (2009). Carboxylic-functionalized water soluble π-conjugated polymer: Highly selective and efficient chemosensor for mercury(II) ions. *Journal of Polymer Science Part A: Polymer Chemistry*, *47*(19), 5144–5157. https://doi.org/10.1002/pola.23566.
67. Kalyanasundaram, K., & Thomas, J. K. (1977). Environmental effects on vibronic band intensities in pyrene monomer fluorescence and their application in studies of micellar systems. *Journal of the American Chemical Society*, *99*(7), 2039–2044. https://doi.org/10.1021/ja00449a004.
68. Rao, G. G., & Sastry, G. S. (1971). Titrimetric determination of ascorbic acid with cerium(IV) sulphate. *Analytica Chimica Acta*, *56*(2), 325–328. https://doi.org/10.1016/S0003-2670(01)82430-2.
69. Yan, Y. E., & Schwartz, F. W. (1999). Oxidative degradation and kinetics of chlorinated ethylenes by potassium permanganate. *Journal of Contaminant Hydrology*, *37*(3–4), 343–365. https://doi.org/10.1016/S0169-7722(98)00166-1.
70. Rao, G. (1966). Potassium dichromate as an oxidimetric reagent. *Talanta*, *13*(11), 1473–1495. https://doi.org/10.1016/0039-9140(66)80096-6.
71. Syrokomsky, W. S., & Stiepin, V. v. (1936). New Oxidation—Reduction Indicators. I. Phenylanthranilic Acid (o-Diphenylamine Carbonic Acid). *Journal of the American Chemical Society*, *58*(6), 928–929. https://doi.org/10.1021/ja01297a024.
72. Sriramam, K. (1973). Some observations on the redox behaviour of N-phenylanthranilic acid indicator in iron(II) titrations. *Talanta*, *20*(4), 383–390. https://doi.org/10.1016/0039-9140(73)80166-3.
73. Kolthoff, I. M., & Sarver, L. A. (1930). Properties of diphenylamine and diphenylbenzidine as oxidation-reduction indicators. *Journal of the American Chemical Society*, *52*(11), 4179–4191. https://doi.org/10.1021/ja01374a001.
74. Bishop, E., & Hartshorn, L. G. (1971). Some observations on oxidation-reduction indicators of the benzidine, naphthidine and diarylamine types. *The Analyst*, *96*(1138), 26. https://doi.org/10.1039/an9719600026.
75. Lederer, M., & Ward, F. L. (1952). The oxidation of the tolyl-anthranilic acids. *Analytica Chimica Acta*, *6*, 1–6. https://doi.org/10.1016/S0003-2670(00)86911-1.
76. Rashidi Nassab, H., Souri, A., Javadian, A., & Amini, M. K. (2015). A novel mercury-free stripping voltammetric sensor for uranium based on electropolymerized N-phenylanthranilic acid film electrode. *Sensors and Actuators B: Chemical*, *215*, 360–367. https://doi.org/10.1016/j.snb.2015.03.086.
77. Hengchang, M., Zhongwei, Z., Yuanyuan, J., Lajia, Z., Chunxuan, Q., Haiying, C., Zengming, Y., Zhiwang, Y., & Ziqiang, L. (2015). Triphenylamine-decorated BODIPY fluorescent probe for trace detection of picric acid. *RSC Advances*, *5*(106), 87157–87167. https://doi.org/10.1039/C5RA12154J.
78. Keizer, J. (1983). Nonlinear fluorescence quenching and the origin of positive curvature in Stern-Volmer plots. *Journal of the American Chemical Society*, *105*(6), 1494–1498. https://doi.org/10.1021/ja00344a013.
79. Borsook, H., & Keighley, G. (1933). Oxidation-Reduction Potential of Ascorbic Acid (Vitamin C). *Proceedings of the National Academy of Sciences*, *19*(9), 875–878. https://doi.org/10.1073/pnas.19.9.875.
80. Mezhuev, Y. O., & Korshak, Y. v. (2020). Theory of chain growth in chemical oxidative polymerization of aniline derivatives. *Synthetic Metals*, *267*, 116445. https://doi.org/10.1016/j.synthmet.2020.116445.

CHAPTER 3

Microscale Redox Titrations Using Poly-N-Phenyl Anthranilic Acid Fluorescent Turn-Off Indicator

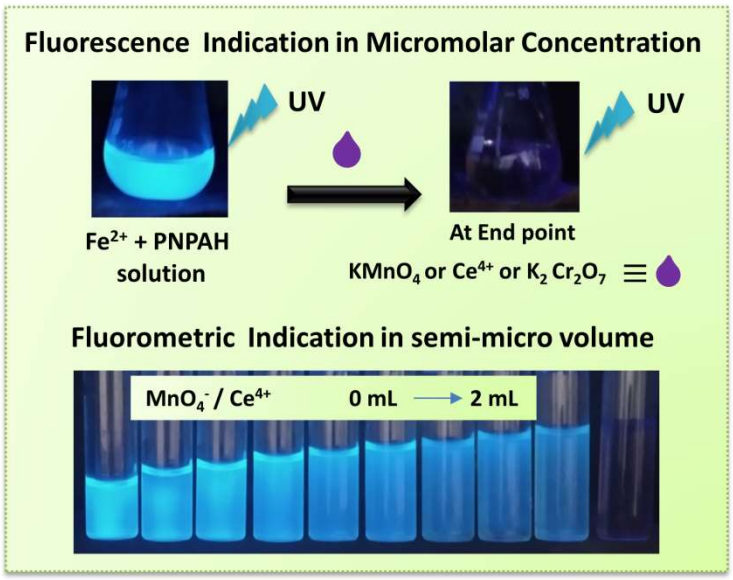

3.1. Introduction

Quantitative analysis is a branch of chemical analysis that includes precise, reliable and accurate determination of the quantity of a substance or substances in the sample. Quantitative analysis has been widely used in biological sample analysis, food analysis, soil analysis, pesticide determination, and environmental pollutant determinations [1-4]. Quantitative analysis is an essential part of quality control procedures to ensure the percentage of purity of products. The methods available for the quantitative analysis can be broadly classified into chemical and physical methods. Titrimetric analysis and colorimetric analysis belong to chemical methods, whereas physical methods include determining physical properties such as refractive index, mass, density, light absorption, magnetic susceptibility, or electromotive force to determine the quantity. Sophisticated instrumentations have improved accuracy of the quantitative analysis, especially at very low concentrations. Chromatographic methods, along with spectroscopic techniques like gas chromatography-mass spectrometry (GC-MS) and liquid chromatography-mass spectroscopy (LC-MS) were commonly used for the determination of the chemical composition of samples [5, 6]. Such sophisticated instrumental methods can detect trace-level quantities of substances, but the need for external calibrations, high maintenance cost, and technical skills reduce their accessibility to common people. In this scenario, one of the earliest chemical methods like titrimetry, remains an important tool still in modern laboratories. The advantages of volumetric or titrimetric analysis are the simple, inexpensive, and well-defined procedures that do not need external calibrations.

Titrimetric analysis is used in pharmaceutical, petroleum, food, and cosmetic industries due to the reliability and accuracy of results, ease of use, and low cost [7]. Advancements in volumetric analysis, such as automated titration systems, were also developed to enhance the speed of titrations and have been used in medical laboratories and hospitals [8, 9]. Microscale titrimetry setup utilizes a microscale apparatus/kit to engage micro-level quantities of analytes (see **Figure 3.1.B.**) [12]. Flint et al. used an automatic pipet to provide micro-volume titrants for microscale acid-base titrations [10]. Gordon et al. determined the hardness of water samples in parts per million quantities using microscale spectrophotometric titration by measuring the absorbance [11]. Richardson et al. used micro-volume quantities of potassium permanganate to determine

water hardness using redox titrations. In this method, the calcium content in water samples was estimated using macroscale titration with 50 mL burette and microscale titrations with 2 mL burette and determined the comparable precision and accuracy of microscale techniques [13]. Microscale analysis has advantages over conventional analysis due to reduced chemical waste and less detrimental effects on environmental pollution. Therefore, microscale titrations allow one to practice green chemistry principles and quantify substances in micromolar concentrations.

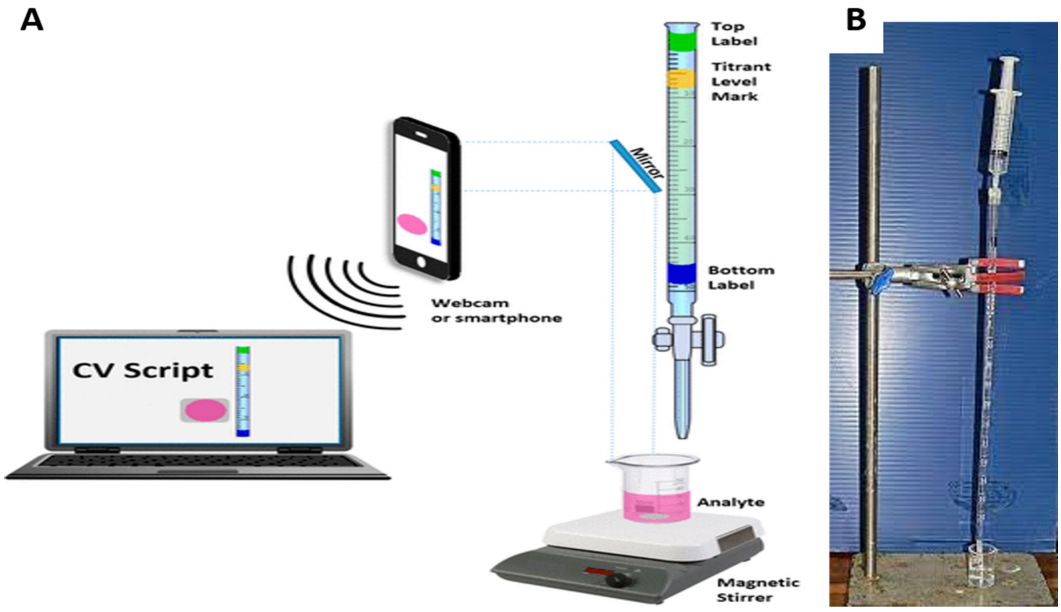

Figure 3.1. *Microscale titration apparatus used in the laboratories. A) Experimental setup for automatic titration (Adapted from Kosenkov et al. 2021). B) Microscale acid-base titration unit (Adapted from RSC Education).*

In titrimetric analysis, the unknown concentration of an analyte is determined by titration, with the titrant having a known concentration. The endpoint of the titration is precisely detected by an indicator that gives a sharp change in colour [15]. The sharp colorimetric transition at the endpoint of indicators was mainly due to a change in light absorption as seen in acid-base titration, complexometric titration, precipitation titrations and redox titrations in response to the change in pH, presence of excess metal ions for complex formation, formation of precipitate, and change in potential respectively [16-21]. Fluorescence is the emission of light in the visible region and, which takes place with high selectivity and sensitivity. Therefore, fluorescence is a widely acceptable tool for various analytical purposes like polymer characterization, monitoring conformational changes, and determining hydration structures [22-24]. Fluorescent indicator

displacement (FID) assays were developed to detect food additives. The interactions between molecules and RNA can also be analysed using fluorescent indicators using their emission properties [25-27]. An efficient fluorescent indicator should satisfy some conditions such as (i) selective fluorescence response with a particular analyte (ii) stability towards chemicals and light (iii) high fluorescence intensity or high quantum yield. Most of the fluorescent indicators have conjugated organic framework, emitting fluorescence after UV light excitation at a particular wavelength [27].

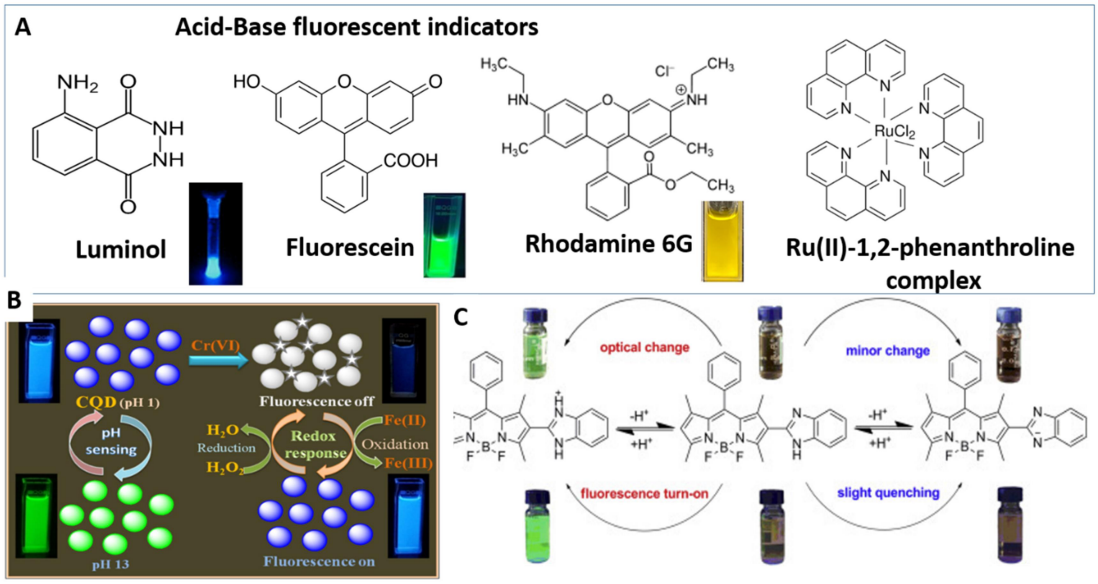

Figure 3.2. *A) Fluorescent organic molecules used in acid-base and redox titrations. B) Quantum dot-based fluorescent indicator for pH sensing and redox titration for* Fe^{2+} *and* Cr^{3+} *(Adapted from Mondal et al. 2019). C) Structural and fluorescence changes associated with Benzimidazole- BODIPY with pH (Adapted from Li et al. 2016).*

Fluorescent indicators detect the end point of the titration either by fluorescence turn on or turn off, which would be sensitive towards metal ion concentration, conformation, redox potential and pH of titrants [28]. Using fluorescent indicators, the titrations of strongly coloured or turbid solutions makes them advantageous over conventional indicators in endpoint detection. Fluorescent indicators have been used in acid-base titrations based on their changes in the fluorescence with respect to pH [29] (see **Figure 3.2.**). Other titrimetry methods that utilize physical properties like pH, potential, turbidity, current, and complex formation are acid-base titrations, potentiometric titrations, precipitation titrations, conductometric titrations, and complexometric titrations. Erdey et al. developed luminol as an acid-base fluorescent indicator used to determine acid content in milk, wine, and cherry juice [30]. Fluorescent indicators for

redox titration have been rarely reported compared to acid-base titrations, complexometric and precipitation titrations [31-34]. The rarity could be due to the mismatched titrant and fluorescent indicator reduction potential, and the less stable fluorescence change at the endpoint. Fluorometric orange-red to non-fluorescent indicating action of 1, 10-phenanthroline and 2, 2'-bipyridine complexes with Ru(II) have been reported for oxidation and reduction titrations [34]. G. Gopala Rao et al reported Rhodamine 6G as a fluorescent indicator for cerimetry and ferrimetry for determination of ascorbic acid, vanadium, molybdenum (V), uranium (IV) [35-37]. The fluorescence indicators used for the titrimetric estimation of various analytes previously reported in the literature were given in **Table 3.1.**

Table 3.1. *Fluorescent indicator, titrant used, estimated analyte and estimated concentration of analytes previously reported in the literature.*

Sl. No.	**Fluorescent indicator**	**Titrant**	**Analyte**	**Concentration of analyte estimated**	**Ref**
1	Ru (II) complex	Iodine	Arsenite or thiosulphate	1×10^{-3} M	37
2	Ru (II) complex	sulfatocerate	Arsenite	1×10^{-6} M	33
3	Rhodamine-6G	Cerium (IV) sulphate	Vanadium	1×10^{-2} M	38
4	Rhodamine-6G	Cerium (IV) sulphate	Molybednum (V) and Uranium (IV)	0.2 mM	35
5	Rhodamine-6G	Fe(III)	Uranium (IV)	0.250 mM	31
6	Rhodamine 6G	Cerium (IV) sulphate	Ascorbic acid	5×10^{-2} M	34
7	Carbon quantum dots from aspartic acid	$K_2Cr_2O_7$	Fe^{2+}	6 mM	39
8	8-Hydroxyquinoline	EDTA	Gallium	50µg/mL	40
9	Acridine Orange, Acriflavin hydrochloride, Safranine O	Cationic polyelectrolyte-Polydiallyl dimethylammonium chloride	Anionic polyelectrolyte-Potassium polyvinyl sulfonate (KPVS)	Charge determination in 1×10^{-4} N KPVS	41

Fluorescent conjugated polymers have broad applications due to their conjugated electronic structures. The excellent electronic and optical properties of conjugated polymers were desirable for developing sensors. Many chemical and biochemical sensors with micro or nano-level detection limits were developed based on fluorescent conjugated polymers because of their enhanced sensitivity to interactions with analytes. The use of fluorescent conjugated polymers as an indicator in the titrations was not reported. The analytical sensing of permanganate ions, cerium (IV) ions, and dichromate ions via fluorescence quenching of bluish-white emission of poly N-phenyl anthranilic acid in acid media (**PNPA-H**) was discussed in Chapter 2. In this chapter, we have introduced poly-N-phenyl anthranilic acid (**PNPA-H)** and N-phenyl anthranilic acid (**NPA-H**) as a fluorescence turn-off indicators for redox titration of ferrous ions against different oxidizing titrants like potassium permanganate, ammonium cerium (IV) sulfate, and potassium dichromate in molar and micromolar (μM) concentrations. Fluorescent indicating actions of **PNPA-H** and **NPA-H** were compared with the standard indicating method and validated the results using student's t-test and F-test. The fluorescent indicators **(PNPA-H** and **NPA-H)** have an added advantage over conventional indicators to detect the endpoint of the analytes in micromolar (μM) concentrations. Additionally, fluorescent indicators **PNPA-H** and **NPA-H** were successfully utilized in semi-micro volume titrations using micro burettes to reduce the excess volume wasted in high concentrations. Microscale redox titration reduces approximately one-ten thousandth of mass, and semi-microvolume titration reduces the one-tenth of volume of analytes than the conventional titrations. Therefore, microscale titrations justify the first principle of green chemistry: "it is better to prevent waste than to treat or clean up waste after it is formed" by reducing quantity of chemicals. [42] In summary, fluorometric endpoint detection of ferrous ion against oxidizing titrants in micromolar redox titration was carried out with one or two drops of fluorescent indicators (**PNPA-H** or **NPA-H**) via a fluorescent turn-off mechanism. A microscale titration experiment, suitable for undergraduate students, was also designed and the results were evaluated based on the students' feedback.

3.2. Experimental

3.2.1 Materials and Reagents: N-Phenyl anthranilic acid (97%) was purchased from LOBA chemicals and further purified by double recrystallization using acetone as

solvent. Poly N-phenyl anthranilic acid was prepared according to the procedure in Chapter 2. [43] Ammonium cerium (IV) sulfate dihydrate (GR), potassium permanganate, potassium dichromate (GR), acetone, and concentrated H_2SO_4 (98%) were purchased from Merck chemicals, India. Ammonium ferrous sulfate hexahydrate (AR) was purchased from Kanton Laboratories. Double-distilled ethanol was used to synthesize polymer, and deionized water was used to prepare solutions of titrants and analytes.

3.2.2. Measurements and Instruments: UV-visible absorption spectra of the samples in deionized water were recorded in 200–800 nm wavelength by Shimadzu UV-Visible spectrophotometer, UV 1800 series. The fluorescence emission of the indicators was checked using long-wavelength UV light in the UV inspection cabinet of Rotek Laboratory Instruments. The UV inspection cabinet can turn on and off for long-wavelength UV light (λ= 365 nm), short-wavelength UV light (λ= 254 nm), and fluorescence tube light. The micro burettes of 10 mL volume capacity with 0.05 mL graduation, 5 mL volume capacity with 20 µL graduation, and 1 mL volume capacity with 10 µL graduation were used. Standard flasks with 10, 100, and 250 mL volumes were used to make up the solutions. In addition, conical flasks or vials of 5, 10, and 50 mL were used to titrate the titrants. A home-built micro-molar titrating setup was used for titrating semi-micro-volume titrations of 1×10^{-4} M solution continuously inside a cardboard box with dimensions 40 × 24 × 12 cms (L × W × H) with amiciVision 21 LED UV torchlight of 395-400 nm wavelength with 3 AAA batteries.

3.2.3. Preparation of indicators

3.2.3.A. Preparation of fluorescent indicator (PNPA-H): PNPA (9.70 mg, 0.046 mmol) was dissolved in 10 mL of concentrated H_2SO_4 (18 M) using a sonicator for 10 minutes. A dark blue-colored solution of **PNPA-H** was obtained. The required indicator concentration was prepared from the stock solution by dilution using deionized water.

3.2.3.B. Preparation of fluorescent indicator NPA-H: NPA (9.70 mg, 0.046 mmol) was dissolved in 10 mL of concentrated H_2SO_4 (18 M) using a sonicator. A pale green color was developed for the **NPA-H** solution. The required indicator concentration was prepared from the stock solution by dilution using deionized water.

3.2.3.C. Preparation of NPA-Na (conventional N-phenyl anthranilic acid indicator): **NPA** (0.1 %, 0.10 g) was dissolved in sodium hydroxide (100 mL, 1 M) solution to get a colorless solution.

3.2.4. Titrations in Micro Molar Concentrations

3.2.4.A. Preparation of standard Mohr's salt solution: The primary standard Mohr's salt (0.98 g) was accurately weighed into a standard flask (250 mL), and sulphuric acid (20 mL, 1 M) was added. The Mohr's salt solution was made up to the mark with deionized water to get 0.01 M standard Mohr's salt solution. Concentrations like 1×10^{-3} M and 1×10^{-4} M were prepared similarly by weighing 0.098 g and 0.0098 g of Mohr's salt, respectively. Other concentrations 1×10^{-5} M, 5×10^{-6} M, and 1×10^{-6} M was prepared from 1×10^{-4} M Mohr's salt solution by dilution using deionized water.

3.2.4.B. Standardization of oxidizing titrants: 0.0790 g of potassium permanganate and 0.1225 g of potassium dichromate were separately dissolved in a 250 mL standard flask using deionized water and made up to the mark to get ~ 0.002 M $KMnO_4$ and 0.0017M $K_2Cr_2O_7$ solutions. 0.6326 g of Ammonium cerium (IV) sulfate dihydrate was gently boiled with sulphuric acid (100 mL, 2 M) to remove ammonia in a beaker and made up to 100 mL in a standard flask for preparing ~ 0.01 M solution. Similarly, we prepared different concentrations of oxidizing analytes like 1×10^{-3} M and 1×10^{-4} M by taking the required mass calculated per the formula MM'V/1000, where M is Molarity, M' is molecular mass and V is volume. Micro-molar concentrations like 1×10^{-5} M, 5×10^{-6} M, and 1×10^{-6} M were prepared from dilution of 1×10^{-4} M.

Standard Mohr's salt solution (10 mL, 1×10^{-4} M), dilute sulphuric acid (5 mL, 1 M), and one drop of **PNPA-H** or **NPA-H** fluorescent indicator were added to 50 mL conical flask. Oxidizing titrant (~ 2×10^{-5} M of potassium permanganate or 1×10^{-4} M cerium ammonium sulfate or 1.7×10^{-5} M potassium dichromate) taken in a micro-burette was added to the Mohr's salt solution taken in a conical flask with manual shaking. Initially, fluorescence intensity was checked after adding 2 mL each of oxidizing agent. When fluorescence intensity changes, volume addition was reduced to 0.5 mL, 0.1 mL, and finally, drop by drop to detect the endpoint. At micro-molar concentration (1×10^{-6} M), the reaction mixture should be thoroughly shaken for 30 seconds near the endpoint due to the low fluorescence intensity of the mixture. Sulphuric acid (5 mL, 2M) was added to the titrating mixture instead of dilute sulphuric acid (1 M) for dichrometry.

3.2.4.C. Estimation of ferrous ion: 3.92 g Mohr's salt was accurately weighed into a 100 mL standard flask, H_2SO_4 (5 mL, 1 M) was added to it and then made up to the mark to 100 mL using deionized water to get ferrous ion solution (1×10^{-1} M). Other concentrations like 1×10^{-2} M, 1×10^{-3} M, 1×10^{-4} M, 1×10^{-5} M, 5×10^{-6} M, and 1×10^{-6} M

was prepared by dilution of bulk concentration or previous higher concentration using deionized water.

Ferrous ion solution (10 mL, ~ 1×10^{-4} M), dilute sulphuric acid (5 mL, 1 M), and one drop of **PNPA-H** or **NPA-H** fluorescent indicator were added to 50 mL conical flask. Oxidizing titrant (~ 2×10^{-5} M potassium permanganate or ~ 1×10^{-4} M cerium ammonium sulfate or ~ 1.7×10^{-5} M potassium dichromate) taken in a 10 mL micro burette was added to the ferrous ion solution taken in a 50 mL conical flask with manual shaking. Fluorescence intensities were checked after 2 mL of volume additions initially. When fluorescence intensity changes, volume addition was reduced to 1 mL, then to 0.1 mL, and finally drop by drop to detect the endpoint. Sulphuric acid (5 mL, 2M) was added to the titrating mixture instead of dilute sulphuric acid (1 M) for dichrometric titrations. Estimating ferrous ions in other micro-molar concentrations like 1×10^{-5}, 5×10^{-6}, and 1×10^{-6} M was conducted by taking the respective concentrations of analytes and titrants.

3.2.5. Titrations in Semi-Micro Volume Scale

Titrations in semi-micro volume utilize titrant volume in 1 mL and 2 mL, significantly reducing the total volume required for the whole batch.

3.2.5.A. Preparation of standard Mohr's salt solution: The primary standard Mohr's salt (0.0392g) was accurately weighed into a standard flask (10 mL) and dilute sulphuric acid was added (20 mL, 1 M). The Mohr's salt solution was made up to the mark with deionized water to get 0.01 M standard Mohr's salt solution.

3.2.5.B. Standardization of oxidizing titrant: Standard Mohr's salt solution (2 mL, ~ 1×10^{-2} M), dilute sulphuric acid (1 mL, 1 M), and one drop of **PNPA-H** fluorescent indicator was added to 10 mL conical flask. An oxidizing titrant (~ 2×10^{-3} M of potassium permanganate or ~ 1×10^{-2} M cerium ammonium sulfate) taken in a 5 mL micro burette was added drop by drop to the Mohr's salt solution. Fluorescence intensity was checked after adding each drop by manual shaking to detect the endpoint.

3.2.5.C. Estimation of ferrous ion: Ferrous ion solution (2 mL, ~ 1×10^{-2} M), dilute sulphuric acid (1 mL, 1 M), and one drop of **PNPA-H** fluorescent indicator was added to 10 mL conical flask. An oxidizing titrant (~ 2×10^{-3} M of potassium permanganate or ~ 1×10^{-2} M cerium ammonium sulfate) taken in a 5 mL micro burette was added drop by drop to the ferrous ion solution. Fluorescence intensity was checked after adding each drop by manual shaking to detect the endpoint.

3.2.6. Procedure for estimation using semi-micro volume in micro molar titrations (1×10^{-4} M**)**: Ferrous ion solution (2 mL, 1×10^{-4} M), dilute sulphuric acid (1 mL, 1 M), and a drop of **PNPA-H** fluorescent indicator was added to a 10 mL conical flask. The oxidizing titrant (~ 2×10^{-5} M of potassium permanganate) taken in a 5 mL micro burette was added to the ferrous ion solution. Fluorescence intensity was checked after adding each drop with manual shaking to detect the endpoint. Similarly, standardization was also performed using semi-micro volume of standard Mohr's salt solution.

3.3. Results and Discussion

Microscale redox titrations in micro-molar concentration reduce chemical waste produced in the lab and avoid over-exposure to concentrated solutions. In addition, microscale titration helps to develop skills in estimating the micro quantities of substances. Redox titrations were usually practiced as a quantitative method for estimating redox analytes in the chemistry lab, especially in undergraduate courses. [44, 45] Microscale redox titrations with good precision and accuracy would be advantageous and align with the green chemistry taught for undergraduate courses. Here, two microscale approaches adopted for redox titrations are micromolar titrations and semi-microvolume titrations. The microscale titrations were carried out with the help of fluorescent indicators like poly-N-phenyl anthranilic acid (**PNPA-H**) or N-phenyl anthranilic acid (**NPA-H**). The UV inspection chamber with UV lamp, UV-torch, and microscale glassware are the primary types of equipment for this method.

3.3.1. Preparation of fluorescent indicators

The fluorescent indicator poly-N-phenyl anthranilic acid (**PNPA**) has been synthesized by the oxidative chemical polymerization of N-phenyl anthranilic acid monomer using ferric chloride as the oxidizing agent in ethanol solvent (**Figure 3.3.**). The polymerization and work-up were completed in five hours without heating, and magnetic stirring.[43] The polymer product has a good yield of 75% and can be stored stably for several months. A stock solution of the fluorescent indicator was prepared by dissolving 9.7 mg **PNPA** in 10 mL concentrated sulphuric acid by sonication for fifteen minutes and kept for one hour without disturbance before its use. The fluorescence of the stock solution of fluorescent indicator **PNPA-H** in H_2SO_4 was stable for up to one month without sonication and shaking.

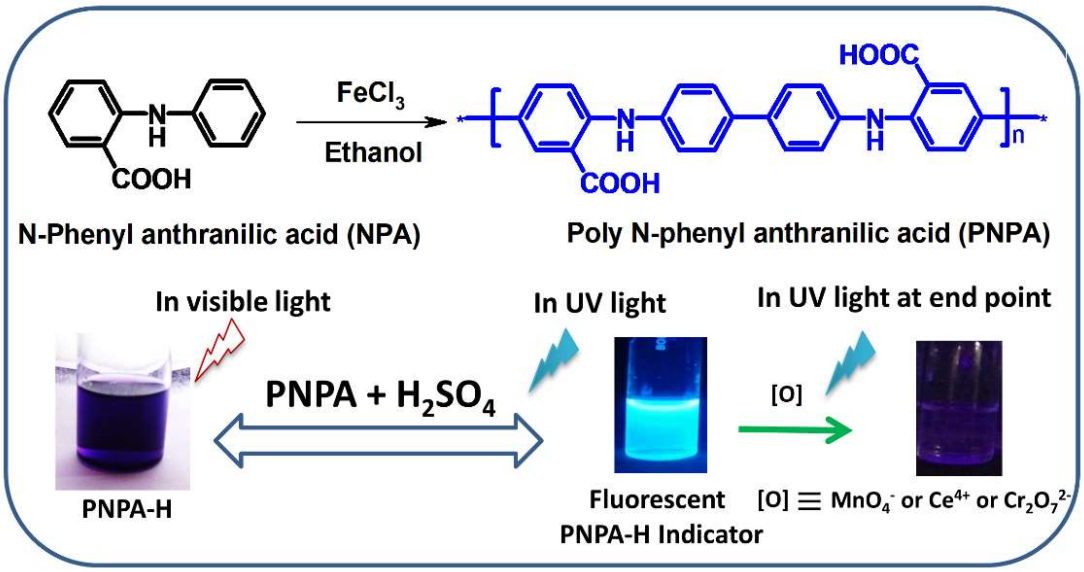

***Figure 3.3**. Synthesis of **PNPA** from **NPA** and its fluorescence quenching action with oxidizing agents in acid media.*

3.3.2. Application of fluorescent PNPA-H and NPA-H in microscale redox titrations

The polymer in a sulphuric acid medium (**PNPA-H)** has intense bluish-white emission, which undergoes fluorescence quenching reaction with oxidizing agents like potassium permanganate, ammonium cerium (IV) sulfate, and potassium dichromate (see **Figure 3.3.**).[43] The [Ox. titrant]/[**PNPA-H**] molar ratios for fluorescence quenching procured by different oxidizing analytes like potassium permanganate, ammonium cerium sulfate, and potassium dichromate were determined to be 7.5, 5, and 250, respectively. [43] Fluorescent indicator (**PNPA-H)** concentration for permanganometry, cerimetry, and dichrometry has to be kept lower than oxidizing titrant concentration as per the molar ratio obtained for fluorescence quenching. The standard redox volumetric method of estimation of ferrous ions, such as dichrometry and cerimetry, uses diphenylamine sulfonate, diphenylamine, and ferroin as indicators. In contrast, permanganometry does not require any external indicators because the permanganate ion has a self-indicting action (colorless to pink) at the endpoint. [46,47] For the present studies, we have selected different concentrations of an analyte such as 1×10^{-2}, 1×10^{-3}, 1×10^{-4}, 1×10^{-5}, 5×10^{-6}, and 1×10^{-6} M (molar to the micromolar) to find out the concentration range applicable for the fluorescent indicators. The higher concentrations like 1×10^{-2} M and 1×10^{-3} M were selected to establish the validity of the results by comparing them with the conventional indicating method. Adding two drops of fluorescence indicator **PNPA-H** to an aqueous

ferrous ion solution (10 mL) produces bright bluish-white fluorescence. Fluorescence emission was checked by irradiating the titrating mixture with long-wavelength UV light (365 nm) repeatedly after adding a definite volume (say 1 mL) of oxidizing titrant, followed by drop-by-drop addition near the endpoint.

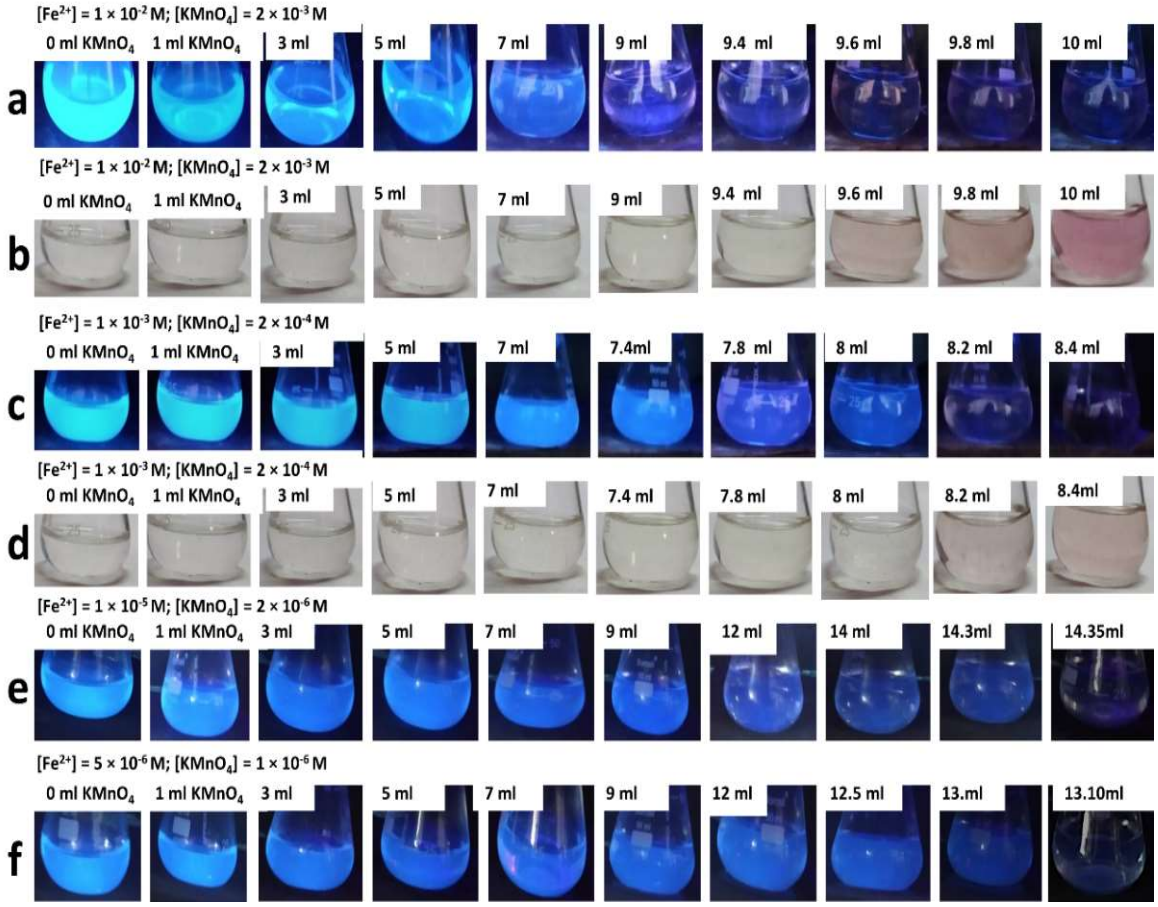

Figure 3.4. *Photographs of endpoint detection in permanaganometry at different concentrations of ferrous ions using* ***PNPA-H*** *as a fluorescent indicator. From top row to bottom a)* 1×10^{-2} *M in UV light, b)* 1×10^{-2} *M in visible light, c)* 1×10^{-3} *M in UV light d)* 1×10^{-3} *M in visible light, e)* 1×10^{-5} *M in UV light and f)* 5×10^{-6} *M in UV light.*

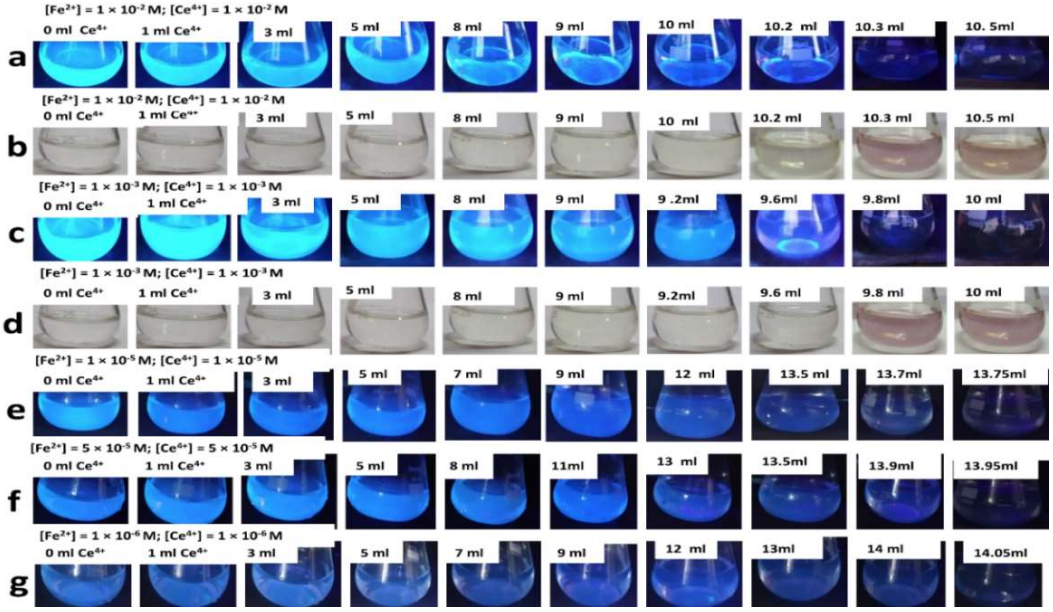

Figure 3.5. *Photographs showing endpoint detection in cerimetry at different concentrations of ferrous ions using* ***PNPA-H*** *as a fluorescent indicator. From top row to bottom a) 1 × 10^{-2} M in UV light b) 1 × 10^{-2} M in visible light c)1×10^{-3} M in UV light d) 1× 10^{-3} M in Visible light e) 1× 10^{-5} M in UV light f) 5×10^{-6} M in UV light and g) 1×10^{-6} M in UV light.*

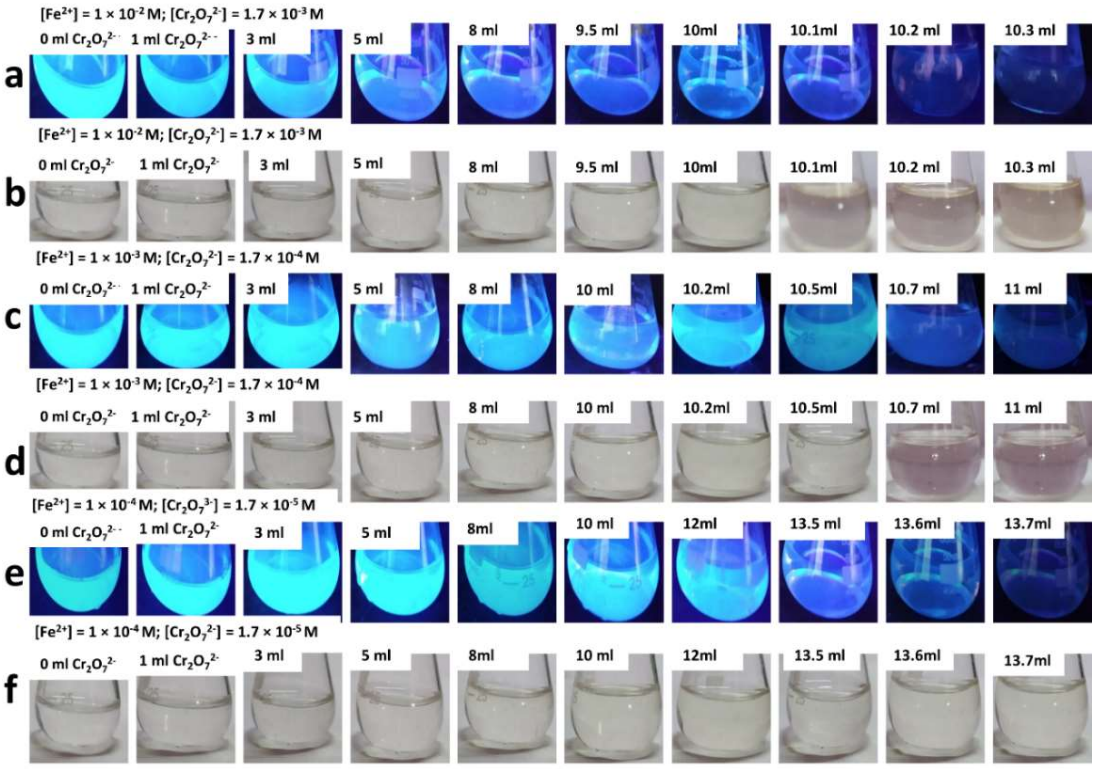

Figure 3.6. *Photographs showing endpoint detection in dichrometry at different concentrations of ferrous ions using* ***PNPA-H*** *as a fluorescent indicator. From top row to bottom a) 1 ×10^{-2} M in UV light, b)1× 10^{-2} M in visible light, c) 1×10^{-3} M in UV light d) 1×10^{-3} M in Visible light, e) 1×10^{-4} M in UV light and f) 1×10^{-4} M in visible light.*

Table 3.2. *Details of analyte, titrant, and indicator concentrations, times of dilution fluorescent indicator from bulk, titrant/ indicator molar ratio, and volume of PNPA-H required for different concentrations.*

Method	Conc. of Fe^{2+} ion (M)	Conc. of oxidizing analyte (M)	Bulk Conc. of PNPA-H Prepared (M)	PNPA-H Conc. (M)	Dilution of FL. Indicator required from bulk Conc.	$[KMnO_4]_{initial}$ /$[PNPA\text{-}H]_{final}$	Drops of PNPA-H
Permanganometry	1×10^{-2}	2×10^{-3}	4.6×10^{-3}	4.6×10^{-3}	1	217.4	1 drops
	1×10^{-3}	2×10^{-4}	4.6×10^{-3}	9.2×10^{-4}	5	108.7	1 drops
	1×10^{-4}	2×10^{-5}	4.6×10^{-3}	4.6×10^{-4}	5-10	10.8- 21.7	1-2 drops
	1×10^{-5}	2×10^{-6}	4.6×10^{-3}	4.6×10^{-5}	100-200	4.3-8.7	5 drops
	5×10^{-6}	1×10^{-6}	4.6×10^{-3}	2.3×10^{-5}	200	8.7	5 drops
	1×10^{-6}	2×10^{-7}	4.6×10^{-3}	9.2×10^{-6}	500	1.1	10 drops
Cerimetry	1×10^{-2}	1×10^{-2}	4.6×10^{-3}	4.6×10^{-3}	5	543	1 drop
	1×10^{-3}	1×10^{-3}	4.6×10^{-3}	9.2×10^{-4}	5	543	1 drop
	1×10^{-4}	1×10^{-4}	4.6×10^{-3}	4.6×10^{-4}	10	108.7	1 drop
	1×10^{-5}	1×10^{-5}	4.6×10^{-3}	9.2×10^{-5}	50	54.3	1 drop
	5×10^{-6}	5×10^{-6}	4.6×10^{-3}	4.6×10^{-5}	100	54.3	1 drops
	1×10^{-6}	1×10^{-6}	4.6×10^{-3}	4.6×10^{-5}	100	10.8	1 drops

The permanganometry titrations of ferrous ion using fluorescent indicator **PNPA-H** at different concentrations 1×10^{-2}, 1×10^{-3}, 1×10^{-5}, and 5×10^{-6} M were shown respectively in **Figure 3.4. (a-f)**. It was evident from the photographs that bluish-white emission from the **PNPA-H** indicator decreased with the addition of potassium permanganate ions near the endpoint. Fluorescence was quenched entirely at the endpoint by adding one or two drops of permanganate solution. The addition of excess drops of $KMnO_4$ did not produce further changes. The indicating effect of **PNPA-H** in the visible light was also checked (see **Figure 3.4.b** and **3.4.d**). Pink and pale pink for 1×10^{-2} and 1×10^{-3} M concentrations were respectively noticed at the endpoint. No noticeable color change was obtained for other lower titrant concentrations. Conventional indicators or self-indicators could not detect the endpoint of the analyte for concentrations lesser than 1×10^{-3} M due to the low optical density and poor color change by mixing with the titrant.

However, fluorescent indicators emit intense fluorescence by applying UV light even at micromolar concentration, which can be detected by the eye. The endpoints of fluorometric and colorimetric indicating methods almost matched each other, as shown in **Figure 3.4**. The molar ratio of **[$KMnO_4$]/ [PNPA-H]** has to be kept between the range 10-650, while varying the analyte concentration from 1×10^{-2} M to 1×10^{-6} M to get precise fluorescence quenching at the endpoint. The concentration range of analytes and indicators used for the titrations are shown in **Table 3.2**. The limit of detection (LOD) of fluorescent indicators (**PNPA-H**) via the naked eye was 0.1 μM, making fluorometric endpoint detection of ferrous ion possible in 1 μM concentration. We have conducted the cerimetry and dichrometry titrations using a **PNPA-H** fluorescent indicator similar to permanganometry titration; see **Figure 3.5. (a-g)** for cerimetry and see **Figure 3.6. (a-f)** for dichrometry**.** The molar ratio of fluorescence quenching for [$\mathbf{Cr_2O_7^{2-}}$]/ [**PNPA-H**] was 250, so we could not conduct the redox titrations below 1×10^{-4} M.

The monomer N-phenyl anthranilic acid is a versatile conventional redox indicator in dichrometry and cerimetry. However, fluorescence indicating actions of **NPA** in an acid medium has not been explored for fluorometric titrations. The N-phenyl anthranilic acid dissolved in concentrated sulphuric acid (**NPA-H**) has developed pale green in visible light and bluish-white emission in UV light. Permanganometric titrations of ferrous ions have been carried out in 1×10^{-2} to 1×10^{-6} M concentrations using **NPA-H** as a fluorescent indicator similar to **PNPA-H,** shown in **Figure 3.7. (a-g)**. The **NPA-H** as a fluorescent indicator at different concentrations in cerimetry and dichrometry was shown in **Figure 3.8. (a-g)** and **Figure 3.9. (a-f).** The fluorometric indicating effect of **PNPA-H** and **NPA-H** have a similar fluorescence quenching effect due to the similar redox mechanism. The advantage of the **NPA-H** indicator is its commercial availability as **NPA**, whereas **PNPA** has to be prepared from **NPA** by a step of 5 h duration. The fluorescence indicator **NPA-H** has the same limit of detection (LOD) of 0.1 μM as **PNPA-H**.

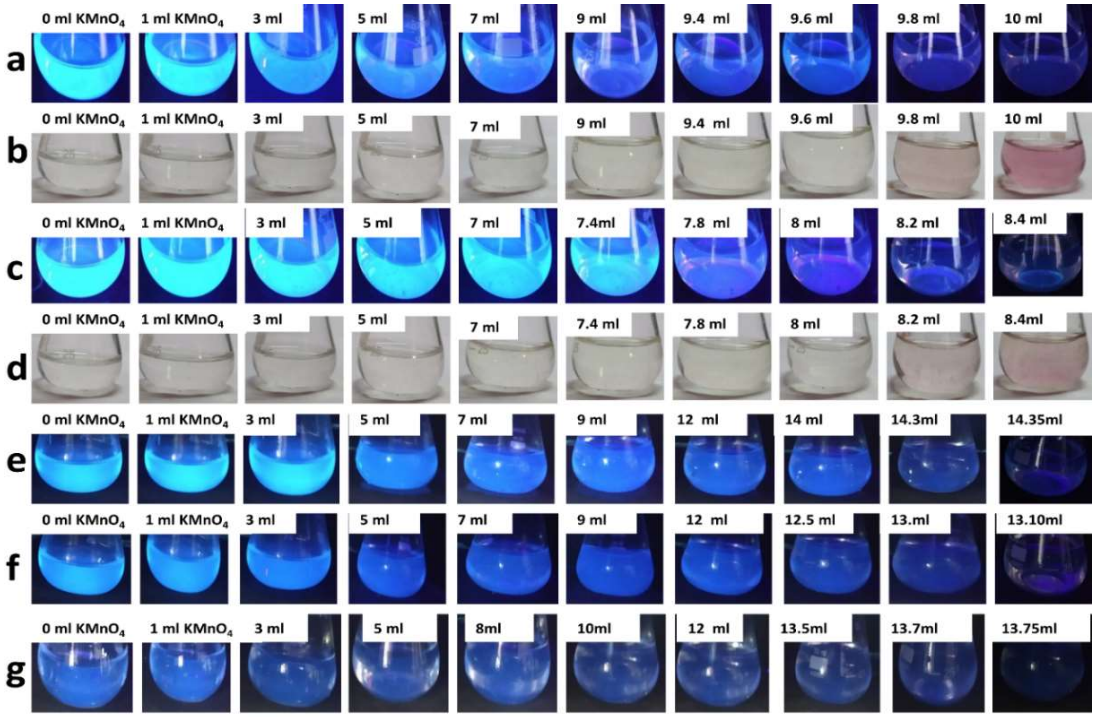

Figure 3.7. *Photographs showing endpoint detection in permanaganometry at different concentrations of ferrous ions using* ***NPA-H*** *as a fluorescent indicator. From top row to bottom a) 1 × 10^{-2} M in UV light, b) 1 × 10^{-2} M in visible light, c) 1 × 10^{-3} M in UV light, d) 1 × 10^{-3} M in Visible light e) 1 × 10^{-5} M in UV light, f) 5 × 10^{-6} M in UV light and g) 1 × 10^{-6} M in UV light.*

Figure 3.8. *Photographs showing endpoint detection in cerimetry at different concentrations of ferrous ions using* ***NPA-H*** *as a fluorescent indicator. From top row to bottom, a) 1× 10^{-2} M in UV light, b) 1× 10^{-2} M in visible light, c) 1× 10^{-3} M in UV light, d) 1× 10^{-3} M in visible light, e) 1× 10^{-5} M in UV light, f) 5× 10^{-6} M in UV light and g) 1× 10^{-6} M in UV light.*

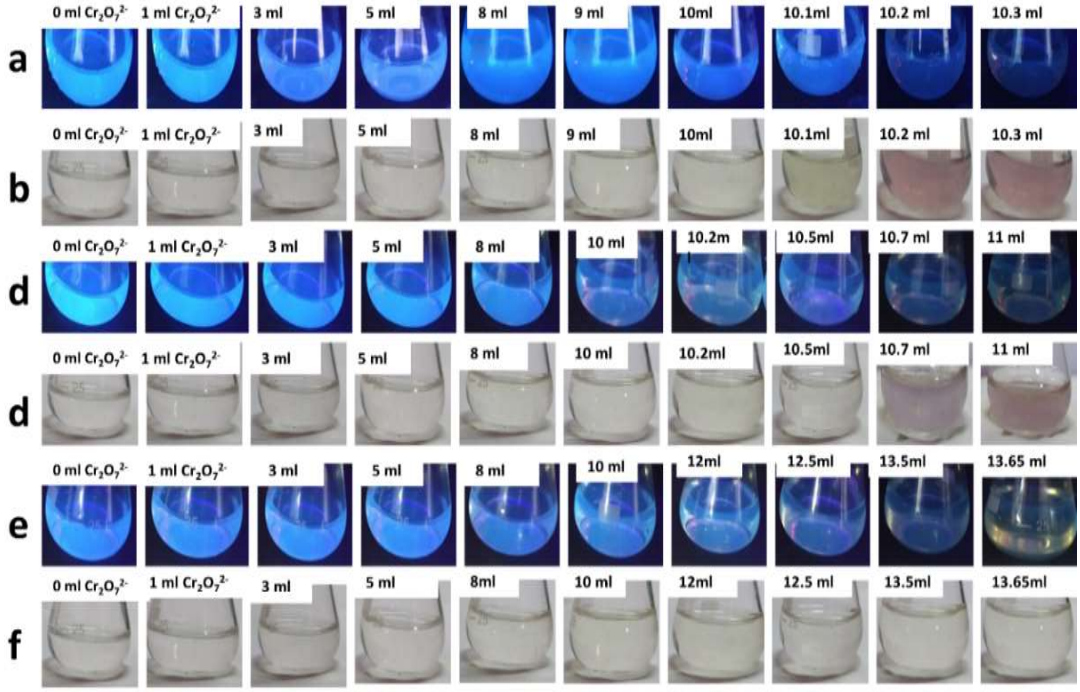

Figure 3.9. *Photographs showing endpoint detection in dichrometry at different concentrations of ferrous ions using* ***NPA-H*** *as a fluorescent indicator. From top row to bottom, a) 1×10^{-2} M in UV light, b) 1×10^{-2} M in visible light, c) 1×10^{-3} M in UV light, d) 1×10^{-3} M in visible light, e) 1×10^{-4} M in UV light, and f) 1×10^{-4} M in visible light.*

3.3.3. Application of fluorescent indicator PNPA-H in semi-micro volume redox titrations

The permanaganometry and cerimetry estimation of ferrous ion was carried out in semi-micro volume (1 mL and 2 mL) by semi-micro burettes using fluorescent indicator **PNPA-H**. The minimum drop volume used in a 1 mL micro burette at the endpoint produces a slight variation in the precision for 1 mL of titrant, and utmost care must be taken to operate such a micro burette to avoid bubbles and breakage. [49] Whereas accurate, precise, and faster results could be easily obtained by taking 2 mL titrant volume in a 5 mL micro burette. The photographs of semi-micro volume titrations in permanganometry and cerimetry were given in **Figure 3.10.** and the mass of ferrous ions in **Table 3.3**. Semi-micro volume titrations with fluorescent indicators have given sharper endpoint detection. Besides reducing the volume of the titrants, the time required for the whole experiment can be reduced to less than one-half of conventional titration carried out in 10 mL or 20 mL.

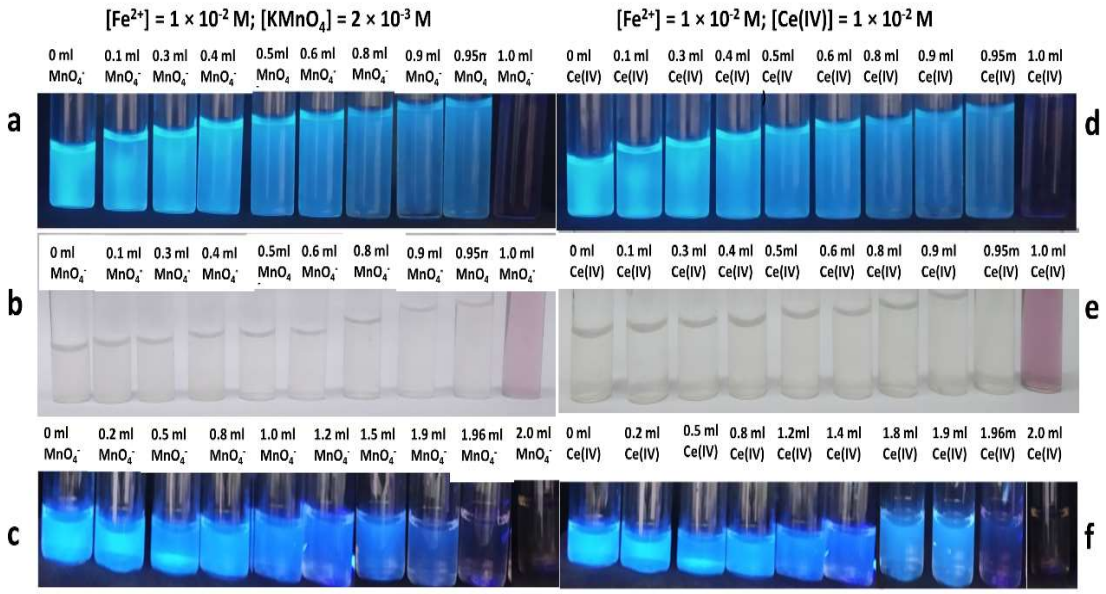

***Figure 3.10**. Photographs show semi-micro volume titrations of ferrous ions with endpoint detection using fluorescence indicator **PNPA-H.** Ferrous ion solution (1 × 10^{-2} M) titrated against potassium permanganate solution (2 × 10^{-3} M) using 1 mL volume in the presence of UV light (a) and visible light (b) and using 2 mL volume in the presence of UV light (c). Ferrous ion solution (1 × 10^{-2} M) titrated against cerium ammonium sulfate solution (1 × 10^{-2} M) using 1 mL in the presence of UV light (d) and visible light (e) and using 2 mL in the presence of UV light (f).*

***Table 3.3.** Comparative mass values of ferrous ions estimated by conventional titrations and semi micro-volume redox titration using fluorescent indicators.*

Sample	Oxidizing Titrant	Estimated Mass of Fe^{2+} Ions for 1×10^{-2} M Concentration, g, by Analyte Volume and Method		
		Conventional Indicating Method	Semi micro Volume Using fluorescent PNPA-H indicator	
		10mL volume	1mL volume	2mL volume
1	$KMnO_4$	5.3378 ×10^{-2}	5.3855 × 10^{-2}	5.3400 × 10^{-2}
2	Ce (IV)	5.3237 ×10^{-2}	5.3616 × 10^{-2}	5.3282 × 10^{-2}

3.3.4. Mechanism of fluorescent indicators

UV-visible absorption spectra of **NPA-H** and **PNPA-H** were recorded before the endpoint and at the endpoint in the presence of ferrous ions and UV-visible spectra show a change in an absorption band. (See **Figure 3.11.**). The broad vibronic peak centered at

around 400 nm was transformed into a new absorption band centred at 525 nm, corresponding to the oxidized form of the diquinoid structure, which has a characteristic wine-red color. [48,49] A colorless **PNPA-H** + Fe^{2+} ions solution mixture in visible light has shown bluish-white emission upon UV irradiation (see the first vial in first-row of **Figure 3.11.A and B** in inset**)**. On the other hand, the photographs of titrating mixture with different analytes at the endpoint were non-fluorescent in the presence of UV light and had a characteristic wine-red color in visible light (especially for higher analyte concentrations). The quenching of fluorescence and the appearance of wine-red was due to the oxidation of **NPA-H** and **PNPA-H**.

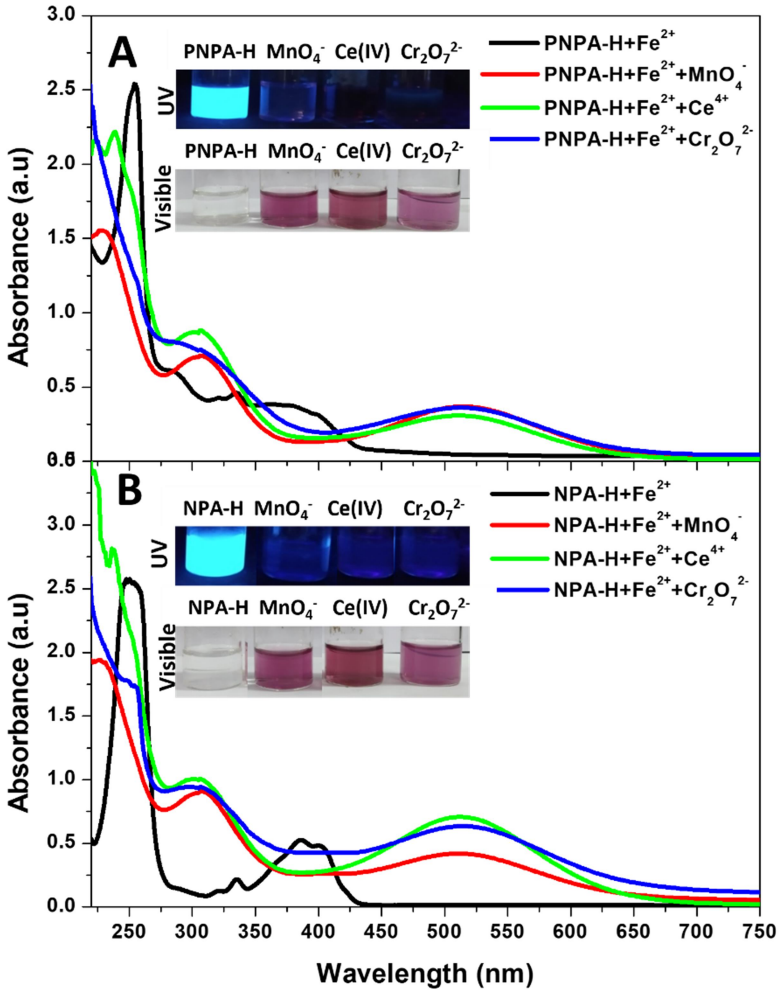

Figure 3.11. *UV-visible absorption spectra of titrating mixture with fluorescence indicators* ***PNPA-H*** *(A) and* ***NPA-H*** *(B) before and at the endpoint in molar concentrations. The inset shows the titrating mixture in UV light (top row) and visible light (bottom row).*

The mechanism of the color change of **NPA** in conventional redox titrations has been reported in the literature. [48] The colorless **NPA** monomer was dimerized irreversibly to diphenyl benzidine dicarboxylic acid (colorless), which subsequently undergoes oxidation at the endpoint to get violet-colored diphenyl diquinoid dicarboxylic acid by oxidizing agents (see **Figure 3.12**). Poly-N-phenyl anthranilic acid (**PNPA)** contains 4-6 repeating diphenyl benzidine dicarboxylic acid units. Ferrous ion was oxidized to ferric ion by adding oxidizing analytes, at the endpoint, the fluorescent indicator **NPA-H** or **PNPA-H** oxidized to non-fluorescent diphenyl diquinoid dicarboxylic acid form. The ferric ions formed as a by-product could not oxidize fluorescent indicators to diquinoid structure due to potential mismatch at those concentrations. [46] The interference of ferric ions was noted when ferric ions were taken directly with the **PNPA-H** fluorescent indicator at a concentration greater than 2.5×10^{-2} M with a higher **[Fe^{3+}]/[PNPA-H]** ratio greater than 650. The redox reactions involved in the permanganometry, cerimetry, and dichrometry were given below.

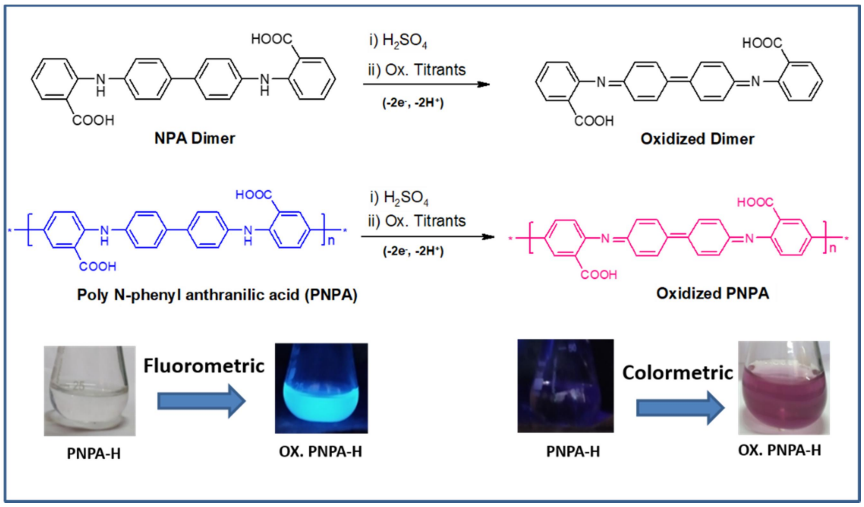

Figure 3.12. *Mechanism of fluorometric indicating action of* ***PNPA-H*** *and* ***NPA-H*** *in the redox titrations.*

3.3.5. Method Validation

Method validations for standardization and estimations of permanganometry, cerimetry, and dichrometry were repeated ten times in 1×10^{-2} M and 1×10^{-3} M concentrations (see **Table 3.4., Table 3.5.**, and **Table 3.6.)**. The narrow distributions of mass obtained from titrations using **PNPA-H and NPA-H** indicated precision of mass obtained from fluorescent indicating methods (**see Figure 3.13.**).

Table 3.4. *Comparative mean mass values of ferrous ions obtained experimentally using conventional indicating method and fluorometric indicating methods in permanganometry.*

Sample	**Fe^{2+} Ion Molarity for Permanagometry**	**Mean mass of Fe^{2+} Ion, g, obtained using these methods**		
		Conventional Indicating Method	**Fluorescent PNPA-H Indicating Method**	**Fluorescent NPA-H Indicating Method**
1	1×10^{-2}	$6.06\times10^{-2}\pm 7.3\times10^{-4}$	$6.02\times10^{-2}\pm 4.9\times 10^{-4}$	$6.03\times10^{-2}\pm 6.0\times 10^{-4}$
2	1×10^{-3}	$5.61\times10^{-3}\pm 4.5\times10^{-5}$	$5.63\times10^{-3}\pm 4.9\times 10^{-5}$	$5.62\times10^{-3}\pm 2.6\times10^{-5}$
3	1×10^{-4}	_	5.74×10^{-4}	5.76×10^{-4}
4	1×10^{-5}	_	5.74×10^{-5}	5.72×10^{-5}
5	5×10^{-6}	_	2.82×10^{-5}	2.80×10^{-5}
6	1×10^{-6}	_	5.67×10^{-6}	5.73×10^{-6}

Table 3.5. *Comparative mass values of ferrous ions estimated by cerimetry using conventional and fluorescent indicators for different molarity range.*

Sample	**Fe^{2+} ion Molarity for Cerimetry**	**The estimated mass of Fe^{2+} ions, g, by analyte concentration and method**		
		Conventional indicating method	**Fluorescent PNPA-H Indicating method**	**Fluorescent NPA-H Indicating Method**
1	1×10^{-2}	$5.70\times10^{-2}\pm 3.7\times 10^{-4}$	$5.71\times10^{-2}\pm 2.5\times 10^{-4}$	$5.6874\times10^{-2}\pm 2.7\times10^{-4}$
2	1×10^{-3}	$5.70\times10^{-3}\pm 2.0\times10^{-5}$	$5.71\times10^{-3}\pm 2.7\times10^{-5}$	$5.7043\times10^{-3}\pm 4.0\times10^{-5}$
3	1×10^{-4}	_	6.0276×10^{-4}	6.0258×10^{-4}
4	1×10^{-5}	_	5.7533×10^{-5}	5.7322×10^{-5}
5	5×10^{-6}	_	2.6962×10^{-5}	2.6764×10^{-5}
6	1×10^{-6}	_	5.7507×10^{-6}	5.7109×10^{-6}

***Table 3.6**. Comparative mass values of ferrous ions estimated by dichromometry using conventional and fluorescent indicators for different molarity range.*

Sample	Fe^{2+} ion Molarity For Dichrometry	The Estimated Mass of Fe^{2+} ions, g, by analyte concentration and method		
		Conventional indicating method	Fluorescent PNPA-H Indicating method	Fluorescent NPA-H Indicating Method
1	1×10^{-2}	$5.69\times10^{-2} \pm 3.5\times10^{-4}$	$5.69 \times10^{-2} \pm 2.6 \times10^{-4}$	$5.70 \times10^{-2} \pm 2.8 \times10^{-4}$
2	1×10^{-3}	5.54×10^{-3}	5.4904×10^{-3}	5.5176×10^{-3}
3	1×10^{-4}	_	5.7100×10^{-4}	5.6899×10^{-4}

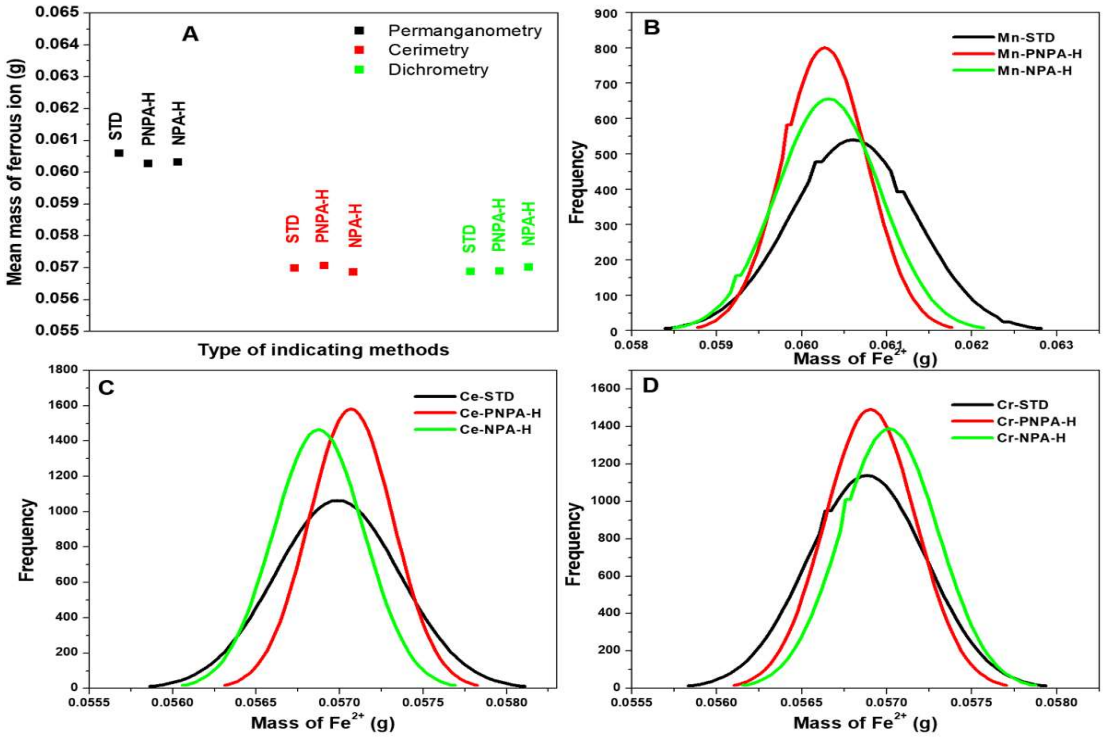

***Figure 3.13.** A) Mean masses of ferrous ion estimated using conventional and fluorometric indicating methods for 10^{-2} M concentration. The standard distribution curves of mass were obtained from B) permanganometry, C) cerimetry and D) dichrometry for 10^{-2} M analyte concentrations.*

Student's t-test and F-test were reported as tests of significance for the fluorometric indicating method by comparing it with the standard indicating method. The

standard deviation of the mass of ferrous ions obtained in both methods was taken to calculate Student's t-test and F-test. The critical values were obtained statistically for the Student's t-test with 18 degrees of freedom and 95% probability, and the variance ratios based on the F-test for 9 degrees of freedom and P = 0.05 (P=0.05 indicates probability level, which corresponds to 95% confidence interval). The calculated values did not exceed the critical values ($t_{critical}$ = 1.74 & $F_{critical}$ = 3.18) in all three redox titrations (see **Table 3.7.** and **Figure 3.14.**). [50-52] The Student's t-test and variance ratio-based F-test show that the fluorescent indicating method using **PNPA-H** and **NPA-H** was significant. Therefore, statistical validations have strengthened the estimation of ferrous ions in micromolar redox titration using fluorescent indicators.

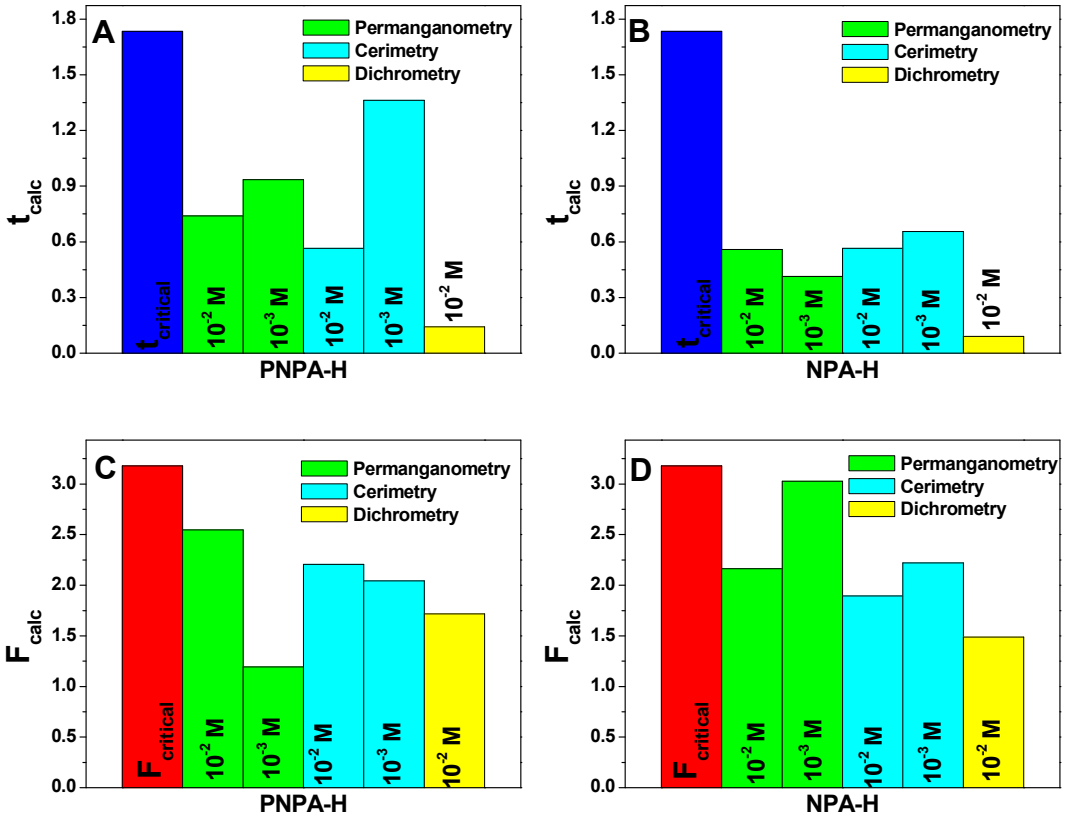

Figure 3.14. *Bar diagram showing the comparison of* $t_{critical}$, $t_{calculated}$, $F_{critical,}$ *and* $F_{calculatd}$ *values for a fluorometric indicating method of* ***PNPA-H*** *(A and C) and* ***NPA-H*** *(B and D).*

Table 3.7. *Comparative results of statistical f test and student's t-test taken for redox titrations using fluorescent and conventional indicators.*

Type of Redox titration & concentrations	Degrees of freedom		F_{calc} PNPA-H	T_{calc} PNPA-H	F_{calc} NPA-H	T_{calc} NPA-H
	F test	Student's t-test				
Permanganometry(10^{-2} M)	9	18	0.24	0.74	2.16	0.55
Permanganometry(10^{-3}M)	9	18	1.19	0.93	3.02	0.41
Cerimetry(10^{-2} M)	9	18	2.20	0.56	1.89	0.76
Cerimetry(10^{-3}M)	9	18	2.04	1.36	2.21	0.65
Dichrometry(10^{-2} M)	9	18	1.71	0.14	1.48	0.091

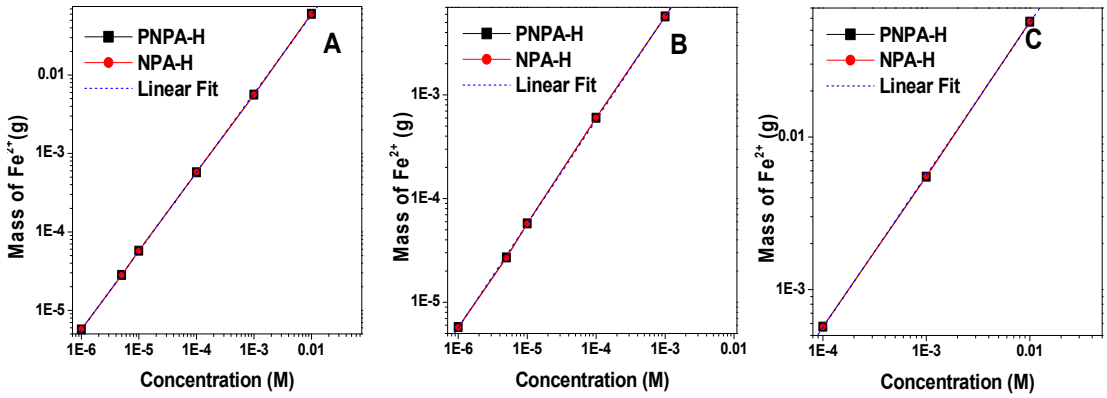

Figure 3.15. *Linear regression of estimated mass of Fe^{2+} ions using fluorometric indicating methods at different concentrations via dilution A) permanganometry, B) cerimetry, and C) dichrometry.*

We have also made a linear regression analysis of the estimated mass of ferrous ions against different concentrations obtained via dilution using fluorometric indicating methods (see **Figure 3.15.**). The plots with good linear response and correlation coefficients equal to 0.999 were obtained. [52] The p-value from linear regression analysis was less than 0.05, indicating the significant dependence between the estimated mass and the concentration of solutions estimated by fluorescent indicating methods. The concentration of titrants and the fluorescent indicator used in the micromolar

concentration reduce chemical waste; thus, the experiment aligns with the concept of the first principle of green chemistry. Further, fluorescence-assisted microscale redox titrations can be extended to volumetric estimations of certain drugs, ascorbic acid, sodium nitrite, hydrogen peroxide, and sodium arsenite.

3.3.6. Experiment overview

Based on the above studies, a microscale redox titration was designed for upper-grade undergraduate students who study green chemistry and photochemistry principles. Microscale analysis primarily involves minimizing the use of the chemical and its exposure without compromising the result and creating an eco-friendly lab experience. The redox titration of ferrous ions against an oxidizing analyte by any titrimetry method includes weighing, standardization, and estimation, usually a minimum two-hour-long experiment. We have carried out the redox titration using fluorescent indicators a) in molar concentrations (1×10^{-2} - 1×10^{-3} M), b) in micromolar concentration (1×10^{-4} - 1×10^{-6} M), and c) in semi-micro volumes (1-2 mL) and results obtained compared to evaluate the benefits of microscale titrations. Before and after the lab session, pre-lab surveys and post-lab surveys were carried out to evaluate students' knowledge and experience on microscale estimations. The micromolar redox titrations reduce the quantities of analytes used, and semi-micro volume titration reduces the volume of analytes and the time required for the titration. Therefore, besides practicing redox chemistry in quantitative analysis, students quickly get the idea of the microscale analysis at the outset of green chemistry and fluorescence turn-off. Significant learning outcomes for the present experiment are focused on the following.

1) To apply the green chemistry principle by microscale redox titration in reducing chemical waste generated in the lab.
2) To develop skills in microscale titrations with the aid of fluorescent indicators.
3) To reduce the exposure and toxicity by taking less mass and volume of titrant and analyte.
4) To estimate the mass of ferrous ions precisely and accurately from micromolar concentrations.

3.3.7. Experiment design

The experiment design involves titrations to estimate the mass of ferrous ions using potassium permanganate or ammonium cerium sulfate in molar concentration (1 × 10^{-2} M), micromolar concentration (1×10^{-4} M or 1×10^{-6}), and semi-micro volume (2 mL, 1×10^{-2} M) with the help of fluorescent **PNPA-H** indicator. Two separate batches of 20 students were allowed to perform the experiment. The first batch was arranged in four groups, with five undergraduate students in each group. The second batch of participants was randomly selected from undergraduates, graduates, and researchers who could give critical feedback on the experiment, and they were allowed to experiment individually as a part of an add-on course introduced for microscale analysis. The first titration uses standard molar concentrations, the second titration uses micromolar concentrations, and the third titration reduces the volume to semi-micro volume. The effectiveness of fluorescent indicating actions can be directly visible from these titrations in different concentrations and volumes. Finally, a fourth titration was used to determine the mass of ferrous ions in molar concentration (1×10^{-2} M) with a self-indicator or conventional indicator. The same ferrous ion solution and titrant solutions can be used for all titrations except micromolar titrations to compare the results. The results of these titrations were assessed in three categories a) fluorescent indicator vs. conventional indicator, b) molar vs. micromolar concentrations, and c) molar vs. semi-micromolar volume. The first category explains the advantage of fluorescent indicators versus conventional indicators. The second and third categories show how much the quantity of the analyte can be reduced very efficiently in micromolar concentrations or semi-micro volumes, besides accurately determining the mass of ferrous ions at low concentrations. The maximum time to complete all the above experiments together is three hours. Therefore, after familiarizing the above titrations, micromolar or semi-micro volume titration can be

directly performed with much less time. A very economical home-built micro-scale titration setup for endpoint detection was applied using a UV torch with a 395 nm LED source, allowing students to continuously do semi-micro molar titration (1×10^{-4} M) inside the setup (see **Scheme 1**).

Figure 3.16. *A) Schematic representation and B) photograph of home-made semi-micro volume titrating setup for fluorometric indicating method.*

3.3.8. Experiment evaluation

Titrations in molar concentration of analyte (1×10^{-2} M) have been carried out using the fluorescent and conventional indicators. Students could easily detect and compare the endpoints in both indicating methods by noting fluorescent turn-off in fluorescent indicators and color change in the conventional method. The titrant volumes obtained in both cases were almost identical in both methods, providing the student and instructor confidence in the new method's accuracy and comfort in using the fluorescent indicator. Placing a reference solution in the UV cabinet was also helpful to detect the endpoint easily. Initial use of the microscale apparatus was slightly unfamiliar for a few students; however, they felt comfortable after second or third titration. Some students first thought fluorescent indicators were an alternate indicating method without recognizing the extended applications. They queried

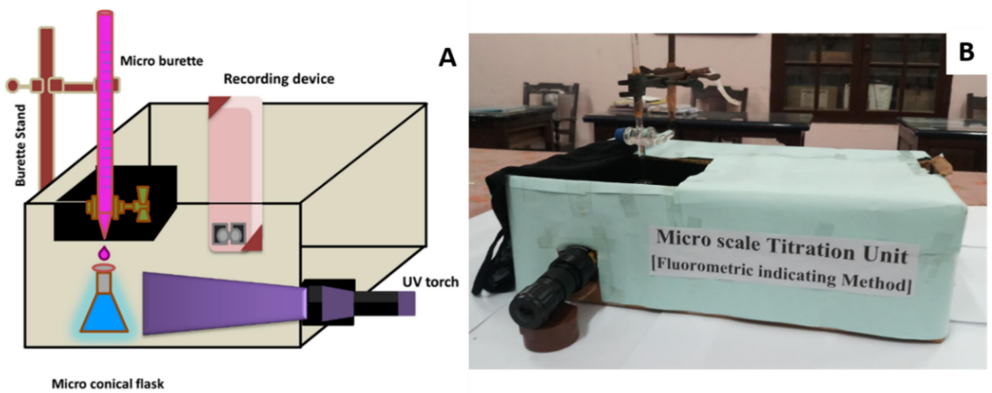

the instructor, "what is the relevance of fluorescent indicators." The titrations in micromolar concentrations (1×10^{-4} - 1×10^{-6} M) have produced fluorescent turn-off in the fluorescent indicating method, whereas no color change in the conventional indicating method. Therefore, students could easily understand working fluorescent indicators in a lower concentration and precise determination of a few micrograms of ferrous ions. Microscale redox titrations allow the students to measure the mass of ferrous ions in between the 5 μg - 500 μg from 1×10^{-6} M to 1×10^{-4} M concentrations. By comparing micro-scale titrations and conventional titrations, the students learned the chemical quantity that could be saved in each lab.

The students have conducted semi-micro volume titrations of ferrous ions in molar concentration (1×10^{-2} M) using a fluorescent **PNPA-H** indicator. The ferrous ion analyte (2 mL) was easily titrated against an oxidizing titrant taken in a 5 mL micro burette within 2-3 minutes. In molar concentrations (1×10^{-2} M), students detected the endpoint as a sharp fluorescence turn-off in UV light and the appearance of wine red color in visible light. The semi-micro volume titrations promote microscale apparatus to limit the volume used for titrations. Few students were concerned about the accuracy of the result before the experiment. They assumed that the accuracy of results would be impoverished by reducing the volume of titrants. The comparable mass of Fe^{2+} ions obtained from conventional and semi-micro volume titrations clarified their apprehension, and they understood that 2 mL was sufficient for precise endpoint detection in this method. The presence of fluorescence indicator in a small volume of 1 or 2 mL had a much-pronounced indicating effect than the conventional indicating method, which can minimize the constant error that can arise when we reduce the volume from higher to lower. Semi-micro volume titrations can be easily extended to micromolar concentrations. Estimation using semi-micro volume in micromolar titration of 1×10^{-4} M solution of ferrous ions against potassium permanganate was carried out in a home-made microscale titrating unit, and checking of the fluorescence emission was monitored continuously inside the setup using a portable UV torch of 395 nm instead of a fixed UV lamp of 365 nm inside UV inspection cabinet. The endpoint was the quenching of the bluish-white color and appearance of the violet from UV source, and the method minimizes any harmful effect of UV radiation. The time taken to complete the titration directly depends on the volume taken, whether it is molar or micromolar titration. Students who experimented with semi-micro volume titration have reduced the time of the entire

experiment by less than one-half the usual way. Students gained awareness about the time benefits of the experiment and reduced the excessive use of the chemicals in the lab as green chemistry practice.

After the experiment, the students submitted their lab reports with tables and calculations to the instructors. The estimated masses of analytes were tabulated in **Table 3.8.** The standard deviations of the estimated mass of ferrous ions obtained from molar concentration, micromolar concentration, semi-micro volume using the fluorescent indicating method and molar concentration using the conventional method were obtained to be as 1.84×10^{-3}, 2.68×10^{-5}, 2.10×10^{-3}, 1.47×10^{-3} respectively. The precision of the results indicates that students have developed skills in semi-micro volume titrations and micromolar titrations using the fluorescent indicator. A post-lab survey was conducted to assess the students' learning outcomes, performance, and lab experience (see **Table 3.9.**). Before the experiment, a pre-lab survey was given to assess the student's awareness about microscale titrations, green chemistry, and fluorescence indicator (see **Table 3.9.**). Before the experiment, students have limited knowledge of microscale titrations and fluorescent indicators. Before the experiment, students (< 30%) perceived that microscale titrations could not be achieved at laboratories as volumetric analysis and were uncertain about the working of fluorescent indicators in endpoint detection. However, after the experiment, they understood the applicability of fluorescent indicators via microscale titrations in the lab. The post-lab survey indicates that microscale redox titration effectively determined analyte concentration at a micromolar concentration using **PNPA-H** (see **Table 3.8.**). Thus, students became aware of the benefit of microscale titrations and the effectiveness of fluorescent indicators in microscale titrations.

Table 3.8. *Comparative estimated mass values of ferrous ions from molar concentration, micromolar concentration, and semimicro volume using different indicating methods and analyte concentrations.*

Sample	**Estimated mass of Fe^{2+} ions, g, by analyte concentration and method**		
	Molar Concentration, 1×10^{-2} M in 10 mL	**Micromolar concentration, 1×10^{-4} M in 10 mL**	**Semimicro Volume, 1×10^{-2} M in 2 mL**

	Fluorescent indicating method using PNPA-H	**Conventional method**	**Fluorescent indicating method using PNPA-H**	**Fluorescent indicating method using PNPA-H**
1	5.50×10^{-2}	5.55×10^{-2}	5.63×10^{-4}	5.54×10^{-2}
2	5.58×10^{-2}	5.55×10^{-2}	5.63×10^{-4}	5.77×10^{-2}
3	5.43×10^{-2}	5.41×10^{-2}	5.40×10^{-4}	5.35×10^{-2}
4	5.47×10^{-2}	5.50×10^{-2}	5.46×10^{-4}	5.63×10^{-2}
5	5.55×10^{-2}	5.50×10^{-2}	5.70×10^{-4}	5.57×10^{-2}
6	5.70×10^{-2}	5.42×10^{-2}	5.22×10^{-4}	5.61×10^{-2}
7	5.40×10^{-2}	5.40×10^{-2}	5.39×10^{-4}	5.50×10^{-2}
8	5.37×10^{-2}	5.35×10^{-2}	5.78×10^{-4}	5.25×10^{-2}
9	5.35×10^{-2}	5.43×10^{-2}	5.75×10^{-4}	5.45×10^{-2}
10	5.28×10^{-2}	5.39×10^{-2}	5.73×10^{-4}	5.87×10^{-2}
11	5.24×10^{-2}	5.22×10^{-2}	5.71×10^{-4}	5.43×10^{-2}
12	5.24×10^{-2}	5.21×10^{-2}	5.59×10^{-4}	5.50×10^{-2}
13	5.08×10^{-2}	5.19×10^{-2}	5.97×10^{-4}	5.54×10^{-2}
14	5.17×10^{-2}	5.17×10^{-2}	5.85×10^{-4}	5.20×10^{-2}
15	5.05×10^{-2}	5.10×10^{-2}	4.92×10^{-4}	5.06×10^{-2}

***Table 3.9**. Pre-lab survey and post-lab survey questions provided to the students.*

	Pre-Lab Survey	**Post-Lab Survey**
1	How can we apply Green chemistry aspects in existing volumetric titrations easily? a) By replacing toxic chemicals b) By recycling solutions c) By employing micro-scale titrations d) others	How to quantitatively estimate the mass of substances less than 5 mg in volumetric titrations? a) Using microscale titrations b) Using fluorescent indicators c) Using conventional colorimetric indicators d) Not possible by volumetric titration
	What are the skills obtained from volumetric	Which of the following skills are mainly

2	titrations? a) Precision and accuracy in quantitative estimations b) Proper Utilization of laboratory glassware c) Detection of the endpoint via Naked-eye d) Others	acquired from micro-scale titrations? a) Expertness in the use of fluorescent indicators b) Comfort in the use of micro burette c) Ability to include green chemistry aspects in experiments d) Precise and accurate titration results
3	What is the difficulty of employing microscale titrations in laboratories? a) Lack of facilities available in the laboratories b) Difficulties in preparing solutions c) Nonavailability of suitable indicators d) Difficulties in endpoint detection with available indicators e) others	Which one do you prefer to perform in the laboratory as an eco-friendly experiment among the following titrations? a) Molar titrations (1×10^{-2} M) b) Micro molar titrations (1×10^{-4} M or 1×10^{-6} M) c) Semi-micro volume titrations (1 mL or 2 mL volume) d) None of the above
4	How can we perform microscale estimations in laboratories? a) By adopting modern instruments b) Using indicators in high concentration c) Using fluorescent indicators d) By adopting methods other than volumetric titrations e) Others	Which of the following experiment is a better way to reduce chemical exposure? a) Molar titrations (1×10^{-2} M) b) Micro molar titrations (1×10^{-4} M or 1×10^{-6} M) c) Semi-micro volume titrations (1 mL or 2 mL volume) d) None of the above
5	Choose the correct statement regarding conventional indicators and fluorescent indicators. a) Conventional indicators cannot be used for micromolar titrations, whereas fluorescent indicators can. b) Both Conventional and fluorescent indicators give endpoint by color change only. c) Conventional indicators give sharp endpoint detection, whereas fluorescent indicators cannot. d) A small quantity of conventional indicators was sufficient for endpoint detection, whereas a high quantity of fluorescent indicators was needed.	Which of the following comparisons was effective for analyzing green chemistry aspects? a) Molar titration vs micro molar titration b) Molar titration vs semi-micro volume titration c) Titrations with conventional indicator vs. titration with fluorescent indicator d) All of the above
6	How can we use fluorescent indicators to detect the endpoint? a) By exhibiting a color change b) By changing fluorescence intensity c) By forming complexes d) By changing the physical property of the indicator	What are the advantages of semi-micro volume estimations using fluorescent indicators? a) Reducing chemical exposure and time b) sharp detection of the endpoint by sharp quenching of fluorescence c) Easy operation of micro burettes

		d) Improvement in precision and accuracy of results
7	Choose the correct statement about micro-scale estimations. i) Microscale estimations will not produce accurate and precise results. ii) Microscale estimations are time-consuming and need high-cost instruments iii) Microscale estimations cannot be performed at laboratories iv) Microscale estimation will produce precise and accurate results v) Microscale estimations are eco friendly a) i, ii & v b) iii, iv & c) i & v d) iv & v	Why are fluorescent indicators necessary in micromolar titrations instead of conventional colorimetric indicators? a) Conventional colorimetric indicators cannot produce a sharp color change at the endpoint. b) Fluorescence indicators show sharp fluorescence quenching at the endpoint in micromolar titrations. c) Conventional colorimetric indicators produce color change at early stages and lead to false endpoint detection. d) Precision and accuracy of results were better using fluorescent indicators.
8	What are the needs of practicing micro-scale titrations? i) To produce accurate and precise estimations ii) To familiarize microscale apparatus iii) To practice green chemistry principles iv) To prevent consumption of chemicals a) i, ii & iii b) iii & iv c) ii, iii, & iv d) i, ii, iii, &iv	Which is the most exciting feature of using fluorescent indicators in permanganometry? a) The detection of endpoints in titration with low concentrations of analytes b) Confirmation of endpoint noted via fluorescence quenching and appearance of wine red color. c) Easy detection of the endpoint by sharp fluorescence quenching d) Others
9	Which of the following titrations are easy to perform in laboratories? a) Conventional titrations with colorimetric indicator b) Microscale titrations with colorimetric indicator c) Microscale titrations with fluorescent indicator d) All the above	Comment on the precision and accuracy of microscale estimations. a) Estimated masses were precise but not accurate. b) Estimated masses were precise and accurate. c) Estimated masses were accurate but not precise. d) Estimated masses were not precise and accurate.
10	Comment on the advantages of titrations. i) Easy to perform ii) Low cost iii) No need of calibrations iv) Precise and accurate results v) Sharp end point detection vi) Less chemical use vii) Less time consumption	How do you rate the entire experiment? a) 4: clearly understood the green chemistry aspect in microscale estimations, the advantage of using fluorescent indicators in titrations, and developed skills for using microscale titrations. b) 3: clearly understood the green

	a) i, ii, v, & vi b) i, ii, iii, iv & v c) iv, v, vi, & vii d) i, ii, iii, iv,& vi	chemistry aspect in micro-scale estimations and the advantage of using fluorescent indicators in titrations. c) 2: developed skills in micro-instruments. d) 1: The use of fluorescent indicators is clearly understood but not the green chemistry aspect in micro-scale estimations.

Table 3.10*. Comparison of Post lab Survey Results for Student Evaluation of the Microscale titrations.*

Item	Question	Students' Most Frequently Chosen Response Options	Option % (N=15)
1	How to quantitatively estimate the mass of substances less than 5 mg in volumetric titrations?	Using microscale titrations	50
		Using fluorescent indicators	50
~~2~~	Which of the following skills are mainly acquired from micro-scale titrations?	Expertness in the use of fluorescent indicators in endpoint detection	60
		Comfort in the use of micro burette	33
3	Which one do you prefer to perform in the laboratory as an eco-friendly experiment among the following titrations?	Micro molar titrations (1×10^{-4} M or 1×10^{-6} M)	86
		Semi-micro volume titrations (1 mL or 2 mL volume)	14
4	Which of the following experiment is a better way to reduce chemical exposure?	Micro molar titrations (1×10^{-4} M or 1×10^{-6} M)	86
		Semi-micro volume titrations (1 mL or 2 mL volume)	14
5	Which of the following comparison was effective for analyzing green chemistry aspects?	Molar titration vs. micro molar titration	60
		Titrations with conventional indicator vs. titration with fluorescent indicator	33
6	What are the advantages of semi-micro volume estimations using fluorescent indicators?	Reducing chemical exposure and time	40
		sharp detection of the	60

		endpoint by sharp quenching of fluorescence	
7	Why are fluorescent indicators necessary in micromolar titrations instead of conventional colorimetric indicators?	Conventional indicators cannot produce a sharp color change in micromolar concentrations.	40
		Fluorescence indicators show sharp fluorescence quenching at the endpoint in micromolar titrations.	60
8	Which is the most exciting feature of using fluorescent indicators in permanganometry?	The detection of endpoints in titration with low concentrations of analytes	50
		Confirmation of endpoint noted via fluorescence quenching and appearance of wine red color.	33
9	Comment on the precision and accuracy of microscale estimations.	Estimated masses were precise and accurate.	93
10	How do you rate the entire experiment?	Choice 4	73
		Choice 3	20

3.4. Conclusion

We have made significant progress in microscale redox titration to estimate the mass of ferrous ions using poly-N-phenyl anthranilic acid (**PNPA-H)** and its monomer N-phenyl anthranilic acid (**NPA-H)** as a fluorescent indicator. The fluorescent indicators like **PNPA-H** and **NPA-H** have shown bluish-white light emission which was quenched by the oxidizing analytes at the endpoint. A comparison of the conventional indicating method with the fluorescence indicating method has been carried out at higher concentrations (1×10^{-2} M and 1×10^{-3} M) to confirm the validity of the fluorescent indicator. The mass of the ferrous ion determined by fluorometric indicating methods has a narrow distribution than conventional indicating methods. Statistical Student's t-test and F-test indicated that fluorometric indicating methods are valid and significant as conventional methods with the additional benefit of detecting micromolar concentration. The micromolar concentrations and semi-micro volumes of titrants ensure these microscale redox titrations follow the first principle of green chemistry. Students' and

participants' feedback shows that fluorescent indicators, micromolar titration, and semi-micro volumetric titrations have produced excellent results. In short, microscale redox titration accurately determines the micromolar concentration of ferrous ions with the help of fluorescent indicators to reduce chemical use and laboratory time in analysis.

Reference

1. Fernando Pérez-Rodríguez, Panagiotis Skandamis, & Vasilis Valdramidis. (2018). *Quantitative Methods for Food Safety and Quality in the Vegetable Industry* (Fernando Pérez-Rodríguez, Panagiotis Skandamis, & Vasilis Valdramidis, Eds.). Springer International Publishing.
2. Soil Science Society of America. Division S-9. (1994). *Quantitative Methods in Soil Mineralogy* (James E. Amonette, L. W. Zelazny, & R. J. Luxmoore, Eds.).
3. Chaudhery Mustansar Hussain, R. K. (2019). *Modern Environmental Analysis Techniques for Pollutants*. Elsevier Science.
4. Hugh A. McKenzie, & Lloyd Earle Smythe (Eds.). (1988). *Quantitative Trace Analysis of Biological Materials*. Elsevier.
5. Koek, M. M., Jellema, R. H., van der Greef, J., Tas, A. C., & Hankemeier, T. (2011). Quantitative metabolomics based on gas chromatography mass spectrometry: status and perspectives. *Metabolomics*, *7*(3), 307–328. https://doi.org/10.1007/s11306-010-0254-3.
6. Pan, X., Welti, R., & Wang, X. (2010). Quantitative analysis of major plant hormones in crude plant extracts by high-performance liquid chromatography–mass spectrometry. *Nature Protocols*, *5*(6), 986–992. https://doi.org/10.1038/nprot.2010.37.
7. Garg, N., Goyal, A., & Das, P. (2022). Recent Advances and Future Perspectives in Volumetric Analysis. In *Advanced Techniques of Analytical Chemistry: Volume 1* (pp. 16–26). bentham science publishers. https://doi.org/10.2174/9789815050233122010005.
8. Boppana, N. P. D., Snow, R., Simone, P. S., Emmert, G. L., & Brown, M. A. (2023). A low-cost automated titration system for colorimetric endpoint detection. *The Analyst*, *148*(9), 2133–2140. https://doi.org/10.1039/D2AN02086F.
9. Kosenkov, Y., & Kosenkov, D. (2021). Computer Vision in Chemistry: Automatic Titration. *Journal of Chemical Education*, *98*(12), 4067–4073. https://doi.org/10.1021/acs.jchemed.1c00810.
10. Flint, E. B., Kortz, C. L., & Taylor, M. A. (2002). Microscale pH Titrations Using an Automatic Pipet. *Journal of Chemical Education*, *79*(6), 705. https://doi.org/10.1021/ed079p705.
11. Gordon, J. S., Harman, S., Weiss, K., & Pettegrew, B. (2001). A Microscale Spectrophotometric Determination of Water Hardness. *Journal of Chemical Education*, *78*(8), 1089. https://doi.org/10.1021/ed078p1089.
12. Royal Society of Chemistry. *A microscale acid–base titration*. https://edu.rsc.org/experiments/a-microscale-acid-base-titration/536.article.
13. Richardson, J. N., Stauffer, M. T., & Henry, J. L. (2003). Microscale Quantitative Analysis of Hard Water Samples Using an Indirect Potassium Permanganate Redox Titration. *Journal of Chemical Education*, *80*(1), 65. https://doi.org/10.1021/ed080p65.
14. Singh, M. M., Szafran, Z., & Pike, R. M. (1999). Microscale Chemistry and Green Chemistry: Complementary Pedagogies. *Journal of Chemical Education*, *76*(12), 1684. https://doi.org/10.1021/ed076p1684.
15. Singh, M. M., McGowan, C. B., Szafran, Z., & Pike, R. M. (2000). A Comparative Study of Microscale and Standard Burets. *Journal of Chemical Education*, *77*(5), 625. https://doi.org/10.1021/ed077p625.
16. Simões, G. B., Badolato, P. V. e S., Ignácio, M. D., & Cerqueira, E. C. (2020). Determination of Zinc Oxide in Pharmaceutical Preparations by EDTA Titration: A

Practical Class for a Quantitative Analysis Course. *Journal of Chemical Education*, *97*(2), 522–527. https://doi.org/10.1021/acs.jchemed.9b00939.

17. Chen, T., Yang, F., Wu, X., Chen, Y., & Yang, G. (2020). A fluorescent and colorimetric probe of carbyne nanocrystals coated Au nanoparticles for selective and sensitive detection of ferrous ions. *Carbon*, *167*, 196–201. https://doi.org/10.1016/j.carbon.2020.06.003.
18. Lu, S., Zhang, X., Chen, L., & Yang, P. (2018). Colorimetric determination of ferrous ion via morphology transition of gold nanorods. *Microchimica Acta*, *185*(1), 76. https://doi.org/10.1007/s00604-017-2602-8.
19. Liu, G., Li, B., Liu, Y., Feng, Y., Jia, D., & Zhou, Y. (2019). Rapid and high yield synthesis of carbon dots with chelating ability derived from acrylamide/chitosan for selective detection of ferrous ions. *Applied Surface Science*, *487*, 1167–1175. https://doi.org/10.1016/j.apsusc.2019.05.069.
20. Du, F., Cheng, Z., Tan, W., Sun, L., & Ruan, G. (2020). Development of sulfur doped carbon quantum dots for highly selective and sensitive fluorescent detection of Fe^{2+} and Fe^{3+} ions in oral ferrous gluconate samples. *Spectrochimica Acta Part A: Molecular and Biomolecular Spectroscopy*, *226*, 117602. https://doi.org/10.1016/j.saa.2019.117602.
21. Zhang, Y.-Y., Chen, X.-Z., Liu, X.-Y., Wang, M., Liu, J.-J., Gao, G., Zhang, X.-Y., Sun, R.-Z., Hou, S.-C., & Wang, H.-M. (2018). A highly sensitive multifunctional sensor based on phenylene-acetylene for colorimetric detection of Fe2+ and ratiometric fluorescent detection of Cd^{2+} and Zn^{2+}. *Sensors and Actuators B: Chemical*, *273*, 1077–1084. https://doi.org/10.1016/j.snb.2018.07.012
22. Nawaz, H., Tian, W., Zhang, J., Jia, R., Chen, Z., & Zhang, J. (2018). Cellulose-Based Sensor Containing Phenanthroline for the Highly Selective and Rapid Detection of Fe^{2+} Ions with Naked Eye and Fluorescent Dual Modes. *ACS Applied Materials & Interfaces*, *10*(2), 2114–2121. https://doi.org/10.1021/acsami.7b17342.
23. Edmund, B. (2013) *Indicators: International Series of Monographs in Analytical Chemistry*. Pergamon Press.
24. Duan, Q., Xing, Y., & Guo, K. (2022). The Detection of Food Additives Using a Fluorescence Indicator Based on 6– p–Toluidinylnaphthalence-2-sulfonate and Cationic Pillar[6]arene. *Frontiers in Chemistry*, *10*. https://doi.org/10.3389/fchem.2022.925881.
25. Murata, A., Harada, Y., Fukuzumi, T., & Nakatani, K. (2013). Fluorescent indicator displacement assay of ligands targeting 10 microRNA precursors. *Bioorganic & Medicinal Chemistry*, *21*(22), 7101–7106. https://doi.org/10.1016/j.bmc.2013.09.007.
26. Wicks, S. L., & Hargrove, A. E. (2019). Fluorescent indicator displacement assays to identify and characterize small molecule interactions with RNA. *Methods*, *167*, 3–14. https://doi.org/10.1016/j.ymeth.2019.04.018.
27. Zhu, X., Duan, Y., Li, P., Fan, H., Han, T., & Huang, X. (2019). A highly selective and instantaneously responsive Schiff base fluorescent sensor for the "turn-off" detection of iron (III), iron (II), and copper (II) ions. *Analytical Methods*, *11*(5), 642–647. https://doi.org/10.1039/C8AY02526F.
28. Li, Z., Li, L.-J., Sun, T., Liu, L., & Xie, Z. (2016). Benzimidazole-BODIPY as optical and fluorometric pH sensor. *Dyes and Pigments*, *128*, 165–169. https://doi.org/10.1016/j.dyepig.2016.01.029.
29. Khatun, S., Biswas, S., Binoy, A., Podder, A., Mishra, N., & Bhuniya, S. (2020). Highly chemoselective turn-on fluorescent probe for ferrous (Fe^{2+}) ion detection in cosmetics and live cells. *Journal of Photochemistry and Photobiology B: Biology*, *209*, 111943. https://doi.org/10.1016/j.jphotobiol.2020.111943.
30. Erdey, L., Buzás, I., & Vigh, K. (1966). Luminol as a fluorescent acid-base indicator. *Talanta*, *13*(3), 463–469. https://doi.org/10.1016/0039-9140(66)80064-4.
31. Krishnankutty, K. (2005). INDICATORS | Complexometric, Adsorption, and Luminescence Indicators. In *Encyclopedia of Analytical Science* (pp. 378–385). Elsevier. https://doi.org/10.1016/B0-12-369397-7/00272-7.

32. Wang, T., Zhang, N., Bai, W., & Bao, Y. (2020). Fluorescent chemosensors based on conjugated polymers with N-heterocyclic moieties: two decades of progress. *Polymer Chemistry*, *11*(18), 3095–3114. https://doi.org/10.1039/D0PY00336K.
33. Kratochvil, Byron., & Zatko, D. A. (1964). Ruthenium 2,2′-Bipyridine Complexes as Fluorescent Oxidation-Reduction Indicators. *Analytical Chemistry*, *36*(3), 527–529. https://doi.org/10.1021/ac60209a060.
34. Rao, G. G., & Sastry, G. S. (1971). Titrimetric determination of ascorbic acid with cerium(IV) sulphate. *Analytica Chimica Acta*, *56*(2), 325–328. https://doi.org/10.1016/S0003-2670(01)82430-2.
35. Sagi, S. R., & Rao, G. G. (1962). Titrimetric determination of molybdenum (V) and uranium(IV) with ceric sulphate using rhodamine 6G as a fluorescent indicator. *Fresenius' Zeitschrift Für Analytische Chemie*, *189*(3), 229–243. https://doi.org/10.1007/BF00497570.
36. Sagi, S., & Rao, G. G. (1960). Ferrimetric determination of uraniumIV using rhodamine 6G as fluorescent indicator. *Talanta*, *5*(3–4), 154–161. https://doi.org/10.1016/0039-9140(60)80167-1.
37. Kratochvil, B., & White, M. C. (1964). Ruthenium complexes of ligands containing the ferroin group as fluorescent precipitation indicators for Iodimetry. *Analytica Chimica Acta*, *31*, 528–533. https://doi.org/10.1016/S0003-2670(00)88872-8.
38. Rao, G. G., & Dikshitulu, L. S. A. (1962). Titrimetric determination of vanadiumIV with ceriumIV sulphate at room temperature using rhodamine 6G as fluorescent indicator. *Talanta*, *9*(3), 289–295. https://doi.org/10.1016/0039-9140(62)80063-0.
39. Mondal, T. K., & Saha, S. K. (2019). Facile Approach To Synthesize Nitrogen- and Oxygen-Rich Carbon Quantum Dots for pH Sensor, Fluorescent Indicator, and Invisible Ink Applications. *ACS Sustainable Chemistry & Engineering*, *7*(24), 19669–19678. https://doi.org/10.1021/acssuschemeng.9b04817.
40. Crawley, R. H. A. (1958). Complexometric titration of gallium with fluorescent indicator. *Analytica Chimica Acta*, *19*, 540–541. https://doi.org/10.1016/S0003-2670(00)88215-X.
41. Tanaka, H., & Sakamoto, Y. (1993). Polyelectrolyte titration using fluorescent indicator. I. Direct titration of anionic and cationic polyelectrolytes with 104N standard solutions. *Journal of Polymer Science Part A: Polymer Chemistry*, *31*(11), 2687–2691. https://doi.org/10.1002/pola.1993.080311103.
42. Anastas, P., & Eghbali, N. (2010). Green Chemistry: Principles and Practice. *Chem. Soc. Rev.*, *39*(1), 301–312. https://doi.org/10.1039/B918763B.
43. Das, K. R., Antony, M. J., & Varghese, S. (2019). Highly bluish-white light emissive and redox active conjugated poly-N-phenyl anthranilic acid polymer fluoroprobe for analytical sensing. *Polymer*, *181*, 121747. https://doi.org/10.1016/j.polymer.2019.121747.
44. Beran, J. A. (2010). *Laboratory Manual for Principles of General Chemitry*, 9th ed..; John Wiley & Sons.
45. McPherson, P. A. (2015). *Practical Volumetric Analysis*, Royal Society of Chemistry.
46. Harris, D. C. (2007). *Quantitative Chemical Analysis*. 7th ed.; W. H. Freeman and Company: New York. pp 327-340.
47. Auwal Balarabe, M., & Zainab Folashade, A. (2019). Determination of Iron in Some Selected Iron Containing Tablets Using Redox Titration. *World Journal of Applied Chemistry*, *4*(3), 42. https://doi.org/10.11648/j.wjac.20190403.13.
48. Sriramam, K. (1973). Some observations on the redox behaviour of N-phenylanthranilic acid indicator in iron(II) titrations. *Talanta*, *20*(4), 383–390. https://doi.org/10.1016/0039-9140(73)80166-3.
49. Singh, M. M., McGowan, C. B., & Szafran, Z. (2002). Precision in Microscale Titration. *Journal of Chemical Education*, *79*(8), 941. https://doi.org/10.1021/ed079p941.2.
50. Miller, J. N. (1991). Basic statistical methods for Analytical Chemistry. Part 2. Calibration and regression methods. A review. *The Analyst*, *116*(1), 3. https://doi.org/10.1039/an9911600003.
51. European Medicines Agency. Note for Guidance on Validation of Analytical Procedures: Text and Methodology. https://www.ema.europa.eu/en/documents/scientific-

guideline/ich-q-2-r1-validation-analytical-procedures-text-methodology-step-5_en.pdf (accessed 2021-12-09).
52. Mendham, J., Denney, R.C., Barnes, J.D., Thomas, M. (2000). *Vogel's Text Book of Quantitative Chemical Analysis*; 6th ed.; Prentice Hall.

CHAPTER 4

Acid Content Sensing and State of Charge Determination of Lead-acid Battery using Poly-N-phenyl-o-phenylenediamine

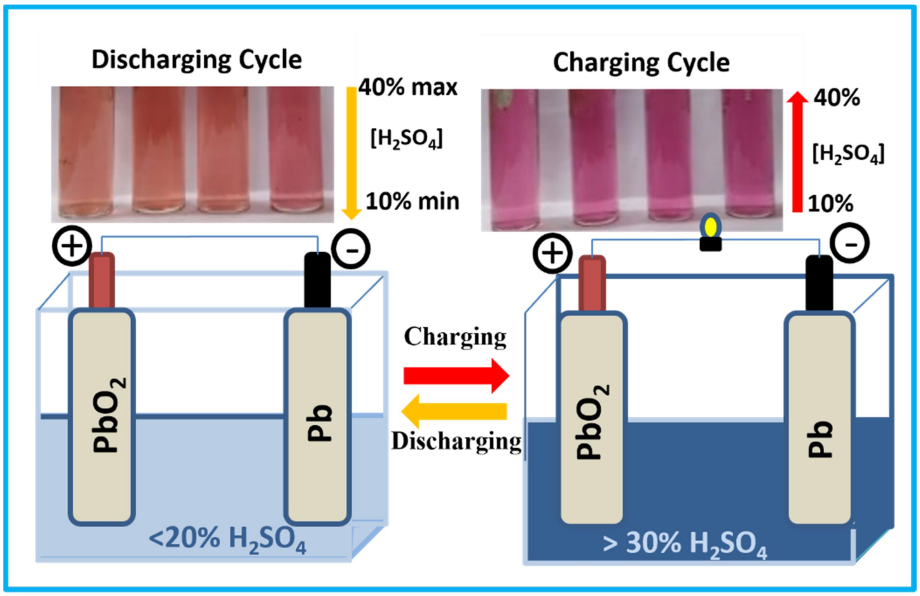

4.1. Introduction

Conjugated polymers were considered as one of the important polymeric chromogenic materials due to their ability to change their color under various conditions [1]. Conjugated polymers exhibit thermochromism, photochromism, solvatochromism, electrochromism, or chemochromism under the action of stimuli like temperature, light, solvent, electric field, and chemical changes like pH, ionic strength etc [2]. Stimuli induces structural changes in conjugated polymer, change in oxidation state, or conformational change in main or side chain. Among different stimuli, pH is one of the important stimuli that impact physical, chemical, and biological properties. pH sensors play an important role in chemical industries, waste-water treatments, pharmaceutical industries, food analysis etc.[3] Conjugated polymer-based optical pH sensors were developed due to their highly sensitive nature and less electrical interferences [4]. Polyaniline is an important pH-sensitive polymer whose optical and electric properties are susceptible to pH [4-7]. Jin et al. developed a stable polyaniline film showing a reversible color change in the pH range of 2-12 [7]. Abu-Tabit et al. used polyaniline-coated polysulfone membranes for pH detection in the range of 4-12 [8] (see **Figure 4.1.**).

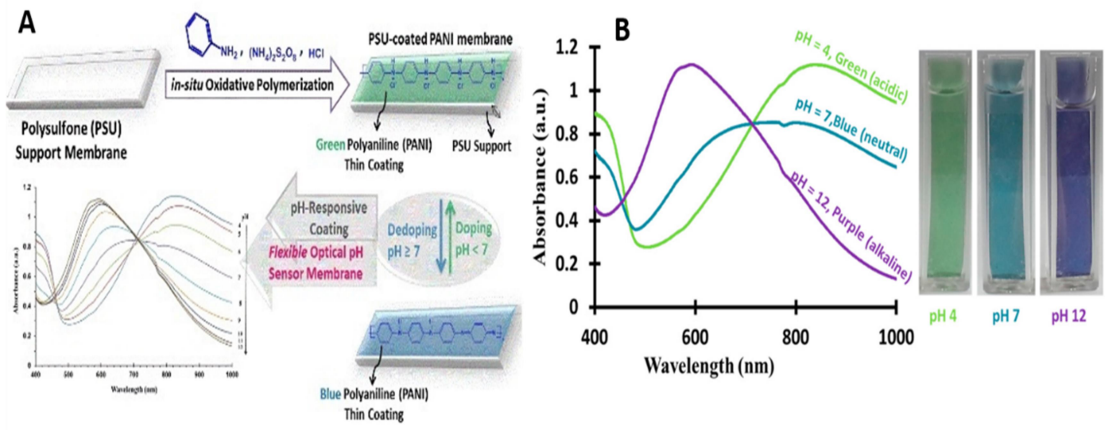

Figure 4.1. *A) pH sensing using polyaniline-coated polysulfone membrane and B) UV-visible absorption spectra of the polymer at different pH with photographs (Adapted from Abu-Thabit et al. 2016).*

Lead-acid batteries are rechargeable batteries, which have an advantage over non-rechargeable batteries because of the multiple-use and reduced battery waste generation in the environment. Lead-acid batteries contain metallic lead dioxide as positive electrode and metallic lead as negative electrode and both the electrodes are dipped in an electrolyte

of sulphuric acid. However, lead acid batteries are more expensive than disposable batteries, but their long-term use from a single investment and technically sound energy storage mechanism makes them more significant than non-rechargeable batteries [10]. The acid content of lead acid batteries changes with charging and discharging. However, it is difficult to measure the acid content of the batteries using a conventional pH meter due to the highly acidic pH of battery acid. The extended use of lead-acid batteries beyond a period produces slow charging rates, self-discharge with battery temperature or time, and causes changes in charging-discharging characteristics. The reasons for the development of the poor performance of lead-acid batteries after a period include draining via electrolysis of water, the reaction of metal with sulphuric acid, impurities in water, and the deposition of lead sulfate (sulphation) and settling of sulphuric acid at the bottom (stratification) [11-12]. Therefore, it is necessary to determine the state of charge in lead-acid batteries. The state of charge (SoC) is the ratio of the remaining capacity to the battery's total capacity, which was necessary to know the lead-acid battery's state of health. [9]

Table 4.1. *Different parameters used to determine the state of charge in batteries, along with advantages and limitations available in the literature.*

Sl. No.	Parameter used to determine the state of charge	Advantage	Limitation	Reference
1	Open circuit voltage (OCV)	Simple and direct SoC determination using a mathematical formula	Need of the long resting time and temperature sensitive	13
2	Terminal voltage	Direct SoC determination using a mathematical formula	Estimated error was high	14
3	Electrochemical impedance spectroscopy	Previous knowledge of initial SoC is not necessary	Sensitive to temperature	9
4	Ampere-hour counting method	Simple and accurate SoC determination	Previous knowledge of SoC is necessary	15
5	Specific gravity using Refractive index	Remote monitoring of SoC is possible	Periodic calibration is needed	16

6	Specific gravity using optical absorption of electrolyte	Accurate measurement	In situ monitoring of SoC is difficult	17
7	Specific gravity using a density meter	Fewer interferences	Indirect SoC measurement	10
8	Specific gravity using electrodes	Reliable and efficient measurement	Periodic replacement of electrodes is necessary	18
9	Refractive index	Direct and in situ monitoring of SoC	Mathematical modeling is required	19
10	Specific gravity using refractive index	Signal processing is not necessary	Indirect SoC measurement	20

The reported methods to determine the state of charge in lead acid batteries available in the literature, along with their advantages and limitations, are given in **Table 4.1**. The SoC of the battery can be determined using electrochemical or electrical methods such as impedance spectroscopy, ampere-hour counting, internal resistance measurement, and voltage measurement [14, 21]. Impedance spectroscopy is a sophisticated method that provides good SoC results without the initial SoC value, whereas the amper-hour counting method needs to know the initial SoC value. The SoC determination from battery voltage required the battery to be in an open circuit for some time after being charged or discharged [13]. Deepti et al. implemented a method of open circuit voltage with a current integration method to determine the state of charge in batteries [22]. The voltage dependence on temperature and current fluctuations on charging/discharging could affect the accurate SoC measurements. A glass hydrometer is a simple and economical instrument for measuring specific gravity; however, it would be a highly skilled method for determining SoC [23-25]. Tang et al. used a hydrometer integrated with a liquid level sensor for gauging the specific gravity of the battery electrolyte to determine battery SoC [26]. The specific gravity measurement using a digital density meter was reported [27]. Hancke et al. described a fiber-optic technique for measuring specific gravity by measuring changes in the refractive index of a solution [16, 28]. The dependence of electrode potential on sulphuric acid concentration was used for developing electrode-based sensors, and this method requires periodic replacement of electrodes [18, 29-32]. Weiss

et al. reported an optical apparatus for measuring the changes in optical absorbance of the electrolyte at 1.45 µm with the change in the composition of the electrolyte to determine the state of charge [17]. The designed sensor shows decreased absorption with lower sulfate ion concentration in the conductor when the battery is used. Therefore, the acid content of lead-acid batteries was correlated to the charging and discharging process [21]. On complete charging of the lead acid battery, acid content increases to 40%, whereas acid content reduces to ~ 10-15 % on normal discharge. An acid content below 10% (specific gravity below 1.106 g/cm^3) indicates a drained or damaged battery (see **Figure 4.2.**) [33-35]. Therefore, a simple and accurate method for determining the state of charge of lead-acid batteries from their acid content in normal atmospheric conditions would benefit battery research.

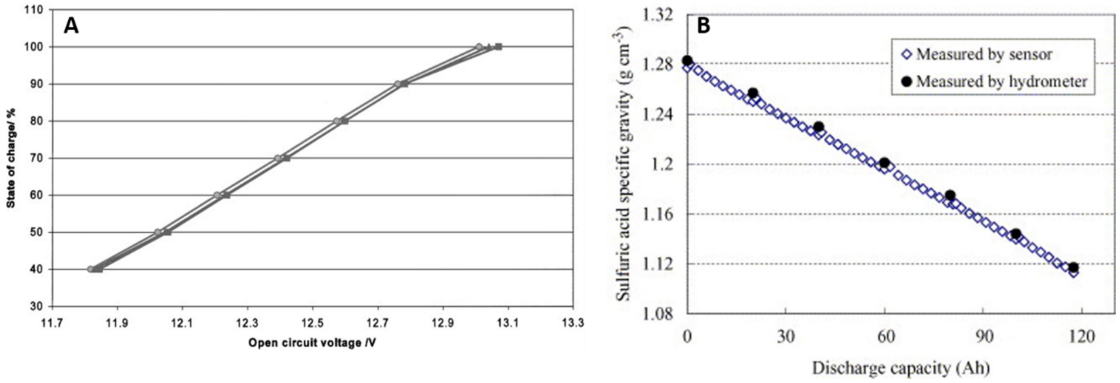

Figure 4.2. *A) Plot showing dependence of the state of charge on open circuit voltage in the lead-acid battery (Adapted from Piller et al. 2001). B) Plot showing the sulphuric acid specific gravity change measured by developed sensor and hydrometer in the lead acid battery during discharging. (Adapted from Guo et al. 2005).*

In the present work, the polymer poly-N-phenyl-o-phenylenediamine (**PPOPD**) solution was used as an ex-situ chemosensor to determine the battery acid content in lead-acid batteries. The change in absorbance of **PPOPD** solution at 518 nm with increase in acid content has shown a linear relationship. The absorbance of the **PPOPD** solution produced in charging and discharging conditions was correlated with the lead-acid battery's acid content and SoC. The acid content corresponding to 40% sulphuric acid would be approximately the same for a lead-acid battery on complete charging. The absorbance corresponding to the minimum acid percentage (10%) on discharging and maximum acid percentage (40%) on complete charging was given as limits to determine the SoC of the battery. Here, an analytical method has been developed to determine

battery acid content and the state of charge of lead-acid batteries through an external calibration-free method by measuring the absorbance of a pH-responsive and water-soluble poly-N-phenyl-o-phenylenediamine.

4.2. Experimental

4.2.1. Materials and Reagents: N-Phenyl-o-phenylenediamine (98%) and anhydrous ferric chloride were purchased from Sigma Aldrich. Concentrated H_2SO_4 (98%) and acetone were purchased from Merck Chemicals. Double-distilled ethanol and deionized water were used to synthesize and purify the polymer.

4.2.2. Measurements and Instruments: UV-Visible absorption spectra of the samples were recorded by Shimadzu UV-Visible spectrometer 1800 series in the 200-800 nm range with deionized water. The proton NMR spectra of the samples were recorded using a 400 MHz Bruker Avance FT-NMR spectrophotometer using DMSO- d_6 as the solvent and TMS as an internal standard. Fourier transform infrared spectra of the powdered samples were recorded using the Shimadzu FT-IR spectrometer IR affinity-1 series by the KBr pellet method in the 400-4000 cm^{-1} range. Powder X-ray diffraction of the samples was measured using PANALYTICAL, Aeris research diffractometer in the range of 2θ values from 4 to 80°. The molecular weight of the **PPOPD** samples has been determined by Bruker Autoflex max LRF MALDI-TOF using sinapinic acid as a matrix. The pH of solutions was measured using a portable pH meter of Hanna instruments. Powersoft automated battery of 12V was used for charging and discharging measurements of the lead acid battery. A digital multimeter was used to measure the battery output voltage. For charging studies, the battery was charged using a power-plus automatic battery charger of 5 amps. For discharging studies, the battery was discharged using a DC bulb of 100 watts. Electrical conductivity of the samples was measured using DFP-RM-200 with constant current source Model CCS-01 and DC microvoltmeter.

4.2.3. Synthesis of poly-N-phenyl-o-phenylenediamine (PPOPD): The monomer N-phenyl-o-phenylenediamine (0.10 g, 0.5 mmol) was dissolved in 3 mL distilled ethanol. Oxidizing agent anhydrous ferric chloride (0.13 g, 0.8 mmol) dissolved in 2 mL ethanol was added to the monomer solution dropwise. The color of the solution immediately changed from pale brown to dark brown upon adding the oxidizing agent. The polymerization reaction was continued for 2 hours without any disturbance, and the solvent evaporated upon reaction completion. The polymer was washed with water and

acetone, filtered, and dried in a vacuum oven at 60°C. Yield = 0.075 g (75%). ^{1}H NMR (400 MHz, DMSO- d_6): δ 6.20 (d, 1H, Ar-H), 7.50 (m, 15H, Ar-H), 8.25 (d, 1H, Ar-H), 9.58 (s, 1H, N-H). FT-IR (KBr, cm^{-1}): 3352, 3176, 3038, 1670, 1517, 1371, 1247, 846, 769, and 693.

4.2.4. Preparation of poly-N-phenyl-o-Phenylenediamine solution (7.5×10^{-5} M): PPOPD (3.4 mg) was accurately weighed into a 250 mL standard flask and made up to the mark using deionized water to get a dark orange-colored **PPOPD** solution.

4.2.5. The pH-dependent absorption studies: The pH of the solutions at different acidic and basic conditions was measured. The pH of the solution was lowered by adding H_2SO_4 and increased by adding NaOH (10 mL) using different concentrations of acid and base between 0.01 M to 4 M.

4.2.6. Electrochemical studies: Poly-N-phenyl-o-phenylenediamine (0.0182 g) was accurately weighed into a 50 mL standard flask and made up to the mark using deionized water to obtain a 2.0×10^{-3} M PPOPD solution. The cyclic voltammogram of 2.0×10^{-3} M PPOPD solution was recorded. The electrochemical activity of POPD solution in an acidic medium was also analyzed in the presence of 1% and 4% H_2SO_4 as an electrolyte. The cyclic voltammetric studies were performed at a scan rate of 20 mV/s between the voltages -1.0 to +1.2 volt.

4.2.7. Calibration plot of PPOPD solution with different known concentrations of acids: Concentrated H_2SO_4 (~0.10 mL, 18 M) was taken in a 10 mL standard flask and made up to the mark using deionized water to get 1 % acid. Similarly, different acid percentages (0.5, 0.6, 0.8, 1.0, 1.2, 1.4, 1.6, 1.8, 2.0, 2.2, 2.4, 2.6, 2.8, 3.0, 3.2, 3.4, 3.6, 3.8, and 4.0 %) were prepared from corresponding acid concentrations in molarity obtained using the formula; $Molarity = \frac{Acid\ Percentage \times density\ of\ H_2SO_4 \times 10}{molar\ mass}$ and volume using $M_1V_1 = M_2V_2$ formula [36]. The density and molar mass of 98% sulphuric acid was 1.83 g/cm^3 and 98.079 g/mol respectively. Each 10 mL of known acid percentage solutions was added to **PPOPD** (10 mL, 7.5×10^{-5} M) solution in a 100 mL beaker. The UV-visible absorbance of the **PPOPD** at 518 nm, noted from UV-visible spectra, has shown a linear response with the increase in the acid concentration (acid %).

4.2.8. Determination of battery acid content: Battery acid (1 mL) was collected from the lead-acid battery during the charging or discharging time intervals. The collected battery acid was diluted to 10 mL in a standard flask using deionized water. The diluted battery acid (10 mL) was mixed with **PPOPD** (10 mL, 7.5×10^{-5} M), and UV-visible absorbance was noted at 518 nm using a UV-visible absorbance spectrometer. The unknown battery acid concentrations during charging or discharging were obtained by extrapolating the obtained absorbance to the linear calibration plot.

4.2.9. Determination of the state of charge of lead-acid batteries from absorbance: The state of charge of a lead-acid battery can be determined from the absorbance of the **PPOPD** solution using the formula

$$SoC\ (t) = \left[\frac{A\ (t) - A_{min}}{A_{max} - A_{min}}\right] * 100 \quad \ldots\ldots\ldots\ldots\ldots\ldots\ldots\ldots\ldots\ldots\ldots\ldots\ldots\ldots\ldots \quad (1)$$

Where, $SoC\ (t)$ was the state of charge of lead-acid batteries at any particular time (state) at different charging or discharging intervals, $A(t)$ was the absorbance of **PPOPD** with battery acid at 518 nm at a particular time (state) at different charging or discharging intervals, The absorbance A_{min} & A_{max}, corresponds to **PPOPD** solution in 10% and 40% acid content, which was set as the lower and upper limits for SoC determination.

4.2.10. Determination of State of Charge of Lead-acid batteries from open circuit voltage: A digital multimeter was used to determine the battery's open circuit voltage. The multimeter was turned on, its positive probe was connected to the battery's positive terminal (red), the negative probe was connected to the battery's negative terminal (black), and the display reading on the multimeter was checked**.** The battery was disconnected from the load for 15 minutes before measuring the open circuit voltage. The state of charge of a lead-acid battery can be determined from open circuit voltage by using the formula adapted from Chang et al. 2013 [14]

$$SoC\ (t) = \frac{V_{oc}\ (t) - a_0}{a_1} \quad \ldots\ldots\ldots\ldots\ldots\ldots\ldots\ldots\ldots\ldots\ldots\ldots\ldots\ldots\ldots\ldots \quad (2)$$

Where SoC (t) was the state of charge of the battery at a particular time (t), V_{oc} (t) was open circuit voltage, a_0 is the terminal voltage of the battery when SoC equals 0%. a_1 is obtained by knowing the value of V_{oc} (t) and a_0, when SoC (t) is 100.

4.2.11. Determination of specific gravity from density measurement: Different percentages of sulphuric acid solution ranging from 5 % to 50% were prepared by diluting concentrated sulphuric acid using double-deionized water. The weight of the empty weighing bottle was measured. Acid solution (5 mL) was added to a pre-weighed weighing bottle and weight was measured. The difference between the weight of an empty bottle and weight of the bottle with acid gives the weight of the acid solution (W_{acid}). Similarly, weight of water was determined by adding water (5 mL) to a pre-weighed bottle and by measuring the weight (W_{water}). The specific gravity ($\boldsymbol{x}$) was calculated by using the formula given below [50].

$$\boldsymbol{x} = \frac{\frac{\boldsymbol{W_{acid}}}{\boldsymbol{V_{acid}}}}{\frac{\boldsymbol{W_{water}}}{\boldsymbol{V_{water}}}}$$

4.3. Results and Discussion

4.3.1. Synthesis of Poly-N-phenyl-o-phenylenediamine

Poly-N-phenyl-o-phenylenediamine has been synthesized by an oxidative chemical polymerization route using ferric chloride as an oxidizing agent in ethanol solvent. The polymer was a dark brown powder soluble in different solvents such as water, chloroform, acetone, ethanol, tertrahydrofuran, and dimethyl sulfoxide. However, monomer N-phenyl-o-phenylene diamine (**POPD**) was insoluble in the water. The orange-colored **PPOPD** solution in water has shown pH-dependent color changes from orange to pink in acidic pH (< 1.5) and from orange to yellow in basic pH (>10) (see **Figure 4.3.**).

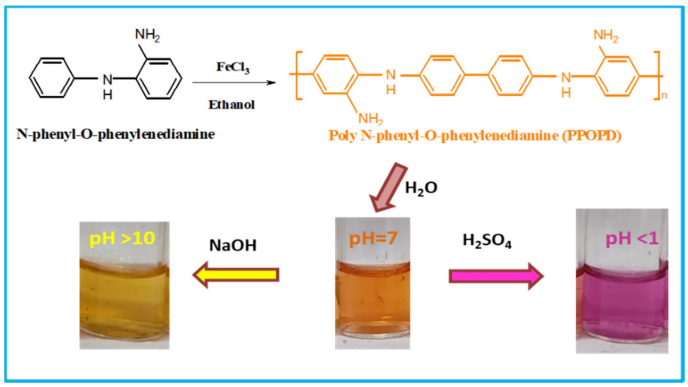

Figure 4.3. *Schematic representation of the synthesis of* ***PPOPD*** *using oxidative chemical polymerization and photographs of the aqueous solution of* ***PPOPD*** *in basic, neutral, and acidic pH.*

4.3.2. Structural characterisation of PPOPD

The complete solubility of polymer and monomer in DMSO enabled us to do their structural characterization by proton NMR spectroscopy (**Figure 4.4.**). The ^{1}H NMR spectra of the monomer contain a multiplet peak at 7.2 ppm, which corresponds to aromatic H_a and H_d protons, and a doublet peak of H_g proton exists at 7.0 ppm as de-shielded peaks mainly due to the electronegative nitrogen at their ortho positions [37]. H_e and H_f protons showed triplets at 6.85 ppm and 6.65 ppm, respectively. The triplet corresponds H_c proton at 6.55 ppm to be the most shielded aromatic proton. The peaks at 4.75 and 6.75 ppm were assigned to the primary $–NH_2$ and secondary –NH– protons. The peak at 8.24 ppm in polymer corresponded to proton H_1, present at the ortho position of the $–NH_2$ group, and was the most de-shielded aromatic proton in the polymer. The multiplets observed between 7 ppm and 8 ppm were assigned to other aromatic protons. In the polymer, secondary –NH protons were present at 9.6 ppm and were most de-shielded, indicating the presence of the –NH group in the polymer [37]. The absence of peaks corresponding to H_c and H_f and aromatic protons in the monomer and the shift in new peaks from 6.5-7.0 ppm to higher δ values confirm the polymer formation.

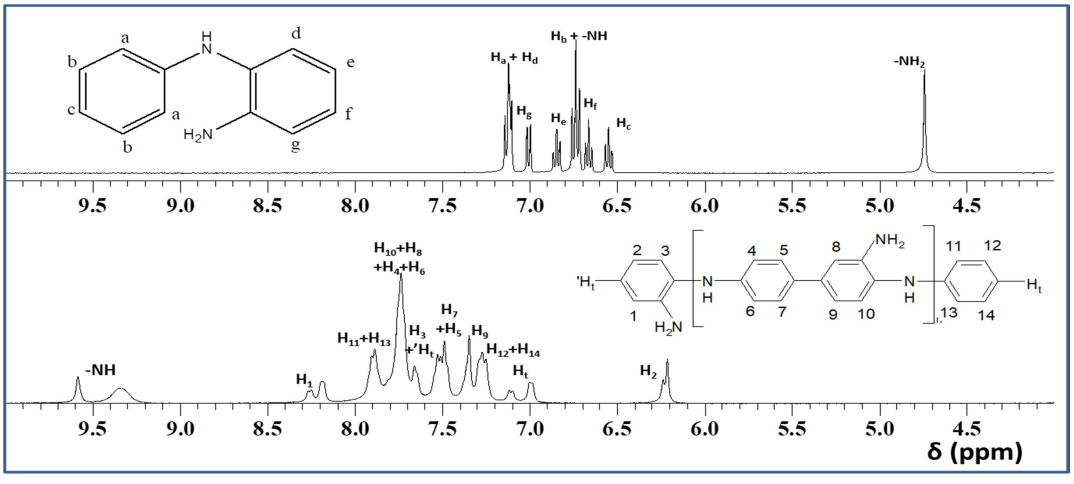

Figure 4.4. *^{1}H NMR Spectra of the monomer* ***POPD*** *and polymer* ***PPOPD*** *in d_6-DMSO.*

The monomer (**POPD**) and polymer (**PPOPD**) were characterized by fourier transform infrared spectroscopy using the KBr pellet method (**Figure 4.5.A**). The monomer showed

characteristic peaks at 1632, 1506, 1319, and 769 cm^{-1} corresponding to –NH bending of primary amine, C=C stretching, C-N stretching, and aromatic C-H out-of-plane bending characteristics of 1, 2-disubstituted phenyl rings respectively. The monomer showed peaks at 3367 and 3080 cm^{-1} corresponding to –NH stretching of a secondary amine and primary amine, respectively [38]. The polymer also showed characteristic peaks at 3352, 3176 and 3038 $cm^{-1,}$ corresponding to –NH stretching of secondary amines and asymmetric and symmetric $–NH_2$ stretching of primary amines, respectively. The moderate peak at 1670 cm^{-1} in the polymer was attributed to the characteristic –NH bending vibration of primary amine, which confirmed the presence of the primary $–NH_2$ group in the polymer. The polymer has shown intense peaks at 1517, 1319, and 769 cm^{-1} corresponding to C=C stretching, C-N stretching, and aromatic C-H out-of-plane bending similar to monomer. The peak at 846 cm^{-1} in the polymer corresponds to C-H out-of-plane bending vibrations characteristic of 1, 2, 4 - trisubstituted phenyl rings [39-41]. The polymer has shown additional moderate peaks at 1247 and 1371 cm^{-1} corresponding to the C-N stretching of secondary aromatic amines, which were weak in monomers. The different peak positions of –NH bending, additional peaks of C-N stretching, and C-H bending indicate polymer formation.

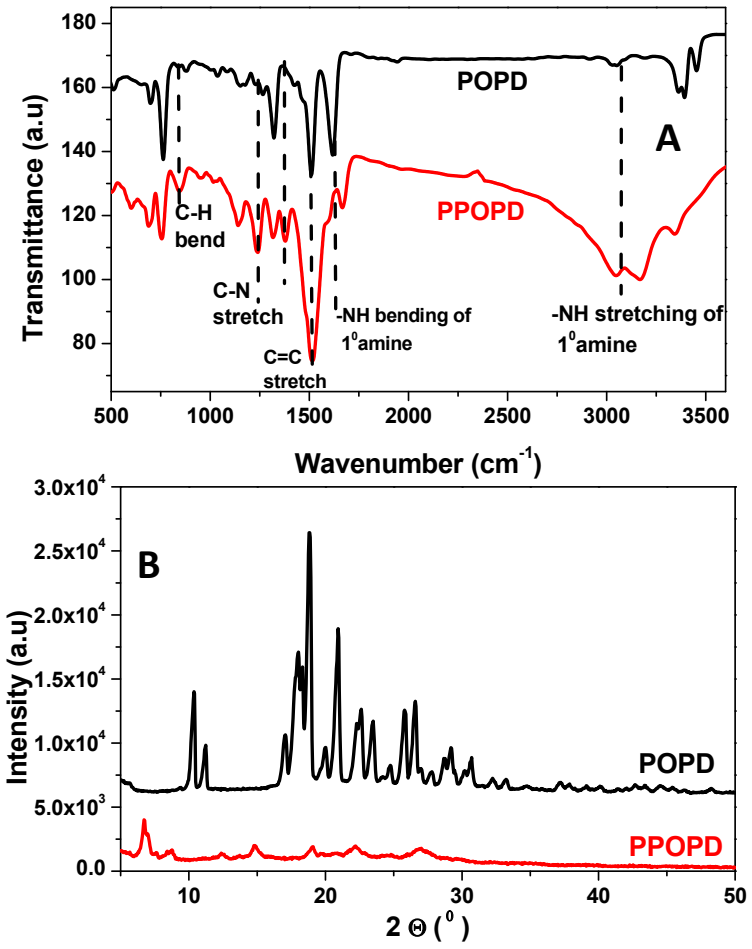

Figure 4.5. *A) FT-IR spectra of* ***POPD*** *and* ***PPOPD*** *and B) Powder WXRD diffractogram of* ***POPD*** *and* ***PPOPD.***

The solid-state ordering of the monomer and polymer was studied by powder X-ray diffractogram (**Figure 4.5.B)**. The powder form of the monomer showed sharp peaks at 2θ values 10.26, 11.39, 18.24, 21.30, 22.44, 23.44, 25.70, 26.55, 28.82, and 30.80, which indicated the crystalline nature of the monomer. The X-ray diffraction pattern of the polymer has shown different peaks with less intensity at 2θ values 6.83, 8.86, 12.23, 14.72, 19.16, 20.55, 22.15, 24.52, and 26.89. The weak inter-chain interactions between the polymer chains could lead to a semi-crystalline nature in the polymer [42-44].

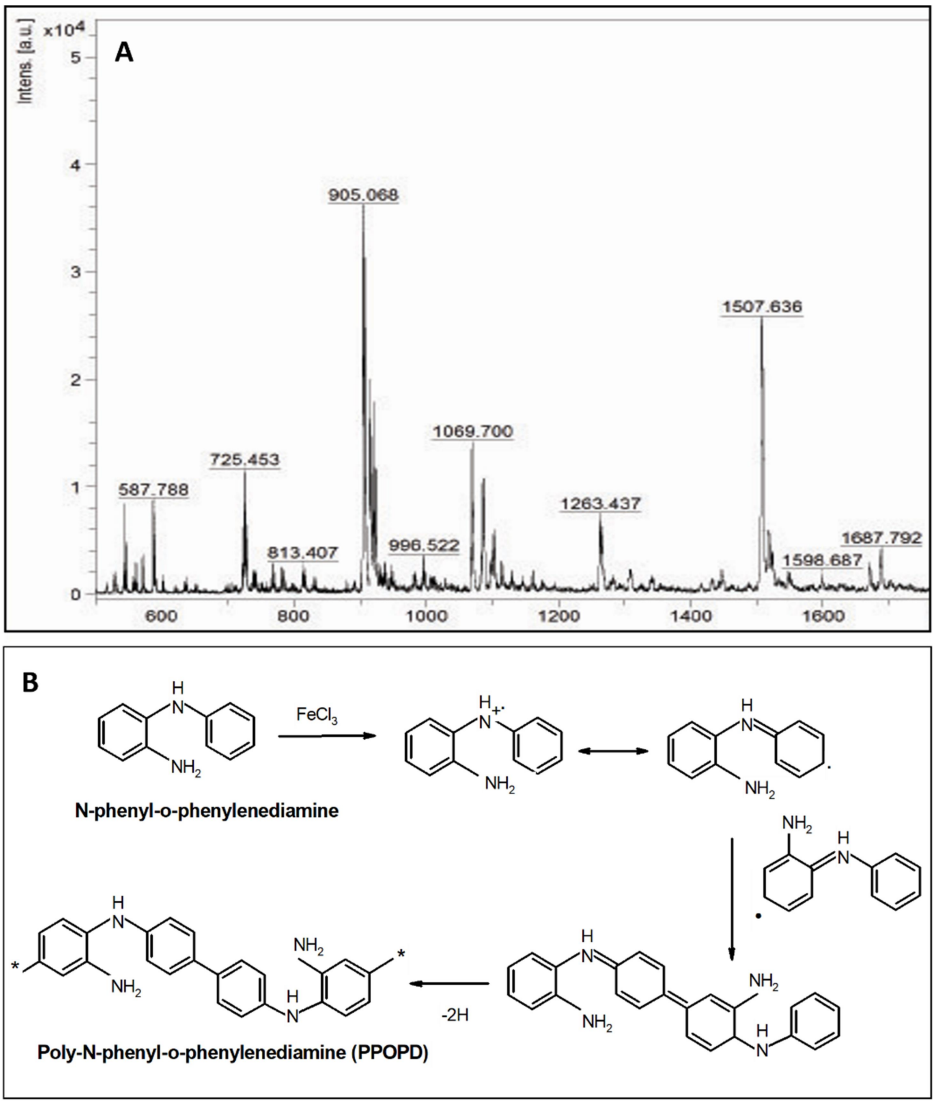

Figure 4.6. *A) MALDI-TOF spectra of* ***PPOPD****. B) Possible mechanism of formation of* ***PPOPD.***

MALDI-TOF analysis of **PPOPD** has been carried out to determine the molecular weight and number of repeating units present in the polymer chains using the sinapinic acid matrix (**Figure 4.6.**). The molecular ion peaks in the polymer have been repeated with an m/z value equal to 182 amu, with the mass ranging between 725-1687 amu indicating the polydispersity of sample. The average repeating units of polymer **PPOPD** were 5 to 6 units with an average molecular mass of 905 amu. Polyaniline and poly-N-phenyl-o-phenylenediamine were structurally different with the coupling of monomer units. The synthesized **PPOPD** existed as a non-conducting conjugate polymer. The molecular weight of polymers affects their mechanical and electrical properties. The high molecular weight polymer provides high mechanical strength, film forming properties, and low processability, whereas low molecular weight polymers impart ease of processability. The electrical conductivity of polymer could also increase with molecular weight, because of the increase in the charge carriers produced with the increase in the polymer chain length [52,53]. But here, even though **PPOPD** has low molecular weight, its conductivity increased by doping. The dried **PPOPD** polymer, after dipping in concentrated sulphuric acid, has shown electrical conductivity of 1.4×10^{-3} S/cm. On the other hand, usually, polyaniline synthesized exists as a conducting polymer with electrical conductivity in the semiconducting range. The possible mechanism of the formation of **PPOPD** is given in **Figure 4.6.B**. The monomer POPD were oxidised to form cation radicals. These cation radicals polymerize together to form a dimer through C-C bond formation similar to polydiphenylamines.

4.3.3. The pH-dependent absorption studies of PPOPD

The UV-visible absorption spectra of the **PPOPD** solution were taken with a change in pH, and corresponding photographs were shown in **Figure 4.7.A**. The high solubility of the polymer in water was attributed to the hydrogen bonding interaction of –NH groups of the polymer and water. The UV-visible absorption spectra of **PPOPD** have shown two absorption maxima at 278 nm and 485 nm in water, which corresponds to л-л* transition and extended л- л* transitions of the benzenoid segments, respectively [37]. The orange color of the aqueous **PPOPD** (7.5×10^{-5} M) solution in water has changed to pink as the pH value decreased to <1.5, showing a concomitant red shift in absorption

maxima to 518 nm. **PPOPD** solution showed a blue shift of absorption maxima to 455 nm with a change to yellow color as the pH value increased to 10. The absorbance maxima of **PPOPD** at three different wavelengths (455, 485, and 518 nm) were plotted against increasing pH in the same plot to see the effect of pH on absorption maximum (see **Figure 4.7.B**).

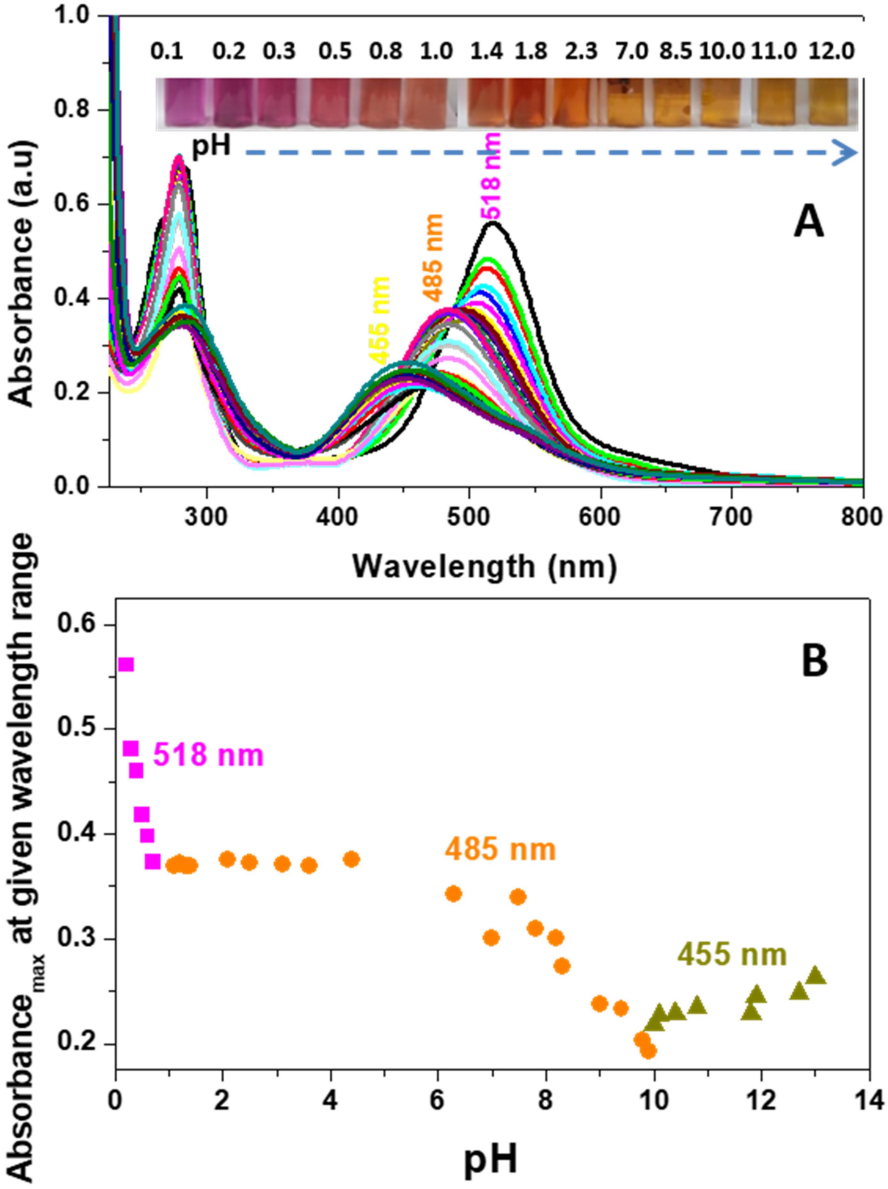

Figure 4.7. *A) pH-dependent UV-visible absorption spectra of 7.5 × 10^{-5} M* ***PPOPD*** *and photographs of aqueous solutions of* ***PPOPD*** *at different pH and B) Plot of absorbance maxima (at 518, 485, and 455 nm) versus increasing pH.*

The absorbance and intensity of the **PPOPD** solution at 518 nm have shown an enhancement with a decrease in pH <1.5, whereas it shows a slight irregular increase in

high pH >9 at 455 nm. The color change of the **PPOPD** solution with a change in pH was reversible and could be repeated. The blue shift in absorbance with increased pH may be due to the formation of partial quinoid rings in the polymer chain similar to the emeraldine base [45]. An enhanced conjugation after protonation results in a bathochromic shift to 518 nm, followed by a hyperchromic shift on decreasing the pH <1.5. A bathochromic shift was observed in the emeraldine form of polyaniline on protonation [46]. The pH-dependent absorbance studies revealed that **PPOPD** has a large pH window as a pH-sensitive material. UV-visible absorption spectra of polymer in water were recorded in different concentrations ranging from 2.5×10^{-4} M to 1×10^{-5} M (see **Figure 4.8.**). The molar extinction coefficient of **PPOPD** has a value of 7290.08 $mol^{-1}Lcm^{-1}$ for absorbance at 485 nm [46]. A relatively high molar extinction coefficient indicated that the polymer has the characteristics of organic polymer dye, which has good absorbance even with a very minimum concentration of sample [47].

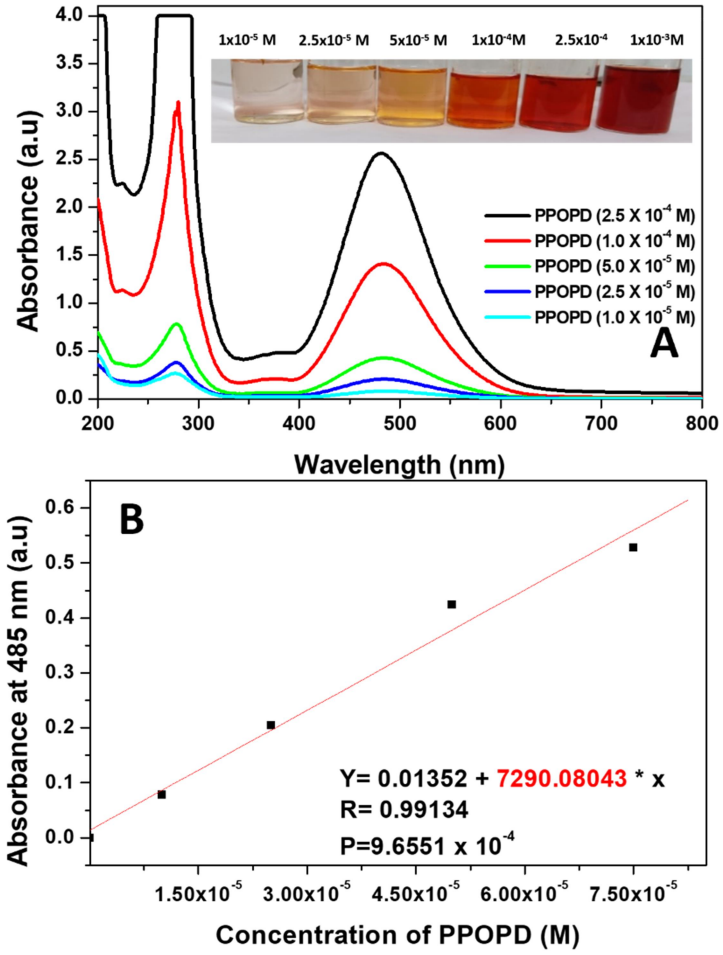

Figure 4.8. *A) UV-visible absorption spectra of different concentrations of* ***PPOPD*** *in water and B) Determination of molar extinction coefficient of* ***PPOPD****.*

Strong and weak acids were added to the **PPOPD** solution (7.5×10^{-5} M) to see the change in absorbance and color with acid strength. The UV-visible absorption spectra of **PPOPD** were recorded in 1 M acid concentration, and their photographs were given in **Figure 4.9.** The absorbance for strong acids at 518 nm followed the order perchloric acid > sulphuric acid > hydrochloric acid > nitric acid > oxalic acid > acetic acid. Despite being dibasic acid, sulphuric acid has less absorbance than mono-basic perchloric acid. Similarly, oxalic acid, being dibasic, was weaker than perchloric, hydrochloric, and nitric acid. Therefore, the absorbance at 518 nm and intensity of the pink color of **PPOPD** depends on acidic strength and not on the basicity of acids. Acids weaker than oxalic acid have shown absorbance at 485 nm in following the order, phosphoric acid (tribasic) > sulphanilic acid > acetic acid **PPOPD** solution (see **Figure 4.9.**).

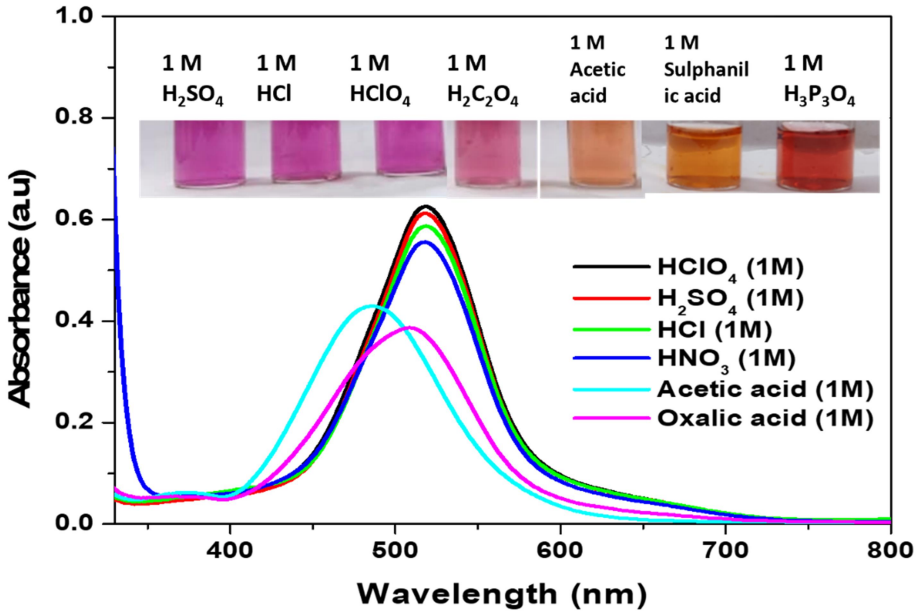

Figure 4.9. *UV-visible absorption spectra of* ***PPOPD*** *solution in different acids having acid strength 1M and photographs of* ***PPOPD*** *in different acids.*

4.3.4. Electrochemical studies

The cyclic voltammogram of **PPOPD** have been recorded in water and in the presence of acid to determine the system's electrochemical stability using a glassy carbon working electrode. The **PPOPD** solution has shown redox activities in the negative potential as well as positive potential sweep, which arose due to the coupled electron and proton transfer in polymer (see **Figure 4.10.A**). The anodic peaks at -0.11 V and +0.40 V

arose due to the oxidation of **PPOPD**. In the cathodic sweep, the peaks at +0.21 V and -0.53 V, were obtained corresponding to the reduction of oxidized **PPOPD**. The cyclic voltammogram of **PPOPD** in 1% and 4% H_2SO_4 were given in **Figure 4.10.B**. The anodic peak potentials corresponding to the oxidation of **PPOPD** at +0.01 V and +0.54 V in the anodic sweep and two peak potentials corresponding to the reduction of **PPOPD** at -0.39 V and + 0.36 V in the cathodic sweep were observed. However, the peak potentials were shifted positively in an acidic medium. The peaks corresponding to the oxidation and reduction of **PPOPD** remained at the same potentials on anodic sweep and cathodic sweep for **PPOPD** in 1% and 4% acid solutions, indicating the electrochemical stability of **PPOPD** in the presence of different acid contents.

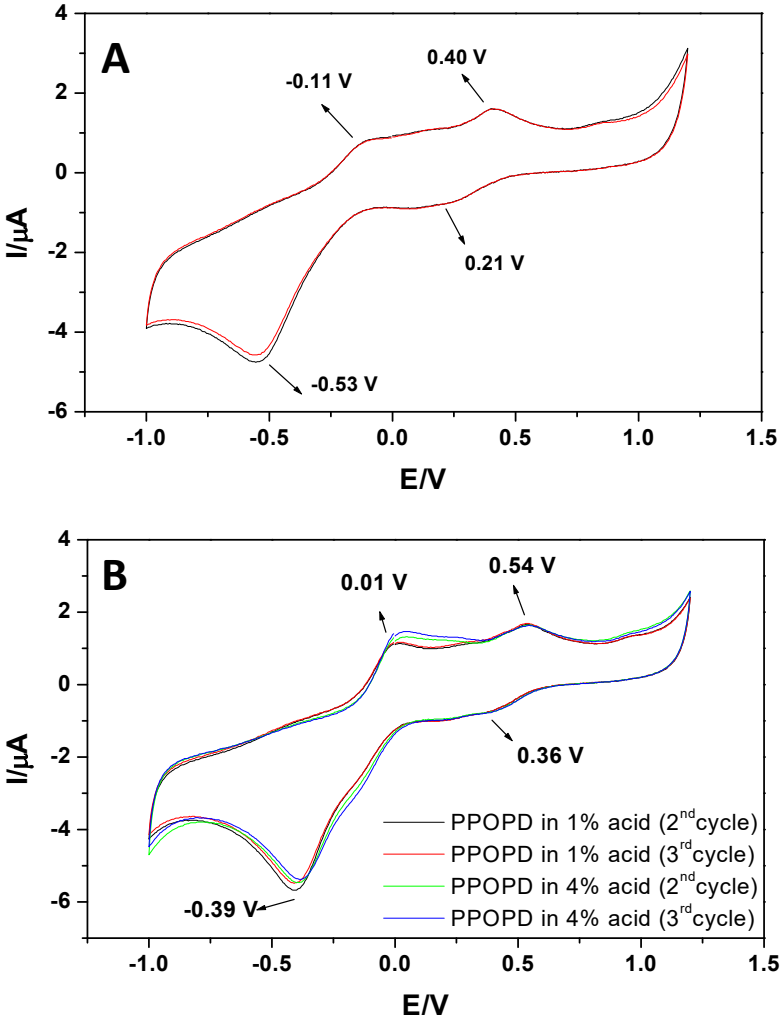

Figure 4.10. *Cyclic voltammogram of* ***PPOPD*** *in A) water and B) 1% and 4% H_2SO_4 solutions.*

The UV-visible absorption spectra of **PPOPD** (7.5×10^{-5} M) were mixed with known sulphuric acid percentages ranging from 0.5 % to 4 %, which is given in **Figure 4.11.A**. The absorbance of the **PPOPD** solution increases with acid strength at 518 nm wavelength. The linear calibration of absorbance with different sulphuric acid concentrations has shown good agreement with R = 0.9963, and P <0.0001 was obtained (see **Figure 4.11.B**). This linear calibration plot of **PPOPD** solution within this acid percentage helps us to determine unknown acid contents. In addition, the stability of the aqueous solution of **PPOPD** and standard deviations in absorbance for calibration were also studied. The calibration plot was repeated using **PPOPD** solutions, which were duplicated four times from the same batch of synthesized polymer (see **Figure 4.11.A.**). The standard deviation for absorbance at 518 nm obtained for 1 % was slightly higher and was 0.010. For other acid percentages (2%, 3%, 4%, and 5%), the standard deviation was less than 0.01.

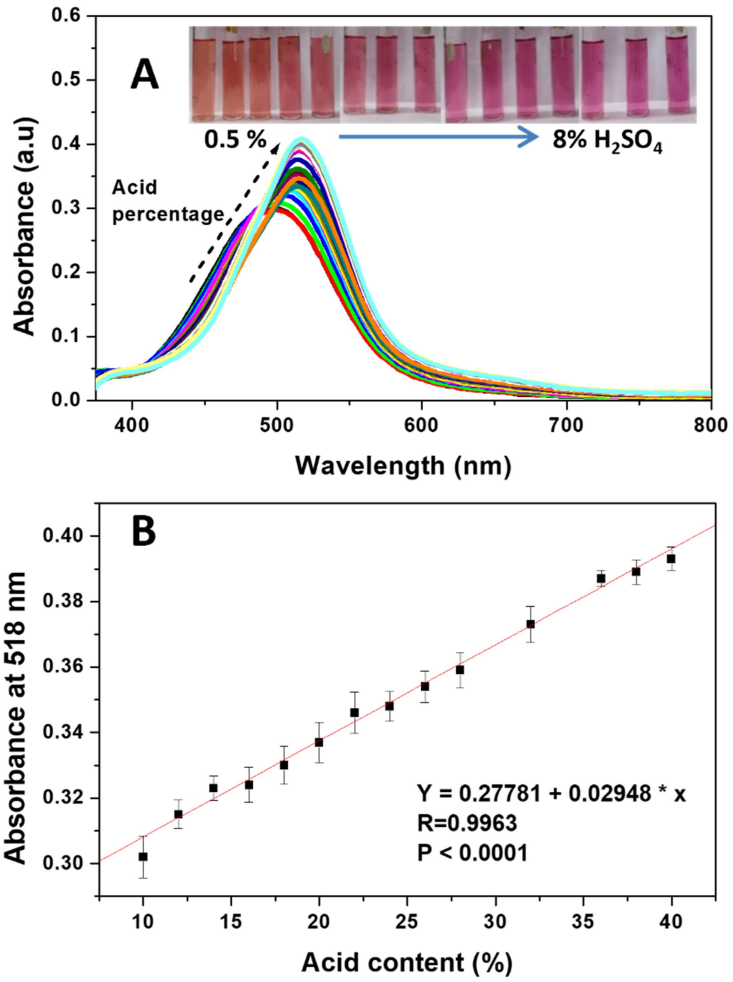

Figure 4.11. *A) UV-visible absorption spectra of* ***PPOPD*** *(7.5×10^{-5} M) and their photographs in solutions having different H_2SO_4 percentages ranging from 0.5 % to 4% and B) Calibration plot (absorbance at 518 nm vs. acid percentage) for the determination of unknown acid content.*

Time-dependent studies were carried out using a bulk quantity of **PPOPD** solution (7.5×10^{-5} M, 1 L) and UV-visible absorption spectra were recorded by adding 1% to 5% acid solutions to different **PPOPD** solutions in the time intervals of qtr. hour (quarter hour), 48 hours, 96 hours, 144 hours, and 384 hours. A standard deviation of less than 0.006 was obtained for the absorbance of **PPOPD** in each acid percentage (see **Figure 4.12.B**.). The stability of **PPOPD** was also checked by recording UV-visible absorption spectra of **PPOPD** alone in different time intervals of 0.25 hours, 48 hours, 96 hours, 144 hours, and 384 hours. The absorbance of **PPOPD** was found to be stable and not diminished with time. The UV-visible absorption spectra of **PPOPD** having concentrations of 7.5×10^{-5} M, 1.0×10^{-4} M, and 2.0×10^{-4} M were recorded by adding acid solutions of 6% to 10%. For **PPOPD** solution with a concentration of 7.5×10^{-5} M, the absorbance at 518 nm ranged from 0.500 to 0.560 (see **Figure 4.12.C.**). For higher concentrations of **PPOPD,** like 1.0×10^{-4} M and 2.0×10^{-4} M, the absorbance at 518 nm was increased and ranged from 0.8 to 1.0 and 1.60 to 1.82, respectively. The absorbance at 518 nm of **PPOPD** was enhanced linearly with higher percentages of acids by increasing the polymer concentration. Thus, higher acid contents could also be determined using the calibration method with **PPOPD** by increasing the polymer concentration. The absorbance maxima may slightly shift with the formation of high molecular weight of polymers, however with the formation of 5-6 repeating units no major change in their optical properties were expected. For very hight molecular weight polymers, the processability could be an issue. The lack of processability of high molecular weight polymer could affect their absorption. But the samples, prepared under similar reaction conditions, have absorbance maxima at 518 nm. The UV-visible absorption spectra of aqueous **PPOPD** solutions prepared from different batches were also recorded in the presence of 1% and 4% acid. The absorbance at 518 nm has shown only slight changes, even with different batches of samples. This indicated the stability of **PPOPD** as well as the practicability of **PPOPD** for determining acid contents (see **Figure 4.13.C** and **4.13.D.**). However, it is recommended that the calibration curve repeated for **PPOPD** synthesized from different batches.

The signal-to-noise ratio was determined by recording UV-visible absorption spectra of **PPOPD** (7.5×10^{-5} M) in the presence of 4% acid for 15 times using the formula [51],

$$\frac{S}{N} = \frac{S_{signal}}{Noise_{rms}} = \frac{\overline{X}}{S}$$

Where $\overline{X}$ is the average of absorbance at a particular wavelength and S is the standard deviation in absorbance at a particular wavelength. The signal-to-noise ratio obtained for absorbance at 518 nm was 457.92, which indicated better signal quality at 518 nm, whereas signal-to-noise ratio of absorbance at 282 nm was obtained as 71.21.

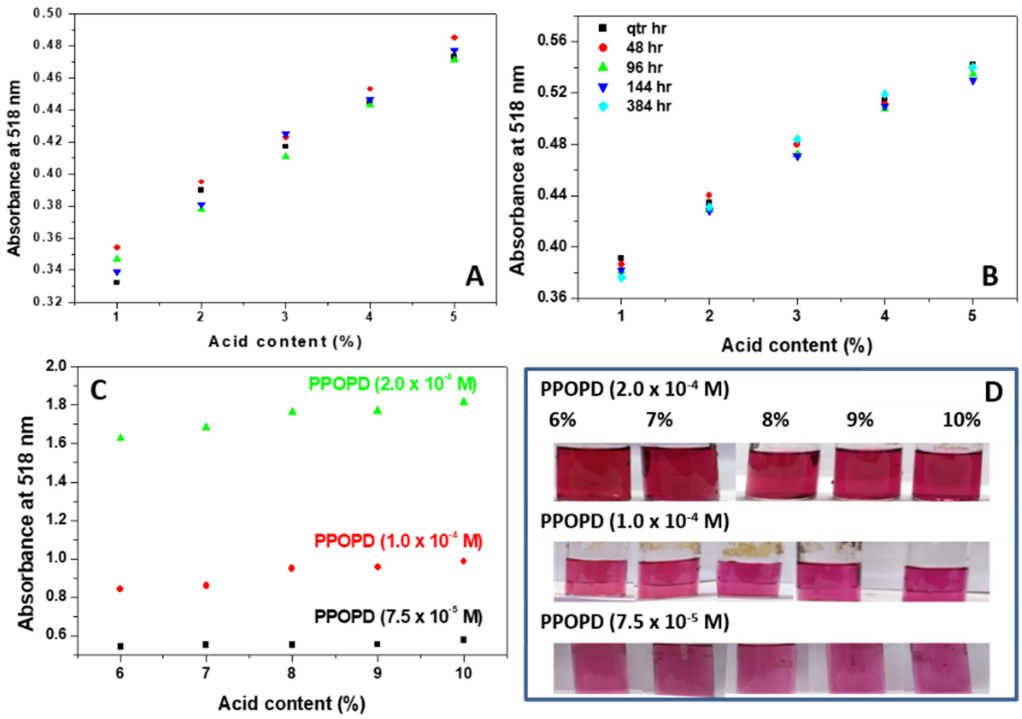

Figure 4.12. *A) Absorbance of **PPOPD** solution duplicated four times from the same solution at 518 nm from known acid percentage. B) Absorbance of **PPOPD**, prepared in bulk quantity measured at 518 nm acid solutions at qtr. hour, 48 hours, 96 hours, 144 hours and 384 hours. C) Absorbance of **PPOPD** solution having concentrations (2×10^{-4} M, 1×10^{-4} M and 7.5×10^{-5} M) at 518 nm taken from known acid solutions and D) corresponding photographs of **PPOPD** solutions.*

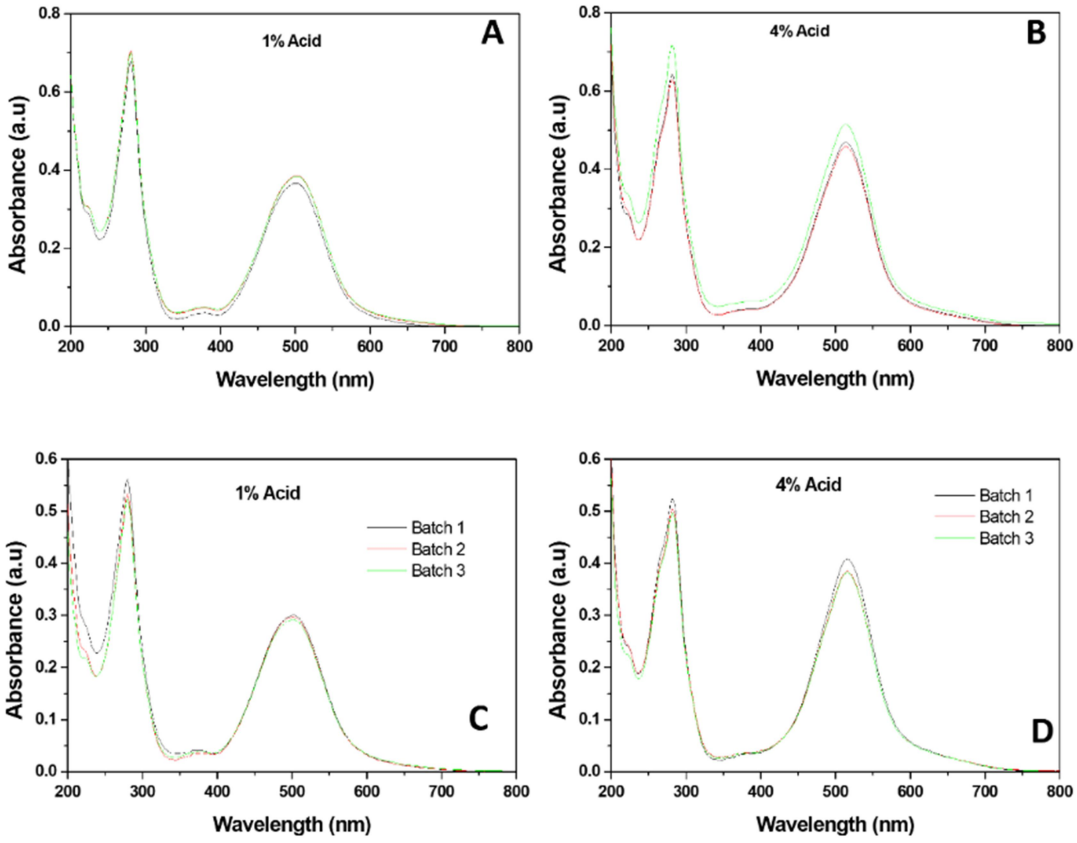

***Figure 4.13**. UV-Visible absorption spectra of **PPOPD** solutions having A) 1% acid, B) 4% acid prepared from bulk solution of **PPOPD** and C) 1% acid, D) 4% acid prepared from three different batches of synthesized **PPOPD** samples.*

The specific gravity of the known sulphuric acid content (5 to 50%) were determined by measuring the density of samples. The plot of known acid content and specific gravity gave a good straight line with R= 0.9961 and P < 0.0001 (see **Figure 4.14**). In lead acid batteries, the specific gravity of battery acid was commonly determined using Hydrometer. The specific gravities of acid solutions having sulfuric acid percentages varying from 5 to 50 % were also determined by using a hydrometer also at 27 °C and obtained standard deviation for specific gravity determined using the hydrometer was higher. Thus, the specific gravity determination using density measurement is more accurate and precise compared to commonly adopted hydrometer measurement.

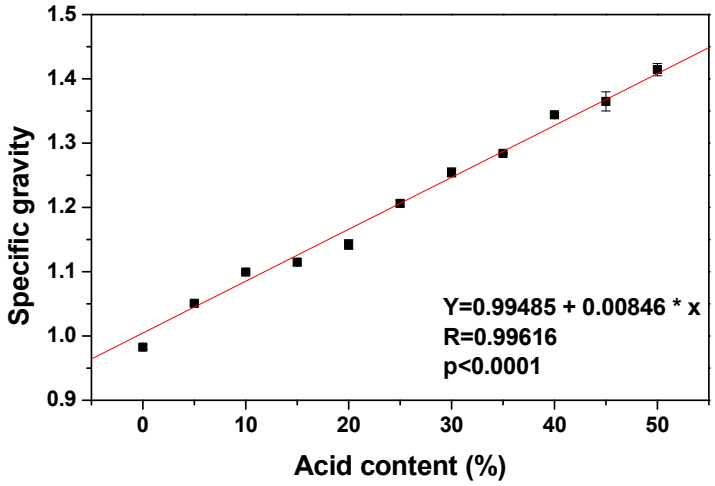

Figure 4.14. *Calibration plot of specific gravity of standard acid solutions from density measurements at 27°C with error bars (N=3).*

4.3.5. State of charge determination in Lead-acid batteries using PPOPD

The aqueous **PPOPD** solutions prepared from the same batch had a negligible change in absorbance even after storing the solution for three weeks. The sharp linear response at 518 nm, with an increase in acidic strength at low pH (<1.5), prompted us to determine the acid percentage of lead-acid batteries. Lead-acid batteries are rechargeable batteries that consist of two electrodes dipped in sulphuric acid as a working electrolyte. The positive electrode was lead dioxide, and the negative electrode was metallic lead. Both electrodes react with the electrolyte during the discharging process, resulting in lead sulfate deposition, whereas during the charging process, the deposited sulfate was removed from the electrodes as sulfuric acid into the electrolyte. Fully charged lead-acid batteries contain approximate sulphuric acid of about 39.7%, whereas its concentration will fall below 10% in completely discharging conditions [48]. Therefore, the change in acid content can be monitored by the ex-situ colorimetric change of the **PPOPD** solution from orange to pink color with a change in absorbance. The acid contents corresponding to battery acids during charging and discharging were determined by extrapolating the absorbance at 518 nm in the calibration plot obtained for known acid percentage or specific gravity. The known acid content used for calibration, absorbance at 518 nm and specific gravity corresponding to the acid content was given in **Table 4.2.**

Table 4.2. *Acid content (%), absorbance of* ***PPOPD*** *at 518 nm having known acid content, and specific gravity determined from direct density and hydrometer.*

Acid content (%)	Absorbance at 518 nm	Specific gravity determined from	
		Direct density measurement	Hydrometer
10	0.306	1.0997	1.16
15	0.322	1.1143	1.19
20	0.337	1.1416	1.21
25	0.352	1.2063	1.22
30	0.365	1.2537	1.26
35	0.381	1.284	1.27
40	0.395	1.3442	1.28

An automated lead-acid battery of 12 V was discharged using a DC bulb of 100 Watts for discharging studies and charged using a 5-ampere automatic battery charger for charging studies. The battery was disconnected from the load/source for 15 minutes to maintain the open circuit, and voltage was determined using a multimeter [8]. First, the open circuit potential of the fully charged or fully discharged battery was checked to determine the values of constants a_1 and a_0 in equation (2), and the specific gravity of battery acid was determined using hydrometer, followed by the collection of battery acid for the colorimetric acid estimation. Battery acid (1 mL) was collected from the lead-acid battery during discharging and charging intervals and was diluted to 10 mL. The battery acids collected during charging or discharging have 10%- 40% acid content. Ten times dilution results in acid content in the range of 1-4%. Therefore, the acid percentage used in the linear calibration plot and the acid percentage from the battery stand in the same range.

The images of the **PPOPD** (7.5×10^{-5} M) solution mixed with ten times diluted battery acids collected from the lead-acid battery during charging and discharging are shown in **Figure 4.15.** During charging, the intensity of the pink color of **PPOPD** increased with an increase in the battery's open circuit voltage, whereas on discharging, the intensity of the pink color decreased with battery voltage. The battery electrodes connected to an external load during discharging deposit the $PbSO_4$ on both electrodes by consuming the sulphuric acid electrolyte. Therefore, the color change and voltage drops were as per the decrease in sulphuric acid percentage. The deposition process was reversed during charging; the deposited $PbSO_4$ was removed from the PbO_2 anode and Pb cathode. The obtained acid content increase was as per the rise in the open circuit voltage

and color change. The completely discharged state of the lead acid battery produces 6.6% sulphuric acid, which may cause battery damage; therefore, we have set a minimum acid content as 10% for determining the SoC.

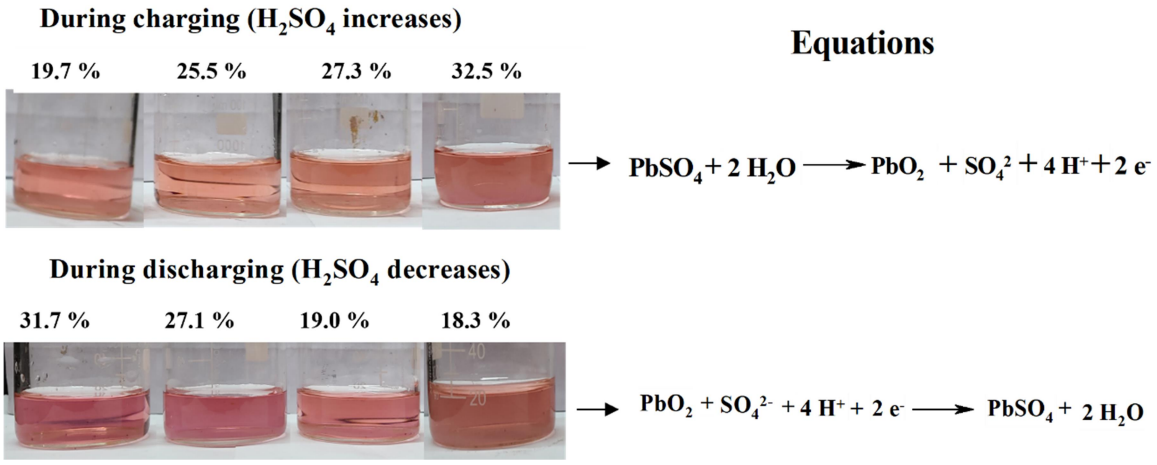

Figure 4.15. *The color change of* ***PPOPD*** *on adding battery acids and the electrochemical reaction inside the battery during charging and discharging.*

Different open circuit voltages noted during discharging of the lead acid battery and corresponding absorbance taken from UV-Visible absorption spectra of the battery acids mixed with **PPOPD** solution were shown in **Figure 4.16.A**. During discharging, the sulphuric acid content in the lead-acid battery decreases, resulting in a decrease in absorbance of **PPOPD** at 518 nm and a decrease in open circuit voltage. The acid contents corresponding to battery acids at different open circuit voltages were determined using extrapolation of absorbance to the linear calibration plot of known acid % (see **Figure 4.16.B**). The UV-Visible absorption spectra of battery acid with **PPOPD** solution during charging were also recorded (see **Figure 4.17.A**). During charging, the lead-acid battery's sulphuric acid content increases, resulting in higher absorbance of **PPOPD** at 518 nm and an increase in open circuit voltage. The acid contents corresponding to battery acids at different open circuit voltages were determined by extrapolating of absorbance obtained from the calibration plot of known acid percentage (see **Figure 4.17.B**).

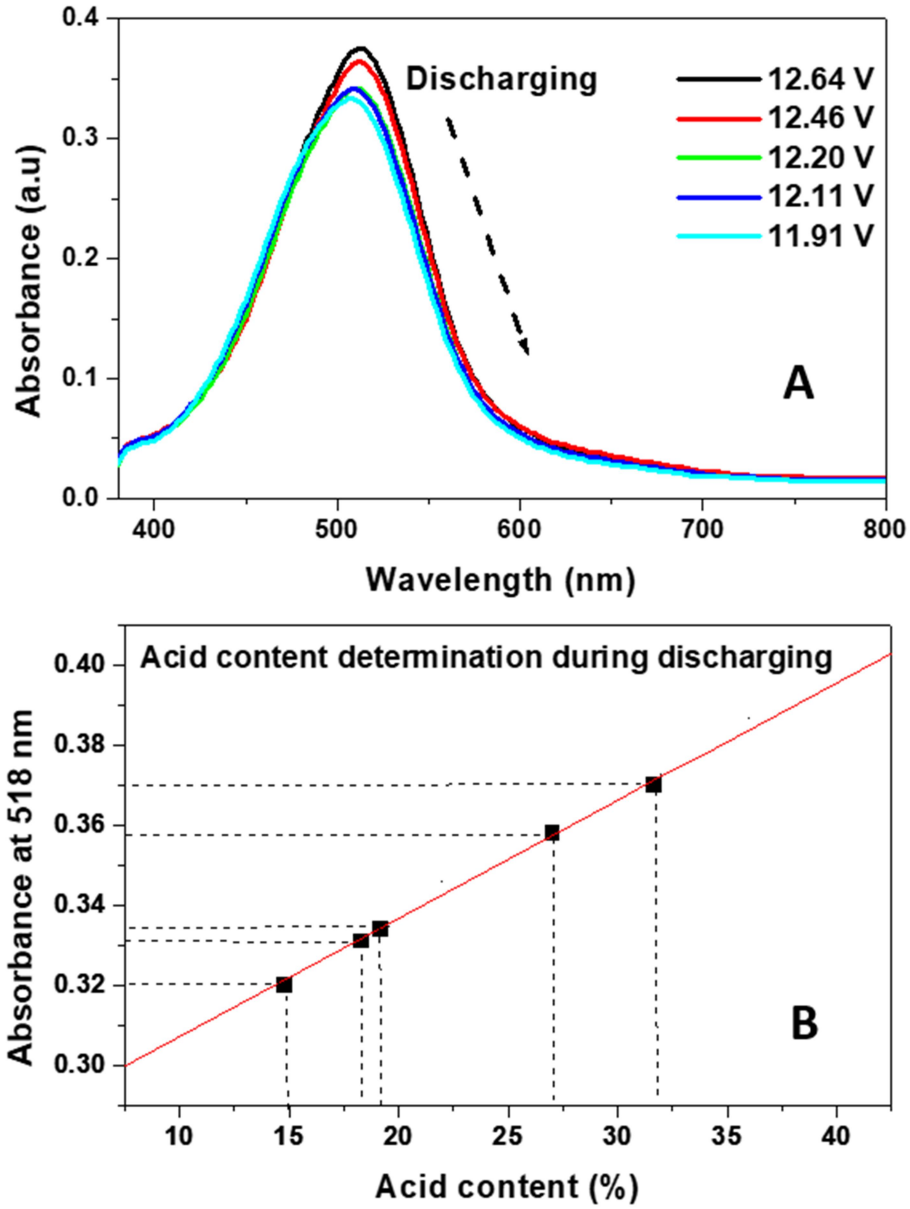

Figure 4.16. *A) UV-Visible absorption spectra of battery acids with* ***PPOPD*** *at different open circuit voltages on discharging conditions and B) Determination of battery acid content taken during discharging via extrapolating absorbance of* ***PPOPD*** *with the linear calibration plot.*

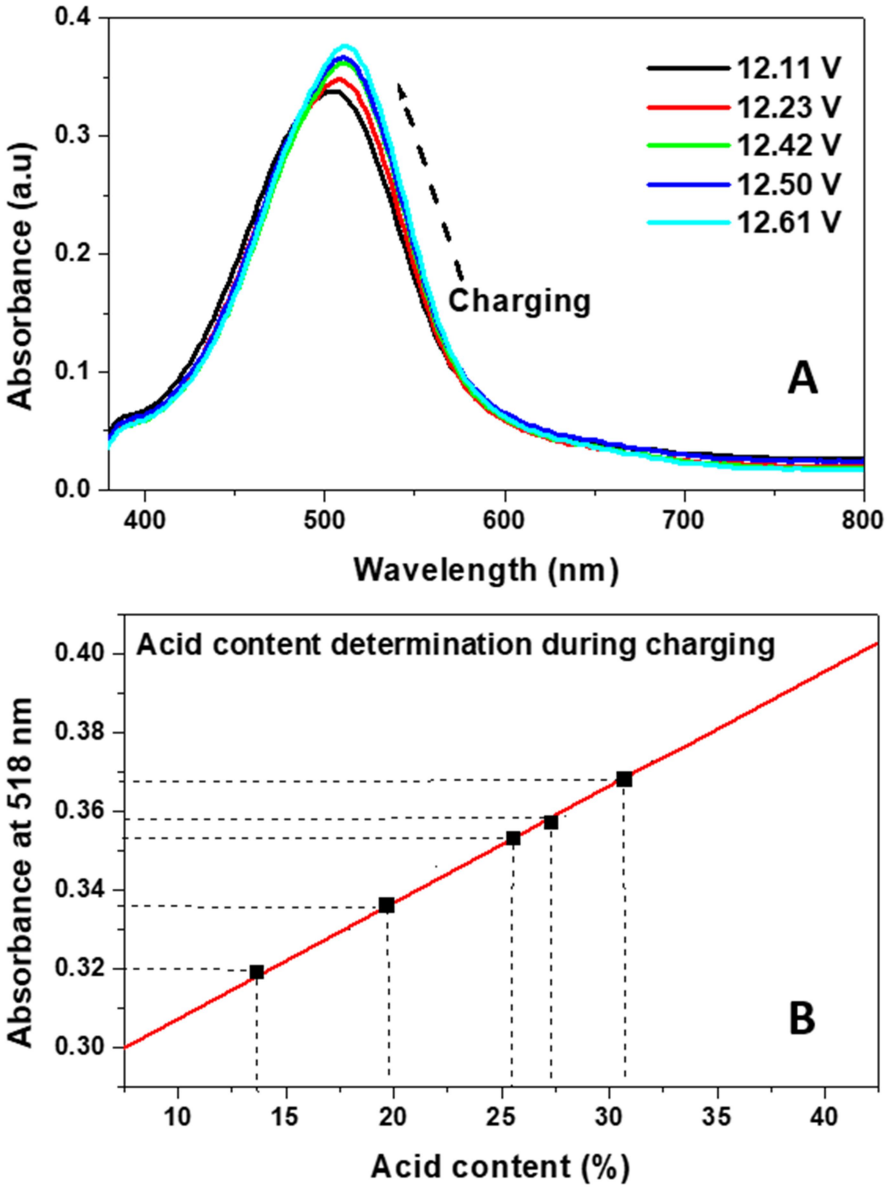

Figure 4.17. *A) UV-Visible absorption spectra of battery acids with* ***PPOPD*** *solution at different open circuit voltages on charging conditions and B) Determination of battery acid content taken during charging via extrapolating absorbance of* ***PPOPD*** *with the linear calibration plot.*

Here, we have proposed a mathematical equation to calculate the state of charge of the battery using the absorbance of **PPOPD** in battery acids at 518 nm.

$$SoC\ (t) = \left[\frac{A\ (t) - A_{min}}{A_{max} - A_{min}}\right] * 100 \quad \ldots\ldots\ldots\ldots\ldots\ldots\ldots\ldots\ (1)$$

Where $SoC\ (t)$ is the state of charge of the battery at a particular time 't', $A\ (t)$ is the absorbance of **PPOPD** from battery acid at a particular time 't' of measurement, and

A_{min}, was the absorbance of **PPOPD** in 10% sulphuric acid taken as 0.302 and A_{max}, was the absorbance of **PPOPD** in 40% sulphuric acid taken as 0.393. A lead-acid battery's maximum sulphuric acid content could not exceed 40%. Therefore, the upper limit of acid content was 40%, and its corresponding absorbance of **PPOPD** solution was 0.393, and the lower limit corresponding to the acid content of 10% was set at 0.302. For **PPOPD** synthesized in different batches, calibrations of acid content to determine A_{max} and A_{min} have to recalibrate to avoid experimental error. The state of charge in lead-acid batteries can thus easily be determined by knowing the absorbance of PPOPD in battery acid at 518 nm at any particular state or at any charging or discharging time of using the above formula. When the measured absorbance of **PPOPD** with battery acids was less than 0.302, the acid percentage would be less than 10%, and the battery's state of health would be in poor condition. Therefore, the absorbance of **PPOPD** on treatment with battery acid provided the battery's state of charge quantitatively. For **PPOPD** solution prepared from the same batch of polymer, only different $A\ (t)$ have to be determined and other parameters are same.

The state of charge was also determined from the open circuit voltage of the lead-acid battery using the formula [14],

$$SoC\ (t) = \left[\frac{V_{oc}\ (t) - a_0}{a_1}\right] \quad \ldots\ldots\ldots\ldots\ldots\ldots\ldots\ldots\ldots \ (2)$$

The value of a_0 was obtained by knowing the open circuit voltage of lead acid batteries in a completely discharged condition and was determined as 11.6 V using a multimeter. The value of a_1 is obtained by knowing the value of a_0 and V_{oc} (t) when SoC (t) =100. On fully charged condition, the open circuit voltage of the lead acid battery was determined as 13.0 V [21]. The state of charge calculated using absorbance values and open circuit voltage was compared on discharging and charging conditions (see **Figure 4.18.**).

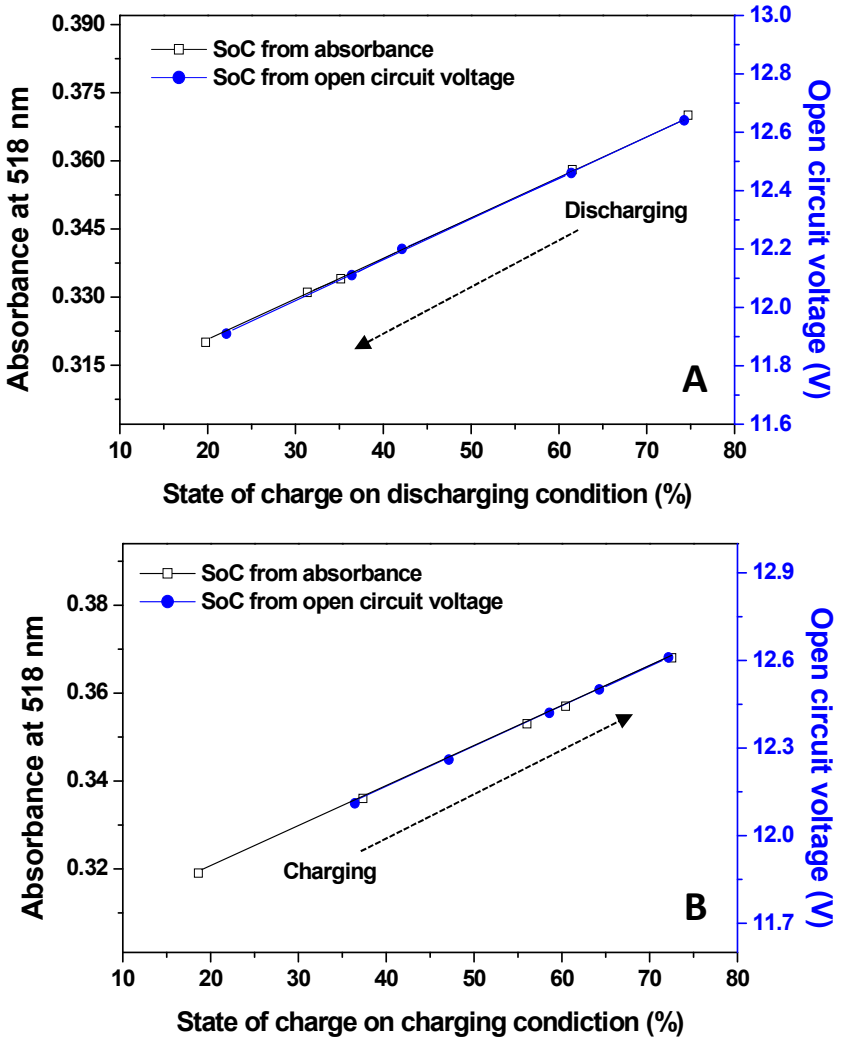

Figure 4.18. *State of charge vs. absorbance of* ***PPOPD*** *solution in battery acid at 518 nm and state of charge vs. open circuit voltage on discharging condition.*

The state of charges calculated from open circuit voltage and absorbance were almost equal at higher SoC, but slight variations were observed at SoC below 30%. It may be attributed to the lower limiting value set in SoC determination corresponding to the voltage (a_0) and absorbance (A_{min}) values. The A_{min} of **PPOPD** was set at 10%, and voltage A_0 was set at 11.6 V. Open circuit voltage value depends on temperature, current, and other electronic parameters [49]. This situation could cause fluctuations in the measured open circuit voltage [13]. Furthermore, the battery has to be disconnected from the source or load for a while to take open circuit voltage. The state of charge calculated from open circuit voltage and the state of charge calculated from absorbance on discharging and charging conditions were given in **Table 4.3** and **Table 4.4**.

Table 4.3. *Specific gravity of battery acid on discharging intervals, open circuit voltage (V) of lead acid battery on discharging intervals, the absorbance of* ***PPOPD*** *in battery acid at 518 nm, battery acid content (%) determined from absorbance, and state of charge (%) calculated from open circuit voltage and absorbance of* ***PPOPD*** *in battery acid.*

Specific Gravity from Hydrometer Reading	Open circuit voltage on discharging (V)	Absorbance of PPOPD with battery acid	Battery acid content determined from absorbance (%)	Calculated SoC (%) from	
				open circuit voltage	Absorbance
1.230	12.64	0.370	31.7	74.285	74.725
1.220	12.46	0.358	27.1	61.428	61.538
1.190	12.20	0.334	19.0	42.142	35.164
1.170	12.11	0.331	18.3	36.428	31.868
1.150	11.91	0.320	14.9	22.142	19.780

Table 4.4. *Specific gravity of battery acid on charging intervals, open circuit voltage (V) of lead acid battery on charging intervals, the absorbance of* ***PPOPD*** *in battery acid at 518 nm, battery acid content (%) determined from absorbance, and state of charge (%) calculated from open circuit voltage and absorbance of* ***PPOPD*** *in battery acid.*

Specific gravity from Hydrometer Reading	Open circuit voltage on charging (V)	Absorbance of PPOPD with battery acid	Battery acid content determined from absorbance (%)	Calculated SoC (%) from	
				open circuit voltage	Absorbance
1.140	12.11	0.319	13.6	36.428	18.681
1.160	12.26	0.336	19.7	47.142	37.362
1.180	12.42	0.353	25.4	58.571	56.043
1.200	12.50	0.357	27.3	64.285	60.439
1.220	12.61	0.368	32.5	72.142	72.527

Thus, the state of charge could be quickly checked using the formula knowing the A_{min}, A_{max} and A(t) of the **PPOPD** solution with battery acid. The state of charge of an inverter battery was determined from absorbance of battery acids in **PPOPD** solution.

The battery was disconnected from the source or the load for 15 minutes. Then, 1 mL of acid was collected and the corresponding open circuit voltage was measured using a digital multimeter. In order to measure the absorbance of **PPOPD** in battery acid, the collected acid (1 mL) was made up to 10 mL using deionized water in a 10 mL standard flask and mixed with 10 mL **PPOPD** solution having a concentration of 7.5×10^{-5} M. The absorbance of **PPOPD** at 518 nm was obtained as 0.387 at an open circuit voltage of 12.89 V. The calculated state of charge of the inverter battery from absorbance was 93.4065 % with A_{max} of 0.393 and A_{min} of 0.302. The state of charge determined from open circuit voltage was 92.14 % with a_0 of 11.6 and a_1 of 0.014. A good agreement in the state of charge obtained from absorbance and open circuit voltage given the practical applicability of the proposed method to battery research. Battery undergoing quick discharge can be detected from the state of charge measured at two different time intervals. In the present work, poly-N-phenyl-o-phenylenediamine (**PPOPD**) was applied as a colorimetric acid content sensor to determine the SoC of lead acid battery using a UV-visible absorption spectrometer as the main equipment. Work is in progress to replace the UV-visible spectrophotometer with a simple colorimeter using a filter for 520 nm to determine the state of charge at an affordable expense in large numbers. Thus, the state of charge and state of health of the battery can be easily determined from the absorbance of poly-N-phenyl-o-phenylenediamine solution with battery acids.

4.4. Conclusion

A ex-situ colorimetric method has been developed to determine the state of charge of lead-acid batteries from their change in acid content during charging or discharging, which have been carried out ex-situ. The basic principle of the method was the colorimetric change of poly-N-phenyl-o-phenylenediamine (**PPOPD**) with different concentrations of battery acid. The oxidative chemical polymerization of monomer N-phenyl-o-phenylenediamine was carried out using ferric chloride as the oxidizing agent in ethanol solvent. The orange-colored **PPOPD** solution changed to pink in an acidic medium, and its absorbance showed a linear increase with acid concentration. The UV-visible absorption spectrometer was used as the primary analytical tool to determine colorimetric change. The absorbance of the **PPOPD** solution versus the known acid percentage was calibrated and used to determine the unknown concentration of battery acid. The absorbance of the **PPOPD** solution was linearly correlated with acid percentage

and the linear calibration curve was used to obtain the unknown battery acid content. An empirical formula have been set to determine the state of charge (SoC) of lead-acid battery by taking absorbance of acid with **PPOPD** at different charging and discharging intervals. The absorbance of **PPOPD** solution for 10% and 40% acid concentration was set as a lower limit and upper limit, respectively, to determine the SoC of battery acid. The SoC determined using the absorbance of the battery acid was accurate and matched with the open circuit voltage method, particularly at higher SoCs. In a nutshell, a colorimetric acid content sensitive method has been proposed to determine the battery acid content and state of charge of the lead acid battery by checking the absorbance of the water-soluble and pH-sensitive poly-N-phenyl-o-phenylenediamine (**PPOPD**) solution.

Reference

1. Batchelder, D. N. (1988). Colour and chromism of conjugated polymers. *Contemporary Physics*, *29*(1), 3–31. https://doi.org/10.1080/00107518808213749.
2. Sadeghi, K., Yoon, J.-Y., & Seo, J. (2020). Chromogenic Polymers and Their Packaging Applications: A Review. *Polymer Reviews*, *60*(3), 442–492. https://doi.org/10.1080/15583724.2019.1676775.
3. Qiao, Y., Xu, T., Zhang, Y., Zhang, C., Shi, L., Zhang, G., Shuang, S., & Dong, C. (2015). Green synthesis of fluorescent copper nanoclusters for reversible pH-sensors. *Sensors and Actuators B: Chemical*, *220*, 1064–1069. https://doi.org/10.1016/j.snb.2015.06.073.
4. Ko, Y., Jeong, H. Y., Kwon, G., Kim, D., Lee, C., & You, J. (2020). pH-responsive polyaniline/polyethylene glycol composite arrays for colorimetric sensor application. *Sensors and Actuators B: Chemical*, *305*, 127447. https://doi.org/10.1016/j.snb.2019.127447.
5. Grummt, U.-W., Pron, A., Zagorska, M., & Lefrant, S. (1997). Polyaniline based optical pH sensor. *Analytica Chimica Acta*, *357*(3), 253–259. https://doi.org/10.1016/S0003-2670(97)00572-2.
6. Antohe, I., Jinga, L.-I., Antohe, V.-A., & Socol, G. (2021). Sensitive pH Monitoring Using a Polyaniline-Functionalized Fiber Optic—Surface Plasmon Resonance Detector. *Sensors*, *21*(12), 4218. https://doi.org/10.3390/s21124218.
7. Jin, Z., Su, Y., & Duan, Y. (2000). An improved optical pH sensor based on polyaniline. *Sensors and Actuators B: Chemical*, *71*(1–2), 118–122. https://doi.org/10.1016/S0925-4005(00)00597-9.
8. Abu-Thabit, N., Umar, Y., Ratemi, E., Ahmad, A., & Ahmad Abuilaiwi, F. (2016). A Flexible Optical pH Sensor Based on Polysulfone Membranes Coated with pH-Responsive Polyaniline Nanofibers. *Sensors*, *16*(7), 986. https://doi.org/10.3390/s16070986.
9. Křivík, P., Vaculík, S., Bača, P., & Kazelle, J. (2019). Determination of state of charge of lead-acid battery by EIS. *Journal of Energy Storage*, *21*, 581–585. https://doi.org/10.1016/j.est.2018.12.020.
10. Megateli, R. M., Idir, G., & Arab, A. H. (2015). Study of the variation of the specific gravity of the electrolyte during charge/discharge cycling of a lead acid battery. *2015 3rd International Conference on Control, Engineering & Information Technology (CEIT)*, 1–4. https://doi.org/10.1109/CEIT.2015.7232980.

11. Catherino, H. A., Feres, F. F., & Trinidad, F. (2004). Sulfation in lead–acid batteries. *Journal of Power Sources*, *129*(1), 113–120. https://doi.org/10.1016/j.jpowsour.2003.11.003.
12. Schiffer, J., Sauer, D. U., Bindner, H., Cronin, T., Lundsager, P., & Kaiser, R. (2007). Model prediction for ranking lead-acid batteries according to expected lifetime in renewable energy systems and autonomous power-supply systems. *Journal of Power Sources*, *168*(1), 66–78. https://doi.org/10.1016/j.jpowsour.2006.11.092.
13. al Hadi, A. Muh. R., Ekaputri, C., & Reza, M. (2019). Estimating the state of charge on lead acid battery using the open circuit voltage method. *Journal of Physics: Conference Series*, *1367*(1), 012077. https://doi.org/10.1088/1742-6596/1367/1/012077.
14. Chang, W.-Y. (2013). The State of Charge Estimating Methods for Battery: A Review. *ISRN Applied Mathematics*, *2013*, 1–7. https://doi.org/10.1155/2013/953792.
15. Zhongxiaoi, L., Zhe, L., & Jianbo, Z. (2018). Alternate Adaptive Extended Kalman Filter and Ampere-hour Counting Method to Estimate the State of Charge. *2018 IEEE International Power Electronics and Application Conference and Exposition (PEAC)*, 1–4. https://doi.org/10.1109/PEAC.2018.8589972.
16. Hancke, G. P. (1990). A fiber-optic density sensor for monitoring the state-of-charge of a lead acid battery. *IEEE Transactions on Instrumentation and Measurement*, *39*(1), 247–250. https://doi.org/10.1109/19.50454.
17. Weiss, J. D. (1999). Optical state-of-charge monitor for batteries. US5949219.
18. Cherng, J. Y. (1994) Capacity indicator for lead-acid batteries. US5304433.
19. Patil, S. S., Labade, V. P., Kulkarni, N. M., & Shaligram, A. D. (2013). Analysis of refractometric fiber optic state-of-charge (SOC) monitoring sensor for lead acid battery. *Optik*, *124*(22), 5687–5691. https://doi.org/10.1016/j.ijleo.2013.04.031.
20. Cortázar, O. D., & Feliu, V. (2006). A simple and robust fiber optics system for measuring the lead-acid battery state-of-charge. *Journal of Power Sources*, *159*(1), 728–733. https://doi.org/10.1016/j.jpowsour.2005.11.052.
21. Piller, S., Perrin, M., & Jossen, A. (2001). Methods for state-of-charge determination and their applications. *Journal of Power Sources*, *96*(1), 113–120. https://doi.org/10.1016/S0378-7753(01)00560-2.
22. Deepti, D. J., & Ramanarayanan, V. (2006). State of charge of lead acid battery. *2006 India International Conference on Power Electronics*, 89–93. https://doi.org/10.1109/IICPE.2006.4685347.
23. Guo, Y. (2005). A sensor of sulfuric acid specific gravity for lead-acid batteries. *Sensors and Actuators B: Chemical*, *105*(2), 194–198. https://doi.org/10.1016/j.snb.2004.05.061.
24. Lorefice, S., & Malengo, A. (2004). An image processing approach to calibration of hydrometers. *Metrologia*, *41*(3), L7–L10. https://doi.org/10.1088/0026-1394/41/3/L02.
25. Ying-Shing Shiao, Ding-Tsair Su, Jui-Liang Yang, R.-W. H. (2008). Electrochemistry Theorem Based State-of-Charge Estimation of the Lead Acid Batteries for Electric Vehicles. *WSEAS Trans. Syst.*, *7* (10), 1092–1103.
26. Tang, C.-Y., & Lin, J.-T. (2020). Online Autonomous Specific Gravity Measurement Strategy for Lead-Acid Batteries. *IEEE Sensors Journal*, *20*(4), 1980–1987. https://doi.org/10.1109/JSEN.2019.2948778.
27. Anton Paar official website. https://wiki.anton-paar.com/in-en/density-and-density-measurement/measuring-the-density-and-specific-gravity-of-battery-acid-in-lead-acid-batteries/. (accessed 2023-04-19).
28. Yamamoto. (1993) Sulfuric acid concentration sensor and lead acid battery equipped with sulfuric acid concentration sensor. US5273841.
29. Yonezu, H.; Nitta, M.; Tsubota. (1987). Specific gravity detecting device for lead-acid battery. US4689571.
30. Spaziante, P. M.; Giuffre, L.; Modica, G. (1981). Measuring electrode for sulfuric acid concentration. US 4262252.
31. Bullock, K. R. (1991). The electromotive force of the lead□acid cell and its half-cell potentials. *Journal of Power Sources*, *35*(3), 197–223. https://doi.org/10.1016/0378-7753(91)80107-9.

32. Ruetschi, P. (2003). Silver–silver sulfate reference electrodes for lead-acid batteries. *Journal of Power Sources*, *113*(2), 363–370. https://doi.org/10.1016/S0378-7753(02)00549-9.
33. Hiller, V.A.W.; Coombes, P. (2004). *Hillier's Fundamentals of Motor Vehicle Technology*; 5th Edition; *Nelson Thornes Pvt. Ltd*.
34. Duan, X., Moghaddam, M., Wenkert, D., Jordan, R. L., & Smrekar, S. E. (2010). X band model of Venus atmosphere permittivity. *Radio Science*, *45*(2), n/a-n/a. https://doi.org/10.1029/2009RS004169.
35. N. Mondol, S.K.Das, N.A.Sultana, & M. R. I. Sheikh. (2011). Design, performance and economic analysis of a solar home system in remote area of bangladesh. *Proceedings of the International Conference on Mechanical Engineering and Renewable Energy 2011*.
36. McMurry, J., Fay, R. C. (2008). Chemistry. United Kingdom: Pearson Prentice Hall.
37. Das, K. R., Antony, M. J., & Varghese, S. (2019). Highly bluish-white light emissive and redox active conjugated poly-N-phenyl anthranilic acid polymer fluoroprobe for analytical sensing. *Polymer*, *181*, 121747. https://doi.org/10.1016/j.polymer.2019.121747.
38. Han, J., Liu, Y., Li, L., & Guo, R. (2009). Poly(*o* -phenylenediamine) Submicrosphere-Supported Gold Nanocatalysts: Synthesis, Characterization, and Application in Selective Oxidation of Benzyl Alcohol. *Langmuir*, *25*(18), 11054–11060. https://doi.org/10.1021/la901373t.
39. Ozkan, S. Zh., Eremeev, I. S., Karpacheva, G. P., Prudskova, T. N., Veselova, E. v., Bondarenko, G. N., & Shandryuk, G. A. (2013). Polymers of diphenylamine-2-carboxylic acid: Synthesis, structure, and properties. *Polymer Science Series B*, *55*(3–4), 107–115. https://doi.org/10.1134/S1560090413030032.
40. Pavia, D. L.; Lampman, G. M.; Kriz, G. S. (2001). *Introduction to Spectroscopy Third Edition*; Thomson Learning, Inc.
41. Rohini Das, K., & Jinish Antony, M. (2016). Synthesis and characterisation of water dispersible copolymer submicron spheres of poly-(phenylenediamine-co-N-sulfopropyl aniline) via random copolymerisation. *Polymer*, *87*, 215–225. https://doi.org/10.1016/j.polymer.2016.01.078.
42. Antony, M. J., & Jayakannan, M. (2011). Polyaniline Nanoscaffolds for Colorimetric Sensing of Biomolecules via Electron Transfer Process. *Langmuir*, *27*(10), 6268–6278. https://doi.org/10.1021/la200047t
43. Zaragoza-Contreras, E. A., Hernández-Escobar, C. A., Estrada-Monje, A., & Kobayashi, T. (2016). Synthesis of diphenylamine-co-aniline copolymers in emulsified systems using a reactive surfactant as the emulsifying agent and aniline monomer. *Synthetic Metals*, *214*, 5–13. https://doi.org/10.1016/j.synthmet.2016.01.007.
44. Showkat, A. M., Cao, X. T., Kim, D. W., Islam, M. R., & Lim, K. T. (2015). Characterization of poly(diphenylamine)-gold nanocomposites obtained by self-assembly. *IOP Conference Series: Materials Science and Engineering*, *77*, 012007. https://doi.org/10.1088/1757-899X/77/1/012007.
45. Djara, R., Holade, Y., Merzouki, A., Masquelez, N., Cot, D., Rebiere, B., Petit, E., Huguet, P., Canaff, C., Morisset, S., Napporn, T. W., Cornu, D., & Tingry, S. (2020). Insights from the Physicochemical and Electrochemical Screening of the Potentiality of the Chemically Synthesized Polyaniline. *Journal of The Electrochemical Society*, *167*(6), 066503. https://doi.org/10.1149/1945-7111/ab7d40.
46. Stejskal, J., Kratochvíl, P., & Radhakrishnan, N. (1993). Polyaniline dispersions 2. UV—Vis absorption spectra. *Synthetic Metals*, *61*(3), 225–231. https://doi.org/10.1016/0379-6779(93)91266-5.
47. Tonga, M., & Lahti, P. M. (2019). Designing conjugation-extended viologens for high molar absorptivity with longer wavelength absorption. *Synthetic Metals*, *254*, 75–84. https://doi.org/10.1016/j.synthmet.2019.06.003.
48. Pavlov, D., Naidenov, V., & Ruevski, S. (2006). Influence of H2SO4 concentration on lead-acid battery performance. *Journal of Power Sources*, *161*(1), 658–665. https://doi.org/10.1016/j.jpowsour.2006.03.081.

49. Man, K. L., Ting, T. O., Krilavicius, T., Wan, K., Chen, C., Chang, J., & Poon, S. H. (2012). Towards a hybrid approach to SoC estimation for a smart Battery Management System (BMS) and battery supported Cyber-Physical Systems (CPS). *2012 2nd Baltic Congress on Future Internet Communications*, 113–116. https://doi.org/10.1109/BCFIC.2012.6217989.
50. Webster.G & Eran.H. Measurement, Instrumentation and Sensors Handbook. Second Edition. CRC Press. (2014).
51. Busch, K. W., & Busch, M. A. (2018). Light Polarization and Signal Processing in Chiroptical Instrumentation. In *Chiral Analysis* (pp. 73–151). Elsevier. https://doi.org/10.1016/B978-0-444-64027-7.00003-3.
52. Walsh, D. J., Schinski, D. A., Schneider, R. A., & Guironnet, D. (2020). General route to design polymer molecular weight distributions through flow chemistry. *Nature Communications*, *11*(1), 3094. https://doi.org/10.1038/s41467-020-16874-6.
53. Pearson, D. S., Pincus, P. A., Heffner, G. W., & Dahman, S. J. (1993). Effect of molecular weight and orientation on the conductivity of conjugated polymers. *Macromolecules*, *26*(7), 1570–1575. https://doi.org/10.1021/ma00059a013.

.

CHAPTER 5

Redox Type Poly-o-phenylenediamine for Reversible Fluorescence Sensing of Silver ion

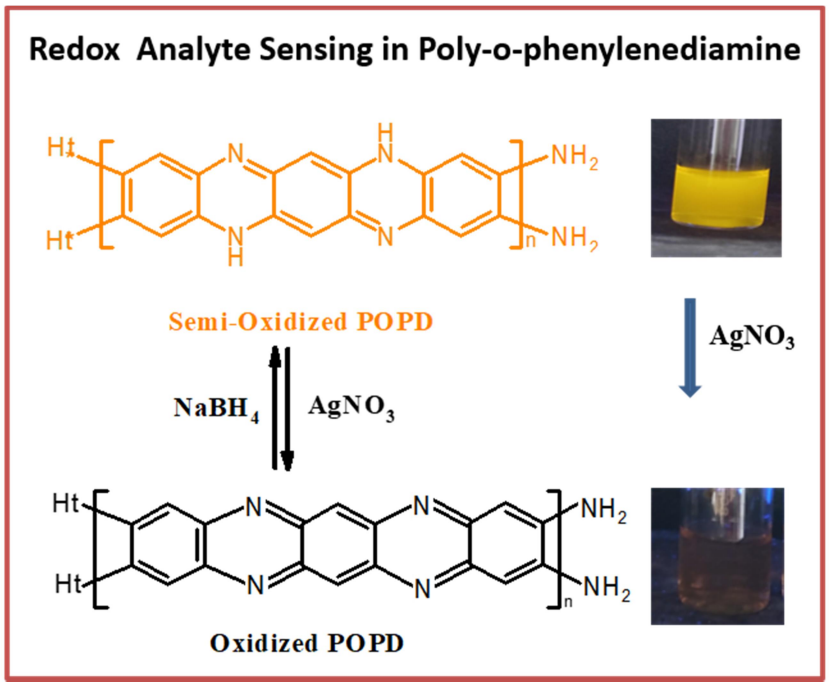

5.1. Introduction

Conjugated polymers have gained a wide research interest in the material development for chemical, electrochemical and biochemical sensors. The good optical, electrical and thermal performances and easy and low production cost of conjugated polymers were attractive for various applications [1, 2]. Polyaniline (PANI) is an important conjugated polymer known for its high conductivity, redox properties, and mechanical strength. However, poor solubility is a major concern in polyaniline. Several chemical methods, like doping or the use of alternate PANI derivatives, have been adopted to improve their solubility [3]. Phenylenediamines are an important group of aniline derivatives. Three isomeric forms of phenylenediamines are o-phenylenediamine, p-phenylenediamine, m-phenylenediamine, based on the positions of $–NH_2$ groups attached to the aromatic ring. These monomers were highly susceptible to either oxidative chemical polymerization, electrochemical polymerization, or enzyme-catalyzed polymerization to produce polyphenylenediamines [4]. The structural difference between polyanilines and polyphenylenediamines endowed them with different chemical and electrochemical properties. The advantage of polyphenylenediamines over polyaniline is the presence of additional –NH and terminal $–NH_2$ groups, which provide them multifunctionality. Better solubility and good opto-electronic properties of polyphenylenediamines make them advantageous over polyanilines.

Among the polyphenylenediamines, poly-o-phenylenediamine emerged as an efficient material due to their potential applications in various fields. Polyphenylenediamines were used in sensors, catalysts, coatings, and energy devices due to their strong opto-electroactivities, and antimicrobial activities, good spectral properties and high environmental and thermal stability [5, 6, 7]. POPD can be easily synthesized by electrochemical polymerization, microwave-assisted polymerization, and oxidative chemical polymerization utilizing oxidizing agents like $K_2Cr_2O_7$, $FeCl_3$, $HAuCl_4$, $(NH_4)_2S_2O_8$, H_2O_2, and $AgNO_3$ [8-17]. The structural properties and morphology of POPD can be controlled by the polymerization medium and reaction conditions [15, 18-20]. Nanorod, nanofibre, nanosphere, microrod, microsphere, and microfiber-shaped POPDs have been synthesized to make them suitable for different applications [18, 21-25]. POPD has also been used to form nanocomposites with graphene oxide, graphene nanosheets, carbon nanocomposites, Fe_3O_4, and $MnCoFe_2O_4$ [26]. These nanocomposites have several

applications in electrochromic devices, smart windows, and anti-corrosion materials due to the combined properties of organic polymer and inorganic materials.

Doping methods have been widely used in conjugated polymers to improve their properties. The excess charges developed in the polymer through the doping process can effectively alter the intrinsic properties of polymers, like conductivity, absorption and emission, and electroactivities. Poly-o-phenylenediamine has a better doping ability, similar to PANI. POPD has been doped with acids like HCl, H_2SO_4, H_3BO_3, inorganic ions like Cu (II), I_2, and organic molecules like luminol [19,27]. The dopant influenced the colour, fluorescence, band gap, electrical conductivity, voltammetric behavior, and POPD morphology. The structural changes and spectral changes associated with POPD during acid doping and undoping were studied by Olgun et al. [19] (see **Figure 5.1.**). The doping in POPD was confirmed using different spectroscopic analysis like proton NMR, FT-IR, and UV-visible absorption [19].

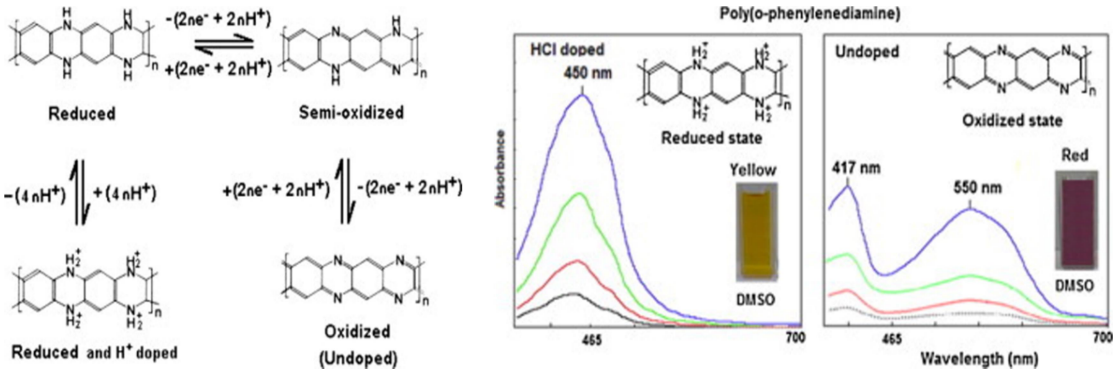

Figure 5.1. *Acid-doped and undoped forms of poly-o-phenylenediamine and corresponding changes in the UV-visible absorption spectra of POPD. (Adapted from Olgun et al. 2014).*

Redox-active conjugated polymers were suitable for efficient charge storage, electrode materials fabrication, and as an electron transfer mediator in living cells [29-31]. Conjugated polymers possess reversible or irreversible conjugated structures, which could be achieved by choosing the appropriate analyte. Therefore, the studies on the structure and redox properties of conjugated polymers like poly-o-phenylenediamine are important, since the properties of POPD and their applications were highly dependent on their structure. Samantha et al. studied the effect of the pH of the reaction medium and the presence of various inorganic acids on the structure and conductivities of POPD [15, 32]. Zhang et al. studied the dependence of the structure of POPD on its electrochemical

performance for the development of cathode material [1]. Wu et al. studied the electrochemical redox process in POPD film and reported three redox states (reduced, semi-oxidized and total oxidized) [20]. Ullah et al. utilized quantum mechanical calculation for the structural elucidation of POPD and determined the ladder-like structure of POPD [33]. The dependence of spectrochemical and electrochemical properties of POPD film and its redox transformations was studied by Bilal et al. [34].

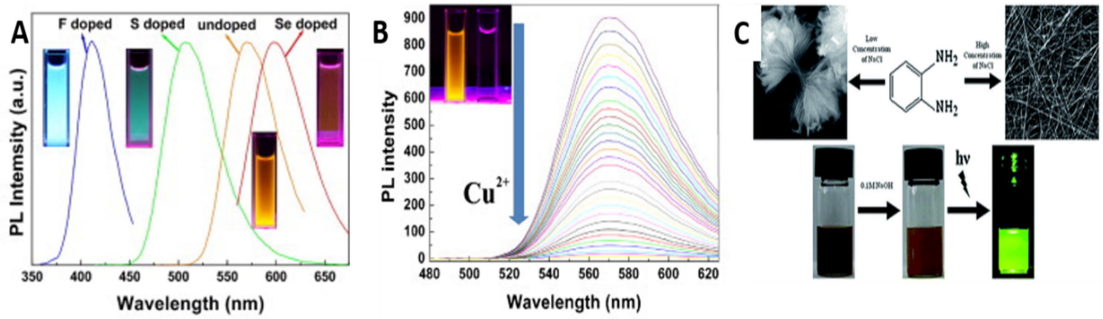

Figure 5.2. *A) Heteroatom-doped fluorescence tuning in POPD and B) fluorescent turn-off sensing of Cu^{2+} ions using POPD. (Adapted from Liao et al. 2014). C) Morphology-controlled fabrication of poly-o-phenyelendiamine and development of POPD-based fluorescent pH sensor (Adapted from Jiang et al. 2014).*

The potential use of POPD was spread across several areas, such as sensors, rechargeable cell electrodes, solar cell films, organic cathode material, corrosion protectors, and biomarkers. Different properties of poly-o-phenylenediamine have been utilized to sense various analytes (see **Table 5.1**). Many electrochemical sensors have been fabricated based on poly-o-phenylenediamines to detect biological analytes like glucose and ascorbic acid [35,36]. Fluorescence sensors based on poly-o-phenylenediamine were also developed and such sensors have an added advantage of amplified light sensitivity. Liao et al. used hetero atom doping to produce fluorescence tuning in POPD (see **Figure 5.2.A.**). An ultrasensitive fluorescence detection system for Cu^{2+}, Ca^{2+}, Hg^{2+} and H_2O_2 was also developed based on fluorescent POPD (see **Figure 5.2.B.**) [14]. Jiang et al. developed a POPD-based pH sensor based on the strong green fluorescence of POPD in basic pH [37]. (See **Figure 5.2.C.**) The yellow fluorescence emission developed during the oxidation of o-phenylenediamine was utilized for the sensing of various analytes. Ye et al. reviewed OPD-based sensors for various analytes like metal ions, chemical reagents, and biological enzymes based on the oxidation of monomer OPD [38].

Table 5.1. *POPD-based sensors reported in the literature.*

Sl. No.	Morphology	Analyte	LOD	Mode of sensing	Ref.
1	POPD nanospheres	Pd^{2+}	1 ppm	Fluorescence enhancement sensor	39
2	POPD microstructure	Basic pH	-	Fluorescence turn-on sensor	37
3	POPD nanospheres	Cu^{2+}, Ca^{2+}, Hg^{2+}, and H_2O_2	10^{-12} M	Fluorescence turn-off sensor	14
4	POPD colloid	Nucleic acids	0.52 ppb	Fluorescence turn-on sensor	40
5	Fluorescein doped POPD	Bovine serum albumin (BSA)	1.35 nM	Fluorescent turn-off sensor	41
6	POPD/Fe_2O_3 Composite	Ribonucleic acid (RNA)	0.1 µg/mL	Fluorescence turn-on sensor	42
7	POPD coated gold electrode	Electroinactive anions	Micromolar concentrations	Amperometric sensor	43
8	Sulphuric acid doped POPD	Ethanol	1.25 ppm	Electrochemical sensor	44
9	POPD and CdS/FeS nanocomposite	E.coli	6.1×10^5 CFU/mL	Electrochemical sensor	45
10	POPD-Graphene oxide composite	Dopamine	7.5 µM	Electrochemical sensor	46
11	POPD-Cu nanoparticle composite	Glucose	5 µM	Electrochemical sensor	47
12	POPD	Perfluorooctane sulfonate	0.4 nM	Electrochemical sensor	48

Silver ion (Ag^+) is an important heavy metal ion with antibacterial action and is used as a precursor for silver metal nanoparticles useful in many applications, including industrial catalysis [49, 50]. The amount of silver ion accumulation increases rapidly in water due to its widespread commercial application [51]. Although silver ions possess extremely low toxicity in topical medical preparation, the exceeding amount of silver (>100µg/L) in water can deactivate proteins in humans and damage cell functions in

humans [52]. Therefore, detecting and quantifying silver ions is a basic step to remedy the polluting effect of silver. Several analytical methods were used for silver ion sensing, such as high-performance liquid chromatography (HPLC), atomic absorption/emission spectroscopy, inductively coupled plasma-mass spectroscopy and electrochemical analysis. Fluorescent conjugated polymers could play a better role in fluorescence sensing due to their stability, reversibility, emission tunability, pH sensitivity, and presence of multiple redox states than small molecules. Conjugated polyquinolines, polytriazoles, polyquinoxalines, and polybenzimidazoles have been reported for silver ion sensing in solvents other than water [53-54]. However, the poor water solubility of these conjugated polymers may cause ineffectual sensing of silver ions in water. Wang et al. used water-soluble Pd (II) acetylide-based conjugated poly electrolyte for the colorimetric and fluorometric detection of silver ions in water [54].

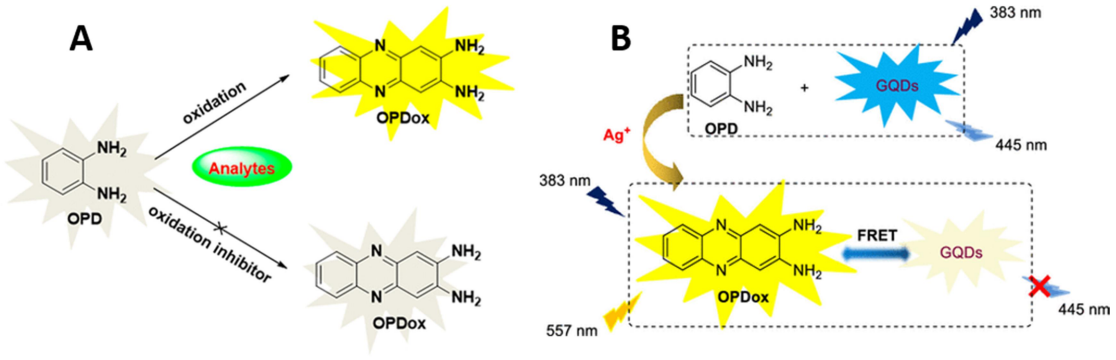

Figure 5.3. *Schematic representations of A) fluorescence sensing of analytes based on the oxidation of o-phenylenediamine and B) fluorescence development during the oxidation of o-phenylenediamine for Ag^+ ion detection (Adapted from Ye. et al., 2020).*

The sensing of Ag^+ ions and Cu^{2+} ions in the presence of autocatalysed metal nanoparticle to oxidize o-phenylenediamine (OPD) have been reported (see **Figure 5.3.**) [54-56]. However, the direct detection of silver ions using the aqueous solution of poly-o-phenylenediamine homopolymer via the oxidative fluorescence turn-off have not reported yet. The structural correlation of redox states of POPD on fluorescence emission and sensing would be an interesting case study. The present studies focus on the synthesis of poly-o-phenylenediamine via chemical oxidative polymerization using ferric chloride as an oxidizing agent in an ethanol medium. FT-IR and proton NMR spectra revealed a semi-oxidized structure of POPD with benzenoid rings and oxidized quinoid rings. The semi-oxidized POPD was further oxidized using $AgNO_3$, resulting in a fluorescent turn-

off in aqueous solution. The oxidized state of POPD undergoes redox reversibility and fluorescence turn-on upon adding $NaBH_4$ as a reducing agent.

5.2. Experimental

5.2.1. Materials and Reagents: O-phenylenediamine was purchased from Loba Chemicals. Anhydrous ferric chloride and sodium borohydride were purchased from Sigma Aldrich. Silver nitrate and concentrated sulphuric acid (98%) were purchased from Merck, India. Double-distilled ethanol and deionized water were used to synthesize and purify the polymer.

5.2.2. Measurements and Instruments: UV-visible absorption spectra of the samples were recorded by Shimadzu UV-visible spectrophotometer 1800 series in the 200-800 nm range using deionized water as solvent. Proton NMR was recorded using a 400 MHz Bruker Avance FT-NMR Spectrophotometer in DMSO-d_6 solvent using trimethyl silane (TMS) as an internal standard. The Fourier transform infrared spectra of the samples were recorded by Cary 660 FT-IR spectrometer using attenuated total reflectance (ATR) Mode. Powder X-ray diffraction of the samples was measured using PANALYTICAL, Aeris research diffractometer in the range of 2θ values from 5 to 80°. Polymer molecular weight determination of the POPD samples has been carried out using Bruker Autoflex max LRF MALDI-TOF using sinapinic acid as a matrix. The pH of solutions was measured using a portable pH meter from Hanna Instruments. Fluorescence spectra of the samples were recorded using a Shimadzu RF 5301-PC spectrofluorophotometer. Thermo gravimetric analysis (TGA) of the samples was measured using a simultaneous thermal analyzer STA 8000. Field emission scanning electron microscopic (FE-SEM) images of the samples were recorded using Zeiss Gemini SEM 300. Cyclic voltammetric studies of polymer were performed by using Ivium compactStat electrochemical interface consisting of a three-electrode electrochemical cell system in which Ag/AgCl is used as the reference electrode, small platinum wire is used as the counter electrode, and glassy carbon is used as the working electrode. Electrical conductivity of the sample was measured using DFP-RM-200 with constant current source Model CCS-01 and DC microvoltmeter.

5.2.3. Synthesis of poly-o-phenylenediamine (POPD): The monomer o-phenylenediamine (0.10 g, 0.93 mmol) was dissolved in 3 mL double distilled ethanol. The oxidizing agent anhydrous $FeCl_3$ (0.23 g, 1.38 mmol) dissolved in 2 mL ethanol was added dropwise into the monomer solution. The color of the solution immediately

changed from pale brown to dark brown upon adding the oxidizing agent. The polymerization was allowed to continue for 2 hours without disturbance. The solvent ethanol was completely evaporated, and the polymer was washed with water and acetone, then filtered and dried in the vacuum oven at 60°C. Yield= 0.070 g (70%). ^{1}H NMR (400 MHz, DMSO-d_6) δ: 7.02 (S, 2H, Ar-H), 7.75 (S, 2H, Ar-H), 8.04 (S, 2H, Ar-H). FT-IR (KBr, cm^{-1}): 3316, 3161, 1694, 1641, 1531, 1357, 1231, 1153, 843, 745 and 589.

5.2.4. Fluorescence turn-off in POPD solution using silver nitrate: Poly-o-phenylenediamine (1.10 mg) was accurately weighed into a 100 mL standard flask and made up to the mark using deionized water to obtain a yellow-colored POPD solution (1.0×10^{-4} M). The pH of the solution was kept at neutral pH (pH=7). To the 3 mL (1.0×10^{-4} M) each of POPD solution taken in different vials, 3 mL $AgNO_3$ solutions having different concentrations (1×10^{-2} M, 5×10^{-3} M, 2.5×10^{-3} M, 1×10^{-3} M, 5×10^{-4} M, 2.5×10^{-4} M, and 1×10^{-4} M) were added. Fluorescence of the polymer-analyte mixture was checked by irradiating UV light (365 nm) on the solutions in the presence of different concentrations of $AgNO_3$. UV-visible absorption and fluorescence spectra of POPD were recorded to get the quenching concentration of silver ion quantitatively.

5.2.5. Electrochemical studies: Poly-o-phenylenediamine (5.4 mg) was accurately weighed into a 10 mL standard flask and made up to the mark using deionized water to obtain a 5.0×10^{-3} M POPD solution. The cyclic voltammogram of 5.0×10^{-3} M POPD solution was recorded. The electrochemical activity of POPD solution in a neutral medium and in the presence of 0.1 M H_2SO_4 has been checked. The cyclic voltammetric studies were performed at a scan rate of 20 mV/s between the voltages -1.0 to +1.5 volt.

5.3. Results and Discussion

5.3.1. Synthesis of Poly-o-phenylenediamine

Poly-o-phenylenediamine (POPD) has been synthesized by oxidative chemical polymerization using anhydrous $FeCl_3$ as an oxidizing agent in an ethanol medium. The reddish-brown POPD powder was soluble in water (neutral, acidic, and alkaline pH), chloroform, acetone, ethanol, and dimethyl sulfoxide. The polymer is yellow in neutral and basic medium, orange in weakly acidic medium, and dark brown in concentrated acid solution (see **Figure 5.4.**).

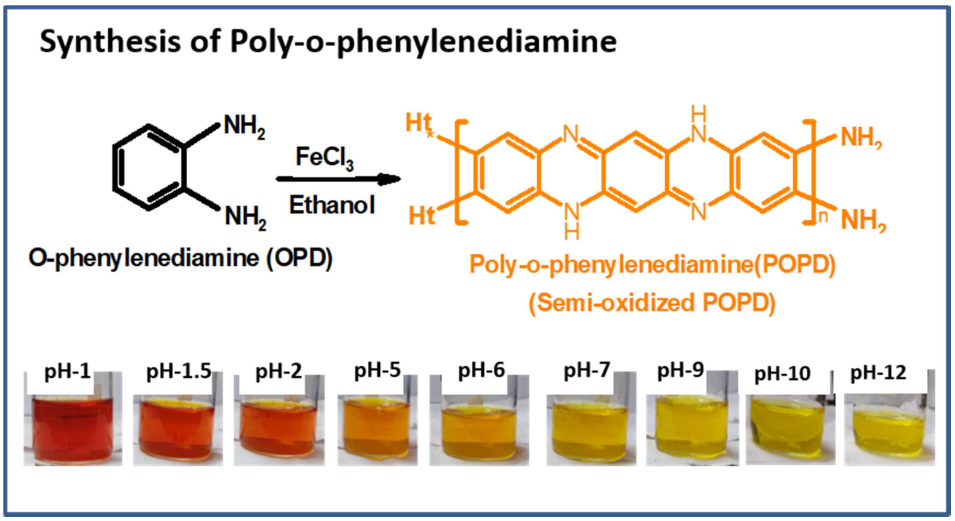

Figure 5.4. *Schematic representation of the synthesis of POPD from OPD by chemical oxidative polymerization and photographs showing pH-dependent color changes of POPD.*

5.3.2. Structural characterisation of POPD

The o-phenylenediamine (OPD) monomer and poly-o-phenylenediamine (POPD) polymer have good solubility in dimethyl sulfoxide (DMSO). The polymer formation was structurally characterized by proton NMR in deuterated DMSO-d_6 solvent, as given in **Figure 5.5**. The OPD monomer has shown three peaks in which the singlet at δ value 4.40 ppm was most shielded, which indicated the presence of $–NH_2$ protons. The multiplet at 6.55 ppm (H_1) and 6.40 ppm (H_2) indicated protons in the benzene ring, in which the later peak was more shielded due to the presence of nearby electron donating $–NH_2$ groups [57,58]. The synthesized POPD polymer was denoted as semi-oxidized POPD, containing benzenoid and oxidized quinoid units. The synthesized POPD polymer was denoted as semi-oxidized POPD, containing benzenoid and oxidized quinoid units. ^1H NMR spectra of semi-oxidized POPD have shown three peaks, the peak at 8.05 ppm indicating the presence of aromatic hydrogens (Ar-H). The peak at 7.75 ppm indicated either the protons in the benzenoid ring or secondary NH protons. Some literature evidence indicated the presence of NH protons in the NMR spectra of POPD at 7.74-7.72 ppm [10,19], whereas some other reports suggested the presence of aromatic hydrogens at 7.70 ppm [9]. The shielded singlet at 7.00 ppm was due to the quinoid protons (Q-H) [17, 59]. The semi-oxidized POPD was more deshielded than the monomer due to the conjugation of the POPD polymer chain.

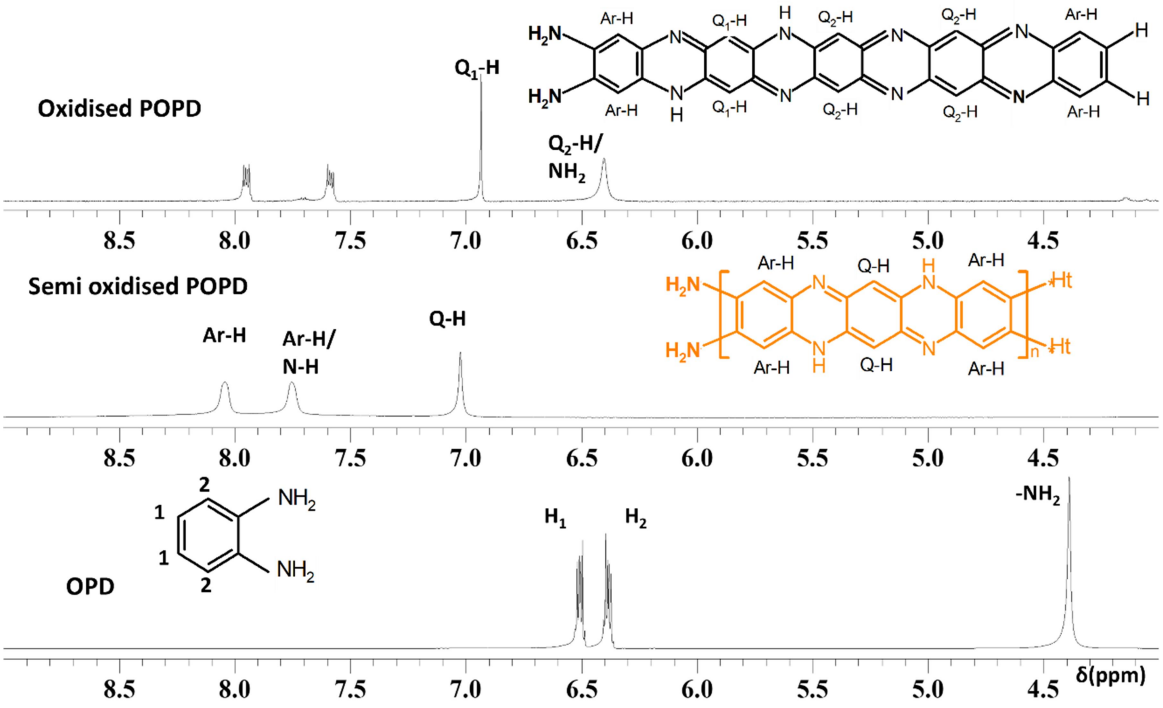

Figure 5.5. *^{1}H NMR spectra of OPD, semi-oxidized POPD and oxidized POPD in DMSO- d_6.*

The monomer (OPD) and polymer (POPD) were characterized by FT-IR spectroscopy by the attenuated total reflectance method (see **Figure 5.6.A.**). The monomer showed peaks at 3337 and 3198 $cm^{-1,}$ corresponding to asymmetric and symmetric –NH stretching vibrations of primary amines [8, 57]. The monomer showed characteristic peaks at 1641, 1498, 1269, and 749 cm^{-1} corresponding to $–NH_2$ bending vibration of the primary amine group, C=C stretching of the benzenoid ring, C-N stretching of the benzenoid ring, and C-H out of plane bending characteristic of 1, 2-disubstituted phenyl rings respectively [21, 57, 59]. The polymer showed a peak at 3316 $cm^{-1,}$ corresponding to –NH stretching of secondary amines [8]. The weak band at 3161 cm^{-1} indicated the presence of terminal primary $-NH_2$ groups. The polymer showed characteristic strong peaks at 1694, 1641, 1531, 1357, 1231, and 1153 cm^{-1} corresponding to C=N stretching of the quinoid ring, C=C stretching of quinoid ring merged with terminal $–NH_2$ bending, C=C stretching of the benzenoid ring, C-N stretching in the neighbourhood of quinoid units, C-N stretching in the neighbourhood of benzenoid ring, and C-H in-plane bending in quinoid rings [27, 60]. The benzenoid to quinoid ratio (B/Q ratio) calculated from C=C stretching vibration in the benzenoid ring at 1531 cm^{-1} and

C=N stretching vibrations in the quinoid ring at 1694 cm^{-1} was in the ratio 3:1, approximately matching with the proposed structure. The peak at 843 cm^{-1} in the polymer corresponds to C-H out-of-plane bending vibrations characteristic of 1, 2, 4, 5- tetra substituted phenyl rings [59]. The 745cm^{-1} and 589 cm^{-1} peaks indicated C-H bending of 1, 2-disubstituted phenyl rings and N-H out-of-plane bending vibrations [59]. The presence of C=N stretching at 1694 cm^{-1}, C-N stretching vibration in the neighbourhood of quinoid rings at 1357$cm^{-1,}$ and C-H out of plane bending at 843 cm^{-1} in polymer indicated the typical ladder-like structure of POPD with both benzenoid and quinoid rings as shown in **Figure 5.4.** [61,33].

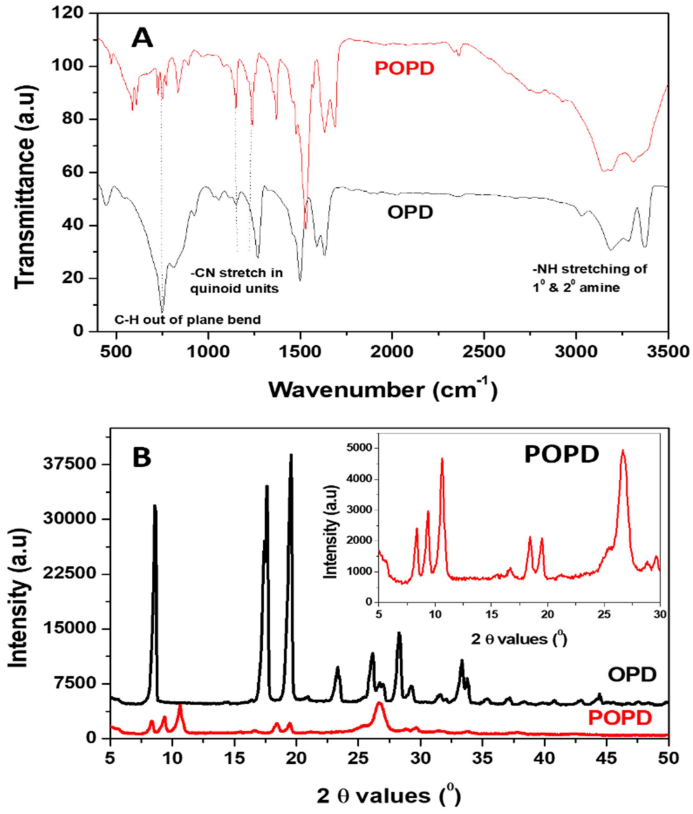

***Figure 5.6**. A) FT-IR spectra of OPD and POPD and B) Powder X-ray diffractogram of OPD and POPD.*

Monomer (OPD) and polymer (POPD) were subjected to powder X-ray diffraction to see the solid-state ordering of the samples (Figure **5.6.B.)**. The monomer showed sharp peaks at 2θ values 8.56, 17.62, 19.58, 23.41, 26.07, 28.29 and 33.36°. The presence of sharp peaks indicated the crystalline nature of the monomer, whereas the powder X-ray diffraction peaks of the polymer were present at 2θ values at 8.41, 9.31, 10.54, 18.32, 19.39, and 26.70°, which was less intense and different from the OPD. The

diffraction peaks of POPD polymer in the 2θ range 10-35° were mainly devoided of the amorphous domain [49] (see inset of **Figure 5.6.B.**). The conductivity of synthesized POPD was determined as 1.73×10^{-6} S/cm in the undoped state. The dried POPD polymer, after dipping in concentrated sulphuric acid, has shown increased electrical conductivity of 8.73×10^{-5} S/cm [10,15,18]. The increase conductivity of POPD films on doping were previously reported [19], which renders them practical use in electronic devices like interconnectors and sensors as electroactive organic materials. The electroactive POPD has been used as cathode for aqueous zinc batteries and anode for nonaqueous lithium batteries [1].

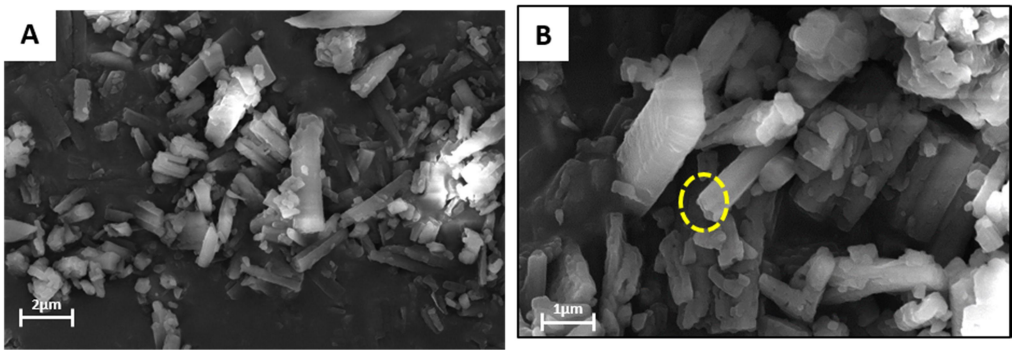

Figure 5.7. *FE-SEM images of POPD with different magnifications A) 2µm and B) 1 µm.*

The surface morphology of the polymer POPD was analyzed using a field emission scanning electron microscope (see **Figure 5.7.).** The polymer has a micro rod-like morphology with a length of around 4±2 µm and a width of around 0.5±0.2 µm. A hollow tube-like morphology was also observed in some areas. POPD micro rods formed due to the self-assembling of OPD oligomers via hydrogen bonds or due to the π to π* interactions [62-63]. The microrod like self-assembly of POPD has advantages in forming well defined, dynamic, and responsive structures. The microrod morphology makes them promising candidates for waste water purification and catalysis due to their high surface to volume ratio. One dimensional structure of microrods enabled their applications in optical wave guides to propagate light in tiny devices. They have also found applications in lithium-ion batteries, because of their rod like morphology can adjust with the volume change in the charge-discharge cycles and can rapidly transport electrons too. Microrods are useful in photonics due to their ability to exhibit an extra liquid crystal structure compared to spherical particles [79]. MALDI-TOF analysis of POPD has been carried out to determine the number of repeating units present in the polymer chains using the sinapinic acid matrix (see **Figure 5.8.A.**). A base peak was observed at m/z equal to 614

amu, indicating the presence of 5-6 monomer units in most of the polymer chains. The peaks at m/z equal to 688, 719, 793, 897, 1004, and 1211 amu indicated the presence of higher molecular weight fragments in the polymer chain. The m/z values of the polymer mainly repeated at a regular pattern of m/z equal to 105 amu for molecular formula [$C_6N_2H_5$] due to the monomeric repeating units. The thermal stability studies of OPD and POPD were carried out by thermogravimetric analysis, and the thermogram is given in **Figure 5.8.B.**. In the case of OPD, a sudden weight loss of 55 % was observed from 110°C to 170°C. But in the case of POPD, the thermogram was entirely different from OPD, in which 10% weight loss observed at 310 °C and then sudden weight loss of of 30% was observed at 348°C, possibly due to the weight loss from very low molecular weight oligomers. The second stage weight loss of 20 % was started from 348°C to 570°C due to the degradation of the polymer chains [10]. Further weight loss upto 50% observed at higher temperatures upto 570 °C. The higher thermal stability of POPD over monomer indicated the rigid ladder like structure of POPD [19]. Thus POPD can withstand high temperature without loss of strength or change in structure and the application studies of POPD like silver ion sensing could be possible at higher temperatures, even at 310˚C. These materials were applicable in aircrafts, space equipment etc, where temperature withstanding is essential.

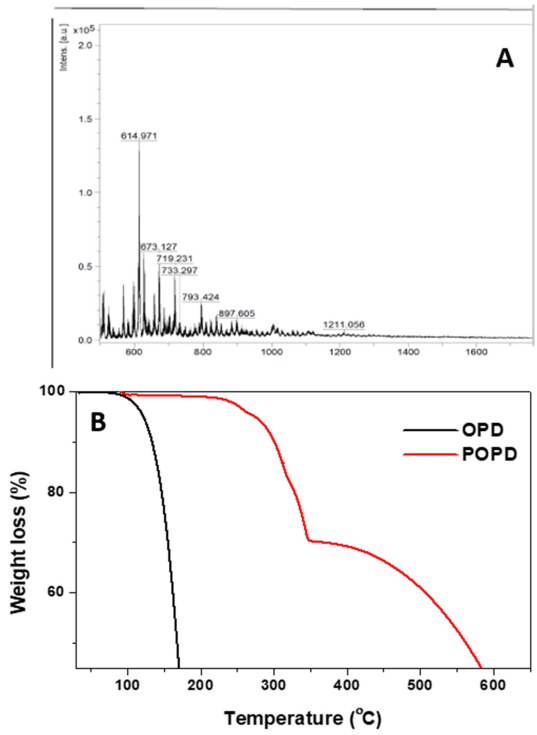

Figure 5.8. *A) MALDI-TOF spectra of POPD and B) Thermograms of OPD and POPD.*

The good solubility of OPD and POPD in water enabled us to record its UV-visible absorption spectra in water. The UV-visible absorption spectra of POPD at different concentrations from 2.3×10^{-4} M to 2.5×10^{-5} M were given in **Figure 5.9.A**. The aqueous polymer solution is yellow, and two absorption peaks were present in the UV-visible absorption spectra. The absorption at 259 nm was due to the π to π* transition and broad absorption at 419 nm was due to the extended π to π* transition associated with conjugated bands, respectively [11,12]. The UV-visible absorption spectra of OPD have shown maximum absorption at 288 nm, corresponding to π to π* transition of the benzene ring [8]. The broad absorption at 419 nm was absent in the monomer. The molar extinction coefficient of POPD was determined as 7387 mol^{-1} L cm^{-1} at 419 nm in water (**Figure 5.9.B.**). The relatively high molar extinction coefficient and yellow color of POPD indicated its suitability in colorimetry analysis at low concentrations.

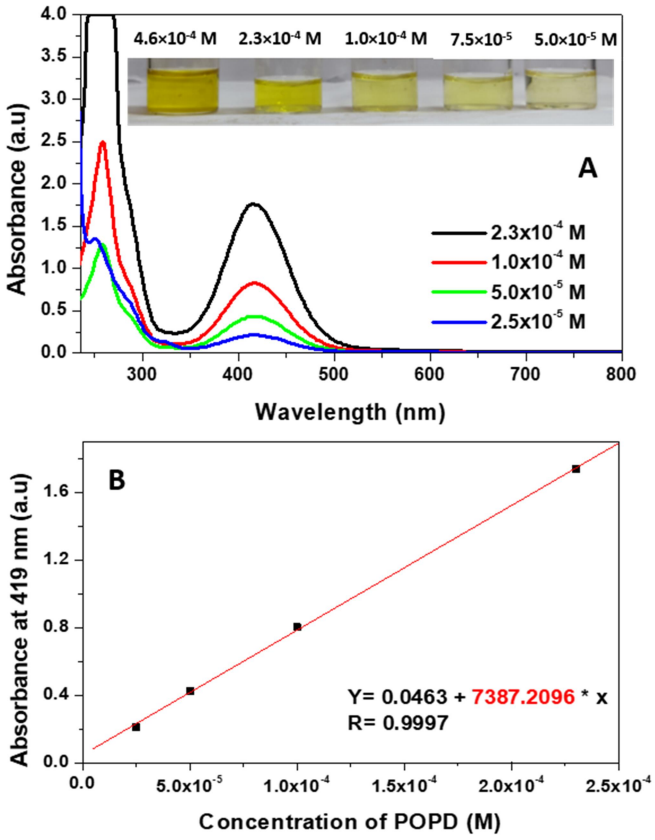

Figure 5.9. *A) UV-visible absorption spectra of POPD at different concentrations in neutral pH. (Inset: Photographs of POPD having different concentrations in visible light) and B) the plot of absorbance at 419 nm vs. concentration of POPD for the determination of the molar extinction coefficient of POPD.*

5.3.3. Fluorescence sensing of $AgNO_3$

The solubility of POPD in water enabled us to study their sensing applications in aqueous medium. The good solubility of polymer could be attributed due to their low molecular weight. The molecular weight of polymers impacts their processability and some of their mechanical properties and morphological behaviour. Once the molecular weight was increased, their processability would decrease, but their mechanical strength and film forming properties would enhance. In our work, application studies of polymers were performed in aqueous medium. The reduced processability would thus adversely affect their applications in aqueous medium.

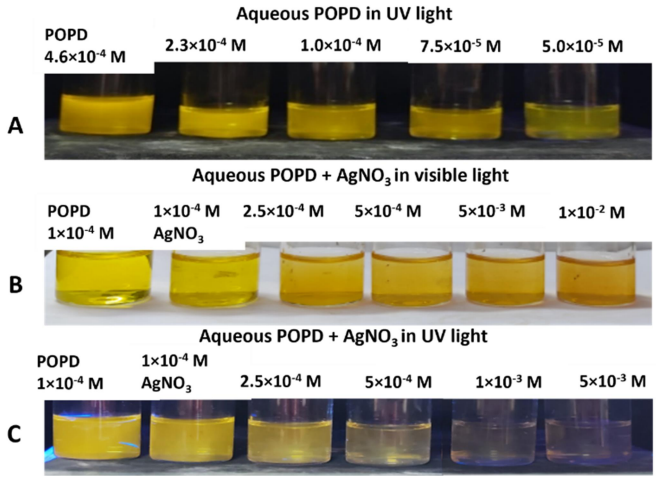

Figure 5.10. *Photographs of POPD solution in A) UV light at different concentrations from 4.6×10^{-4} M to 5×10^{-5} M. Photographs of POPD solution in B) visible and C) UV light on adding different concentrations of $AgNO_3$ solution to 1×10^{-4} M POPD.*

The fluorescence emission of the POPD in water at different concentrations has been checked by irradiating UV light at 365 nm. The bright yellow emission of the polymer gets reduced as we decrease the POPD concentration (see **Figure 5.10.A.**). In the present study, we have selected $AgNO_3$ to oxidize POPD due to its moderately strong oxidizing behavior with a standard reduction potential value of 0.80 V [64]. Effective strategies for silver ion detection in water are highly demanded nowadays due to their high concentrations in water higher than the tolerance level. The aqueous poly-o-phenylenediamine solution with yellow emission was switched to a non-emissive solution by adding silver nitrate via an oxidative fluorescence quenching of the POPD solution. The fluorescence turn-off in POPD in the presence of analyte $AgNO_3$ has given a new

platform for Ag^{+} ion sensing in water. The oxidation of POPD was achieved by adding equal volumes of aqueous $AgNO_3$ having concentrations of 1×10^{-4} M, 2.5×10^{-4} M, 5×10^{-4} M, 1×10^{-3} M, 2.5×10^{-3} M, 5×10^{-3} M, and 1×10^{-2} M to POPD solution having concentration 1×10^{-4} M. The photographs of oxidative quenching in POPD solutions in the presence of different concentrations of $AgNO_3$ are given in **Figure 5.10.B & C.** The POPD solution with concentration 1×10^{-4} M has intense yellow emission, which was seen in naked-eye detection. The yellow emission of the POPD decreased gradually on increasing $AgNO_3$ concentration and completely quenched at 1×10^{-3} M $AgNO_3$. The mole ratio [$AgNO_3$]/[POPD] calculated for visual detection was 10.

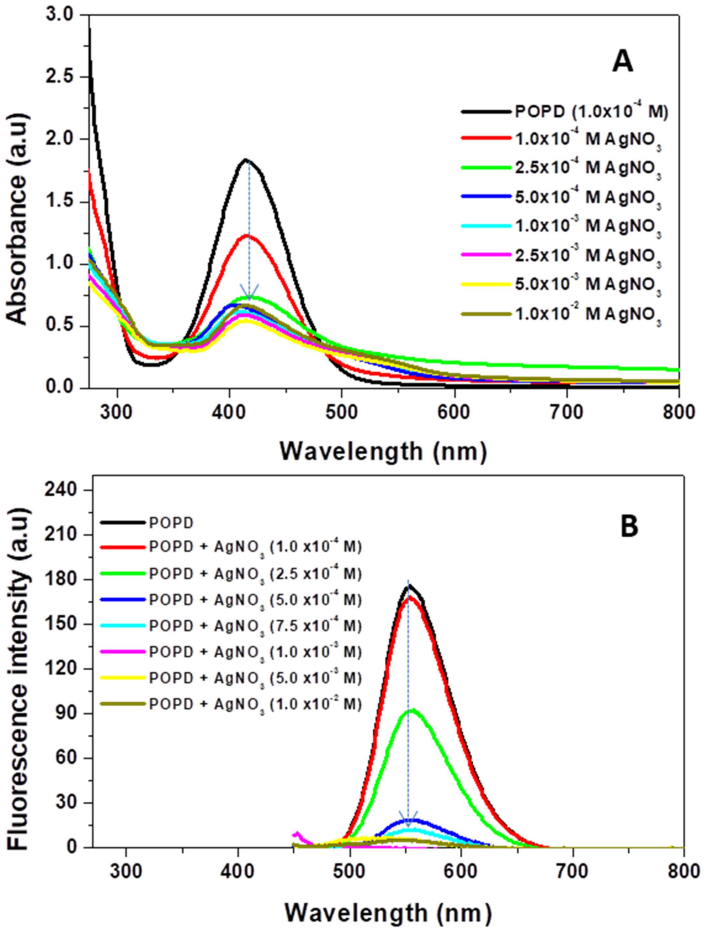

Figure 5.11. *A) UV-visible absorption spectra and B) Fluorescence spectra of POPD with different concentrations of $AgNO_3$.*

UV-visible absorption spectra of the POPD (1×10^{-4} M) after adding different concentrations of $AgNO_3$ were given in **Figure 5.11. A** and corresponding photographs of POPD solutions in visible light were given in **Figure 5.10.C.** The absorbance of the POPD at 419 nm was gradually decreased by adding 1×10^{-4} M, 2.5×10^{-4} M, and 5×10^{-4} M

$AgNO_3$ and then reached a constant value on adding still higher concentrations of $AgNO_3$ solution. The surface plasmon resonance of reduced silver nanoparticles and absorbance of oxidized POPD may coexist as a weak and broad absorption at 419 nm[65]. The fluorescence spectra of POPD were recorded by varying the concentration of $AgNO_3$ (see **Figure 5.11.B.).** The peak at 550 nm in the fluorescence spectra of POPD was attributed to the S_1 to S_0 transition [66]. It could be seen that the fluorescence intensity of POPD at 550 nm decreased with the increase in the concentration of $AgNO_3$ and completely disappeared on adding 1×10^{-3} M $AgNO_3$, which was evident from the fluorescence intensity vs. $AgNO_3$ mole plot (see **Figure 5.12.A.**). The detectable decrease in the fluorescence intensity was observed at a mole ratio of [$AgNO_3$]/[POPD] at 5, while complete quenching was obtained at a mole ratio of 10. The absorbance of POPD at 419 nm plotted against the concentration of $AgNO_3$ was shown in in **Figure 5.12.B.** The absorbance of POPD was considerably decreased linearly on adding $AgNO_3$, indicating the oxidation of the POPD from a semi-oxidized state. The [analyte]/[polymer] mole ratio for fluorescence quenching obtained from fluorescence spectra, naked-eye detection and absorption spectra were in good agreement.

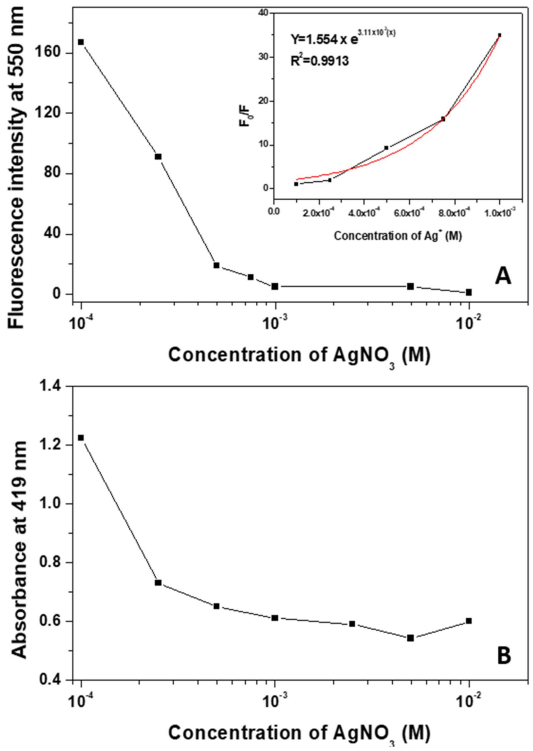

***Figure 5.12**. A) Fluorescence intensity of POPD at 550 nm plotted vs. concentration of $AgNO_3$. Stern-Volmer plot with non-linear curve fitting was shown in the inset, and B) absorbance of POPD at 419 nm plotted vs concentration of $AgNO_3$.*

The Stern-Volmer plot of the POPD at different quencher concentrations was plotted against the corresponding F_0/F (see **Figure 5.12.A).** The deviation of the Stern-Volmer plot from linearity indicated the possibility of chromophoric aggregation or variation in the association constant with quencher concentration or mixed static and dynamic quenching [67, 68]. We have applied the following exponential quenching equation, $\frac{F_0}{F} = Ae^{k[Q]} + B$, where A, B, and k are constants to fit the non-linear stern-volmer plot [69, 70]. From the exponential curve fitting, $\frac{F_0}{F} = 1.55\, e^{3.11x10^3[Ag^+]}$, ($R^2$=0.9913), the stern-volmer quenching constant was calculated as 4.82×10^3 L mol^{-1} by multiplying the constants A (1.55) and k (3.11×10^3). The quenching constant value indicated the quencher availability to the fluorophore excited state and the strong ability to quench silver ions towards poly-o-phenylenediamine. According to the exponential quenching equation $\frac{F_0}{F} = 1.55\, e^{3.11x10^3[Ag^+]}$, the value of F_0/F becomes 1 at $AgNO_3$ concentrations less than 1×10^{-4} M, and the maximum value of F_0/F was obtained at $AgNO_3$ having concentration of 5×10^{-3} M. Thus, exponential quenching equation was valid from 1×10^{-4} M $AgNO_3$ to 5×10^{-3} M $AgNO_3$ in the case of 1×10^{-4} M POPD.

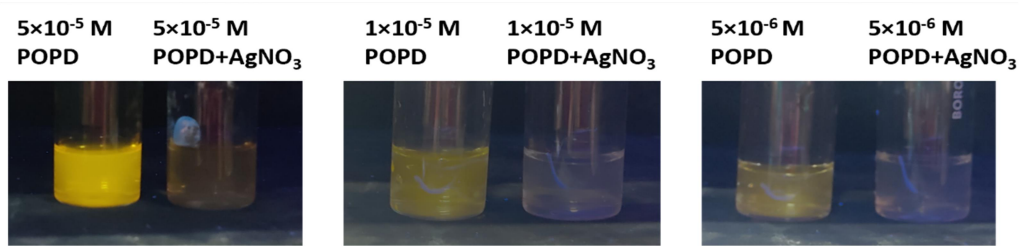

Figure 5.13*. Photographs under UV light of different concentrations of POPD (5×10^{-5} M, 1×10^{-5} M, 5×10^{-6} M) with $AgNO_3$ at a mole ratio of [$AgNO_3$]/[POPD] as 10 respectively.*

The limit of detection (LOD) of $AgNO_3$ for simple naked eye fluorescence detection has been found to be 50 μM by taking the lowest naked eye emissive polymer concentration as 5×10^{-6} M (see **Figure 5.13.**).

5.3.4. Fluorescence reversibility of oxidized POPD

The fluorescence reversibility of oxidized POPD was studied by adding sodium ascorbate. The color and fluorescence of POPD were not changed by adding sodium ascorbate since the reduction potential of sodium ascorbate was not sufficient to reduce

the polymer (standard reduction potential of ascorbate (DHA/AH^-) is + 0.19 V) [71]. Sodium borohydride ($NaBH_4$) is a strong reducing agent with a standard reduction potential of -1.24 V for $NaBH_4/NaBO_2$ [72]. The reappearance of the yellow emission of POPD was masked by the reaction between $NaBH_4$ and excess $AgNO_3$ remaining in the solution. In order to avoid the reaction between $NaBH_4$ and excess $AgNO_3$ in the reaction medium, oxidized POPD was synthesized in powder form using poly-o-phenylenediamine and $AgNO_3$ in the ratio 1:3. The oxidized form of POPD has orange color in water and has a very weak orange fluorescence in UV light (see **Figure 5.14.**).

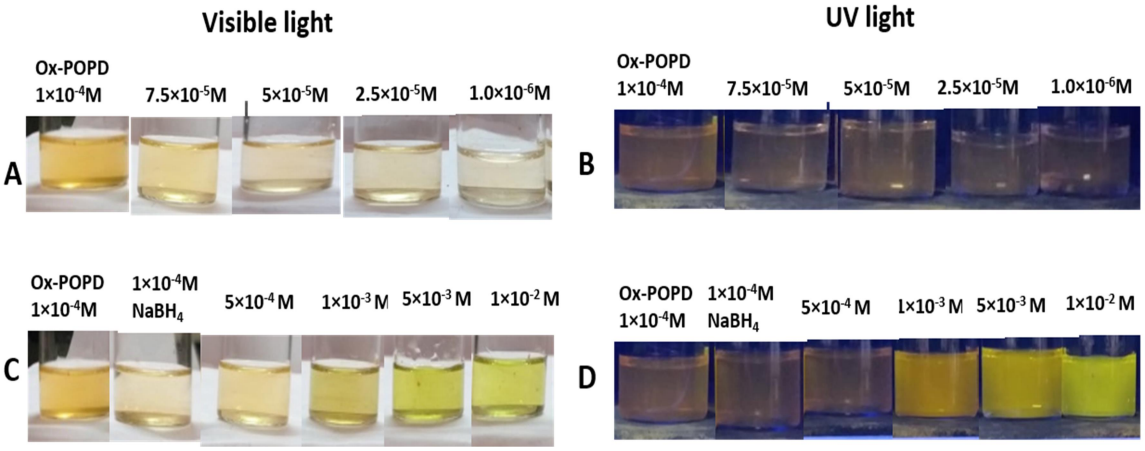

Figure 5.14. *A) Photographs of Ox-POPD solution at different concentrations from 1.0×10^{-4} M to 1×10^{-6} M, A) in visible light, B) in UV light and on adding different concentrations of $NaBH_4$ solution to 1×10^{-4} M Ox. POPD C) in visible light, and D) in UV light.*

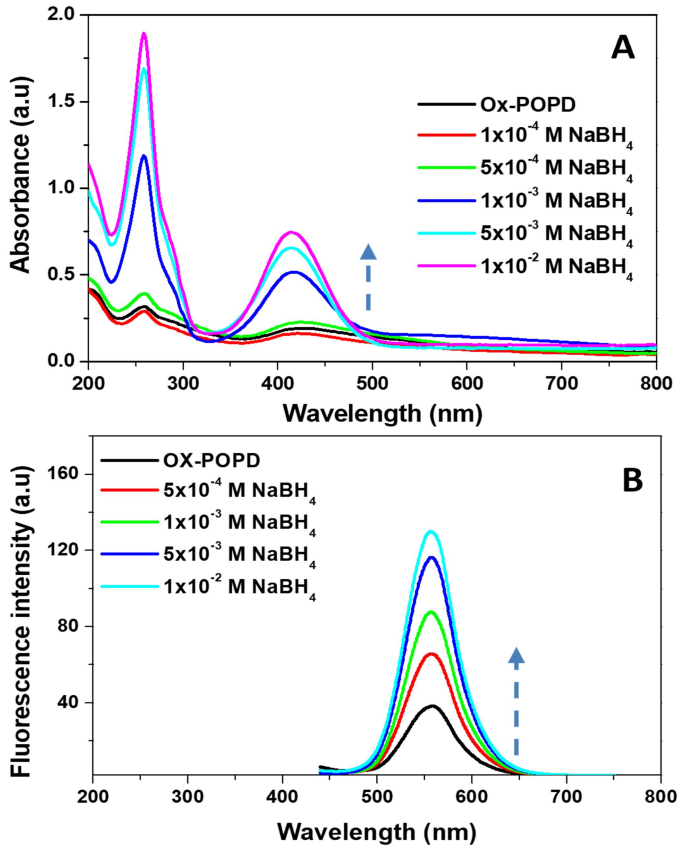

Figure 5.15. *A) UV-visible absorption spectra and B) Fluorescence spectra of oxidized POPD having concentration 1×10^{-4} M on adding different concentrations of $NaBH_4$.*

The UV-visible absorption spectra of oxidized POPD were recorded in water and showed a broad absorption at 419 nm, similar to that of POPD in the presence of $AgNO_3$ (see **Figure 5.15.A.**). The reduction of oxidized POPD by $NaBH_4$ was carried out in the water by mixing 3 mL of each oxidized POPD having a concentration of 1×10^{-4} M and $NaBH_4$ having different concentrations between 1×10^{-4} M, 5×10^{-4} M, 1×10^{-3} M, 5×10^{-3} M, to 1×10^{-2} M. The absorbance of the oxidized POPD at 419 nm was increased by adding $NaBH_4$. In order to confirm the reduction of oxidized POPD, the fluorescence emission changes associated with the polymer were checked under UV light by adding $NaBH_4$ (see **Figure 5.14.**). The appearance of yellow fluorescence emission on adding $NaBH_4$ has confirmed the reduction of oxidized POPD. The fluorescence spectra of oxidized POPD were also recorded by adding $NaBH_4$, and the fluorescence intensity at 419 nm was increased by adding $NaBH_4$ (see **Figure 5.15.B.**). The concentration of $NaBH_4$ required for the fluorescence turn-on was determined as 1×10^{-3} M and the corresponding mole ratio of $[NaBH_4]/[POPD]$ was calculated as 10 by visual detection. The mole ratio of

[$AgNO_3$]/[POPD] for fluorescence tun-off in POPD and the mole ratio of [$NaBH_4$]/[POPD] for fluorescence turn-on in oxidized POPD were comparable.

Fluorescence reversibility in POPD was studied by another oxidizing reagent like iodine solution (1×10^{-2} M) to avoid interference from excess silver ion and then reduced back using $NaBH_4$ (1×10^{-2} M). The fluorescence quenching of POPD by iodine and fluorescence reappearance using $NaBH_4$ for two oxidation-reduction cycles have been carried out. The fluorescence spectra of POPD solutions also confirm the same fluorescence quenching and reappearance (See **Figure 5.16.A.**). Although the dilution effect decreases the fluorescence intensity on reduction, the fluorescence turns-off and turn-on was clear. UV-visible absorption spectra of POPD in the presence of 5×10^{-3} M $AgNO_3$ have been taken at intervals like 0.25 hrs, 24 hrs., and 48 hrs have shown fair stability without any change absorption (see **Figure 5.16.B.**).

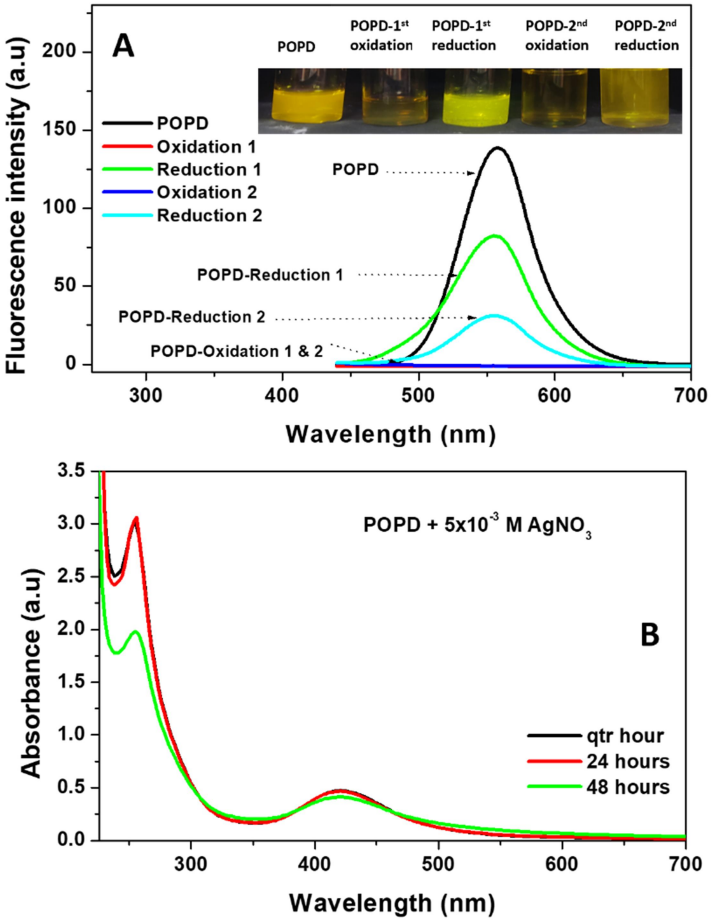

Figure 5.16. *A) Fluorescence spectra of POPD on multiple oxidation and reduction for reversibility studies and corresponding photographs under UV light in the inset. B) UV-*

visible absorption spectra of POPD solution with 5×10^{-3} M $AgNO_3$ taken at different time intervals 0.25 hrs, 24 hrs, and 48 hrs.

5.3.5. Mechanism of fluorescence sensing

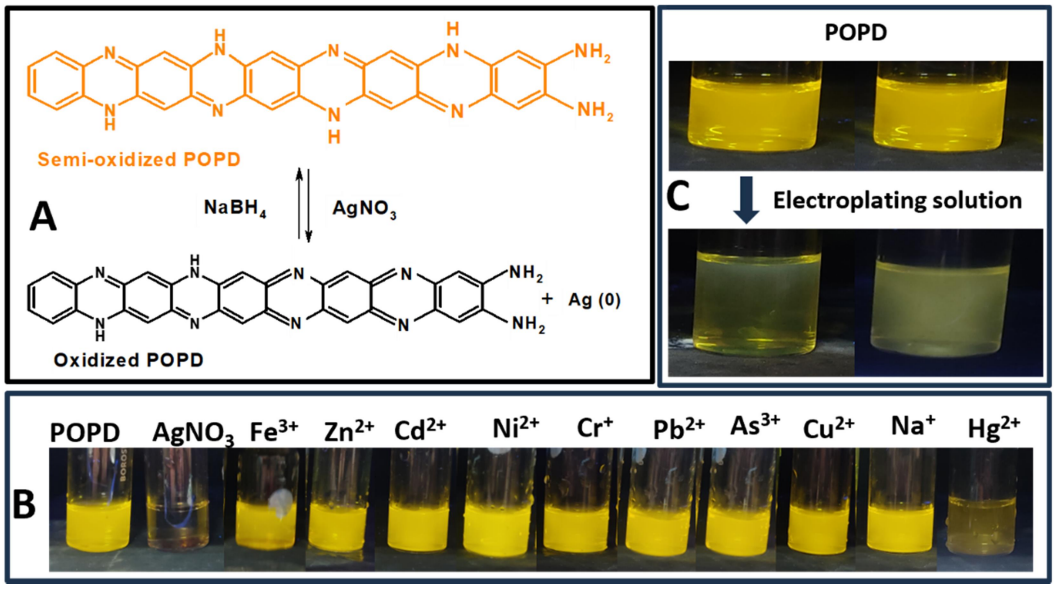

Figure 5.17. *A) Possible mechanism of oxidation and reduction in POPD B) Photographs of POPD solution (1×10^{-4} M) with different metal ion analytes having concentration 1×10^{-3} M under UV light and C) Photographs of POPD under UV light in the presence of silver discarded electroplating solution.*

The Mechanism of oxidation of POPD by $AgNO_3$ and reduction of oxidized POPD by $NaBH_4$ is given in **Figure 5.17.A**. The synthesized POPD was termed semi-oxidized POPD, which contains typical benzenoid and quinoid rings. The oxidizing agents like $AgNO_3$ remove two electrons per aromatic ring to oxidize POPD and vice versa. Thus, yellow emissive semi-oxidized POPD was oxidized to non-emissive phenazine units. Similarly, the non-emissive oxidized POPD was reduced to yellow emissive semi-oxidized POPD by adding $NaBH_4$. The experimental support for the oxidation was obtained from ^{1}H NMR spectra of oxidized POPD in DMSO-d_6 solvent (see **Figure 5.5.**). Oxidized POPD was synthesized from semi-oxidized POPD by adding $AgNO_3$. ^{1}H NMR spectra of oxidized POPD have shown four peaks, which were more shielded than semi-oxidized polymer. It could be due to the lack of conjugation in the oxidized structure of the POPD compared to its semi-oxidized structure. The possible structure of oxidized POPD with five monomer units is also given in **Figure 5.5**. Four

peaks in the proton NMR spectra of oxidized POPD corresponded to four types of protons present in the different chemical environments. The most deshielded peaks at 7.95 ppm corresponded to the aromatic benzenoid protons and the peak at 7.60 ppm corresponded to either aromatic protons or secondary -NH proton. Two singlets at 6.95 and 6.4 ppm were present in the ratio 1:2 indicated the presence of quinoid protons. Literature report suggest that $-NH_2$ protons can be present at 6.4 ppm in the NMR spectra [1]. The structural difference between semi-oxidized POPD and oxidized POPD was thus confirmed from ^1H NMR spectra. We have also studied the effect of interfering analytes Fe^{3+}, Zn^{2+}, Cd^{2+}, Ni^{2+}, Cr^{2+}, Pb^{2+}, As^{3+}, Cu^{2+}, and Na^+ on the fluorescence turn off of POPD using a naked-eye detection test (see **Figure 5.17.B**). It has been found that no analytes other than Hg^{2+} have an effect on the fluorescence quenching of POPD. However, Hg^{2+} was found to quench the fluorescence of POPD at a very high mole ratio of $[Hg^{2+}]$/[POPD] as 100. The higher difference between mole ratios of $[AgNO_3]$/[POPD] and $[Hg^{2+}]$/[POPD] indicated less interference of Hg^{2+} ions on the fluorescence sensing of $AgNO_3$. The silver ion sensing ability of POPD in industrial samples were also tested. The discarded electroplating solutions of silver were collected from local plating industries. The electrolytic solution was composed of AgCl, KCN, and $Na_2S_2O_3$, and the concentration of silver ions after sufficient electroplating would be reduced between 2500 mg/L to 5000 mg/L [78]. The fluorescence intensity of POPD was decreased slowly with the addition of an electroplating solution, which indicated the sensing of silver ions. Unlike silver nitrate solution, the fluorescence emission was quenched entirely after 48 hours (See **Figure 5.17.C**). The presence of reducing agents like $Na_2S_2O_3$ and the complex formation of sodium silver cyanide in the silver electroplating water could slow down the oxidation of POPD.

5.3.6. Electrochemical activities of POPD

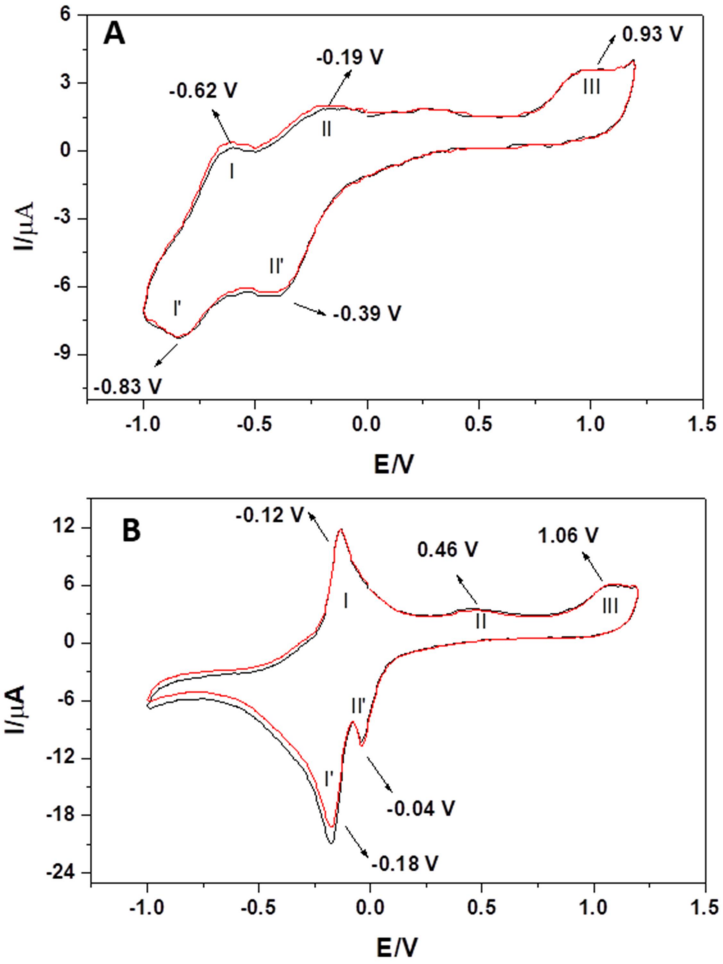

Figure 5.18. *The cyclic voltammograms of POPD in A) water and B) 0.1 M H_2SO_4.*

The electrochemical activities of redox states in POPD were studied by recording the cyclic voltammogram of POPD in water using a glassy carbon working electrode. The polymer solution has shown redox activities in the negative potential region (see **Figure 5.18.A**), which arose due to the coupled electron and proton transfer in polymer and their structural changes [73-75]. The first anodic peak (I) at -0.62 V arose due to reaction I, in which reduced POPD was oxidized to semi-oxidized POPD [76] (see **Figure 5.19.**). The oxidation of semi-oxidized POPD to oxidized POPD resulted in the anodic peak (II) at -0.19 V [77] (see reaction II in **Figure 5.19.**). An anodic peak around 0.93 V (III) indicated further oxidation of POPD (see reaction III in **Figure 5.19.**) [10,20]. The reduction peaks at -0.83 V (I') and -0.39 V (II') in the cathodic sweep corresponded to the reversible oxidation peaks at -0.62 V (I) and -0.19 V (II) in the anodic sweep, respectively. In the cyclic voltammogram of POPD, the anodic oxidation potential at 0.93 V was not

reversed, indicating the sluggish reversibility of reaction III [20]. The cyclic voltammogram of POPD in 0.1 M H_2SO_4 is given in **Figure 5.18.B**. Three anodic peak potentials corresponding to the oxidation of POPD at -0.12 V, 0.46 V, and 1.06 V in the anodic sweep, and two cathodic peak potentials corresponding to the reduction of POPD at -0.18 V and -0.04 V in the cathodic sweep were observed similar to the oxidations and reductions of POPD in water. However, anodic and cathodic peak potentials were shifted to a positive direction in 0.1 M H_2SO_4. The increase in the anodic and cathodic peak potentials of poly-o-phenylenediamine with a decrease in pH indicates excellent electrochemical activity required for electrochemical sensing [76,78]. The redox states of POPD were as proposed in **Figure 5.19.**

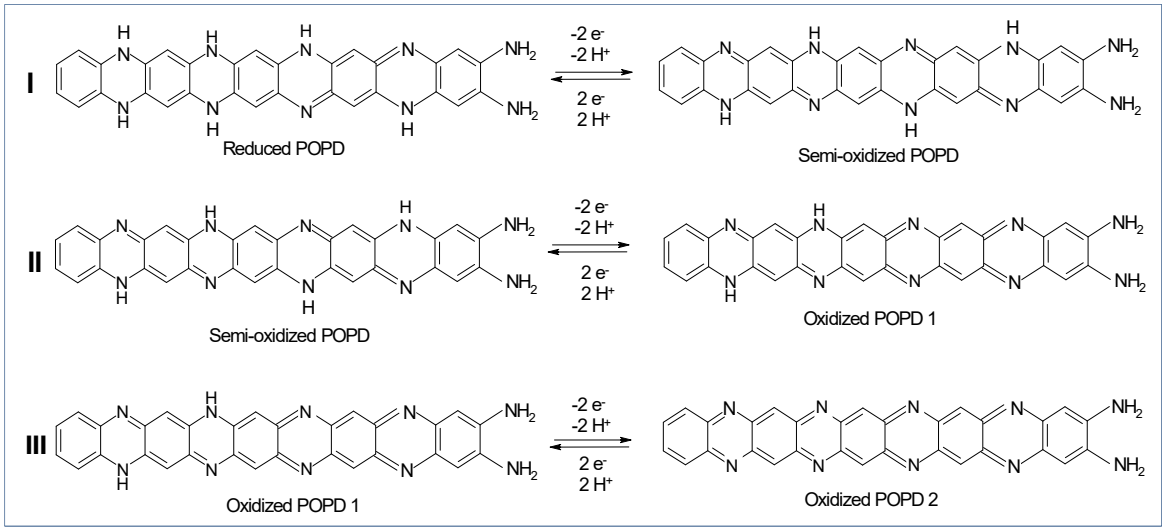

***Figure 5.19**. Possible redox states in poly-o-phenylenediamine.*

In a nutshell, the yellow fluorescence turn-off in poly-o-phenylenediamine was obtained by oxidizing agent $AgNO_3$, providing a sensing platform for the silver ion. The non-fluorescent oxidized state of the POPD state can be reverted to the semi-oxidized state with yellow fluorescence by adding sodium borohydride as a reducing agent. Therefore, the present study emphasizes the relationship between different redox states of POPD and their fluorescence properties, which may be suitable for sensing various reducing analytes.

5.4. Conclusion

The fluorescence turn-off and turn-on associated with different redox states of poly-o-phenylenediamine were studied, and oxidative yellow fluorescence quenching of POPD

with $AgNO_3$ was used for silver ion sensing. Poly-o-phenylenediamine was synthesized by chemical oxidative polymerization using $FeCl_3$ as an oxidizing agent. The presence of C=N stretching and C-N stretching peaks associated with benzenoid and quinoid rings in the FT-IR spectra of POPD confirmed the semi-oxidized structure of the polymer. The presence of 5-6 monomer units in the polymer was evident from MALDI-TOF spectra. FE-SEM images revealed the self-assembled micro rod-like morphology in POPD. The water-soluble POPD has shown broad absorption at 419 nm and yellow fluorescence emission. The quenching of the yellow fluorescence emission of POPD with $AgNO_3$ indicated the oxidation of POPD. This oxidative fluorescence turn-off in POPD was effectively used for silver ion sensing. The enhancement of yellow fluorescence of oxidized POPD with $NaBH_4$ confirmed the reversibility in redox states of POPD. The structural evidence for semi-oxidized POPD and oxidized POPD were obtained from ^1H NMR spectra. Thus, water-mediated oxidative fluorescence turn-off in semi-oxidized POPD and reductive fluorescence turn-on in oxidized POPD have great potential for quantifying various oxidizing and reducing analytes.

Reference

1. Zhang, X., Li, G., Wang, J., Chu, J., Wang, F., Hu, Z., & Song, Z. (2022). Revisiting the Structure and Electrochemical Performance of Poly(*o* -phenylenediamine) as an Organic Cathode Material. *ACS Applied Materials & Interfaces*, *14*(24), 27968–27978. https://doi.org/10.1021/acsami.2c06208.
2. Lan, H., Muslim, A., Hojiahmat, M., Wang, L., Meng, Y., & Zhong, Q. (2021). Morphology formation mechanism and electrochemical performance of poly(o-phenylenediamine) based electrode materials. *Synthetic Metals*, *273*, 116688. https://doi.org/10.1016/j.synthmet.2020.116688.
3. Jaymand, M. (2013). Recent progress in chemical modification of polyaniline. *Progress in Polymer Science*, *38*(9), 1287–1306. https://doi.org/10.1016/j.progpolymsci.2013.05.015.
4. Li, X. G., Huang, M. R., Duan, W., & Yang, Y. L. (2002). Novel multifunctional polymers from aromatic diamines by oxidative polymerizations. *Chemical Reviews*, *102*(9), 2925–3030. https://doi.org/10.1021/cr010423z.
5. Xu, L., Sun, Y., Han, B., & Su, C. (2019). Electrochemical Performances on Both poly(Phenylenediamine) Derivatives as Anode of Lithium-Ion Batteries. *Journal of The Electrochemical Society*, *166*(8), A1363–A1369. https://doi.org/10.1149/2.0351908jes.
6. Duran, B., Bereket, G., & Duran, M. (2012). Electrochemical synthesis and characterization of poly(m-phenylenediamine) films on copper for corrosion protection. *Progress in Organic Coatings*, *73*(2–3), 162–168. https://doi.org/10.1016/j.porgcoat.2011.10.008.
7. Ghahremanloo, A., Zare, E. N., Salimi, F., & Makvandi, P. (2022). Electroconductive and photoactive poly(phenylenediamine)s with antioxidant and antimicrobial activities for potential photothermal therapy. *New Journal of Chemistry*, *46*(13), 6255–6266. https://doi.org/10.1039/D1NJ06145C.
8. Sayyah, S. M., Khaliel, A. B., Aboud, A. A., & Mohamed, S. M. (2014). Chemical Polymerization Kinetics of Poly-O-Phenylenediamine and Characterization of the

Obtained Polymer in Aqueous Hydrochloric Acid Solution Using $K_2Cr_2O_7$ as Oxidizing Agent. *International Journal of Polymer Science*, *2014*, 1–16. https://doi.org/10.1016/j.jlumin.2016.04.053.

9. Sun, X., & Hagner, M. (2007). Mixing Aqueous Ferric Chloride and *O* -Phenylenediamine Solutions at Room Temperature: A Fast, Economical Route to Ultralong Microfibrils of Assemblied *O* -Phenylenediamine Dimers. *Langmuir*, *23*(21), 10441–10444. https://doi.org/10.1021/la701378y.
10. Olmedo-Martínez, J. L., Farías-Mancilla, B. I., Vega-Rios, A., & Zaragoza-Contreras, E. A. (2017). Poly(ortho-phenylenediamine-co-aniline) based copolymer with improved capacitance. *Journal of Power Sources*, *366*, 233–240. https://doi.org/10.1016/j.jpowsour.2017.09.030.
11. Sayyah, S. M., El-Deeb, M. M., Kamal, S. M., & Azooz, R. E. (2009). Electropolymerization of *o* -phenylenediamine on Pt-electrode from aqueous acidic solution: Kinetic, Mechanism, electrochemical studies and characterization of the polymer obtained. *Journal of Applied Polymer Science*, *112*(6), 3695–3706. https://doi.org/10.1002/app.29802.
12. Riaz, U., Ashraf, S. M., Aleem, S., Budhiraja, V., & Jadoun, S. (2016). Microwave-assisted green synthesis of some nanoconjugated copolymers: characterisation and fluorescence quenching studies with bovine serum albumin. *New Journal of Chemistry*, *40*(5), 4643–4653. https://doi.org/10.1039/C5NJ02513C.
13. Han, J., Liu, Y., Li, L., & Guo, R. (2009). Poly(*o* -phenylenediamine) Submicrosphere-Supported Gold Nanocatalysts: Synthesis, Characterization, and Application in Selective Oxidation of Benzyl Alcohol. *Langmuir*, *25*(18), 11054–11060. https://doi.org/10.1021/la901373t.
14. Liao, F., Yang, S., Li, X., Yang, L., Xie, Z., Hu, C., Yan, S., Ren, T., & Liu, Z. (2014). Preparation of heteroatom doped poly(o-phenylenediamine) fluorescent nanospheres: Tunable fluorescent spectrum and sensing performance. *Synthetic Metals*, *189*, 126–134. https://doi.org/10.1016/j.synthmet.2014.01.008.
15. Samanta, S., Roy, P., & Kar, P. (2015). Influence of pH of the Reaction Medium on the Structure and Property of Conducting Poly(o-Phenylenediamine). *Materials Today: Proceedings*, *2*(4–5), 1301–1308. https://doi.org/10.1016/j.matpr.2015.07.046.
16. K Gopalakrishnan , M Elango, M tamil selvan. (2012). Optical studies on nano-structured conducting Polyaniline prepared by chemical oxidation method, *Archives of phy.Research.* 3, 315-319.
17. Sun, X., Dong, S., & Wang, E. (2005). Formation ofo-Phenylenediamine Oligomers and their Self-Assembly into One-Dimensional Structures in Aqueous Medium. *Macromolecular Rapid Communications*, *26*(18), 1504–1508. https://doi.org/10.1002/marc.200500502.
18. Samanta, S., Roy, P., & Kar, P. (2017). Synthesis of poly(*o* -phenylenediamine) nanofiber with novel structure and properties. *Polymers for Advanced Technologies*, *28*(7), 797–804. https://doi.org/10.1002/pat.3981.
19. Olgun, U., & Gülfen, M. (2014). Doping of poly(o-phenylenediamine): Spectroscopy, voltammetry, conductivity and band gap energy. *Reactive and Functional Polymers*, *77*, 23–29. https://doi.org/10.1016/j.reactfunctpolym.2014.02.006.
20. Wu, L.-L., Luo, J., & Lin, Z.-H. (1996). Spectroelectrochemical studies of poly-o-phenylenediamine. Part 1. In situ resonance Raman spectroscopy. *Journal of Electroanalytical Chemistry*, *417*(1–2), 53–58. https://doi.org/10.1016/S0022-0728(96)04759-6.
21. Zoromba, M. Sh., Abdel-Aziz, M. H., Bassyouni, M., Bahaitham, H., & Al-Hossainy, A. F. (2018). Poly(o-phenylenediamine) thin film for organic solar cell applications. *Journal of Solid State Electrochemistry*, *22*(12), 3673–3687. https://doi.org/10.1007/s10008-018-4077-x.
22. Liao, F., Yang, S., Li, X., Yang, L., Xie, Z., Hu, C., He, L., Kang, X., Song, X., & Ren, T. (2014). Poly(o-phenylenediamine) and benzeneselenol copolymer fluorescent nanorod: An ultra-sensitive fluorescent probe and a fluorescent switch triggered by redox

procedure. *Synthetic Metals*, *189*, 135–142. https://doi.org/10.1016/j.synthmet.2014.01.020.
23. Wang, Z., & Liao, F. (2012). Synthesis of Poly(Ortho-Phenylenediamine) Fluffy Microspheres and Application for the Removal of Cr(VI). *Journal of Nanomaterials*, *2012*, 1–7. https://doi.org/10.1155/2012/682802.
24. Han, J., Dai, J., & Guo, R. (2011). Highly efficient adsorbents of poly(o-phenylenediamine) solid and hollow sub-microspheres towards lead ions: A comparative study. *Journal of Colloid and Interface Science*, *356*(2), 749–756. https://doi.org/10.1016/j.jcis.2011.01.038
25. Yan, S., Yang, S., He, L., Ye, C., Song, X., & Liao, F. (2014). Quantum size effect of poly(o-phenylenediamine) quantum dots: From controllable fabrication to tunable photoluminescence properties. *Synthetic Metals*, *198*, 142–149. https://doi.org/10.1016/j.synthmet.2014.10.014.
26. Zare, E. N., Lakouraj, M. M., Ghasemi, S., & Moosavi, E. (2015). Emulsion polymerization for the fabrication of poly(o-phenylenediamine)@multi-walled carbon nanotubes nanocomposites: characterization and their application in the corrosion protection of 316L SS. *RSC Advances*, *5*(84), 68788–68795. https://doi.org/10.1039/C5RA11295H.
27. Riaz, U., Jadoun, S., Kumar, P., Arish, M., Rub, A., & Ashraf, S. M. (2017). Influence of Luminol Doping of Poly(*o* -phenylenediamine) on the Spectral, Morphological, and Fluorescent properties: A Potential Fluorescent Marker for Early detection and Diagnosis of *Leishmania donovani*. *ACS Applied Materials & Interfaces*, *9*(38), 33159–33168. https://doi.org/10.1021/acsami.7b10325.
28. Samanta, S., Roy, P., & Kar, P. (2017). Influence of structure of poly(o-phenylenediamine) on the doping ability and conducting property. *Ionics*, *23*(4), 937–947. https://doi.org/10.1007/s11581-016-1904-x.
29. Samuel, J. J., Karrothu, V. K., Canjeevaram Balasubramanyam, R. K., Mohapatra, A. A., Gangadharappa, C., Kankanallu, V. R., Patil, S., & Aetukuri, N. P. B. (2021). Ionic Charge Storage in Diketopyrrolopyrrole-Based Redox-Active Conjugated Polymers. *The Journal of Physical Chemistry C*, *125*(8), 4449–4457. https://doi.org/10.1021/acs.jpcc.0c11635.
30. Molina, A., Patil, N., Ventosa, E., Liras, M., Palma, J., & Marcilla, R. (2020). Electrode Engineering of Redox-Active Conjugated Microporous Polymers for Ultra-High Areal Capacity Organic Batteries. *ACS Energy Letters*, *5*(9), 2945–2953. https://doi.org/10.1021/acsenergylett.0c01577.
31. Kaneko, M., Ishihara, K., & Nakanishi, S. (2020). Redox-Active Polymers Connecting Living Microbial Cells to an Extracellular Electrical Circuit. *Small*, *16*(34), 2001849. https://doi.org/10.1002/smll.202001849.
32. Samanta, S., Roy, P., & Kar, P. (2016). Structure and properties of conducting poly(o-phenylenediamine) synthesized in different inorganic acid medium. *Macromolecular Research*, *24*(4), 342–349. https://doi.org/10.1007/s13233-016-4054-0.
33. Ullah, H., Shah, A.-H. A., Ayub, K., & Bilal, S. (2013). Density Functional Theory Study of Poly(*o* -phenylenediamine) Oligomers. *The Journal of Physical Chemistry C*, *117*(8), 4069–4078. https://doi.org/10.1021/jp311526u.
34. Bilal, S., Ali Shah, A.-H., & Holze, R. (2011). Spectroelectrochemistry of poly(o-phenylenediamine): Polyaniline-like segments in the polymer structure. *Electrochimica Acta*, *56*(9), 3353–3358. https://doi.org/10.1016/j.electacta.2011.01.005.
35. Guo, Y., Wang, L., Xu, L., Peng, C., & Song, Y. (2020). A ascorbic acid-imprinted poly(o-phenylenediamine)/zeolite imidazole frameworks-67/carbon cloth for electrochemical sensing ascorbic acid. *Journal of Materials Science*, *55*(22), 9425–9435. https://doi.org/10.1007/s10853-020-04687-3.
36. Wang, J., & Wu, H. (1993). Permselective lipid□poly(o-phenylenediamine) coatings for amperometric biosensing of glucose. *Analytica Chimica Acta*, *283*(2), 683–688. https://doi.org/10.1016/0003-2670(93)85282-O

37. Jiang, K., Ma, S., Bi, H., Chen, D., & Han, X. (2014). Morphology controllable fabrication of poly-o-phenylenediamine microstructures tuned by the ionic strength and their applications in pH sensors. *J. Mater. Chem. A*, *2*(45), 19208–19213. https://doi.org/10.1039/C4TA04269G.
38. Ye, Q., Ren, S., Huang, H., Duan, G., Liu, K., & Liu, J.-B. (2020). Fluorescent and Colorimetric Sensors Based on the Oxidation of *o* -Phenylenediamine. *ACS Omega*, *5*(33), 20698–20706. https://doi.org/10.1021/acsomega.0c03111.
39. Wang, Z., & Liao, F. (2012). Fluorescent probes for Pd^{2+} detection by poly(o-phenylenediamine) nanospheres with fluorescence enhancement. *Synthetic Metals*, *162*(5–6), 444–447. https://doi.org/10.1016/j.synthmet.2012.01.013.
40. Tian, J., Li, H., Luo, Y., Wang, L., Zhang, Y., & Sun, X. (2011). Poly(*o* -phenylenediamine) Colloid-Quenched Fluorescent Oligonucleotide as a Probe for Fluorescence-Enhanced Nucleic Acid Detection. *Langmuir*, *27*(3), 874–877. https://doi.org/10.1021/la103799e.
41. Riaz, U., Ashraf, S. M., Jadoun, S., Budhiraja, V., & Kumar, P. (2019). Spectroscopic and Biophysical Interaction Studies of Water-soluble Dye modified poly(o-phenylenediamine) for its Potential Application in BSA Detection and Bioimaging. *Scientific Reports*, *9*(1), 8544. https://doi.org/10.1038/s41598-019-44910-z.
42. Wang, Z., & Liao, F. (2011). Synthesis of hollow microspheres poly(o-phenylenediamine)/iron oxide composites and application of fluorescence probe in yeast RNA detection. *Synthetic Metals*, *161*(21–22), 2506–2509. https://doi.org/10.1016/j.synthmet.2011.08.024.
43. Xu, Q., Xu, C., Wang, Y., Zhang, W., Jin, L., Tanaka, K., Haraguchi, H., & Itoh, A. (2000). Amperometric detection studies of poly-o-phenylenediamine film for the determination of electroinactive anions in ion-exclusion chromatography. *The Analyst*, *125*(8), 1453–1457. https://doi.org/10.1039/b004085l.
44. Samanta, S., Roy, P., & Kar, P. (2020). Sensing of ethanol and other alcohol contaminated ethanol by conducting functional poly(o-phenylenediamine). *Materials Science and Engineering: B*, *256*, 114541. https://doi.org/10.1016/j.mseb.2020.114541.
45. Hernández, Loreto. A., Martín, F., Berrios, E., Riveros, G., González, D. M., González, E., Lizama, S., & Hernández, F. (2020). Novel electrosynthesis of CdS/FeS nanocomposite-modified poly(o-phenylenediamine) with views to their use as a biosensor for Escherichia coli. *Arabian Journal of Chemistry*, *13*(12), 8758–8767. https://doi.org/10.1016/j.arabjc.2020.10.006.
46. Liu, X., Zhu, H., & Yang, X. (2014). An electrochemical sensor for dopamine based on poly(o-phenylenediamine) functionalized with electrochemically reduced graphene oxide. *RSC Adv.*, *4*(8), 3743–3749. https://doi.org/10.1039/C3RA45234D.
47. Liu, L., Chen, Y., Lv, H., Wang, G., Hu, X., & Wang, C. (2015). Construction of a non-enzymatic glucose sensor based on copper nanoparticles/poly(o-phenylenediamine) nanocomposites. *Journal of Solid State Electrochemistry*, *19*(3), 731–738. https://doi.org/10.1007/s10008-014-2659-9.
48. Karimian, N., Stortini, A. M., Moretto, L. M., Costantino, C., Bogialli, S., & Ugo, P. (2018). Electrochemosensor for Trace Analysis of Perfluorooctanesulfonate in Water Based on a Molecularly Imprinted Poly(*o* -phenylenediamine) Polymer. *ACS Sensors*, *3*(7), 1291–1298. https://doi.org/10.1021/acssensors.8b00154.
49. Li, X.-G., Ma, X.-L., Sun, J., & Huang, M.-R. (2009). Powerful Reactive Sorption of Silver(I) and Mercury(II) onto Poly(*o* -phenylenediamine) Microparticles. *Langmuir*, *25*(3), 1675–1684. https://doi.org/10.1021/la802410p.
50. Swathy, T. S., Jinish Antony, M., & George, N. (2021). Active Solvent Hydrogen-Enhanced *p* -Nitrophenol Reduction Using Heterogeneous Silver Nanocatalysts@Surface-Functionalized Multiwalled Carbon Nanotubes. *Industrial & Engineering Chemistry Research*, *60*(19), 7050–7064. https://doi.org/10.1021/acs.iecr.1c01371.
51. Manzoli, A., Steffens, C., Paschoalin, R. T., Correa, A., Alves, W., Leite, F., & Herrmann, P. (2011). Low-Cost Gas Sensors Produced by the Graphite Line-Patterning

Technique Applied to Monitoring Banana Ripeness. *Sensors*, *11*(6), 6425–6434. https://doi.org/10.3390/s110606425.
52. Pak, Y. L., Wang, Y., & Xu, Q. (2021). Conjugated polymer based fluorescent probes for metal ions. *Coordination Chemistry Reviews*, *433*, 213745. https://doi.org/10.1016/j.ccr.2020.213745.
53. Qin, C., Wong, W.-Y., & Wang, L. (2011). A Water-Soluble Organometallic Conjugated Polyelectrolyte for the Direct Colorimetric Detection of Silver Ion in Aqueous Media with High Selectivity and Sensitivity. *Macromolecules*, *44*(3), 483–489. https://doi.org/10.1021/ma102373y.
54. Yang, X., & Wang, E. (2011). A Nanoparticle Autocatalytic Sensor for Ag^{+} and Cu^{2+} Ions in Aqueous Solution with High Sensitivity and Selectivity and Its Application in Test Paper. *Analytical Chemistry*, *83*(12), 5005–5011. https://doi.org/10.1021/ac2008465.
55. Dai, H., Ni, P., Sun, Y., Hu, J., Jiang, S., Wang, Y., & Li, Z. (2015). Label-free fluorescence detection of mercury ions based on the regulation of the Ag autocatalytic reaction. *The Analyst*, *140*(10), 3616–3622. https://doi.org/10.1039/C4AN02162B.
56. Li, R., Lei, C., Zhao, X.-E., Gao, Y., Gao, H., Zhu, S., & Wang, H. (2018). A label-free fluorimetric detection of biothiols based on the oxidase-like activity of Ag+ ions. *Spectrochimica Acta Part A: Molecular and Biomolecular Spectroscopy*, *188*, 20–25. https://doi.org/10.1016/j.saa.2017.06.056.
57. Zhang, Q., Wang, R., Feng, B., Zhong, X., & Ostrikov, K. (2021). Photoluminescence mechanism of carbon dots: triggering high-color-purity red fluorescence emission through edge amino protonation. *Nature Communications*, *12*(1), 6856. https://doi.org/10.1038/s41467-021-27071-4.
58. Atac, A., Karaca, C., Gunnaz, S., & Karabacak, M. (2014). Vibrational (FT-IR and FT-Raman), electronic (UV–Vis), NMR (1H and 13C) spectra and reactivity analyses of 4,5-dimethyl-o-phenylenediamine. *Spectrochimica Acta Part A: Molecular and Biomolecular Spectroscopy*, *130*, 516–525. https://doi.org/10.1016/j.saa.2014.04.003.
59. He, D., Wu, Y., & Xu, B.-Q. (2007). Formation of 2,3-diaminophenazines and their self-assembly into nanobelts in aqueous medium. *European Polymer Journal*, *43*(9), 3703–3709. https://doi.org/10.1016/j.eurpolymj.2007.06.038.
60. Kellenberger, A., Dmitrieva, E., & Dunsch, L. (2011). The stabilization of charged states at phenazine-like units in polyaniline under p-doping: an in situ ATR-FTIR spectroelectrochemical study. *Physical Chemistry Chemical Physics*, *13*(8), 3411. https://doi.org/10.1039/c0cp01264e.
61. Huang, M.-R., Li, X.-G., & Duan, W. (2005). Effect of polymerization conditions ono-phenylenediamine ando-phenetidine oxidative copolymers. *Polymer International*, *54*(1), 70–82. https://doi.org/10.1002/pi.1618.
62. Tu, X., Xie, Q., Xiang, C., Zhang, Y., & Yao, S. (2005). Scanning Electrochemical Microscopy in Combination with Piezoelectric Quartz Crystal Impedance Analysis for Studying the Growth and Electrochemistry as Well as Microetching of Poly(*o* -phenylenediamine) Thin Films. *The Journal of Physical Chemistry B*, *109*(9), 4053–4063. https://doi.org/10.1021/jp044731n.
63. Lu, X., Mao, H., Chao, D., Zhao, X., Zhang, W., & Wei, Y. (2007). Preparation and characterization of poly(o-phenylenediamine) microrods using ferric chloride as an oxidant. *Materials Letters*, *61*(6), 1400–1403. https://doi.org/10.1016/j.matlet.2006.07.040.
64. D. C.Harris. (2007). Quantitative Chemical Analyisis, 7th edn., W.H Freeman and Company, United states of America.
65. Ayaz Ahmed, K. B., P, S. K., & Veerappan, A. (2016). A facile method to prepare fluorescent carbon dots and their application in selective colorimetric sensing of silver ion through the formation of silver nanoparticles. *Journal of Luminescence*, *177*, 228–234. https://doi.org/10.1016/j.jlumin.2016.04.053.
66. Liao, F., Song, X., Yang, S., Hu, C., He, L., Yan, S., & Ding, G. (2015). Photoinduced electron transfer of poly(o-phenylenediamine)–Rhodamine B copolymer dots: application

in ultrasensitive detection of nitrite in vivo. *Journal of Materials Chemistry A*, *3*(14), 7568–7574. https://doi.org/10.1039/C5TA00675A.

67. Qin, Y., Ge, Y., Zhang, S., Sun, H., Jing, Y., Li, Y., & Liu, W. (2018). A series of Ln_4^{III} clusters: Dy_4 single molecule magnet and Tb_4 multi-responsive luminescent sensor for Fe^{3+}, CrO_4^{2-}/$Cr_2O_7^{2-}$ and 4-nitroaniline. *RSC Advances*, *8*(23), 12641–12652. https://doi.org/10.1039/C8RA01485J.
68. Malik, A. H., Habib, F., Qazi, M. J., Ganayee, M. A., Ahmad, Z., & Yatoo, M. A. (2023). A short review article on conjugated polymers. *Journal of Polymer Research*, *30*(3), 115. https://doi.org/10.1007/s10965-023-03451-w.
69. Wei, W., Lu, R., Tang, S., & Liu, X. (2015). Highly cross-linked fluorescent poly(cyclotriphosphazene-co-curcumin) microspheres for the selective detection of picric acid in solution phase. *Journal of Materials Chemistry A*, *3*(8), 4604–4611. https://doi.org/10.1039/C4TA06828A.
70. Das, R., Bej, S., Hirani, H., & Banerjee, P. (2021). Trace-Level Humidity Sensing from Commercial Organic Solvents and Food Products by an AIE/ESIPT-Triggered Piezochromic Luminogen and ppb-Level "OFF–ON–OFF" Sensing of Cu^{2+}: A Combined Experimental and Theoretical Outcome. *ACS Omega*, *6*(22), 14104–14121. https://doi.org/10.1021/acsomega.1c00565.
71. Shen, J., Griffiths, P. T., Campbell, S. J., Utinger, B., Kalberer, M., & Paulson, S. E. (2021). Ascorbate oxidation by iron, copper and reactive oxygen species: review, model development, and derivation of key rate constants. *Scientific Reports*, *11*(1), 7417. https://doi.org/10.1038/s41598-021-86477-8.
72. Chakrapani, K., & Sampath, S. (2015). The dual role of borohydride depending on reaction temperature: synthesis of iridium and iridium oxide. *Chemical Communications*, *51*(47), 9690–9693. https://doi.org/10.1039/C5CC03182F.
73. Muthirulan, P., & Rajendran, N. (2012). Poly(o-phenylenediamine) coatings on mild steel: Electrosynthesis, characterization and its corrosion protection ability in acid medium. *Surface and Coatings Technology*, *206*(8–9), 2072–2078. https://doi.org/10.1016/j.surfcoat.2011.09.008.
74. Vanossi, D., Pigani, L., Seeber, R., Ferrarini, P., Baraldi, P., & Fontanesi, C. (2013). Electropolymerization of ortho-phenylenediamine. Structural characterisation of the resulting polymer film and its interfacial capacitive behaviour. *Journal of Electroanalytical Chemistry*, *710*, 22–28. https://doi.org/10.1016/j.jelechem.2013.04.028.
75. Parsa, A., & Ab Ghani, S. (2008). Electrocopolymerization of aniline and ortho-phenylenediamine via facile negative shift of polyaniline redox peaks. *Polymer*, *49*(17), 3702–3708. https://doi.org/10.1016/j.polymer.2008.06.044.
76. Oyama, N., Ohsaka, T., Chiba, K., & Takahashi, K. (1988). Effects of Supporting Electrolyte and pH on Charge Transport within Electropolymerized Poly(*o* -phenylenediamine) Films Deposited on Graphite Electrodes. *Bulletin of the Chemical Society of Japan*, *61*(4), 1095–1101. https://doi.org/10.1246/bcsj.61.1095.
77. Barbero, C., Silber, J. J., & Sereno, L. (1989). Formation of a novel electroactive film by electropolymerization of ortho-aminophenol. *Journal of Electroanalytical Chemistry and Interfacial Electrochemistry*, *263*(2), 333–352. https://doi.org/10.1016/0022-0728(89)85103-4.
78. Du, Y., Wang, H., Zhang, A., & Lu, J. (2007). Electrosynthesis of poly(o-phenylenediamine) in ionic liquid and its properties. *Chinese Science Bulletin*, *52*(16), 2174–2178. https://doi.org/10.1007/s11434-007-0331-9.
79. Wittmann, M., Henze, K., Yan, K., Sharma, V., & Simmchen, J. (2023). Rod-shaped microparticles — an overview of synthesis and properties. *Colloid and Polymer Science*, *301*(7), 783–799. https://doi.org/10.1007/s00396-023-05111-3.

CHAPTER 6

Random Block Type Copolymers of Poly-N-phenyl anthranilic acid-co-Poly-o-phenylenediamine for Oxidizing Analyte Selective Fluorescence Sensing

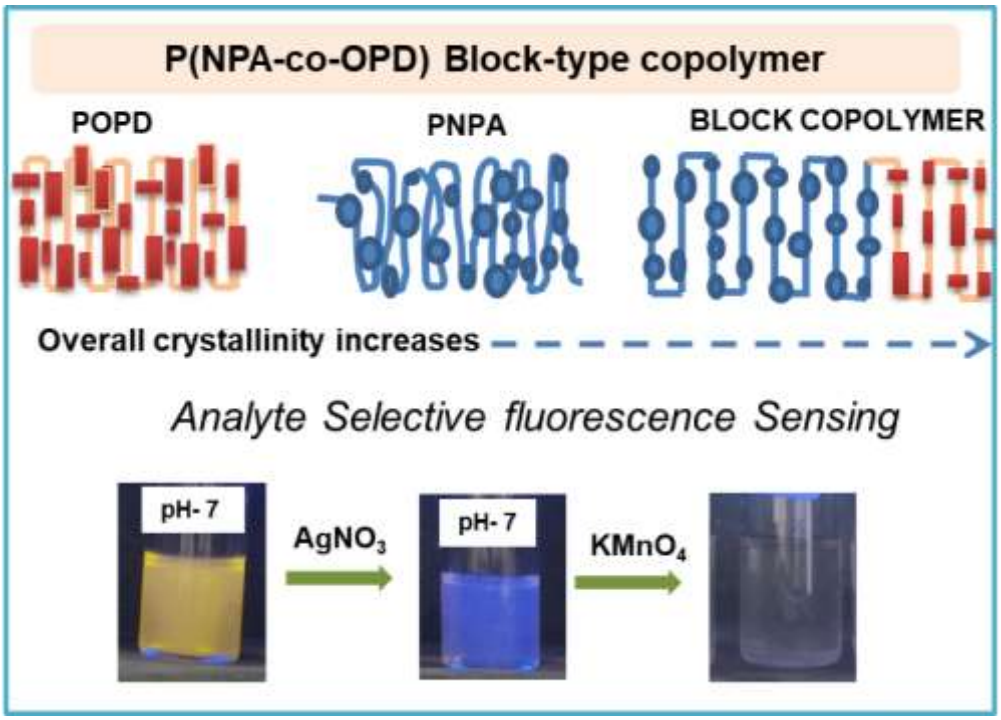

6.1. Introduction

Conjugated polymers are suitable for applications in optoelectronics, electrochemical and biomedical fields due to their diverse structure-property relationships [1-2]. However, their extensive applications were limited by low processability/solubility, less conductivity, and broad photo-emission. The polymer backbone and tailor-made structural modifications on the backbone and side chains provide the desired properties. Water-processable conjugated polymers can be synthesized by polymerizing water-soluble monomers with polar groups on the main or side chain or by palladium cross-coupling reactions [3]. Copolymerization is the best and easiest way to improve properties of conjugated homopolymers. Improvements in the solubility, thermal stability, morphology, and fluorescence properties could be achieved as the significant benefits of copolymerization [4, 5]. Copolymerization could leads to the formation of copolymers with synergistic and improved properties due to the co-monomeric units of homopolymers [6].

Copolymerization of two or more monomers would form either bipolymer, terpolymer, tetrapolymer, or multicomponent polymer [7]. The copolymers can be obtained as random, alternate, block, gradient, or graft based on the reactivity of monomers towards copolymerization [8] (see **Figure 6.1**.). In random copolymers, monomer units are randomly oriented, whereas in alternate copolymers, monomer units are oriented alternatively. Block copolymer contains blocks of monomer units and graft copolymer contains grafted branches of one monomer block from the backbone [9]. In gradient copolymers, the monomer composition varies gradually, whereas block copolymers have abrupt changes and random copolymers have no continuous change in composition [10]. Block copolymers have advantages over random and alternate copolymers, as the desired properties can be selectively tuned without affecting other characteristic properties [11].

Physical blending of homopolymers is an interesting concept in which homopolymers are mixed by physical processes in solid or solution states. Physical blending differed from copolymerization as different monomer units were not linked in a single polymer chain as in the copolymer [12]. Polymer blends can be homogeneous or heterogeneous based on the physical properties of homopolymers. The properties of physical blends depend on the concentrations, viscosities, and miscibility of blended homopolymers [13]. The overlapping energy levels and alterations in electronic transitions via charge transfer occurring during physical blending can influence their photophysical

properties [14]. The intimate interactions between homopolymer chains in the physical blends can also lead to optical properties tuning [15]. Therefore, organic light-emitting diodes and lasers have used stable emission colour tuning by physically blending electro-luminescent or photoluminescent homopolymers [16-18].

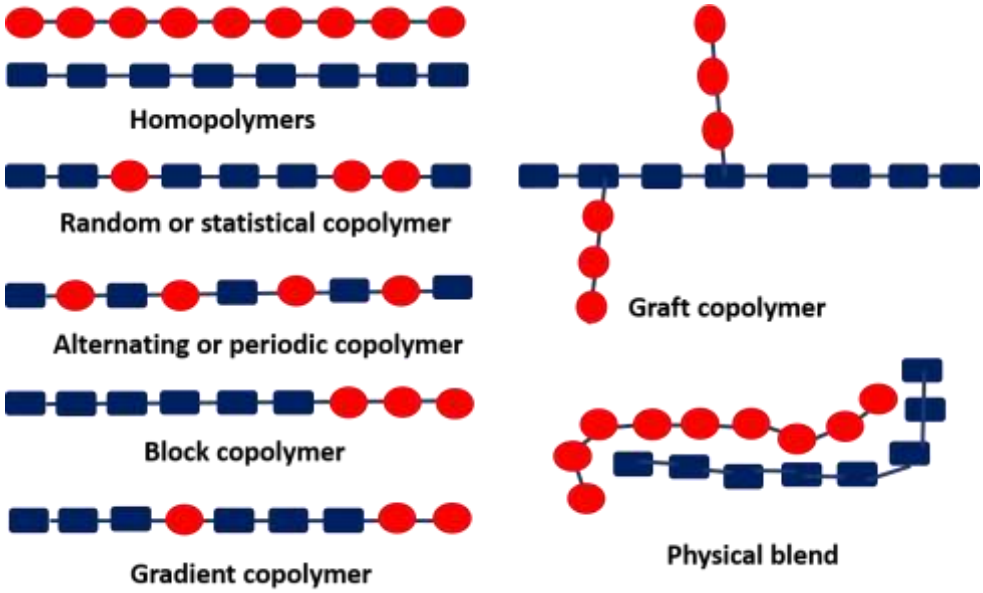

Figure 6.1. *Schematic representation of different types of copolymers and physical blends.*

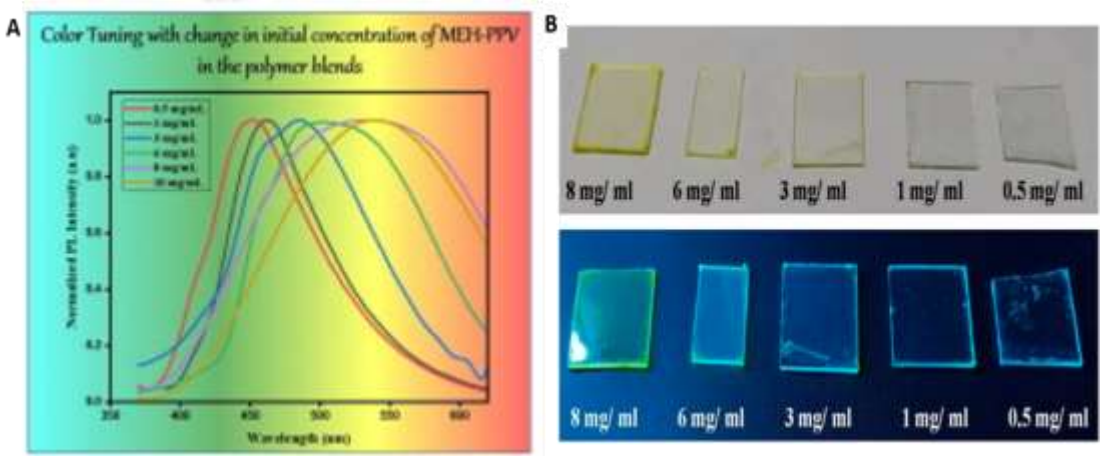

Figure 6.2. *A) Emission tuning in polymer blend composed of poly-2-methoxy-5-(2-ethylhexyloxy)-1,4-phenylene vinylene (MEH-PPV) and a nonconjugated polymer – poly (methyl methacrylate) (PMMA) and B) photos of polymer blend films with various MEH-PPV concentrations in visible light and UV light (Adapted from Ashok Kumar et al. 2021).*

Table 6.1. *Co-monomers used to copolymerize with o-phenylenediamine via chemical oxidative polymerization, the structure of copolymer, and improved properties/applications via copolymerization reported in the literature.*

Sl. No.	**Co-monomer**	**Structure reported**	**Improved property on copolymerization & Application**	**Ref.**
1	1-Naphthylamine	Random copolymer	Fluorescence sensing of Bovine Serum Albumine	32
2	O-Anisidine	Random copolymer	Crystallinity	32
3	Carbazole	Random copolymer	Organic light-emitting diodes	29
4	Vaniline	Alternating copolymer	Optoelectronics and biomedicine	33
5	Luminol	Random copolymer	Fluorescence quantum yield for Cell imaging	30
6	3-Amino-5-methylthio-1H-1,2,4-triazole	Random copolymer	Optoelectronics and biomedicine	6
7	Pyrrole	Random copolymer	Optoelectronics	31
8	O-phenetidine	Random copolymer	Solvatochromism and solubility	34
9	2-pyramidylamine	Random copolymer	Thermal stability	35
10	p-Toluidine	Random copolymer	The power conversion efficiency for Solar cell	36
11	Aniline	Random copolymer	Capacitance for super capacitor	37
12	Aniline	Block copolymer	Electrochromism for electrochromic devices	38
13	N-sulfopropylaniline	Random copolymer	Solubility	39

Polyaniline (PANI) is a conducting polymer with good thermal/environmental stability and semiconducting on doping. However, pristine polyaniline has weak emission and less processability, preventing its applications in optoelectronic devices. Copolymerization was a chemical modification adopted in polyaniline to improve their limitations, like low processability [19]. Water-soluble polyaniline copolymers were obtained from the copolymerization of aniline with suitable monomers [20-23]. Poly-o-phenylenediamine (POPD) has better solubility/processability and fluorescence properties than PANI [24-25]. Aniline and o-phenylenediamine were copolymerized for the sensing, supercapacitance and solar cell applications [26-28]. Copolymers of o-phenylenediamine with other monomers were reported with improved physical and chemical properties suitable for different applications via the chemical oxidative polymerization route (see **Table 6.1**). Jadoun et al. used ultrasonically copolymerized carbazole and o-phenylenediamine for applications in organic light-emitting diodes [29]. Co-monomer composition-dependent fluorescence quantum yield of POPD copolymers has been reported [30-31].

Electrochemically synthesized copolymers of o-phenylenediamine and other monomers were also used for the sensing of different analytes [40-42]. The copolymers of o-phenylenediamine with other fluorescent co-monomers were developed for fluorescence sensing applications and biological studies [43]. Liao et al synthesized poly-o-phenylenediamine and rhodamine-B copolymer dots (Pp-RhB dot) by chemical oxidative polymerization using ammonium persulfate as an oxidizing agent. The weakened fluorescence emission of copolymer dot by photoinduced electron transfer between poly-o-phenylenediamine and rhodamine B was enhanced in the presence of nitrite ions. The copolymer dot was thus used for nitrite ion detection and fluorescent cell imaging of HeLa cells (see **Figure 6.3.A.**) [44]. Liao et al. synthesized copolymers of poly-o-phenylenediamine and benzeneselenol to develop an oxidation-reduction fluorescent switch. The redox reversible fluorescent probe detected hydrogen peroxide and glutathione [45]. Riaz et al. synthesized poly-o-phenylenediamine and luminol fluorescent copolymer and was used for the fluorescence cell imaging of HeLa cells (see **Figure 6.3.B-D**) [30].

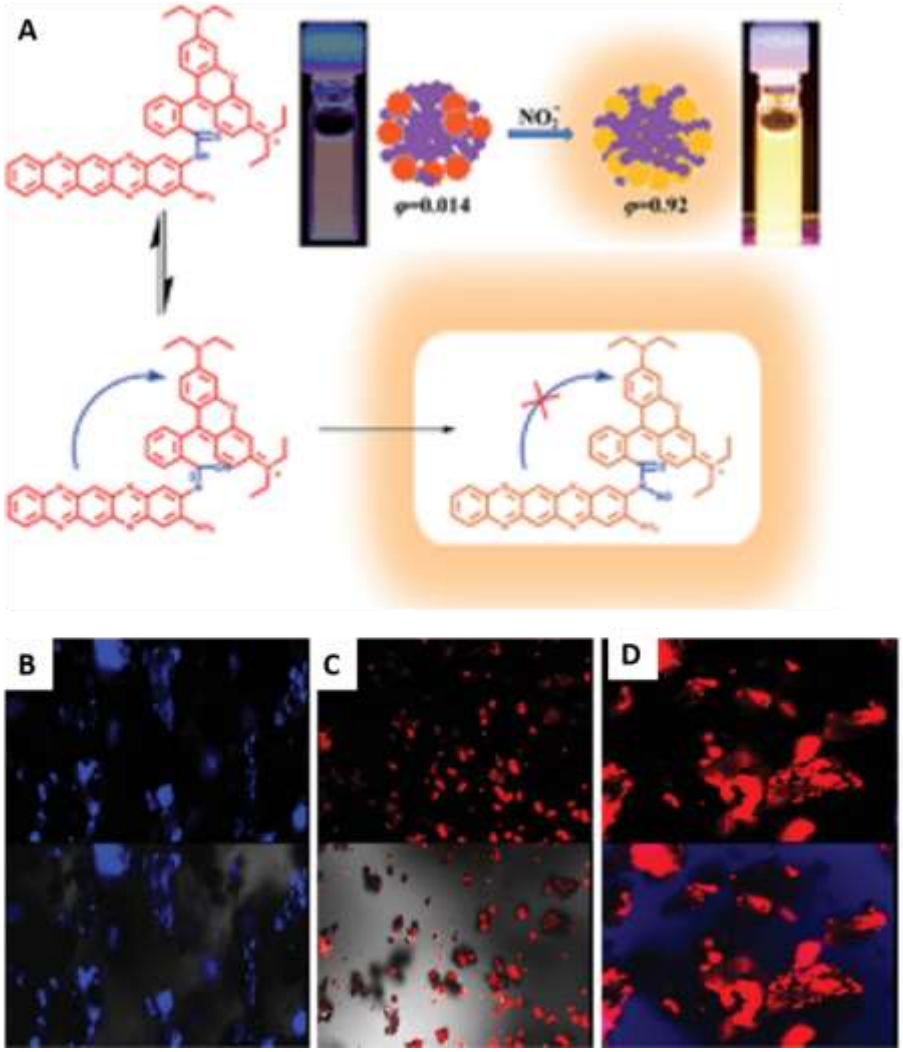

Figure 6.3. *A) Photoinduced electron transfer in poly-o-phenylenediamine and rhodamine B copolymer dot for nitrite detection (Adapted from Liao et al. 2015). Fluorescent cell imaging of HeLa cells using B) polyluminol (PLU) C) poly-o-phenylenediamine (POPD) and D) PLU-POPD copolymer (Adapted from Riaz et al. 2018).*

The synthesis, characterization, and fluorescence properties of poly-N-phenyl anthranilic acid (PNPA) homopolymer were given in Chapter 2. Similarly, o-phenylenediamine undergoes oxidative chemical polymerization in the presence of various oxidizing agents to produce poly-o-phenylenediamine, which has given yellow fluorescence emission [29,47]. The present investigation uses a copolymerization strategy to synthesize N-phenyl anthranilic acid and o-phenylenediamine copolymers to fine-tune the emission characteristics. The emission colour tuning of conjugated polymers via the copolymerization route was rarely reported in the literature [48-49]. Emission control in redox copolymer by oxidizing analytes is a different approach. Furthermore, the physical blends

of bluish-white fluorescent poly-N-phenyl anthranilic acid (PNPA) and yellow fluorescent poly-o-phenylenediamine (POPD) have been utilized to fine-tune the fluorescence emission at different pHs. The structure, reactivity, and photophysical properties of the copolymers of P(NPA-co-POPD) were compared with blend PNPA-blend-POPD and homopolymers. Monomer reactivity ratios determined by the Fineman-Ross method using FT-IR spectra indicated the presence of blocks of NPA units in the copolymers due to the high reactivity of NPA compared to OPD. The present work proposes a distinct method of analyte oxidative power-controlled fluorescent sensing of silver nitrate and potassium permanganate in P(NPA-co-OPD) in water.

6.2. Experimental

6.2.1. Materials and Reagents: O-phenylenediamine and N-Phenyl anthranilic acid (97%) were purchased from LOBA chemicals. N-Phenyl anthranilic acid was further purified by recrystallization method using acetone as solvent. Anhydrous ferric chloride, silver nitrate, potassium permanganate, and concentrated sulphuric acid (98%) were purchased from Merck Chemicals. Double-distilled ethanol and deionized water were used to synthesize and purify the polymer and copolymers.

6.2.2. Measurements and Instruments: UV-visible absorption spectra of the samples were recorded by the Shimadzu UV-Visible spectrometer 1800 series in the 200-800 nm wavelength range using deionized water as solvent. Proton NMR spectra of the samples were recorded using a 400 MHz Bruker Avance III FT-NMR Spectrophotometer using d_6-DMSO as the solvent and TMS as an internal standard. The fourier transform infrared spectra of the samples were recorded by Cary 660 FT-IR spectrometer using ATR Mode in the wavenumber range 400-4000 cm^{-1}. Powder X-ray diffraction of the samples was measured using PANalytical, Aeris research diffractometer in the 2θ range 5 to 80°. Polymer molecular weight determination of the samples has been carried out using Bruker Autoflex max LRF MALDI-TOF using sinapinic acid as a matrix. The pH of solutions was measured using a portable pH meter of Hanna instruments. Fluorescence spectra of the samples were recorded using a Shimadzu RF 5301-PC spectrofluorophotometer. Thermo gravimetric analysis (TGA) of the samples was measured using STA 8000. FE-SEM images of the samples were recorded using Zeiss Gemini SEM 300 with 12-2,000,000 × magnifications.

6.2.3. Synthesis of homopolymers: Synthesis of homopolymer poly-N-phenyl anthranilic acid was given in chapter 2 and the synthesis of homopolymer poly-o-phenylenediamine was given in chapter 5.

6.2.4. Synthesis of copolymers of NPA and OPD

6.2.4.A. Synthesis of copolymer P(NPA-co-OPD) 10:90: The recrystallized monomer N-phenyl anthranilic acid (0.04 g, 0.189 mmol) was dissolved in 2 ml double distilled ethanol. The other monomer, o-phenylenediamine (0.36g, 3.33 mmol) was dissolved in 5 mL double distilled ethanol. Both monomer solutions were mixed together and anhydrous $FeCl_3$ (0.46g, 2.84 mmol), dissolved in 5 mL double distilled ethanol, was added to the monomer mixture, and polymerization was allowed to continue for 2 hours without any disturbance. The ethanol was completely evaporated, and the copolymer was washed with water and acetone, filtered, and dried in a vacuum oven at 60°C. Yield = 0.095 g (23.75 %). ^{1}H NMR (400 MHz, DMSO-d_6) δ: 7.02 (S, 2H, Ar-H), 7.75 (S, 2H, Ar-H), 8.04 (S, 2H, Ar-H). FT-IR (KBr, cm^{-1}): 3316, 3161, 1687, 1628, 1531, 1357, 1231, 1153, 843, 745, and 589.

6.2.4.B. Synthesis of copolymer P(NPA-co-OPD) 25:75: The recrystallized monomer N-phenyl anthranilic acid (0.10 g, 0.469 mmol) was dissolved in 2 mL double distilled ethanol. The other co-monomer, o-phenylenediamine (0.30g, 2.77 mmol), was dissolved in 5 mL double distilled ethanol. Both monomer solutions were mixed, and oxidizing agent anhydrous $FeCl_3$ (0.46g, 2.84 mmol) dissolved in 5 mL double distilled ethanol was added to the monomer mixture. The polymerization was allowed to continue for 2 hours without disturbance, and then the ethanol was completely evaporated. The copolymer was washed with water and acetone, filtered, and dried in a vacuum oven at 60°C. Yield = 0.145 g (36 %). ^{1}H NMR (400 MHz, d_6 DMSO) δ: 6.80 (m, 1H, Ar-H), 7.02 (m, 1H, Ar-H), 7.10 (m, 1H, Ar-H), 7.25 (m, 3H, Ar-H), 7.40 (m, 3H, Ar-H), 7.75 (m, 2H, Ar-H) , 7.90 (m, 1H, Ar-H), 8.05 (t, 2H, Ar-H) and 9.65 (s, 1H, N-H). FT-IR (KBr, cm^{-1}): 3337, 3157, 1694, 1601, 1531, 1451, 1366, 1321, 1272, 1142, 902, 842, 753, 652 and 593.

The digits 25:75 in P(NPA-co-OPD) 25:75 in the sample code implies that 25 weight % feed of NPA monomer and 75 weight % feed of OPD, and the term 'co' represents copolymerization. Other copolymers, P(NPA-co-OPD) 50:50 and P(NPA-co-OPD) 75:25, were also prepared by changing the weight percentage of co-monomers taken in the feed of N-phenyl anthranilic acid (NPA) and o-phenylenediamine (OPD) as given in **Table 6.2.**

6.2.5. Synthesis of physical blends of PNPA and POPD

6.2.5.A. Synthesis of PNPA-blend-POPD 10:90

Poly-N-phenyl anthranilic acid (0.04 g) and poly-o-phenylenediamine (0.36 g) were accurately weighed into a mortar and grounded well for 15 minutes to form a homogenized mixture using a pestle. The resultant blend was used for structural characterization and comparison of properties with the copolymer. Yield = 0.40 g (100%). FT-IR (KBr, cm^{-1}): 3337, 3157, 1694, 1641, 1531, 1366, 1272, 1242, 1142, 842, 753 and 593.

6.2.5.B. Synthesis of PNPA-blend-POPD 25:75: Poly-N-phenyl anthranilic acid (0.10 g) and poly-o-phenylenediamine (0.30 g) were accurately weighed into a mortar and grounded well for 15 minutes to form a homogenized blend using a pestle. The resultant blend was used for structural characterization and comparison of properties with P(NPA-co-OPD) 25:75. Yield = 0.40 g (100%). ^{1}H NMR (400 MHz, DMSO-d_6) δ: 6.75 (m, 1H, Ar-H), 6.95 (m, 1H, Ar-H), 7.05 (m, 1H, Ar-H), 7.25(m, 3H, Ar-H), 7.35 (m, 3H, Ar-H), 7.65 (m, 2H, Ar-H) , 7.90 (m, 1H, Ar-H), 8.00 (t, 2H, Ar-H) and 9.65 (s, 1H, N-H). FT-IR (KBr, cm^{-1}): 3337, 3157, 1694, 1641, 1531, 1366, 1272, 1242, 1142, 842, 753 and 593.

The digits 25:75 in the sample code of PNPA-blend-POPD 25:75 imply 25 weight % feed of PNPA polymer and 75 weight % feed of POPD polymer in blend. Other blends, such as PNPA-blend-POPD 10:90, PNPA-blend-POPD 50:50, and PNPA-blend-POPD 75: 25, were prepared by changing the weight percentage of homopolymers of poly-N-phenyl anthranilic acid (PNPA) and poly-o-phenylenediamine (POPD) as given in **Table 6.2.**

6.2.6. Preparation of $AgNO_3$ and acidified $KMnO_4$ solutions as oxidising analytes: Silver nitrate (16.98 mg) was accurately weighed into a 10 mL standard flask. Double deionised water was added and made up to the mark to obtain 1.0×10^{-2} M $AgNO_3$ solution. From the stock solution, different molarity of $AgNO_3$ (5.0×10^{-3} M, 1.0×10^{-3} M, 7.5×10^{-4} M, 5.0×10^{-4} M, 2.5×10^{-4} M, and 1.0×10^{-4} M) was prepared by diluting stock using double deionised water. Potassium permanganate (1.58 mg) was accurately weighed into a 10 mL standard flask. H_2SO_4 (1 M) was added and made up to the mark to obtain acidified $KMnO_4$ solution having concentration 1.0×10^{-3} M. From the stock solution, different molarity of acidified $KMnO_4$ (7.5×10^{-4} M, 5.0×10^{-4} M, and 2.5×10^{-4} M) was prepared by diluting stock using dilute H_2SO_4.

6.2.7. The pH-dependent studies of homopolymers, copolymers, and blends: The weight of PNPA, POPD, P(NPA-co-OPD) copolymers, and PNPA-blend-POPD blends was fixed as 5.0 mg dissolved in 4 mL conc. H_2SO_4. Half of the above solution (2 mL) was diluted to 20 mL using deionized water in a 100 mL beaker, and the pH was increased to neutral and basic pH by adding 4 M NaOH.

6.2.8. Analyte selective oxidation in P(NPA-co-OPD) 10:90 with $AgNO_3$ and $KMnO_4$: P(NPA-co-OPD) 10:90 (0.50 mg) was dissolved in conc. H_2SO_4 (4 mL). Half of the above solution (2 mL) was diluted to 20 mL using double deionized water. The pH of the solution was maintained at neutral (pH=7) by adding 4 M NaOH (~ 20 mL) solution. To 3 mL of each of neutral P(NPA-co-OPD) 10:90 solution (6.25×10^{-5} g/mL) taken in different vials, 3 mL of $AgNO_3$ having different concentrations like 1×10^{-2}, 5×10^{-3}, 2.5×10^{-3}, 1×10^{-3}, 5×10^{-4}, 2.5×10^{-4}, 1×10^{-4} M were added for the oxidation of POPD fragments. A strong oxidizing agent acidified $KMnO_4$ (5×10^{-4} M, 3 mL) was added to oxidize POPD and PNPA fragments completely. The fluorescence of semi-oxidized and completely oxidized copolymer solutions was noted using the UV Inspection cabinet. UV-visible absorption spectra and fluorescence spectra of each copolymer and copolymer-analyte solution were recorded.

6.3. Results and Discussion

6.3.1. Synthesis of homopolymers, copolymers and physical blends

Homopolymers and copolymers of o-phenylenediamine (OPD) and N-phenyl anthranilic acid (NPA) have been synthesized by chemical oxidative polymerization using anhydrous $FeCl_3$ as an oxidizing agent in ethanol solvent. Different copolymers like P(NPA-co-OPD) 10:90, P(NPA-co-OPD) 25:75, P(NPA-co-OPD) 50:50, and P(NPA-co-OPD) 75:25 have been synthesized by varying the weight percentage of monomers OPD and NPA. For example, sample code P(NPA-co-OPD) 10:90 denoted that the copolymer was synthesized from 10% by weight of NPA and 90% by weight of OPD (see **Figure 6.4.)**. Physical blends of homopolymers (PNPA-blend-POPD 10:90, PNPA-blend-POPD 25:75, PNPA-blend-POPD 50:50, and PNPA-blend-POPD 75:25) were obtained by gentle grinding of different weight percentages of POPD and PNPA powders using mortar and pestle (See **Table 6.2.**).

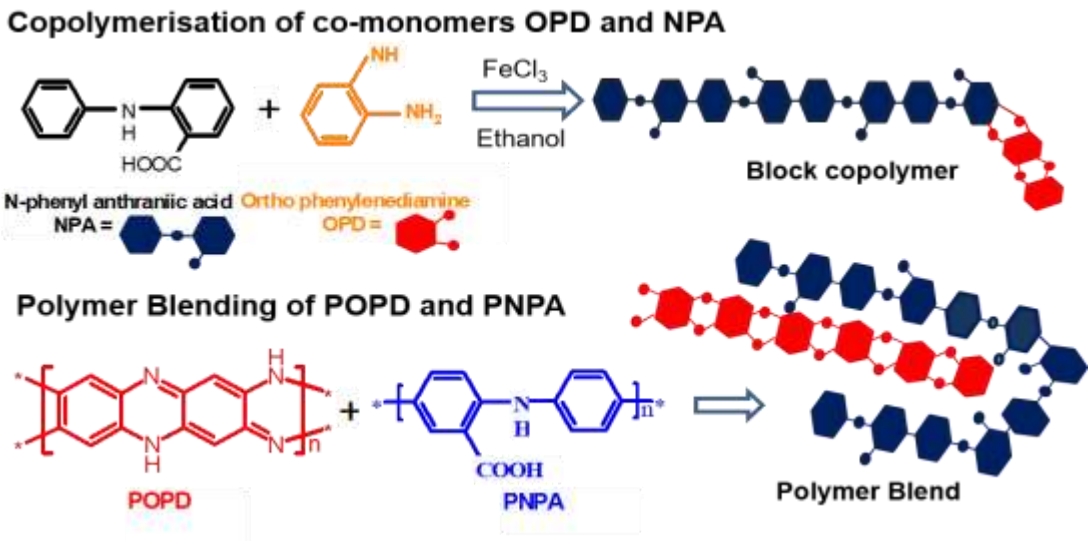

***Figure 6.4**. Schematic representation of the synthesis of copolymers from co-monomers OPD and NPA by oxidative chemical polymerization and physical blending of homopolymers POPD and PNPA.*

The homopolymer POPD was a reddish-brown powder soluble in water, chloroform, acetone, ethanol, and dimethyl sulfoxide (DMSO). The homopolymer PNPA was a bluish-black powder insoluble in water and soluble in concentrated acids, chloroform, acetone, ethanol, and dimethyl sulfoxide. The general strategy for preparing solutions of PNPA, POPD, P(NPA-co-OPD), and PNPA-blend-POPD was to dissolve the sample in an acidic solution, then increase the pH to neutral and to alkaline pH by adding a sufficient quantity of sodium hydroxide. The blue color of PNPA in concentrated acid became colorless by adding H_2O or NaOH solution. The dark brown POPD in the concentrated acid medium became orange in the weakly acidic medium and yellow in the neutral and basic medium. As a result, the copolymer and blends have shown brown to orange color in acidic pH and yellow in neutral and basic pH (see **Figure 6.5.**).

Table 6.2. *The mass of co-monomers NPA and OPD taken for copolymer synthesis, the mass of PNPA and POPD taken for blending, the weight ratio of NPA: OPD or PNPA: POPD, the mole ratio of NPA/OPD or PNPA/POPD, and corresponding yields of copolymers and blends.*

Sample	Mass of NPA or PNPA (g)	Mass of OPD or POPD (g)	Weight ratio NPA: OPD or PNPA: POPD	NPA/OPD or PNPA/POPD Mole ratio	Yield (g)
P(NPA-co-OPD) 10:90	0.04	0.36	10:90	0.057	0.095
P(NPA-co-OPD) 25:75	0.10	0.30	25:75	0.171	0.145
P(NPA-co-OPD) 50:50	0.20	0.20	50:50	0.512	0.270
P(NPA-Co-OPD) 75:25	0.30	0.10	75:25	1.535	0.367
PNPA-blend-POPD 10:90	0.04	0.36	10:90	0.055*	0.40
PNPA-blend-POPD 25:75	0.10	0.3	25:75	0.164*	0.40
PNPA-blend-POPD 50:50	0.20	0.2	50:50	0.493*	0.40
PNPA-blend-POPD 75:25	0.30	0.1	75:25	1.479*	0.40

*The molecular mass of one monomeric/repeating unit was taken as the molecular weight of the polymer to calculate the mole ratio of blends.

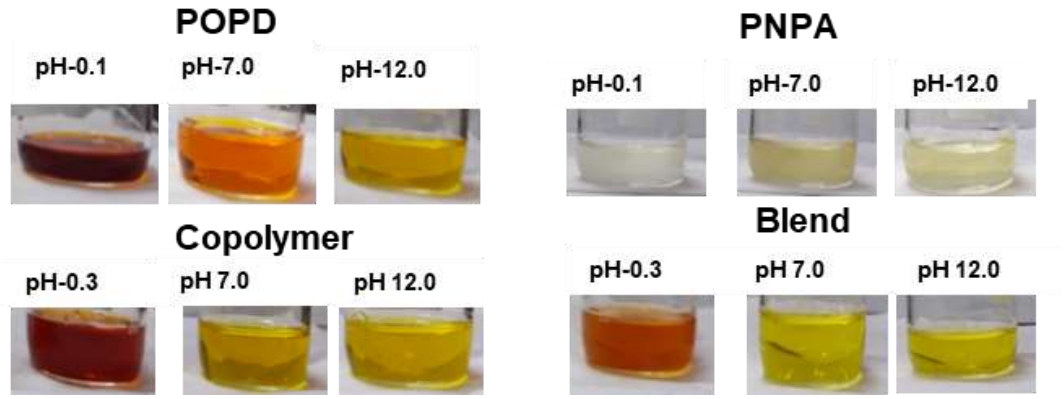

Figure 6.5. *Photographs of homopolymers POPD, PNPA, copolymer and blend at acidic, neutral and basic pH in visible light.*

6.3.2. Structural characterization of copolymers and physical blends

The good solubility of homopolymers, copolymers, and blends in dimethyl sulfoxide (DMSO) enabled us to do their structural characterization by ^{1}H NMR (see

Figure 6.6.). The ^{1}H NMR spectra of homopolymer POPD have three peaks at 7.02, 7.75, and 8.04 ppm [50-52], whereas PNPA has multiplets at 6.80, 7.10, 7.25, 7.40, and 7.90 ppm corresponding to aromatic protons. The ^{1}H NMR spectra of copolymers P(NPA-co-OPD) 25:75 and 50:50 have shown peaks at 7.02, 7.75, and 8.05 ppm corresponding to aromatic protons POPD fragments and other multiplets at 6.80, 7.10, 7.25, 7.40, and 7.90 corresponding to aromatic protons in PNPA fragments. The ^{1}H NMR spectra of the copolymer P(NPA-co-OPD) 10:90 have shown peaks at δ values 7.02, 7.75, and 8.04 ppm corresponding to POPD fragment and weak peaks at 7.10 and 7.25 ppm corresponding to aromatic protons of PNPA. The intensity of peaks corresponding to aromatic protons of PNPA in PNPA-co-POPD 10:90 was low due to the low quantity of PNPA (10 weight percent) taken for the copolymerization. Interestingly, as we increase 10% NPA in feed to 50% NPA in feed, the intensity of the NPA fragment overtakes the OPD fragment due to its high reactivity. The peak intensity of aromatic protons in PNPA fragments in the P(NPA-co-OPD) 25:75 matched the homopolymer PNPA, indicating the better reactivity of PNPA fragments. In contrast, the peaks of aromatic protons in POPD fragments in the copolymer P(NPA-co-OPD) 25:75 have less intensity than those of aromatic protons in homopolymer POPD, indicating the less reactive nature of POPD fragments. Studies on the block copolymers suggest that their ^{1}H NMR spectra were superimposed on that of the homopolymers [53]. The peaks in P(NPA-co-OPD) 25:75 and P(NPA-co-OPD) 50:50 was present at the same chemical shift values as that of the homopolymers PNPA and POPD, indicating the possibility of blocks in copolymers [53]. Block copolymer has the advantage of better crystalline properties of polymers without significant changes in the elastic properties by choosing a suitable co-monomer [54]. The physical blend PNPA-blend-POPD 25:75 has slightly broadened peaks present at δ values 6.75, 6.95, 7.05, 7.25, 7.35, 7.65, 7.9 and 8.0 ppm in contrast to P(NPA-co-OPD) 25:75) (see **Figure 6.6.**). The intensity of POPD and PNPA polymers that take part in PNPA-blend-POPD 25:75 have the same intensity as in homopolymers; however, the peaks corresponding to POPD have slightly upfield chemical shifts. The peak corresponds to secondary –NH protons at δ value 9.65 ppm were present in P(NPA-co-OPD) 25:75 and PNPA-blend-POPD 25:75 similar in PNPA, which confirmed the presence of PNPA fragments in the copolymer and blend [46].

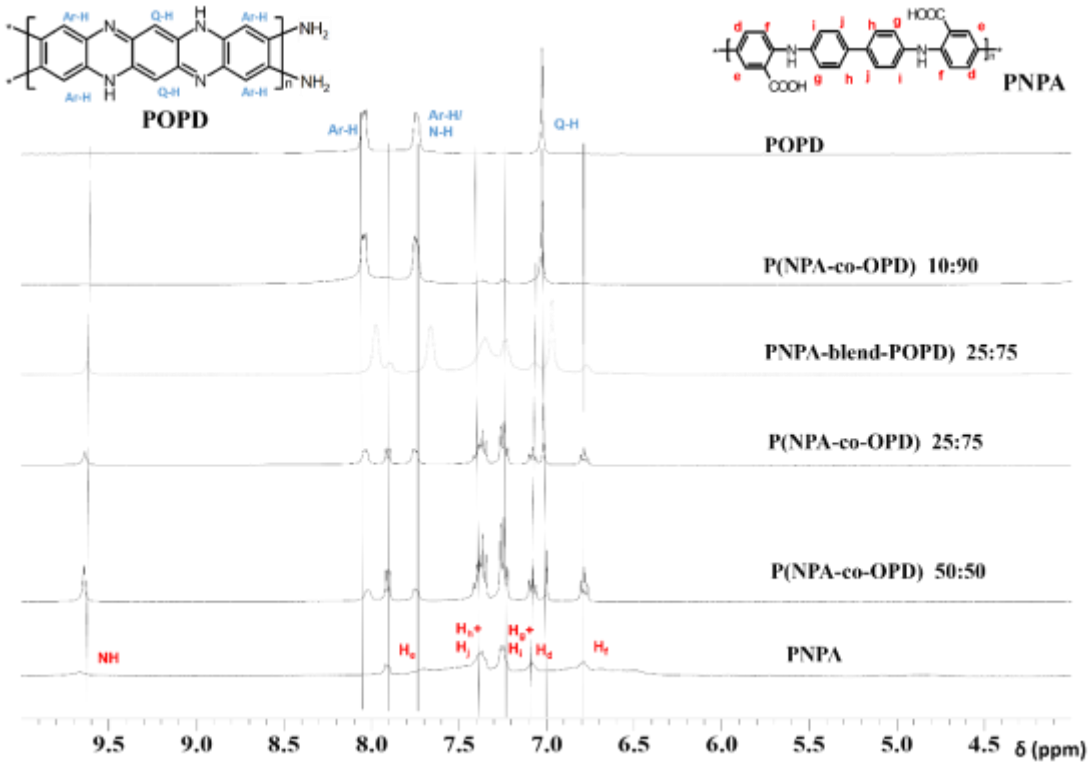

Figure 6.6. *^{1}H NMR spectra of homopolymers POPD, PNPA, copolymers P(NPA-co-OPD) 10:90, P(NPA-co-OPD) 25:75, P(NPA-co-OPD) 50:50, and physical blend PNPA-blend-POPD 25:75 in DMSO- d_6 solvent.*

Carbon-13 NMR spectra of homopolymers and copolymers were also recorded in DMSO-d_6 solvent (see supporting information **Figure 6.7.**). The ^{13}C NMR spectra of POPD has shown only one peak at 131 ppm, which indicated the symmetric chemical environment of carbon atoms in the structure of POPD [37]. The NMR spectra of PNPA has shown peaks at 114.20, 117.89, 121.85, 123.52, 129.87, 132.35, 134.59, 141.00, and 147.42 ppm corresponded to the aromatic carbon atoms, whereas the peak at 170.42 ppm corresponded to –COOH carbon atom [44]. In the case of copolymer P(NPA-co-OPD) 10:90, the peaks corresponded to POPD and PNPA carbon atoms were present, however the intensity of PNPA peaks were very weak due to the lower PNPA co-monomeric fragments in the copolymer. The spectra of P(NPA-co-OPD) 25:75 and P(NPA-co-OPD) 50:50 have shown gradual hike in ^{13}C peak intensity of PNPA fragment and an additional peak was observed at 113.00 ppm indicated the bonding between POPD and PNPA blocks. The peak corresponded to POPD carbon atoms in P(NPA-co-OPD) 25:75 was not visible in P(NPA-co-OPD) 50:50 due to greater reactivity of NPA units.

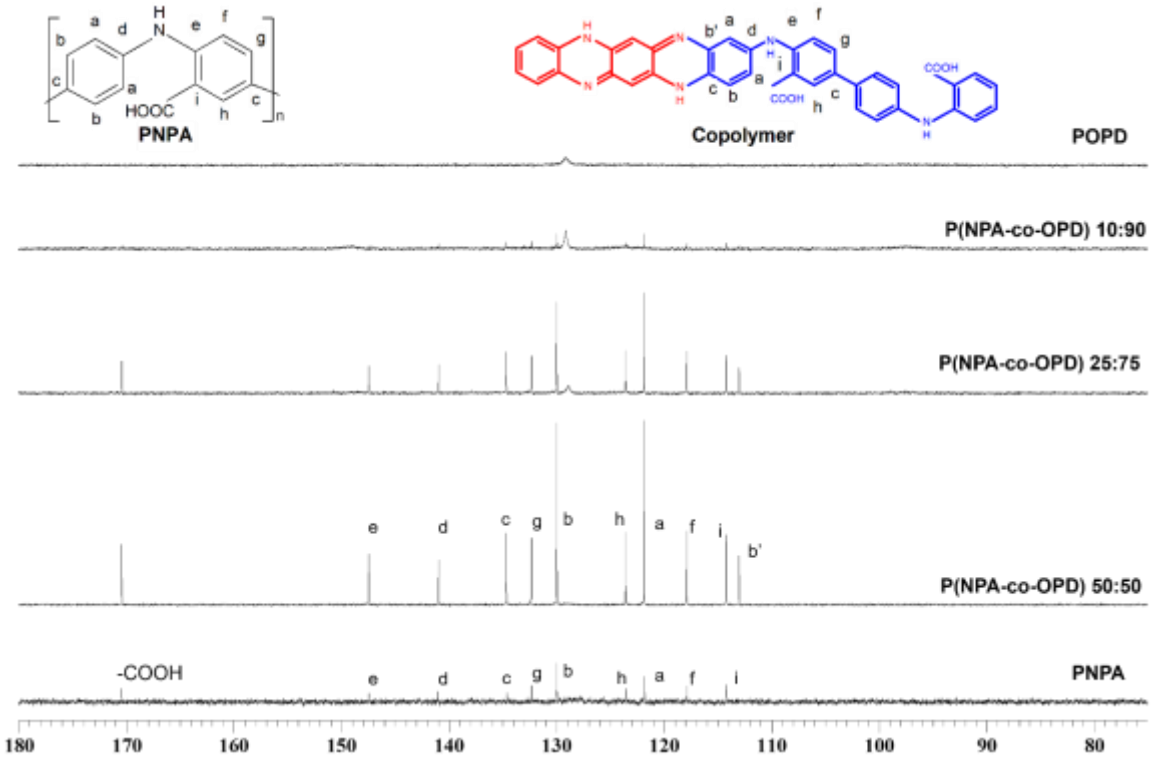

Figure 6.7*. [13]C NMR spectra of homopolymers POPD, PNPA copolymer P(NPA-co-OPD) 10:90, P(NPA-co-OPD) 25:75, and P(NPA-co-OPD) 50:50 in d_6-DMSO solvent.*

The homopolymers POPD, PNPA, and copolymers P(NPA-co-OPD) 10:90, 25:75, 50:50, and 75:25 was characterized by fourier transform infrared spectroscopy (see **Figure 6.8.A** and **Table 6.3.**). The homopolymer POPD showed peaks at 3316, 3161, 1694, 1635, 1531, 1357, 1243, 1153, 837, 752 and 589 cm^{-1} corresponding to –NH stretching of secondary amines, –NH stretching of terminal primary amines, C=N quinoid stretching, C=C quinoid stretching, C=C benzenoid stretching, C-N stretching in the neighbourhood of quinoid units, C-N stretching in the neighbourhood of benzenoid rings, C-H in-plane bending in benzenoid rings, C-H out of plane bending of 1,2,4,5-tetra substituted phenyl rings, C-H bending of 1,2-disubstituted phenyl rings and N-H out of plane bending vibrations respectively [55-60]. The homopolymer PNPA showed peaks at 3347, 3038, 1601, 1582, 1504, 1451, 1393, 1272, 1153, 753 and 503 cm^{-1} corresponding to –NH asymmetric stretching, carboxylic O-H stretching, C=O stretching, C-C aromatic asymmetric stretching, C-C symmetric aromatic stretching, carboxylic O-H bending, C-N stretching, C-O stretching, C-H in-plane bending in benzenoid rings, C-H out of plane bending and N-H out of plane bending respectively [46, 61-62]. The copolymer P(NPA-co-OPD) 10:90 showed peaks similar to POPD, as it may contain higher POPD fragments. The FT-IR

spectrum of copolymer P(NPA-co-OPD) 25:75 indicated the greater reactivity of NPA in the copolymer by showing peaks at 1661, 1451, and 1261 cm^{-1} corresponding to quinoid C=N merged with C=O stretching, carboxylic O-H bending and C-O stretching, respectively. Some additional peaks at 1321 cm^{-1} correspond to C-N stretching and 902 cm^{-1} correspond C-H bending vibrations in the copolymer. In the FT-IR spectra of copolymer P(NPA-co-OPD) 50:50 and P(NPA-co-OPD) 75:25, quinoid C=N peaks at 1694 and C-N peak at 1366 cm^{-1} corresponding to POPD fragment almost diminished, which indicated the less reactivity of OPD in the copolymer formation. FT-IR spectra of physical blends PNPA-blend-POPD 10:90, PNPA-blend-POPD 25:75, and PNPA-blend-POPD 50:50 were also given in **Figure 6.7.B**.

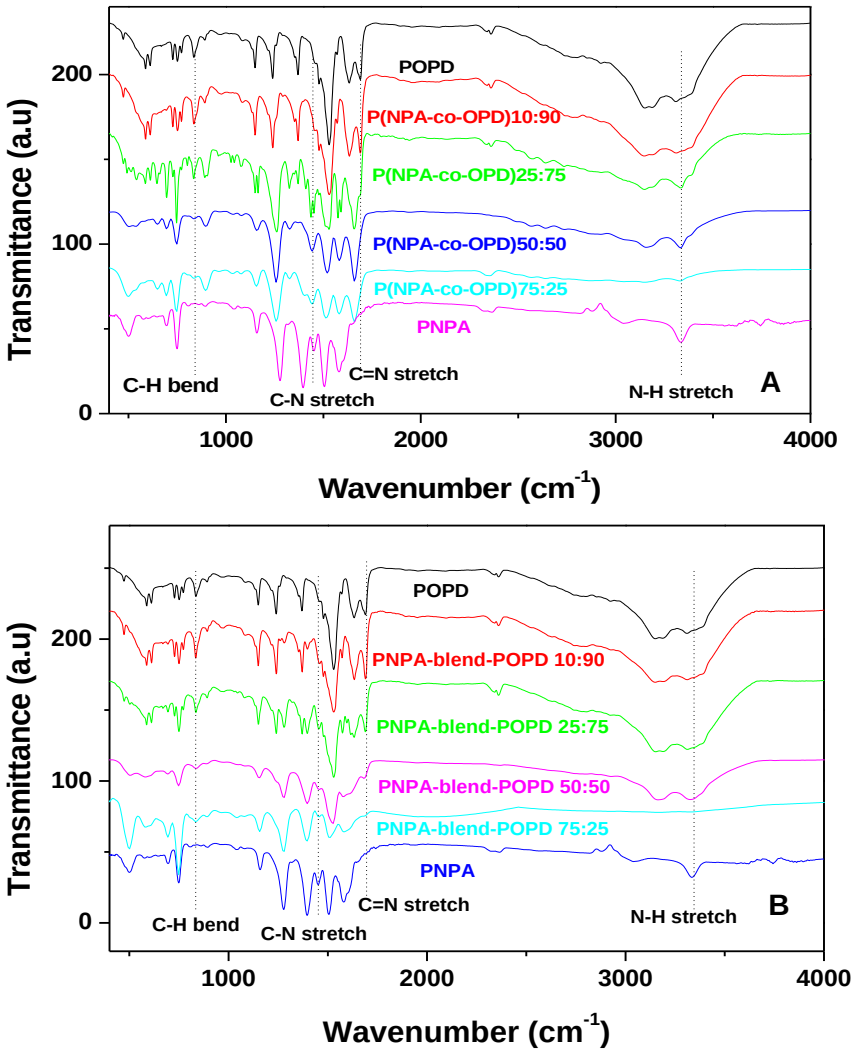

Figure 6.8*. FT-IR spectra of A) homopolymers POPD, PNPA, and copolymers P(NPA-co-OPD) 10:90, P(NPA-co-OPD) 25:75, P(NPA-co-OPD) 50:50, and P(NPA-co-OPD) 75:25 and B) homopolymers POPD, PNPA, and blend PNPA-blend-POPD 10:90, PNPA-blend-POPD 25:75, PNPA-blend-POPD 50:50, and PNPA-blend-POPD 75:25.*

Table 6.3. *FT-IR spectral data of homopolymers, copolymers and physical blends.*

Vibrations of characteristics group	**Wavenumber (cm^{-1}) with relative intensity**									
	Homopolymers		**Copolymers P(NPA-co-OPD)**				**Physical Blends PNPA-blend-POPD**			
	POPD	**PNPA**	**10:90**	**25:75**	**50:50**	**75:25**	**10:90**	**25:75**	**50:50**	**75:25**
–NH stretching of secondary amines	3316 b)	3347 (b)	3316 (b)	3316 (b)	3347 (b)	3347 (w)	3316 (b)	3347 (b)	3347 (b)	-
–NH stretching of primary amines	3161 (b)	-	3161 (b)	3161 (b)	3161 (b)	-	3161 (b)	3161 (b)	3161 (b)	-
carboxylic O-H stretching	-	3038 (b)	-	-	-	-	-	-	-	-
C=N quinoid stretching	1694 (m)	-	1694 (m)	1694 (w)	1694 (w)	1694 (w)	1694 (m)	1694 (m)	1694 (w)	1694 (w)
C=C quinoid stretching	1641 (m)	-	1641 (m)	1641 (w)	-	-	1641 (m)	1641 (m)	1641 (w)	1641 (w)
C=O stretching	-	1601 (w)	-	1601 (w)	1601 (w)	1601 (w)	-	1601 (w)	1601 (w)	1601 (w)
C=C benzenoid stretching	1531 (s)	1501 (m)	1531 (s)	1531 (m)	1531 (m)	1531 (m)	1531 (s)	1531 (m)	1531 (w)	1531 (w)
carboxylic O-H bending	-	1451 (w)	-	1451 (w)	1451 (w)	1451 (w)	-	1451 (w)	1451 (w)	1451 (w)
C-N quinoid stretching	1357 (m)	-	1357 (m)	1357 (w)	-	-	1357 (m)	1357 (w)	-	-
C-N benzenoid stretching	1231 (m)	1401 (m)	1231 (m)	-	-	-	1231 (m)	1231 (w)	-	-

C-O stretching	-	1272 (s)	-	1258 (s)	1258 (s)	1258 (s)	-	1272 (w)	1272 (w)	1272 (w)
C-H in plane bending	1153 (m)	1153 (w)	1153 (m)	1153 (m)	1153 (w)	1153 (w)	1153 (m)	1153 (m)	1153 (w)	1153 (w)
C-H out of plane bending	843 (w)	753 (m)	843 (w)	843 (w)	753 (w)	753 (w)	843 (w)	843 (w)	753 (w)	753 (m)
C-H bending of 1,2-disubstituted phenyl rings	745 (w)	-	745 (w)	745 (m)	745 (w)	745 (w)	745 (w)	745 (m)	745 (w)	745 (w)
N-H out of plane bending	589 (w)	503 (w)	589 (w)	503 (w)	503 (w)	503 (w)	589 (w)	589 (w)	503 (w)	503 (w)

b, s, m, w indicates broad, strong, medium, and weak peaks in the FT-IR spectra.

PNPA-blend-POPD 10:90 showed peaks similar to the homopolymer POPD, whereas, in PNPA-blend-POPD 25:75, the peak corresponding to C-O stretching at 1275 cm^{-1} was obtained, indicating the presence of PNPA fragments in the blend. In the case of PNPA-blend-POPD 50:50, unlike P(NPA-co-OPD) 50:50, the vibrations corresponding to quinoid rings 1694 cm^{-1} and C-N stretch at 1235 cm^{-1} did not considerably diminish. Thus, the difference in the reactivity of PNPA and POPD between copolymers and blends was evident from the FT-IR spectra. The B/Q ratio (Benzenoid C=C stretching at 1531cm^{-1} and quinoid C=N stretching at 1694 cm^{-1}) calculated for POPD was 3.00, which indicated the presence of 3:1 ratio for benzenoid and quinoid units in POPD, approximately matching the proposed structure. The FT-IR peaks at 1694 cm^{-1}, 1635 cm^{-1} and 1357 cm^{-1} corresponding to quinoid C=N stretching, quinoid C=C stretching and C-N stretching in the neighbouring quinoid rings present in POPD decreased with a decrease in the OPD/POPD weight percentage in the copolymer and blend (see **Figure 6.9.**). It indicated the decrease in the number of quinoid units in the copolymer and the blend with the decrease in the OPD/POPD content.

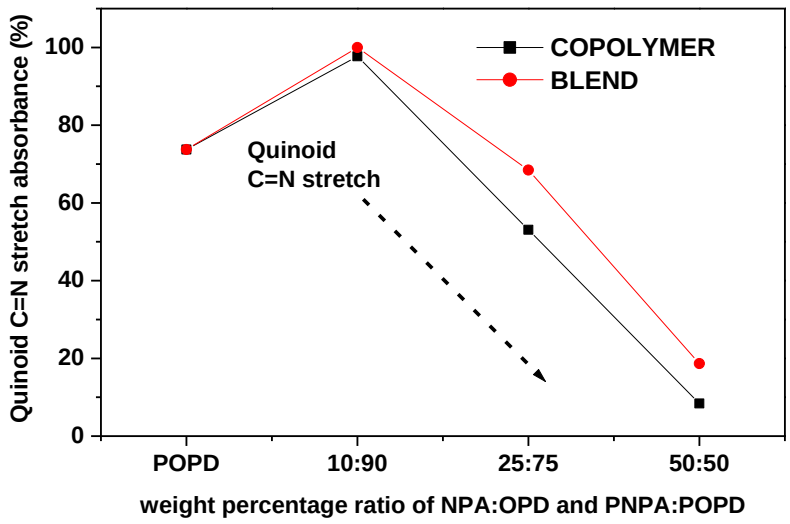

***Figure 6.9**. FT-IR absorbance percentage of quinoid C=N stretch vs. weight percentage ratio NPA: OPD or PNPA: POPD.*

The monomer reactivity ratio in the copolymer was determined using Fineman-Ross (FR) equation [29, 63-64].

$$\frac{F(f-1)}{f} = r_1\left(\frac{F^2}{f}\right) - r_2 \qquad (1)$$

Where, F = [$M_{OPD\ (feed)}$]/ [$M_{NPA\ (feed)}$], f = [m_{OPD}/m_{NPA}], and r_1 and r_2 are reactivity ratios of OPD and NPA, respectively. M_{OPD} and M_{NPA} are mole fractions of OPD and NPA in the co-monomer feed, and m_{OPD} and m_{NPA} are mole fractions of OPD and NPA in the copolymer from FT-IR spectra, respectively. The FT-IR absorption ratios between characteristic analytical bands (A_i) of 1694 cm^{-1} (C=N of OPD unit) and 1272 cm^{-1} (C-O stretching of NPA units) to the least changing absorption band of 1153 cm^{-1} (A_{1153}) as a standard band was used to determine the copolymer compositions. The mole fractions of OPD and NPA in the copolymer were determined from FT-IR peak absorbance values using the formulas

$$m_{OPD} = \frac{(\Delta A_{OPD}/MW_1)}{\left(\frac{\Delta A_{OPD}}{MW_1}\right)+\left(\frac{\Delta A_{NPA}}{MW_2}\right)} \qquad (2)$$

$$m_{NPA} = \frac{(\Delta A_{NPA}/MW_2)}{\left(\frac{\Delta A_{NPA}}{MW_2}\right)+\left(\frac{\Delta A_{OPD}}{MW_1}\right)} \qquad (3)$$

Where $\Delta A_{i=} A_i/A_{1153}$ and MW_1 and MW_2 are the molecular weight of OPD and NPA, respectively. The monomer composition in the copolymer determined from FT-IR analysis

was given in **Table 6.4.** The obtained mole ratio of OPD in the copolymer was lower than OPD taken in feed; on the other hand, NPA content increased. The monomer reactivity ratios were obtained from the Fineman-Ross plot of F(f-1)/f vs. F^2/f for OPD and NPA was determined as $r_1 = 0.241$ and $r_2 = 4.928$ (see **Figure 6.10.A.**). The determined value of r_1 (k_{11}/k_{12}) is smaller than r_2 (k_{22}/k_{21}). Thus, the monomer NPA ($r_2 = 4.918$) was more reactive towards adding its own units than adding OPD units. On the other hand, OPD ($r_1 = 0.241$) was less reactive. As a result ($r_2>1$), the copolymer tends to contain large blocks of NPA monomeric units with small blocks of OPD units in random manners [64-65]. The Fineman-Ross method was used in blends to determine how much the Fineman-Rose curve fit with homopolymer blends with the same feed ratio. Interestingly, the homopolymer blend has shown excellent linear fit with ($R^2 = 0.9998$), indicating the accuracy of the method (see **Figure 6.10.B** and **Table 6.4.**). The slight deviations in the reactivity of the copolymer from linearity was due to the high reactivity of the NPA monomer in P(NPA-co-OPD) 25:75.

Table 6.4*. Monomer/ homopolymer feed ratio, copolymer/homopolymer composition from FT-IR analysis, monomer/homopolymer ratio in the copolymer/blend, and Fineman-Ross parameters for copolymers/blends having different weight percentages of monomers/homopolymers.*

Weight percentages of monomers/ homopolymers		**Mole fractions of monomers/homopolymers in feed**		**Monomer feed ratio $F=M_{OPD}/M_{NPA}$**	**ΔA_{NPA}**	**ΔA_{OPD}**	**Copolymer/ homopolymer composition from FT-IR analysis**		**Monomer /homopolymer ratio in copolymer $f = m_{OPD}/m_{NPA}$**	**Parameters of Fineman-Ross equation**	
Copolymers											
OPD	NPA	M_{OPD}	M_{NPA}				m_{OPD}	m_{NPA}		F(f-1)/f	F^2/f
90	10	0.946	0.053	17.748	0.625	1.406	0.817	0.182	4.489	13.794	70.169
75	25	0.855	0.144	5.9101	2.00	1.070	0.489	0.505	0.968	-0.1954	36.084
50	50	0.663	0.336	1.9714	4.39	1.352	0.378	0.622	0.607	-1.2764	6.4026
25	75	0.397	0.603	0.6584	4.61	1.029	0.305	0.695	0.438	-0.8448	0.9897

Physical blends											
POPD	PNPA	M_{POPD}	M_{PNPA}				M_{POPD}	m_{PNPA}		F(f-1)/f	F^2/f
90	10	0.948	0.052	18.265	0.481	1.337	0.845	0.154	5.4870	14.94	60.728
75	25	0.858	0.141	6.0864	1.198	1.062	0.689	0.311	2.2154	3.339	16.721
50	50	0.669	0.330	2.0290	2.176	1.000	0.475	0.525	0.9048	-0.2137	4.5505
25	75	0.398	0.601	0.6622	2.283	0.448	0.279	0.721	0.3869	-1.0493	1.1339

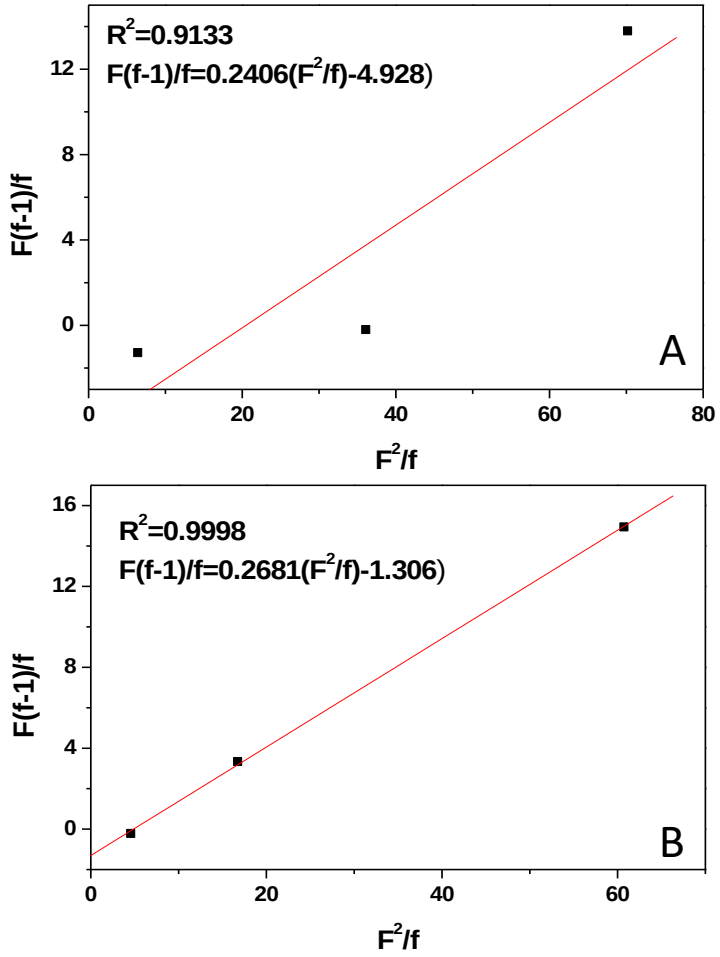

Figure 6.10. *Fineman-Ross plot of F(f-1)/f vs. F^2/f to determine A) monomer reactivity ratio in copolymers and B) reactivity ratio of homopolymers in blends.*

The powder X-ray diffraction method characterized the solid-state ordering of PNPA, POPD, and their copolymers and blends (see **Figure 6.11.A.)**. The homopolymer POPD showed sharp crystalline peaks at 2θ values 8.41, 9.31, 10.54, 18.32, 19.39, and

26.70°, whereas homopolymer PNPA showed semi-crystalline peaks at 2θ values 6.32, 11.31, 16.92, 19.54, 22.31 and 25.94° as well as some amorphous domains [66-67,46]. The XRD patterns of the copolymers P(NPA-co-OPD) 25:75, P(NPA-co-OPD) 50:50, and P(NPA-co-OPD) 75:25 have shown both the sharp peaks of homopolymers along with some additional peaks at 13.13, 20.13, and 23.31. The intensity of peaks in the XRD patterns of the copolymers varies with their co-monomer contents. The copolymer P(NPA-co-OPD) 75:25, P(NPA-co-OPD) 50:50 and P(NPA-co-OPD) 25:75 showed peaks at 2θ values 6.32, 11.31, 16.92, 19.31 and 25.94° with higher intensity than that of the homopolymer PNPA. The copolymer P(NPA-co-OPD) 10:90, which contains 10% NPA and 90% OPD in feed, showed peaks corresponding to POPD with the same intensity as that of homopolymer, whereas peaks corresponding to PNPA were very weak due to its low composition. The more reactive nature of PNPA fragments in the copolymers P(NPA-co-OPD) 25:75 and P(NPA-co-OPD) 50:50 was evident from the XRD pattern of PNPA, which appeared as sharp peaks in the copolymer. Therefore, WXRD studies showed the same trend in higher reactivity of NPA for the copolymer formation as revealed by ^{1}H NMR and FT-IR spectroscopy. WXRD profiles of physical blends have shown sharp peaks of POPD, whereas broad and weak peaks of PNPA fragments were also observed, similar to its homopolymer (see **Figure 6.11.B)**. The blend formation was not affected to increase the semi-crystallinity of PNPA peaks as seen in copolymers. Therefore, highly crystalline peaks were evident in the P(NPA-co-OPD) copolymers, indicating the possibility of block type random copolymers [80].

MALDI-TOF analysis of homopolymers POPD, PNPA, and copolymer P(NPA-co-OPD) 25:75 have been carried out using the sinapinic acid matrix to determine the molecular weight and number of repeating units present in the polymer chains (see **Figure 2.8.B**. in chapter 2 for PNPA, **Figure 5.8.A.** in chapter 5 for POPD and **Figure 6.12.A.**). The average molecular ion peaks in POPD and PNPA have m/z values of 614.97 and 832.71 amu, indicating the presence of six OPD and four NPA units in the homopolymers, respectively. In the case of copolymer P(NPA-co-OPD) 25:75, molecular ion peak was present at m/z value 1092.10 & 1242 amu, which indicated the OPD: NPA fragment ratio 2:4 and 2:5, respectively.

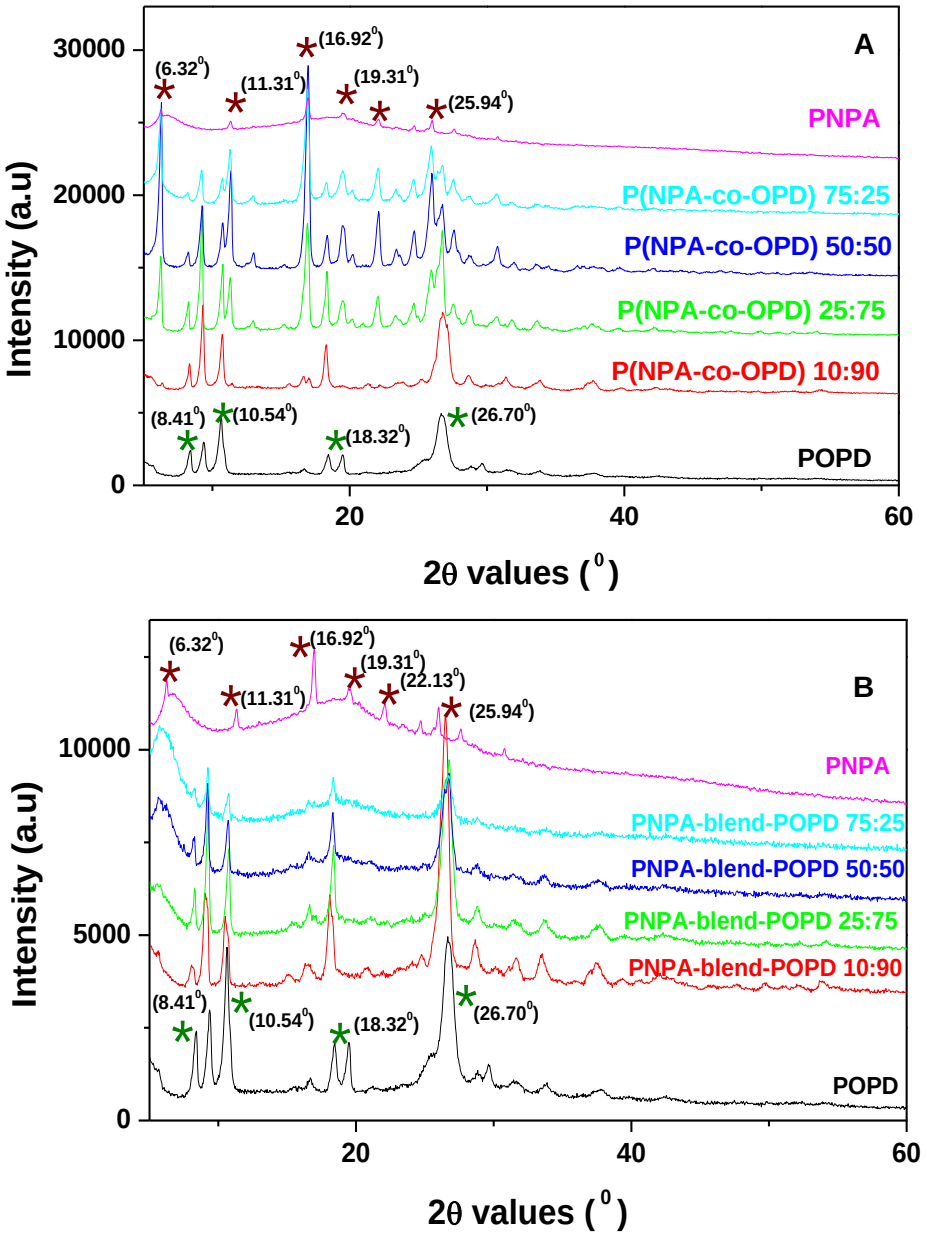

Figure 6.11. *Powder WXRD pattern of A) PNPA, P(NPA-co-OPD) 75:25, P(NPA-co-OPD) 50:50, P(NPA-co-OPD) 25:75 P(NPA-co-OPD) 10:90 and POPD B) PNPA, PNPA-blend-POPD 75:25, PNPA-blend-POPD 50:50, PNPA-blend-POPD 25:75, PNPA-blend-POPD 10:90 and POPD.*

Thermogravimetric analysis of POPD, PNPA, P(NPA-co-OPD) 25:75, and PNPA-blend-POPD 25:75 were studied, and the thermogram was given in **Figure 6.12.B.** In the case of homopolymer POPD, a 10% weight loss was observed at 298° C, and a major weight loss of up to 30% was obtained at 350°C due to the loss of low molecular weight oligomers[37]. In the case of PNPA, a 10% weight loss was observed at 230°C, and 60% degradation was

obtained up to 360°C [46]. The copolymer P(NPA-co-OPD) 25:75 had 10% weight loss at 204° C, and a sudden 45% degradation was obtained at 240° C and then a gradual degradation of 70% up to 350°C. For blend, PNPA-blend-POPD 25:75, a 10% weight loss was observed at 232°C, and then a 60% weight loss occurred up to 487°C. The homopolymer POPD and blend PNPA-blend-POPD 25:75 have more thermal stability than PNPA and copolymer P(NPA-co-OPD) 25:75.

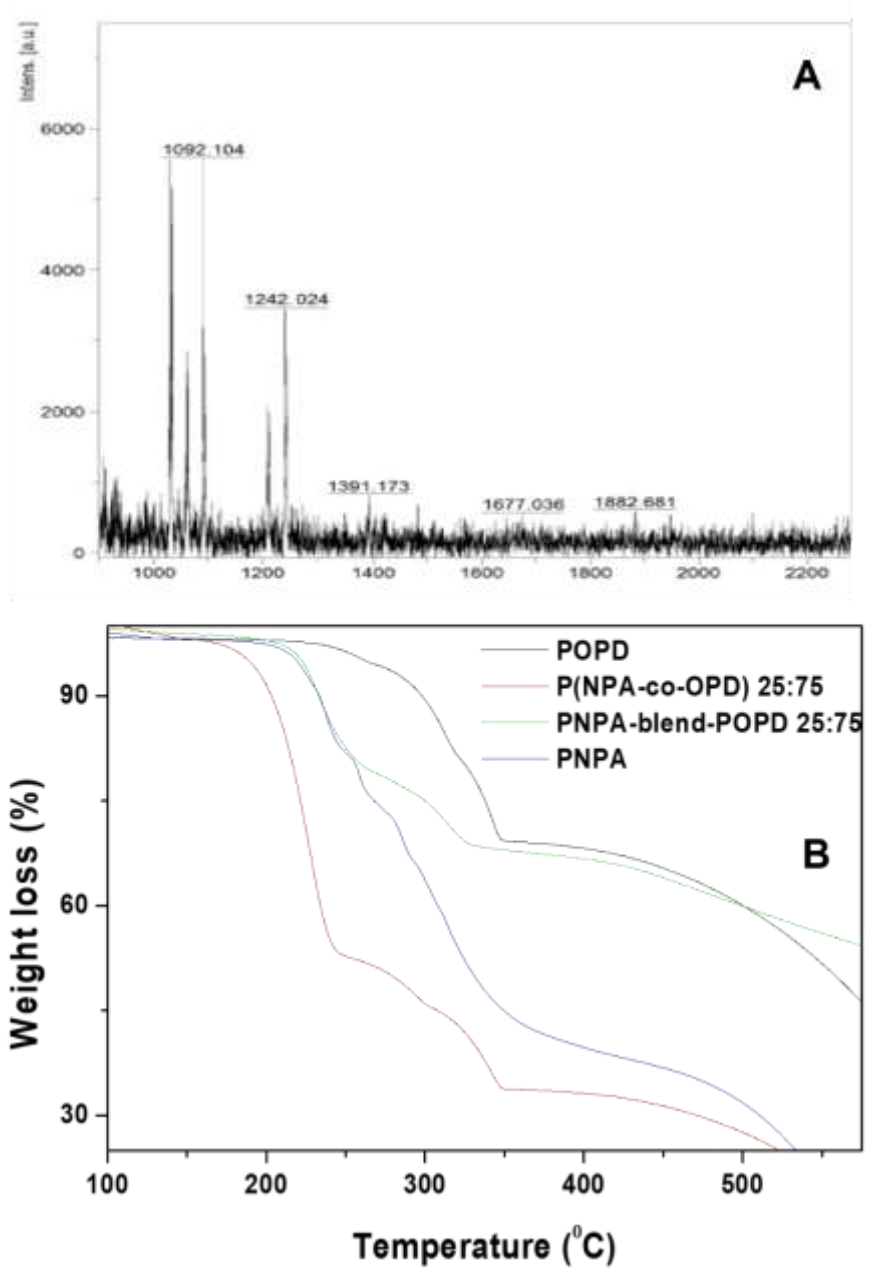

Figure 6.12. *A) MALDI-TOF spectra copolymer P(NPA-co-OPD) 25:75 and B) Thermogram of PNPA, POPD, copolymer P(NPA-co-OPD) 25:75 and blend PNPA-blend-POPD 25:75.*

Surface morphology of the homopolymers POPD, PNPA, copolymer P(NPA-co-OPD) 25:75, and blend PNPA-blend-POPD 25:75 were analyzed using field emission scanning electron microscopy (see **Figure 6.13.).** The polymer POPD has a micro rod-like morphology with a length of around 4±2 µm and a width of around 0.5±0.2 µm, which was due to the self-assembling of OPD oligomers by the formation of hydrogen bonds or due to the π to π* interactions [68-69]. PNPA has semi-microspherical morphology with an average size of 0.25 ± 0.05 µm. In the case of copolymer P(NPA-co-OPD) 25:75, most of the spheres vanished, and only a few spheres were present on a sharp-edged and well-defined block-like copolymer surface. The blend PNPA-blend-POPD 25:75 has shown a mixed morphology of micro-rods and microspheres. The FE-SEM images showed the morphological transition in homopolymers, copolymers, and physical blends.

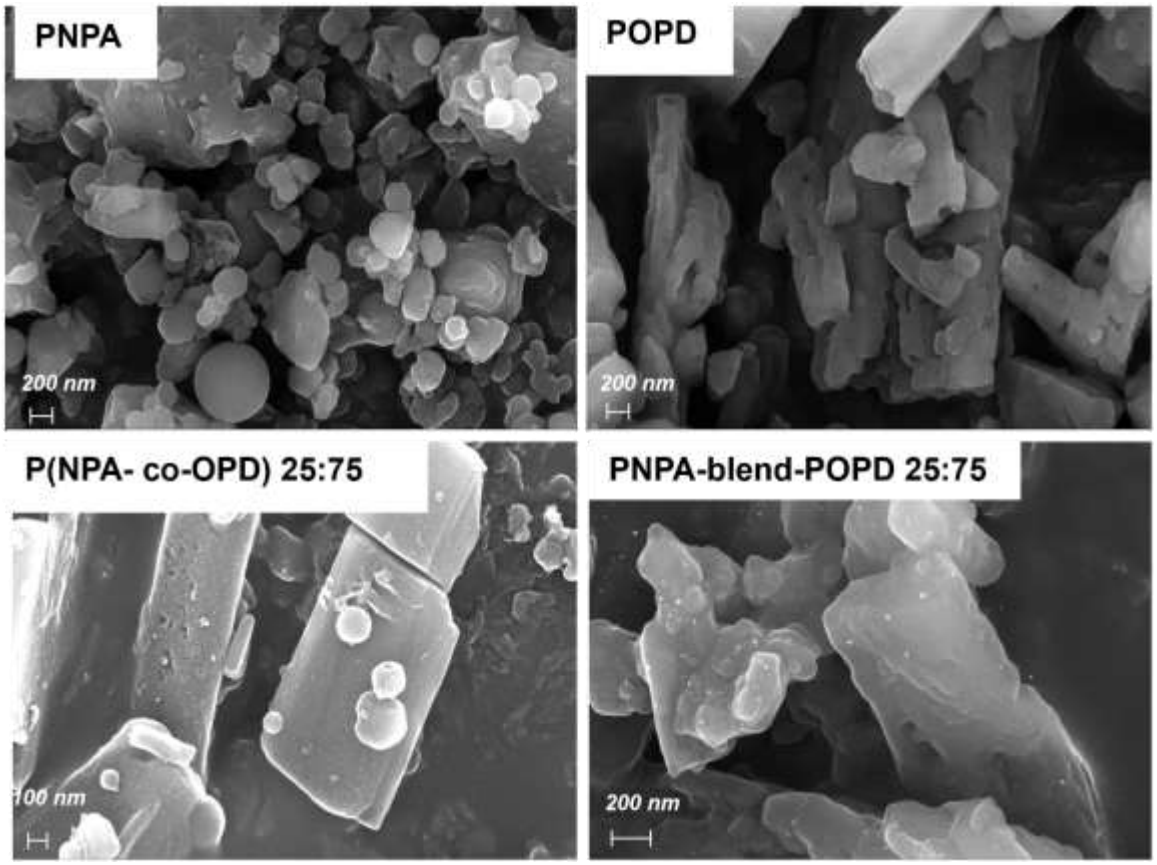

Figure 6.13. *FE-SEM images of homopolymers PNPA, POPD, and copolymers P(NPA-co-OPD) 25:75 and blend PNPA-blend-POPD 25:75.*

The enthalpy changes of the POPD, PNPA, P(NPA-co-OPD) 25:75, P(NPA-co-OPD) 50:50, and P(NPA-co-OPD) 75:25 and physical blend PNPA-blend-POPD 25:75 was recorded using differential scanning calorimeter (see **Figure 6.14.**). The polymer

POPD showed a broad melting peak at 111.51˚C with ΔH of 411.4 J/g, indicated crystalline nature of POPD. The absence of melting peak in PNPA indicated their amorphous nature [62]. In the case of copolymer P(NPA-co-OPD) 25:75, two melting peaks were observed. The peak at 103.65˚C with ΔH of 163.4 J/g indicated the melting of POPD fragments, whereas the peak at 184.5˚C with ΔH of 37.43 J/g indicated the melting of PNPA fragments. Similarly, the copolymer P(NPA-co-OPD) 50:50 showed two melting peaks at 106.81˚C and 190.33˚C, corresponding to the melting of POPD and PNPA fragments respectively. In the case of P(NPA-co-OPD) 75:25, the melting peak of PNPA fragments was observed at 186.86˚C with ΔH of 75.35 J/g. However, the melting peak corresponding to POPD fragments was observed as weak multiplet indicating the random orientation of POPD blocks in the copolymer. The physical blend of PNPA-blend-POPD 25:75 showed only one broad melting peak at 93.94˚C with ΔH of 266.8 J/mol, corresponding to the melting of POPD fragment. The presence of sharp melting peaks of PNPA fragments existed only in the copolymer indicated crystallinity development via random blocks. The temperature shift associated with the melting peaks in the copolymer indicated the structural changes within copolymer. The DSC thermogram is also in agreement with the crystalline nature of copolymers as revealed by powder XRD.

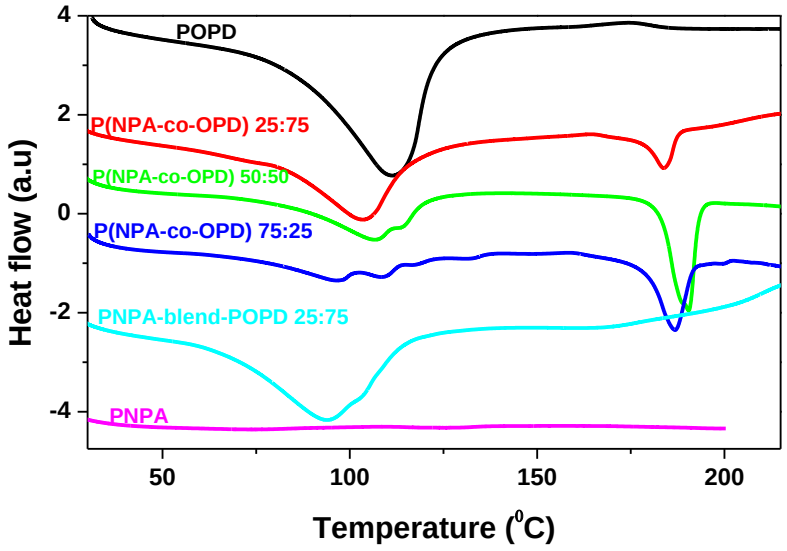

Figure 6.14. *DSC thermograms of homopolymers PNPA, POPD, and copolymers P(NPA-co-OPD) 25:75, P(NPA-co-OPD) 50:50, P(NPA-co-OPD) 75:25 and blend PNPA-blend-POPD 25:75.*

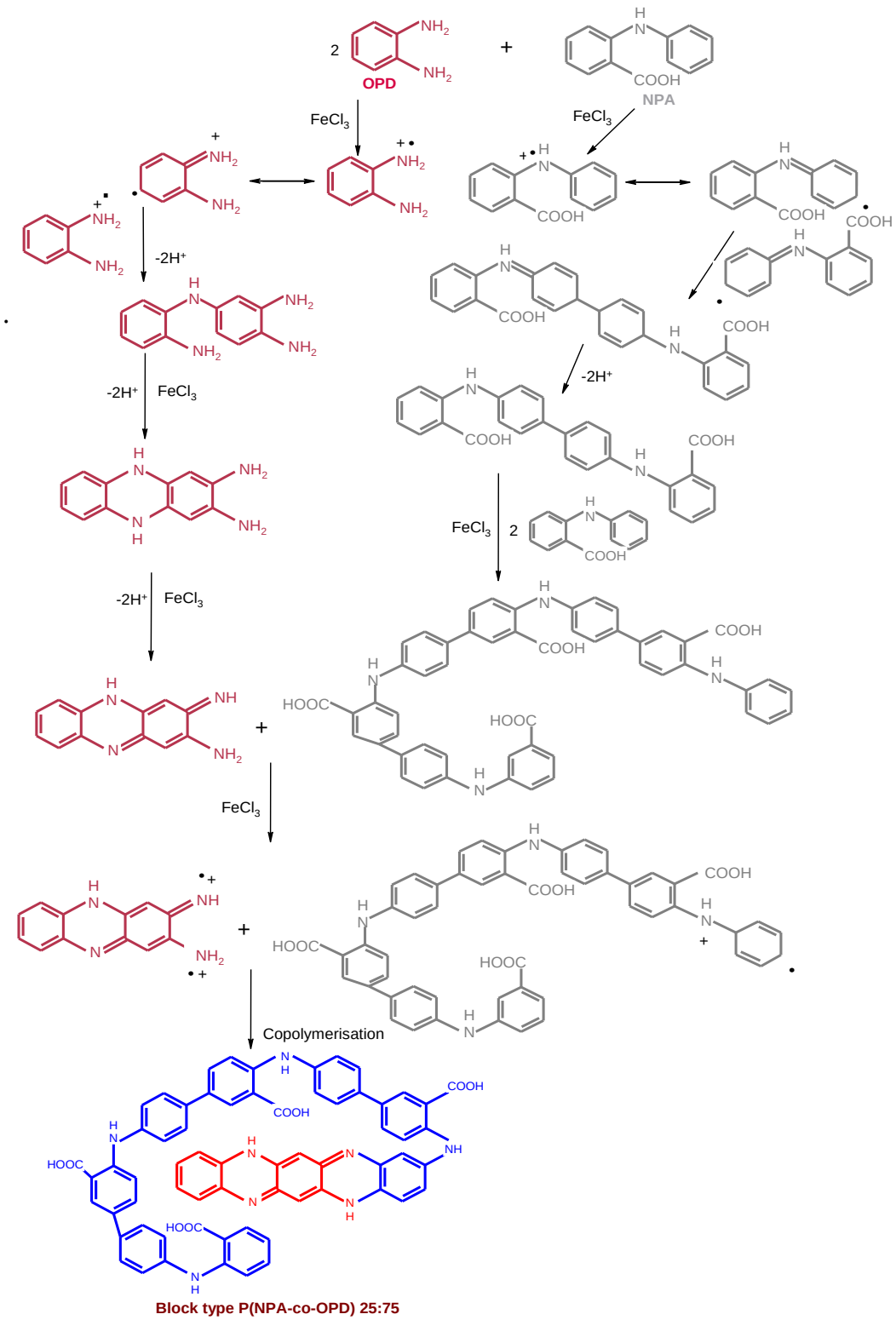

Figure 6.15. *Possible mechanism of copolymer P(NPA-co-OPD) 25:75 formation.*

The possible mechanism of the formation of copolymers P(NPA-co-OPD) 25:75 is given in **Figure 6.15.** The previous works of poly-o-phenylenediamine copolymers reported the formation of POPD blocks due to the higher reactivity of OPD compared to

other co-monomers [29, 32, 70]. However, in the copolymer of OPD and NPA, the monomer reactivity ratios indicated higher NPA reactivity than OPD. Here o-phenylenediamine and N-phenyl anthranilic acid were oxidized to form corresponding cation radicals [71]. Thus, four NPA cation radicals polymerize together to form a tetramer through C-C bond formation similar to polydiphenylamines and, and a dimer of OPD was linked to the tetramer of NPA using two C-N bonds [72]. The presence of multiplets in ^{1}H NMR spectra of copolymer P(NPA-co-OPD) 25:75 with equal intensity as that of the PNPA and the increase in the solid-state ordering of copolymer in XRD suggested the formation of block-type copolymer with the proposed structure. The solid-state ordering of PNPA was improved through copolymerization with POPD, however later has a rigid structure with good crystallinity.

6.3.3. pH dependent emission tuning in copolymers and blends

The UV-visible absorption and fluorescence emission of homopolymers at different pH were studied by recording their UV-visible absorption spectra and fluorescence spectra (see **Figure 6.16.**). The PNPA solution at acidic, neutral, and basic pH has shown two absorption maxima (see **Figure 6.16.A**). The absorption maximum at 252 nm was due to the π to π* transition and a broad absorption maximum at 398 nm was due to the extended π to π* transition [39]. The homopolymer POPD has shown two absorption maxima at acidic pH (pH=0.1) (see **Figure 6.16.B**). The absorption at 259 nm was due to the π to π* transition and absorption at 495 nm was due to the extended π to π* transition associated with extended conjugation of chromophoric rings, respectively[32]. The absorption corresponding to the extended π to π* transition of POPD solution has shown a blue shift to 454 nm at pH 2.7 with a change in color from dark brown to orange[73]. At neutral and basic pH, the absorption peak undergoes a further blue shift to 419 nm with a change in color from orange to yellow[74]. Fluorescence spectra of PNPA and POPD at different pH have been carried out to study the effect of pH on fluorescence intensity (see **Figures 6.16.B** and **6.16.D**). PNPA has the highest fluorescence intensity at a highly acidic pH (pH=0.1) than neutral and basic pH. The photographs of POPD and PNPA solutions in visible light and UV light were shown in the inset, corresponding to the absorption/fluorescence spectra. In the case of PNPA, the fluorescence maximum at 460 nm was responsible for its bluish-white emission in acidic pH (**see Figure 6.16.C**). The fluorescence maximum was blue shifted to 445 nm on increasing pH to 2, 7, and 10. POPD has no fluorescence at acidic pH, but yellow fluorescence with a fluorescence maximum at

550 nm was observed at neutral and basic pH. The peak at 550 nm in the fluorescence spectra of POPD was attributed to the S_1 to S_0 transition [32].

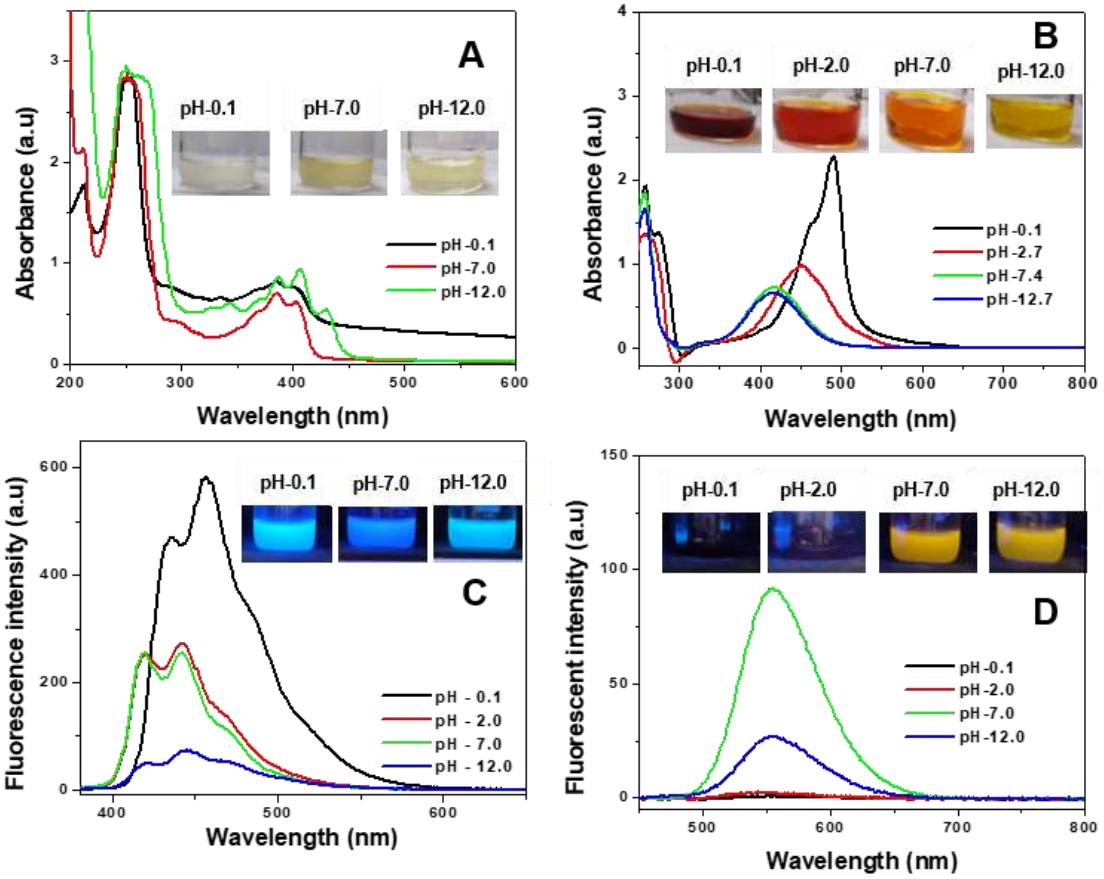

Figure 6.16. *UV-visible absorption spectra of A) PNPA, B) POPD, and fluorescence spectra of C) PNPA and D) POPD at different pH.*

The UV-visible absorption spectra of blend PNPA-blend-POPD 25:75 and copolymer P(NPA-co-OPD) 25:75 at different pH were given in **Figure 6.17.A and 6.17.B.** The absorption peak at 490 nm at acidic pH was blue-shifted to 450 nm at pH 2.5 and then shifted to 420 nm at neutral and basic pH. Therefore, the dark brown colored solutions of both the copolymer and blend were changed to orange at neutral pH and yellow at basic pH. A blue shift in the absorption of the copolymer and blend solutions was obtained, similar to POPD with increased pH. The absorbance of PNPA at 398 nm was merged with the absorbance of POPD at 420 nm. The fluorescence spectra of the blend PNPA-blend-POPD 25:75 at different pH have been recorded (**Figure 6.18.B.)**. At acidic pH (pH = 0.1 and 2.0), the fluorescence intensity corresponding to the PNPA was present at 425 nm, whereas the peak corresponding to the fluorescence of POPD at 550 nm appeared weak. A strong vibronic emission peak at 470 nm with shoulder overlap on both PNPA and POPD

emission has appeared in neutral and basic pH. The maximum overlap in the fluorescence intensity was observed in basic pH at 470 nm. An effective spectral overlap between PNPA and POPD at neutral and basic pH could lead to energy transfer and thus enhanced emission intensity.

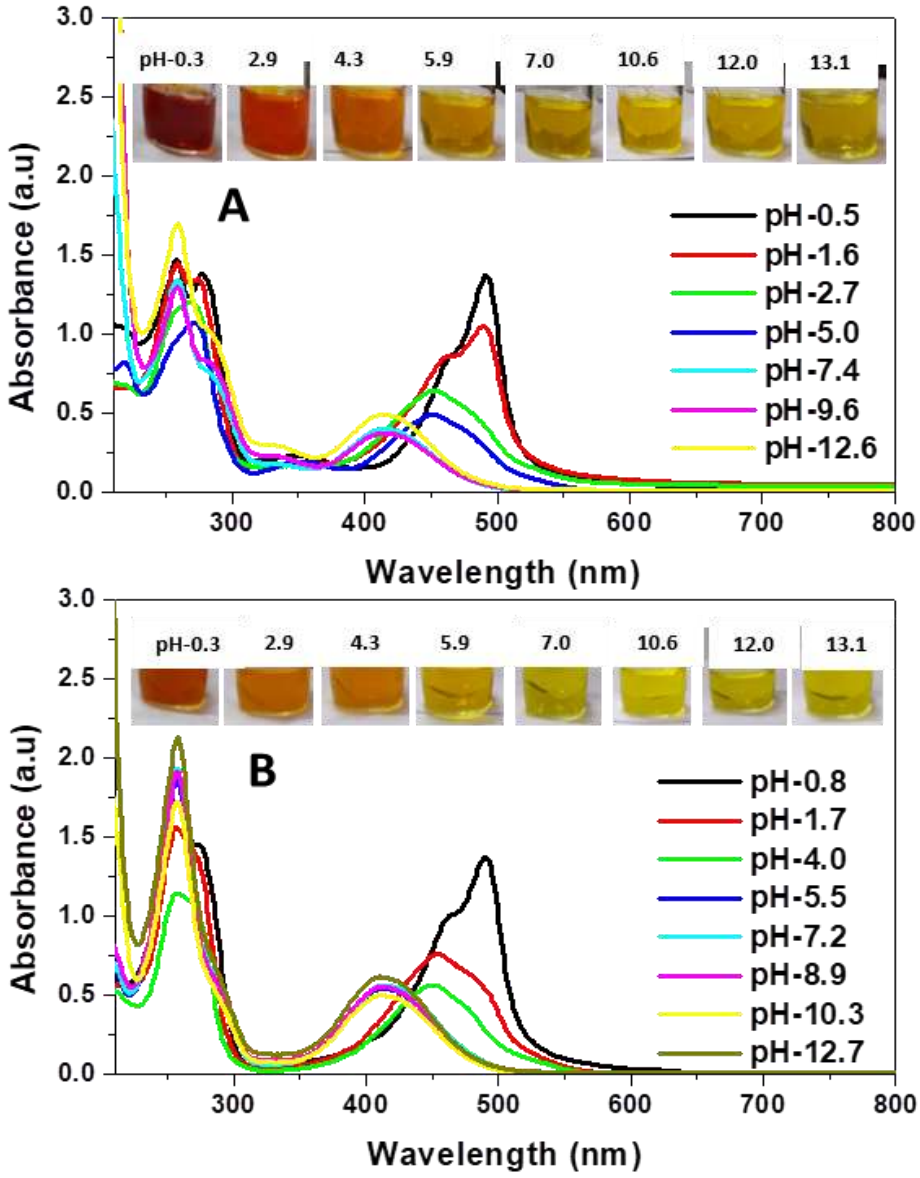

Figure 6.17. *UV-Visible absorption spectra of A) copolymer P(NPA-co-OPD) 25:75 and B) blend PNPA-blend-POPD 25:75 at different pH.*

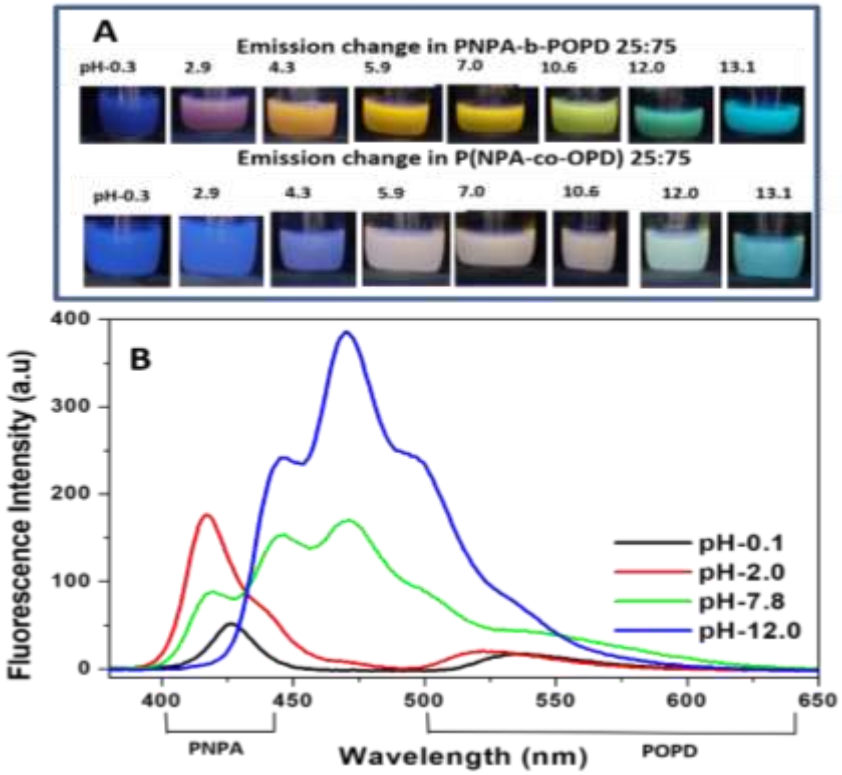

***Figure 6.18**. A) The photographs of P(NPA-co-OPD) 25:75 and PNPA-blend-POPD 25:75 solutions in UV light at different pH and B) fluorescence spectra of blend PNPA-blend-POPD 25:75.*

The fluorescence of PNPA-blend-POPD 25:75 was checked in UV inspection cabinet (see **Figure 6.18.A**). PNPA homopolymer solution has intense bluish fluorescence remains at all pH (acidic, neutral, and basic). The POPD polymer solution has yellow emission in neutral and basic pH. The blend PNPA-blend-POPD 25:75 have produced tuning in emission colors in UV light with a change in pH. In PNPA-blend-POPD 25:75, blue fluorescence of PNPA was produced at an acidic pH (pH = 0.3) because the fluorescence quenching of POPD occurs at acidic pH. As pH increased to 2.9, a combination of blue emission of PNPA and weak orange emission of POPD produces a violet emission in the blend at pH 2.3. The yellow emission of POPD was intensified at neutral pH, dominating the yellow emission of POPD in the blend by masking the emission of PNPA. At pH-10.6, both the yellow emission of POPD and the blue emission of PNPA became active, and a green emission was produced in the blend as the combination of yellow and blue emissions. At basic pH (pH >12), the blend has the cyan emission of PNPA due to the weak yellow emission of POPD above pH-12. The homopolymers PNPA and POPD polymer were involved in the emission tuning of blend PNPA-blend-POPD 25:75 with pH. The pH-

dependent fluorescence of POPD can control the emissions of blend into blue, violet, yellow, green, and cyan with a change in pH. The copolymers of N-phenyl anthranilic acid and o-phenylenediamine were synthesised to fine tune the emission characteristics. But the copolymer P(NPA-co-OPD) 25:75 has less emission tuning due to predominant blue emission from the PNPA fragment at acidic, neutral, and basic pH (see **Figure 6.16.A).** The yellow emission of POPD was not visible at neutral pH due to the combination of blue and yellow emissions. The predominant blue emission in the copolymer P(NPA-co-OPD) 25:75 indicates the higher reactivity of NPA fragments than OPD fragments in the copolymer formation. The pH-dependent absorptions and emissions of blend PNPA-blend-POPD 25:75 was reversible. Therefore, PNPA-blend-POPD may find several applications in pH sensors and fluorescent indicators. The pH dependent changes in the emission of copolymers P(NPA-co-OPD) 10:90, and P(NPA-co-OPD) 50:50 and blends PNPA-blend-POPD 10:90, and PNPA-blend-POPD 50:50 was given in **Figure 6.19.** For P(NPA-co-OPD) 10:90 emission at acidic pH was a weak blue due to the presence of very small PNPA content in the copolymer and yellow emission of POPD were dominated at neutral and basic pH. For P(NPA-co-OPD) 50:50 and PNPA-blend-POPD 50:50, the emission of POPD was completely hidden by the bright bluish white emission of PNPA.

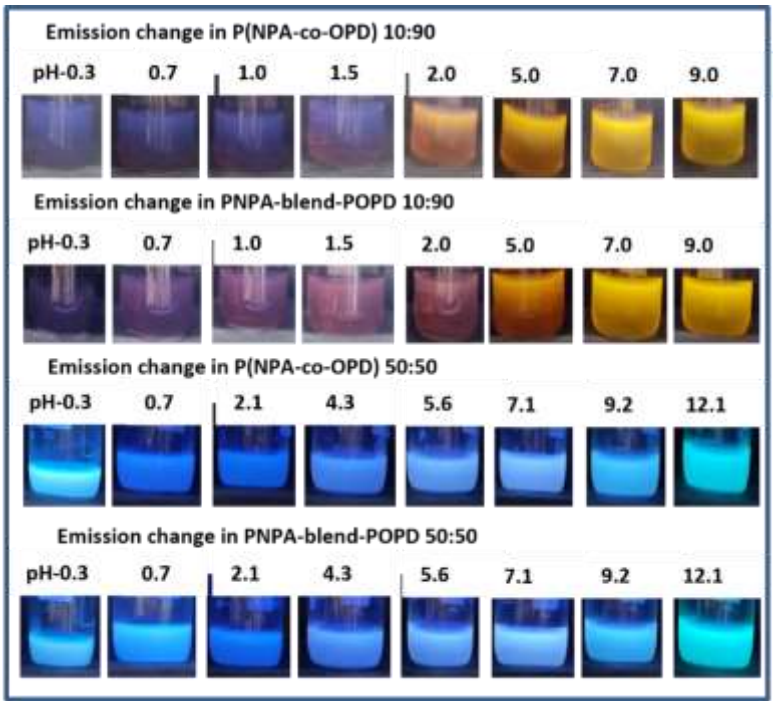

Figure 6.19. *Photographs of copolymer solutions P(NPA-co-OPD) 10:90, P(NPA-co-OPD) 50:50 and blend solutions PNPA-blend-POPD 10:90, PNPA-blend-POPD 50:50 at different pH in UV light.*

6.3.4. Fluorescent sensing of oxidizing analytes

Conjugated polymers on oxidation/reduction in the presence of suitable redox reagents change optical and electrical properties via changing the redox state and band gap. Silver nitrate is a moderately strong oxidizing agent with a standard reduction potential of 0.80 V [75]. The silver nitrate oxidizes POPD, resulting in the quenching of yellow emission. Silver nitrate did not oxidize PNPA, so the blue emission of PNPA remains unchanged. The potassium permanganate is a strong oxidizing agent in an acid medium with a standard reduction potential of 1.51 V for MnO_4^-/Mn^{2+} [75]. Therefore, $KMnO_4$ oxidizes PNPA, resulting in the quenching of bluish emission[39]. $KMnO_4$ can oxidize both POPD for complete quenching of the yellow emission of POPD (see **Figure 6.20.**) and PNPA-H for complete quenching of blue emission (see **Figure 2.15A**).

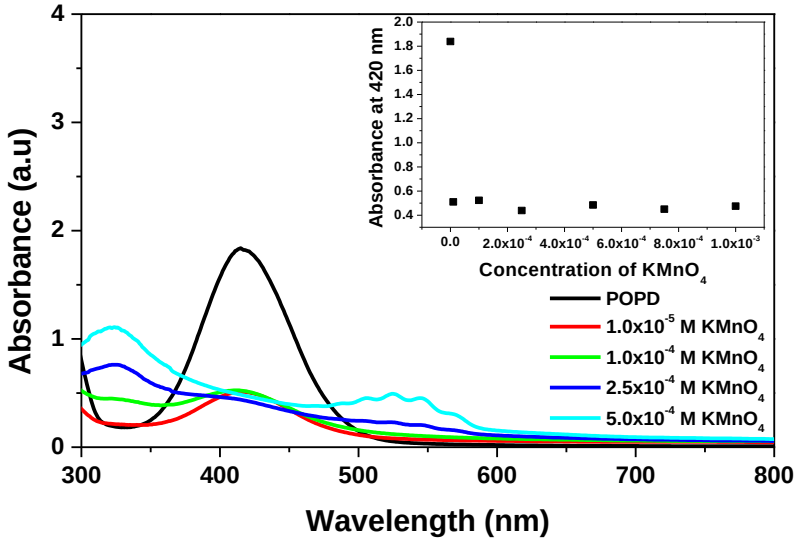

Figure 6.20. *UV-Visible absorption spectra of POPD on adding different $KMnO_4$ concentrations (1×10^{-5} M, 1×10^{-4} M, 2.5×10^{-4} M, and 5.0×10^{-4} M). The plot of absorbance at 420 nm of POPD vs concentrations of $KMnO_4$ in the inset.*

The effect of oxidizing power of analyte on the emission of copolymer P(NPA-co-OPD) 10:90 was systematically studied using $AgNO_3$ and $KMnO_4$ as selective analytes. The copolymer solution has yellow emission at neutral pH, to which aqueous $AgNO_3$ with different concentrations of 1.0×10^{-4} M, 2.5×10^{-4} M, 5.0×10^{-4} M, 1.0×10^{-3} M, and 5.0×10^{-3} M were added. The yellow emission of POPD fragments was weakened on adding 1.0×10^{-4} M and 2.5×10^{-4} M $AgNO_3$ solutions and completely quenched on adding 5×10^{-4} M $AgNO_3$ solutions (see **Figure 6.21.A.)**. Thus, the yellow emission of the copolymer

disappeared on adding $AgNO_3$ due to the oxidation of POPD fragments, whereas the blue emission of PNPA fragments persists. Therefore, a resultant change in the emission from yellow to blue was observed in the copolymer P(NPA-co-OPD) 10:90. The strong oxidizing agent $KMnO_4$ was added to the semi-oxidized copolymer solution for complete oxidation. The oxidation by $KMnO_4$ was most effective in the acidic medium; therefore, acidified $KMnO_4$ with a concentration of 5×10^{-4} M was added to the copolymer solutions. After semi oxidation of copolymer with 1.0×10^{-4} M $AgNO_3$ or 2.5×10^{-4} M $AgNO_3$, the remaining blue emission of copolymer solutions was completely quenched by adding acidified $KMnO_4$ (see **Figure 6.21.A.**). The color change of the copolymer solution after adding $AgNO_3$ and $KMnO_4$ were given in **Figure 6.21.B.** Orange colored P(NPA-co-OPD) 10:90 at neutral pH changed to yellow color on oxidation with $AgNO_3$ and on further oxidation with acidified $KMnO_4$ changes to colorless Thus an analyte-selective fluorescence sensing was observed in P(NPA-co-OPD) 10:90 with $AgNO_3$ and $KMnO_4$. The blend were also suitable for analyte-selective fluorescence sensing, but their applications were mainly focused on emission tuning due to their ability to produce different emission colours with pH.

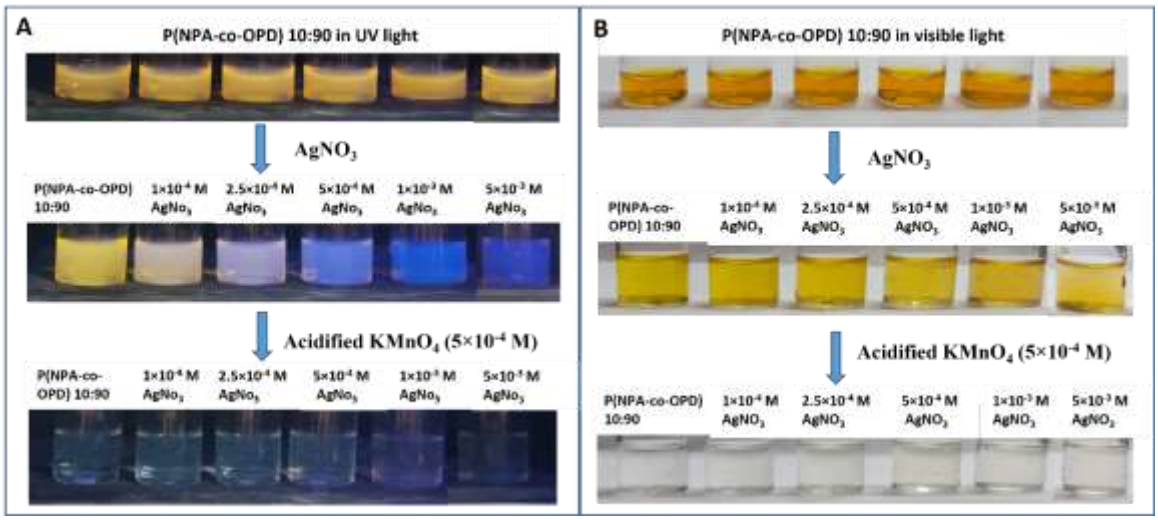

Figure 6.21. *Photographs showing changes in A) the emission in UV light and B) colour in visible light of P(NPA-co-OPD) 10:90 on adding $AgNO_3$ followed by acidified $KMnO_4$.*

The UV-visible absorption spectra of copolymer P(NPA-co-OPD) 10:90 on adding different concentrations of $AgNO_3$ and corresponding photographs were given in **Figure 6.22.A**. The copolymer has two absorption maxima at 250 nm and 420 nm, which correspond to π to π* and extended π to π* transitions, respectively, similar to peaks obtained for POPD at pH 7. The absorbance at 250 nm and 420 nm in the copolymer was decreased with an increase in concentrations of $AgNO_3$ from 1×10^{-4} M to 1×10^{-2} M.

Fluorescence spectra of the copolymer P(NPA-co-OPD) 10:90 on adding different concentrations of $AgNO_3$ were given in **Figure 6.22.B**. The fluorescence intensity at 445 nm, corresponding to the emission of PNPA, was enhanced, and the fluorescence intensity at 550 nm, corresponding to the emission of POPD, was reduced simultaneously with an increase in the concentration of $AgNO_3$, which indicated the oxidation of POPD fragment (see **Figure 6.23.**)[76]. The reduction in the fluorescence intensity at 550 nm resulted in the quenching of yellow emission in the UV light (see inset of **Figure 6.22.B**). The fluorescence intensity of PNPA at 445 nm has enhanced with the fluorescence quenching of POPD fragment on adding $AgNO_3$.The fluorescence spectra provided evidence for the change in emission exhibited by the copolymer from yellow to blue on its partial oxidation using $AgNO_3$.

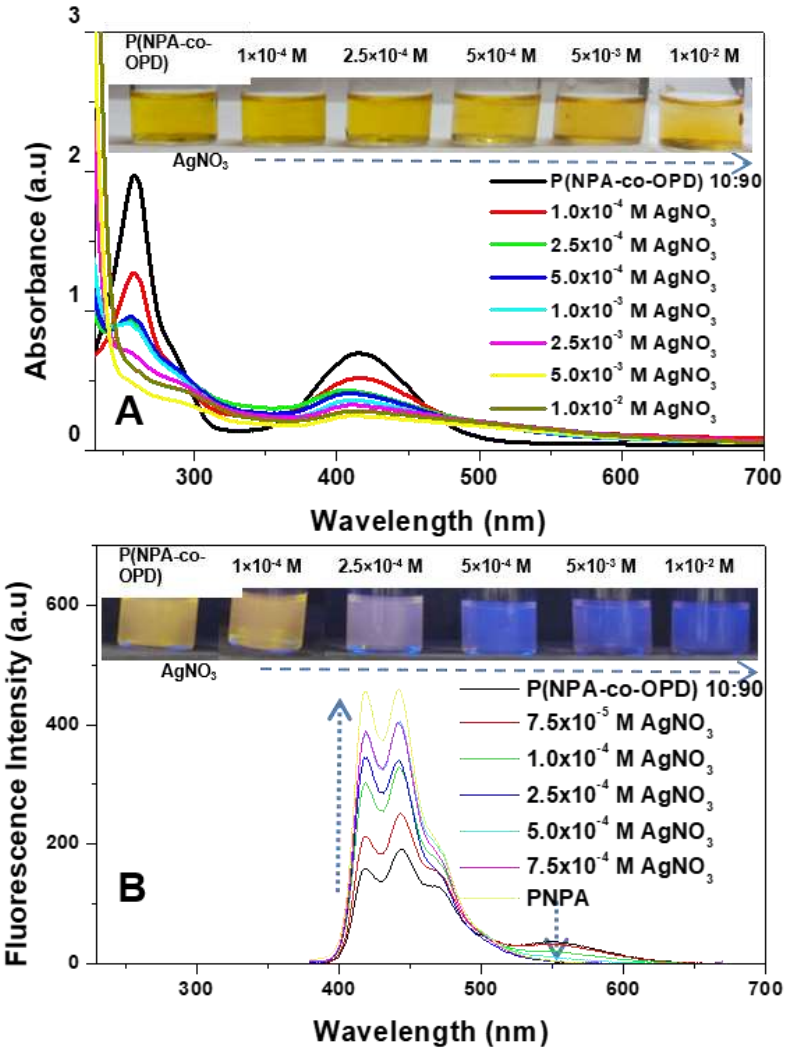

Figure 6.22*. A) UV-visible absorption spectra of copolymer P(NPA-co-OPD) 10:90 and B) fluorescence spectra of copolymer P(NPA-co-OPD) 10:90 on adding different*

concentrations of $AgNO_3$ at neutral pH. (Inset: photographs of copolymer solution on adding $AgNO_3$ in visible light and UV light).

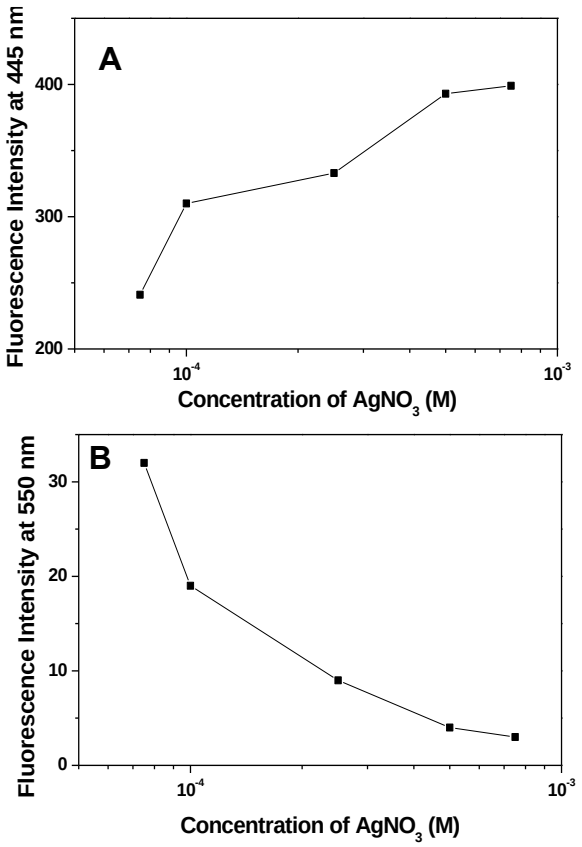

Figure 6.23. *A) Change in fluorescence intensity A) at 445 nm and B) at 550 nm in copolymer P(NPA-co-OPD) 10:90 on adding different concentrations of $AgNO_3$.*

The UV-visible absorption spectra of semi-oxidized copolymer P(NPA-co-OPD) 10:90 (semi-oxidized with $AgNO_3$) on adding acidified $KMnO_4$ (5×10^{-4} M) were given in **Figure 6.24.A** The absorbance around 420 nm corresponding to copolymer disappeared completely. The two new absorption peaks with weak absorbance appeared in the spectra at 230 nm and 320 nm, corresponding to slight excess $KMnO_4$ [77]. As a result, the yellow-colored copolymer solution became colorless on complete oxidation. The evidence for the complete quenching of fluorescence in semi-oxidized P(NPA-co-OPD) 10:90 was obtained from the changes in the emission spectra on adding acidified $KMnO_4$ having a concentration 5×10^{-4} M (see **Figure 6.24.B.)** The fluorescence intensity of the semi-oxidized copolymer at 445 nm corresponding to POPD fragment disappeared on adding $AgNO_3$ alone. Complete quenching of the emission peaks at 445 nm and 550 nm, corresponding to PNPA and POPD fragments, confirm the complete oxidation of the

copolymer in the presence of acidified $KMnO_4$. Furthermore, the effect of different concentrations of acidified $KMnO_4$ (2.5×10^{-4} M and 5×10^{-4} M) on fluorescence intensity of copolymer P(NPA-co-OPD) 10:90 and PNPA at neutral pH was given in **Figure 6.25.**

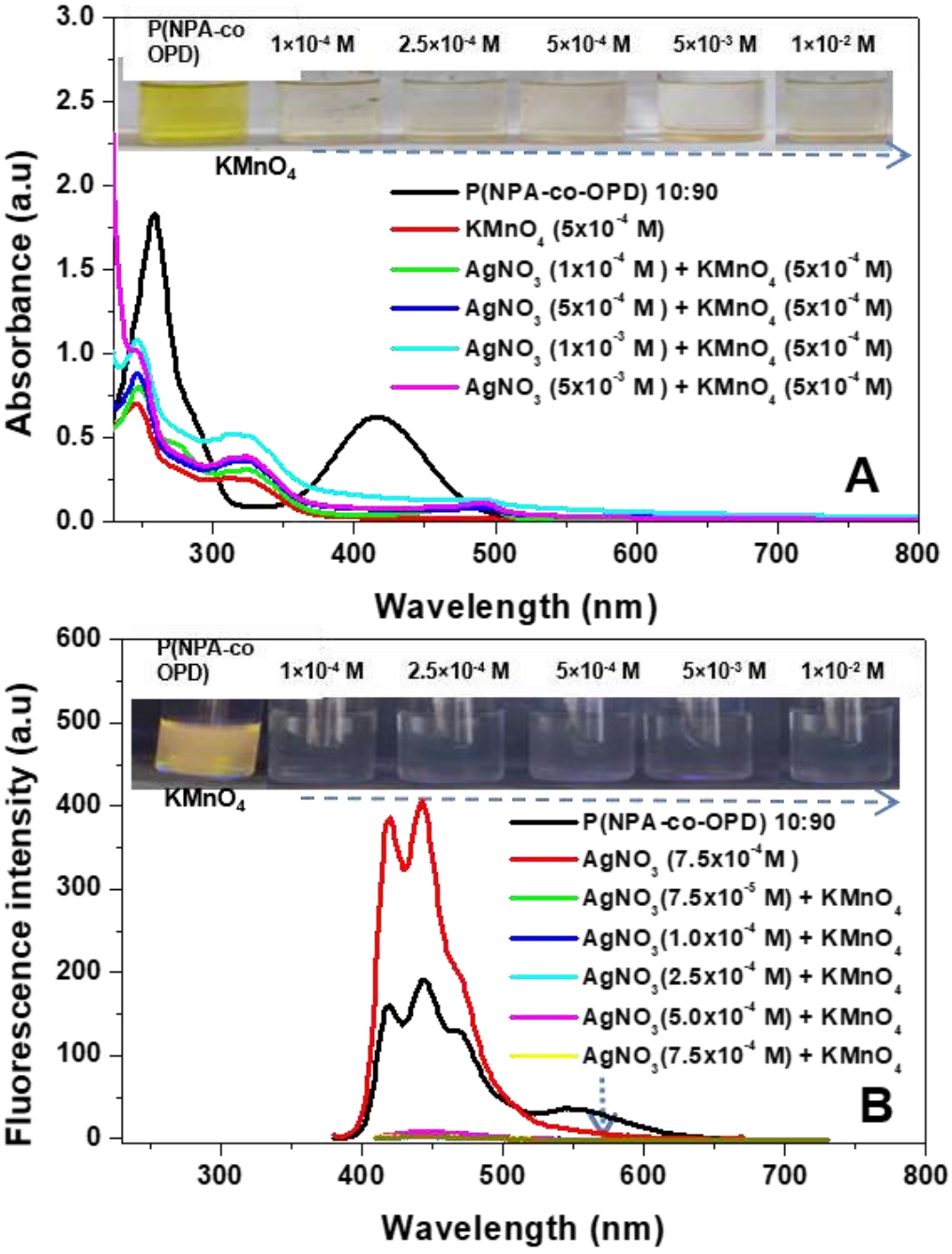

Figure 6.24*. A) UV-visible absorption spectra of copolymer P(NPA-co-OPD) 10:90 and B) fluorescence spectra of copolymer P(NPA-co-OPD) 10:90 on adding different concentrations of $AgNO_3$ and fixed concentration of 5×10^{-4} M acidified $KMnO_4$ (Inset:*

photographs of copolymer solution on adding $AgNO_3$ followed by 5×10^{-4} M acidified $KMnO_4$ in visible light and UV light).

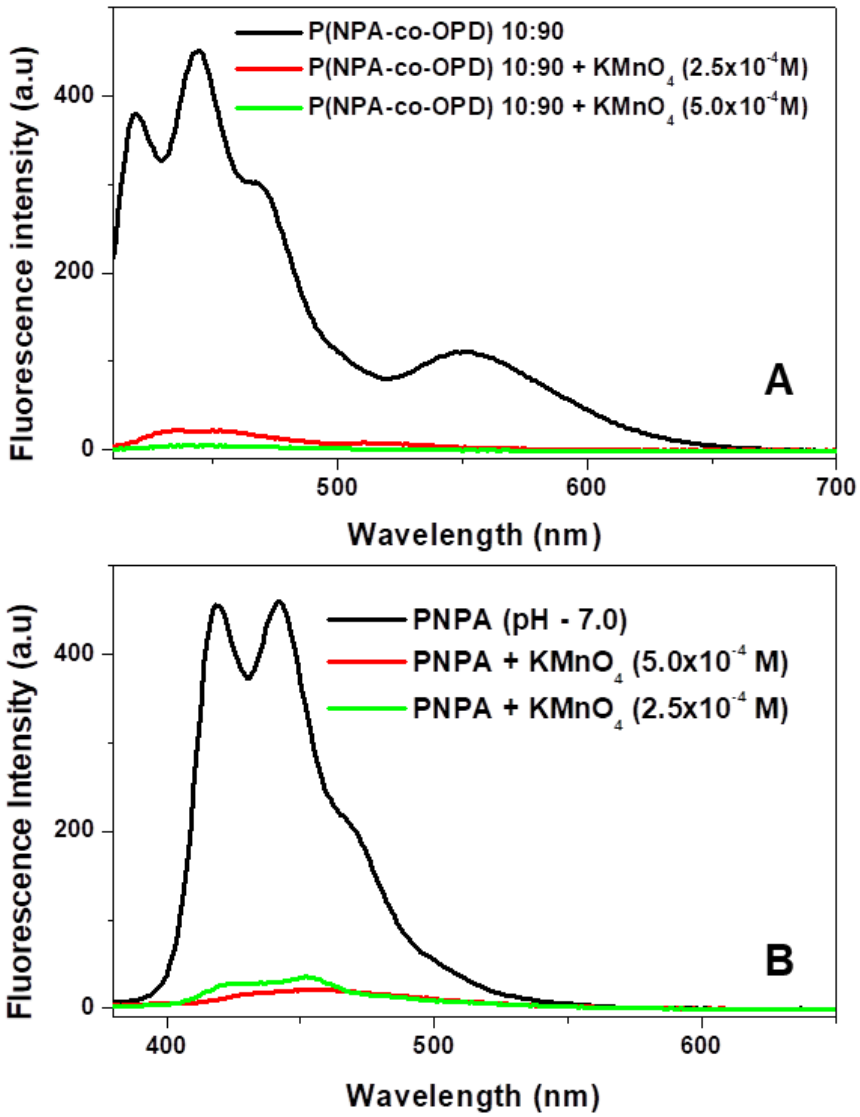

Figure 6.25. *Fluorescence spectra of A) copolymer P(NPA-co-OPD) 10:90 and B) PNPA on adding acidified $KMnO_4$ having concentrations 2.5×10^{-4} M and 5.0×10^{-4} M.*

The fluorescence properties of two pure homopolymers and emission tuning in copolymers and blends have been carried out in the present studies. Fluorescence control in materials is a major interest for light-emitting devices, fluorescence biomarkers, and so on [78]. Alterations in emission colors were usually required in artificial structures like microcavities, photonic crystals, and modifications in quantum dots [79]. Here, the simple physical blending of fluorescent homopolymers PNPA and POPD was produced, which have been used in emission control. The copolymer P(NPA-co-OPD) 10:90 showed a redox

selective fluorescence change from yellow to blue on adding $AgNO_3$ and blue to colorless on adding $KMnO_4$, depending on the oxidation power of analytes. In short, the studies on the fluorescence emission of copolymers and physical blends of PNPA and POPD provide insight into oxidative power-controlled analyte selective oxidation and pH-dependent emission tuning.

6.4. Conclusion

Copolymers of N-phenyl anthranilic acid and o-phenylenediamine were synthesized by oxidative chemical polymerization using $FeCl_3$ as an oxidizing agent by changing the co-monomer weight percentage. Physical blends of poly-N-phenyl anthranilic acid and poly-o-phenylenediamine were prepared by mixing the different weight percentages of homopolymers using a mortar and pestle. ^{1}H NMR and FT-IR spectra of copolymers indicated the possibility of block-type copolymerization and also showed comparatively high reactivity of PNPA fragments in the copolymer P(NPA-co-OPD) 25:75. Additional vibrations corresponding to C-N stretching and C-H bending in the FT-IR spectra and additional peaks in the powder XRD of copolymer confirmed the structural difference between copolymers and blends. The presence of crystalline peaks in the x-ray diffractogram of copolymers indicated blocks in copolymers. A combined morphology of micro rods of POPD and microspheres of PNPA was obtained in the FE-SEM images of the physical blend, whereas few microspheres were present on the sharp-edged microblocks in the copolymer. MALDI-TOF analysis of copolymer PNPA-co-POPD 25:75 indicated the presence of 4-5 NPA fragments and 2 OPD fragments in the copolymer. Thermogravimetric analysis revealed high thermal stability of POPD and PNPA-blend-POPD. The pH-dependent UV-visible absorption spectra of copolymer PNPA-co-POPD 25:75 and blend PNPA-blend-POPD 25:75 showed the merging of absorptions of PNPA with POPD. Mixing of PNPA and POPD in blend PNPA-blend-POPD 25:75 produced different emission color combinations at different pH. In contrast, predominant blue emission of PNPA fragments was observed in copolymer P(NPA-co-OPD) 25:75. Fluorescent sensing was achieved by analyte selective oxidation in copolymer P(NPA-co-OPD) 10:90 with oxidizing agents $AgNO_3$ and acidified $KMnO_4$. An emission change of yellow to blue was obtained due to the partial oxidation of POPD fragments in the copolymer by $AgNO_3$, and the blue emission was quenched entirely due to the complete oxidation of both POPD and PNPA fragments by acidified $KMnO_4$. An oxidative power

selective fluorescence sensing of analytes using a block-type copolymer P(NPA-co-OPD) was developed and pH-controlled attractive emission tuning was achieved using blends P(NPA-blend-OPD).

Reference

1. Ansari, S. P., & Ali, F. (2018). *Conjugated Organic Polymers for Optoelectronic Devices* (pp. 1–40). https://doi.org/10.1007/978-3-319-92067-2_21-1.
2. Lin, H., Bai, H., Yang, Z., Shen, Q., Li, M., Huang, Y., Lv, F., & Wang, S. (2022). Conjugated polymers for biomedical applications. *Chemical Communications*, *58*(52), 7232–7244. https://doi.org/10.1039/D2CC02177C.
3. Beaumont, C., Naqvi, S., & Leclerc, M. (2022). Strategies for the synthesis of water-soluble conjugated polymers. *Trends in Chemistry*, *4*(8), 714–725. https://doi.org/10.1016/j.trechm.2022.05.002.
4. Jadoun, S., Rathore, D. S., Riaz, U., & Chauhan, N. P. S. (2021). Tailoring of conducting polymers via copolymerization – A review. *European Polymer Journal*, *155*, 110561. https://doi.org/10.1016/j.eurpolymj.2021.110561.
5. Li, X.-G., Huang, M.-R., & Yang, Y. (2001). Synthesis and characterization of o-phenylenediamine and xylidine copolymers. *Polymer*, *42*(9), 4099–4107. https://doi.org/10.1016/S0032-3861(00)00661-3.
6. Khokhar, D., Jadoun, S., Arif, R., Jabin, S., & Budhiraja, V. (2021). Copolymerization of o-phenylenediamine and 3-Amino-5-methylthio-1H-1,2,4-triazole for tuned optoelectronic properties and its antioxidant studies. *Journal of Molecular Structure*, *1228*, 129738. https://doi.org/10.1016/j.molstruc.2020.129738.
7. Semenov, A. N., & Nyrkova, I. A. (2012). Statistical Description of Chain Molecules. In *Polymer Science: A Comprehensive Reference* (pp. 3–29). Elsevier. https://doi.org/10.1016/B978-0-444-53349-4.00002-9.
8. Umoren, S. A., Solomon, M. M., & Saji, V. S. (2022). Copolymers. In *Polymeric Materials in Corrosion Inhibition* (pp. 489–519). Elsevier. https://doi.org/10.1016/B978-0-12-823854-7.00020-5.
9. Hatada, K., Kitayama, T., & Ute, K. (1991). Preparation of Random, Block and Graft Copolymers of High Stereoregularity and their Characterization. In *Progress in Pacific Polymer Science* (pp. 131–142). Springer Berlin Heidelberg. https://doi.org/10.1007/978-3-642-84115-6_18.
10. Coldstream, J. G., Camp, P. J., Phillips, D. J., & Dowding, P. J. (2022). Gradient copolymers *versus* block copolymers: self-assembly in solution and surface adsorption. *Soft Matter*, *18*(35), 6538–6549. https://doi.org/10.1039/D2SM00741J.
11. Kenney, J. F. (1968). Properties of block versus random copolymers. *Polymer Engineering and Science*, *8*(3), 216–226. https://doi.org/10.1002/pen.760080307.
12. Scott, A. J., & Penlidis, A. (2017). Copolymerization. In *Reference Module in Chemistry, Molecular Sciences and Chemical Engineering*. Elsevier. https://doi.org/10.1016/B978-0-12-409547-2.13901-0.
13. Ramesh, M., & Muthukrishnan, M. (2022). Biodegradable polymer blends and composites for food-packaging applications. In *Biodegradable Polymers, Blends and Composites* (pp. 693–716). Elsevier. https://doi.org/10.1016/B978-0-12-823791-5.00004-1.
14. Ak, M., Cetişli, H., & Toppare, L. (2013). Blend or copolymer? Spectroelectrochemical evidence of copolymerization and blending of two electrochromic monomers. *Colloid and Polymer Science*, *291*(4), 767–772. https://doi.org/10.1007/s00396-012-2787-7.
15. Ananthakrishnan, N., Padmanaban, G., Ramakrishnan, S., & Reynolds, J. R. (2005). Tuning Polymer Light-Emitting Device Emission Colors in Ternary Blends Composed of Conjugated and Nonconjugated Polymers. *Macromolecules*, *38*(18), 7660–7669. https://doi.org/10.1021/ma050787j.

16. Ashok Kumar, S., Gouthaman, S., Shankar, J. S., Periyasamy, B. K., & Nayak, S. K. (2021). Stable and color tunable MEH-PPV/PMMA polymer blends for light-emitting applications. *Chemical Physics Letters*, *770*, 138462. https://doi.org/10.1016/j.cplett.2021.138462.
17. de Azevedo, D., Freitas, J. N., Domingues, R. A., Faleiros, M. M., & Atvars, T. D. Z. (2017). Correlation between the PL and EL emissions of polyfluorene-based diodes using bilayers or polymer blends. *Synthetic Metals*, *233*, 28–34. https://doi.org/10.1016/j.synthmet.2017.08.015.
18. Tozoni, J. R., Marletta, A., Arantes, A. do N., & de Oliveira, L. R. (2017). PMMA/MEH-PPV Photoluminescent Polymer Blend as a Long Time Exposure Blue-light Dosimeter. *Proceedings of the 5th International Conference on Photonics, Optics and Laser Technology*, 317–322. https://doi.org/10.5220/0006261403170322.
19. Jaymand, M. (2013). Recent progress in chemical modification of polyaniline. *Progress in Polymer Science*, *38*(9), 1287–1306. https://doi.org/10.1016/j.progpolymsci.2013.05.015.
20. Yin, W., & Ruckenstein, E. (2000). Water-Soluble Self-Doped Conducting Polyaniline Copolymer. *Macromolecules*, *33*(4), 1129–1131. https://doi.org/10.1021/ma991626g.
21. Xiao, Y., Wang, Y., Wu, X., & Ma, Y. (2022). Research progress on preparation methods of water-soluble polyaniline. *High Performance Polymers*, 095400832211314. https://doi.org/10.1177/09540083221131456.
22. Prokes, J., Krivka, I., Kuzel, R., Stejskal, J., & Kratochvil, P. (1996). Electrical properties of poly(aniline-co-p-phenylenediamine) copolymers. *International Journal of Electronics*, *81*(4), 407–417. https://doi.org/10.1080/002072196136580.
23. Durgaryan, A. H., Durgaryan, N. A., Arakelyan, R. H., & Miraqyan, N. A. (2017). Copolymerization of Aniline with P-Phenylenediamine in an Acetic Acid Medium. In *Chemical Engineering of Polymers* (pp. 3–14). Apple Academic Press. https://doi.org/10.1201/9781315365985-1.
24. Li, X.-G., Huang, M.-R., Duan, W., & Yang, Y.-L. (2002). Novel Multifunctional Polymers from Aromatic Diamines by Oxidative Polymerizations. *Chemical Reviews*, *102*(9), 2925–3030. https://doi.org/10.1021/cr010423z.
25. Jadoun, S., Riaz, U., Yáñez, J., & Pal Singh Chauhan, N. (2021). Synthesis, characterization and potential applications of Poly(o-phenylenediamine) based copolymers and Nanocomposites: A comprehensive review. *European Polymer Journal*, *156*, 110600. https://doi.org/10.1016/j.eurpolymj.2021.110600.
26. Umare, S. S., Waware, U. S., Ingole, S., & Viswanath, S. G. (2005). Influence of Copolymer Composition on the Structure of Conducting Poly(aniline-co-o-phenylenediamine). *International Journal of Polymer Analysis and Characterization*, *10*(1–2), 1–13. https://doi.org/10.1080/10236660500345398.
27. Zhou, T., Wu, S., Cai, J., & Ruan, W. (2020). Rapid humidity sensors based on poly(o-phenylenediamine-co-aniline) spherical nanoparticles. *Polymer Bulletin*, *77*(3), 1095–1105. https://doi.org/10.1007/s00289-019-02794-z.
28. Gicevicius, M., Kucinski, J., Ramanaviciene, A., & Ramanavicius, A. (2019). Tuning the optical pH sensing properties of polyaniline-based layer by electrochemical copolymerization of aniline with o-phenylenediamine. *Dyes and Pigments*, *170*, 107457. https://doi.org/10.1016/j.dyepig.2019.04.002.
29. Jadoun, S., Ashraf, S. M., & Riaz, U. (2017). Tuning the spectral, thermal and fluorescent properties of conjugated polymers via random copolymerization of hole transporting monomers. *RSC Advances*, *7*(52), 32757–32768. https://doi.org/10.1039/C7RA04662F.
30. Riaz, U., Jadoun, S., Kumar, P., Kumar, R., & Yadav, N. (2018). Microwave-assisted facile synthesis of poly(luminol- *co* -phenylenediamine) copolymers and their potential application in biomedical imaging. *RSC Advances*, *8*(65), 37165–37175. https://doi.org/10.1039/C8RA08373H.
31. Jadoun, S., Biswal, L., & Riaz, U. (2018). Tuning the optical properties of poly(o-phenylenediamine-co-pyrrole) via template mediated copolymerization. *Designed Monomers and Polymers*, *21*(1), 75–81. https://doi.org/10.1080/15685551.2018.1459078.
32. Riaz, U., Ashraf, S. M., Aleem, S., Budhiraja, V., & Jadoun, S. (2016). Microwave-assisted green synthesis of some nanoconjugated copolymers: characterisation and fluorescence

quenching studies with bovine serum albumin. *New Journal of Chemistry*, *40*(5), 4643–4653. https://doi.org/10.1039/C5NJ02513C.

33. Khokhar, D., Jadoun, S., Arif, R., & Jabin, S. (2022). Tuning the spectral, thermal and morphological properties of Poly(o-phenylenediamine-co-vaniline). *Materials Research Innovations*, *26*(1), 25–35. https://doi.org/10.1080/14328917.2020.1870330.
34. Huang, M.-R., Li, X.-G., & Duan, W. (2005). Effect of polymerization conditions ono-phenylenediamine ando-phenetidine oxidative copolymers. *Polymer International*, *54*(1), 70–82. https://doi.org/10.1002/pi.1618.
35. Huang, M.-R., Li, X.-G., & Yang, Y. (2000). Oxidative polymerization of o-phenylenediamine and pyrimidylamine. *Polymer Degradation and Stability*, *71*(1), 31–38. https://doi.org/10.1016/S0141-3910(00)00137-3.
36. Zoromba, M. Sh., & Al-Hossainy, A. F. (2020). Doped poly (o-phenylenediamine -co- p-toluidine) fibers for polymer solar cells applications. *Solar Energy*, *195*, 194–209. https://doi.org/10.1016/j.solener.2019.11.064.
37. Olmedo-Martínez, J. L., Farías-Mancilla, B. I., Vega-Rios, A., & Zaragoza-Contreras, E. A. (2017). Poly(ortho-phenylenediamine-co-aniline) based copolymer with improved capacitance. *Journal of Power Sources*, *366*, 233–240. https://doi.org/10.1016/j.jpowsour.2017.09.030.
38. Li, X.-G., Wang, H.-Y., & Huang, M.-R. (2007). Synthesis, Film-Forming, and Electronic Properties of *o* -Phenylenediamine Copolymers Displaying An Uncommon Tricolor. *Macromolecules*, *40*(5), 1489–1496. https://doi.org/10.1021/ma062463g.
39. Rohini Das, K., & Jinish Antony, M. (2016). Synthesis and characterisation of water dispersible copolymer submicron spheres of poly-(phenylenediamine-co-N-sulfopropyl aniline) via random copolymerizeation. *Polymer*, *87*, 215–225. https://doi.org/10.1016/j.polymer.2016.01.078.
40. Yan, C., Zhang, R., Chen, Y., & Wang, G. (2017). Electrochemical determination of enrofloxacin based on molecularly imprinted polymer via one-step electro-copolymerization of pyrrole and o -phenylenediamine. *Journal of Electroanalytical Chemistry*, *806*, 130–135. https://doi.org/10.1016/j.jelechem.2017.10.047.
41. Kong, Y., Shan, X., Ma, J., Chen, M., & Chen, Z. (2014). A novel voltammetric sensor for ascorbic acid based on molecularly imprinted poly(o-phenylenediamine-co-o-aminophenol). *Analytica Chimica Acta*, *809*, 54–60. https://doi.org/10.1016/j.aca.2013.12.003.
42. Zhao, F., Li, X., Xu, W., Zhang, W., & Ying, X. (2014). An Electrochemical Sensor for L-Tryptophan Using a Molecularly Imprinted Polymer Film Produced by Copolymerization of o-Phenylenediamine and Hydroquinone. *Analytical Letters*, *47*(10), 1712–1725. https://doi.org/10.1080/00032719.2014.880172.
43. Song, X., Sun, H., Yang, S., Zhao, S., & Liao, F. (2016). Synthesis of photoluminescent o-phenylenediamine–m-phenylenediamine copolymer nanospheres: An effective fluorescent sensing platform for selective and sensitive detection of chromium(VI) ion. *Journal of Luminescence*, *169*, 186–190. https://doi.org/10.1016/j.jlumin.2015.08.041.
44. Liao, F., Song, X., Yang, S., Hu, C., He, L., Yan, S., & Ding, G. (2015). Photoinduced electron transfer of poly(o-phenylenediamine)–Rhodamine B copolymer dots: application in ultrasensitive detection of nitrite in vivo. *Journal of Materials Chemistry A*, *3*(14), 7568–7574. https://doi.org/10.1039/C5TA00675A.
45. Liao, F., Yang, S., Li, X., Yang, L., Xie, Z., Hu, C., He, L., Kang, X., Song, X., & Ren, T. (2014). Poly(o-phenylenediamine) and benzeneselenol copolymer fluorescent nanorod: An ultra-sensitive fluorescent probe and a fluorescent switch triggered by redox procedure. *Synthetic Metals*, *189*, 135–142. https://doi.org/10.1016/j.synthmet.2014.01.020.
46. Das, K. R., Antony, M. J., & Varghese, S. (2019). Highly bluish-white light emissive and redox active conjugated poly-N-phenyl anthranilic acid polymer fluoroprobe for analytical sensing. *Polymer*, *181*, 121747. https://doi.org/10.1016/j.polymer.2019.121747.
47. Liao, F., Yang, S., Li, X., Yang, L., Xie, Z., Hu, C., Yan, S., Ren, T., & Liu, Z. (2014). Preparation of heteroatom doped poly(o-phenylenediamine) fluorescent nanospheres:

Tunable fluorescent spectrum and sensing performance. *Synthetic Metals*, *189*, 126–134. https://doi.org/10.1016/j.synthmet.2014.01.008.

48. Ouyang, M., Xiang, W., Xu, Y., Zhang, Y., Qian-pingLou, & Zhang, C. (2012). Tuning the Emission Color of Conjugated Polymers *via* Oxidation Copolymerization of Fluorene and 3,4-Ethylenedioxythiophene. *Polymers and Polymer Composites*, *20*(1–2), 21–26. https://doi.org/10.1177/0967391112020001-205.
49. Song, H. J., Kim, D. H., Lee, T. H., & Moon, D. K. (2012). Emission color tuning of copolymers containing polyfluorene, benzothiadiazole, porphyrin derivatives. *European Polymer Journal*, *48*(8), 1485–1494. https://doi.org/10.1016/j.eurpolymj.2012.06.002.
50. He, D., Wu, Y., & Xu, B.-Q. (2007). Formation of 2,3-diaminophenazines and their self-assembly into nanobelts in aqueous medium. *European Polymer Journal*, *43*(9), 3703–3709. https://doi.org/10.1016/j.eurpolymj.2007.06.038.
51. Sun, X., & Hagner, M. (2007). Mixing Aqueous Ferric Chloride and *O* -Phenylenediamine Solutions at Room Temperature: A Fast, Economical Route to Ultralong Microfibrils of Assemblied *O* -Phenylenediamine Dimers. *Langmuir*, *23*(21), 10441–10444. https://doi.org/10.1021/la701378y.
52. Sestrem, R. H., Ferreira, D. C., Landers, R., Temperini, M. L. A., & do Nascimento, G. M. (2010). Synthesis and spectroscopic characterization of polymer and oligomers of ortho-phenylenediamine. *European Polymer Journal*, *46*(3), 484–493. https://doi.org/10.1016/j.eurpolymj.2009.12.007.
53. Kitayama, T., Ute, K., Yamamoto, M., Fujimoto, N., & Hatada, K. (1991). 1H NMR spectroscopic differentiation of block copolymer, random copolymer and mixture of the corresponding homopolymers through end group and monomer sequence analyses. *Polymer Bulletin*, *25*(6), 683–688. https://doi.org/10.1007/BF01032665.
54. Kenney, J. F. (1968). Properties of block versus random copolymers. *Polymer Engineering and Science*, *8*(3), 216–226. https://doi.org/10.1002/pen.760080307.
55. Sayyah, S. M., Khaliel, A. B., Aboud, A. A., & Mohamed, S. M. (2014). Chemical Polymerization Kinetics of Poly-O-Phenylenediamine and Characterization of the Obtained Polymer in Aqueous Hydrochloric Acid Solution Using $K_2Cr_2O_7$ as Oxidizing Agent. *International Journal of Polymer Science*, *2014*, 1–16. https://doi.org/10.1155/2014/520910.
56. Zoromba, M. Sh., Abdel-Aziz, M. H., Bassyouni, M., Bahaitham, H., & Al-Hossainy, A. F. (2018). Poly(o-phenylenediamine) thin film for organic solar cell applications. *Journal of Solid State Electrochemistry*, *22*(12), 3673–3687. https://doi.org/10.1007/s10008-018-4077-x.
57. Zoromba, M. Sh., Al-Hossainy, A. F., Mahmoud, S. A., Bourezgui, A., & Shaaban, E. R. (2020). Improvement of the thermal stability and optical properties for poly (ortho phenylene diamine) using soft templates. *Journal of Molecular Structure*, *1221*, 128792. https://doi.org/10.1016/j.molstruc.2020.128792.
58. Ullah, H., Shah, A.-H. A., Ayub, K., & Bilal, S. (2013). Density Functional Theory Study of Poly(*o* -phenylenediamine) Oligomers. *The Journal of Physical Chemistry C*, *117*(8), 4069–4078. https://doi.org/10.1021/jp311526u.
59. Wang, Z., & Liao, F. (2012). Fluorescent probes for Pd^{2+} detection by poly(o-phenylenediamine) nanospheres with fluorescence enhancement. *Synthetic Metals*, *162*(5–6), 444–447. https://doi.org/10.1016/j.synthmet.2012.01.013.
60. Han, J., Liu, Y., Li, L., & Guo, R. (2009). Poly(*o* -phenylenediamine) Submicrosphere-Supported Gold Nanocatalysts: Synthesis, Characterization, and Application in Selective Oxidation of Benzyl Alcohol. *Langmuir*, *25*(18), 11054–11060. https://doi.org/10.1021/la901373t.
61. Ozkan, S. Zh., Eremeev, I. S., Karpacheva, G. P., Prudskova, T. N., Veselova, E. v., Bondarenko, G. N., & Shandryuk, G. A. (2013). Polymers of diphenylamine-2-carboxylic acid: Synthesis, structure, and properties. *Polymer Science Series B*, *55*(3–4), 107–115. https://doi.org/10.1134/S1560090413030032.
62. Ozkan, S. Zh., Bondarenko, G. N., & Karpacheva, G. P. (2010). Oxidative polymerization of diphenylamine-2-carboxylic acid: Synthesis, structure, and properties of polymers.

Polymer Science Series B, *52*(5–6), 263–269. https://doi.org/10.1134/S1560090410050015.
63. Fineman, M., & Ross, S. D. (1950). Linear method for determining monomer reactivity ratios in copolymerization. *Journal of Polymer Science*, *5*(2), 259–262. https://doi.org/10.1002/pol.1950.120050210.
64. Odian, G. (2004). *Principles of Polymerization*. Wiley. https://doi.org/10.1002/047147875X.
65. Al-Deyab, S. S., El-Newehy, M. H., & Al-Hazmi, A. M. (2010). Synthesis, Characterization and Reactivity Ratio Study of Poly(di(tri-n-butyltin) citraconate-co-N-vinylimidazole). *Molecules*, *15*(7), 4750–4756. https://doi.org/10.3390/molecules15074750.
66. Wang, L., Guo, S., & Dong, S. (2008). Facile synthesis of poly(o-phenylenediamine) microfibrils using cupric sulfate as the oxidant. *Materials Letters*, *62*(17–18), 3240–3242. https://doi.org/10.1016/j.matlet.2008.02.031.
67. Yang, S.-W., & Liao, F. (2011). Characterization And Morphology Control Of Poly(P-Phenylenediamine) Microstructures In Different pH. *Nano*, *06*(06), 597–601. https://doi.org/10.1142/S1793292011002925.
68. Tu, X., Xie, Q., Xiang, C., Zhang, Y., & Yao, S. (2005). Scanning Electrochemical Microscopy in Combination with Piezoelectric Quartz Crystal Impedance Analysis for Studying the Growth and Electrochemistry as Well as Microetching of Poly(*o* -phenylenediamine) Thin Films. *The Journal of Physical Chemistry B*, *109*(9), 4053–4063. https://doi.org/10.1021/jp044731n.
69. Lu, X., Mao, H., Chao, D., Zhao, X., Zhang, W., & Wei, Y. (2007). Preparation and characterization of poly(o-phenylenediamine) microrods using ferric chloride as an oxidant. *Materials Letters*, *61*(6), 1400–1403. https://doi.org/10.1016/j.matlet.2006.07.040.
70. Sayyah, S. M., Abd El-Rehim, S. S., Kamal, S. M., El-Deeb, M. M., & Azooz, R. E. (2011). Electropolymerization kinetics of a binary mixture of o-phenylenediamine and 2-aminobenzothiazole and characterization of the obtained polymer films. *Journal of Applied Polymer Science*, *119*(1), 252–264. https://doi.org/10.1002/app.32534.
71. Kazemipour, M., Behzadi, M., & Ahmadi, R. (2016). Poly(o -phenylenediamine-co- o -toluidine)/modified carbon nanotubes composite coating fabricated on a stainless steel wire for the headspace solid-phase microextraction of polycyclic aromatic hydrocarbons. *Microchemical Journal*, *128*, 258–266. https://doi.org/10.1016/j.microc.2016.05.004.
72. Kim, M. H., Bae, D. H., Choi, H. J., & Seo, Y. (2017). Synthesis of semiconducting poly(diphenylamine) particles and analysis of their electrorheological properties. *Polymer*, *119*, 40–49. https://doi.org/10.1016/j.polymer.2017.05.017.
73. Wang, Z., Liao, F., Yang, S., & Guo, T. (2011). A novel route synthesis of poly(ortho-phenylenediamine) fluffy microspheres self-assembled from nanospheres. *Fibers and Polymers*, *12*(8), 997–1001. https://doi.org/10.1007/s12221-011-0997-0.
74. Muthirulan, P., Kannan, N., & Meenakshisundaram, M. (2013). Synthesis and corrosion protection properties of poly(o-phenylenediamine) nanofibers. *Journal of Advanced Research*, *4*(4), 385–392. https://doi.org/10.1016/j.jare.2012.07.007.
75. C.Harris, D. (2007). *Quantitative Chemical Analyisis*, 7th edn.; W.H Freeman and Company: United states of America.
76. Johnson, K., Huang, Y.-S., Huettner, S., Sommer, M., Brinkmann, M., Mulherin, R., Niedzialek, D., Beljonne, D., Clark, J., Huck, W. T. S., & Friend, R. H. (2013). Control of Intrachain Charge Transfer in Model Systems for Block Copolymer Photovoltaic Materials. *Journal of the American Chemical Society*, *135*(13), 5074–5083. https://doi.org/10.1021/ja3121247.
77. You, X., & Li, Y. (2019). Direct chemiluminescence of fluorescent gold nanoclusters with classic oxidants for hydrogen peroxide sensing. *Arabian Journal of Chemistry*, *12*(1), 69–74. https://doi.org/10.1016/j.arabjc.2015.05.019.

78. Moritake, Y., Kanamori, Y., & Hane, K. (2016). Emission wavelength tuning of fluorescence by fine structural control of optical metamaterials with Fano resonance. *Scientific Reports*, *6*(1), 33208. https://doi.org/10.1038/srep33208.
79. Leng, J., Xu, Y., Chan, Y., Wang, P., Ryuzaki, S., Okamoto, K., & Tamada, K. (2020). Tuning the Emission Colors of Self-Assembled Quantum Dot Monolayers via One-Step Heat Treatment for Display Applications. *ACS Applied Nano Materials*, *3*(4), 3214–3222. https://doi.org/10.1021/acsanm.9b02358.
80. Mineeva, K. O., Medentseva, E. I., Plutalova, A. v., Serkhacheva, N. S., Bol'shakova, A. v., Lysenko, E. A., & Chernikova, E. v. (2021). Block Random Copolymers of Styrene and Acrylic Acid: Synthesis and Properties. *Polymer Science, Series B*, *63*(6), 821–832. https://doi.org/10.1134/S156009042106018X.

CHAPTER 7

Poly-N-Phenyl Anthranilic Acid Fluorescent Polymer Dye for Cell Imaging and Secret Writing Applications

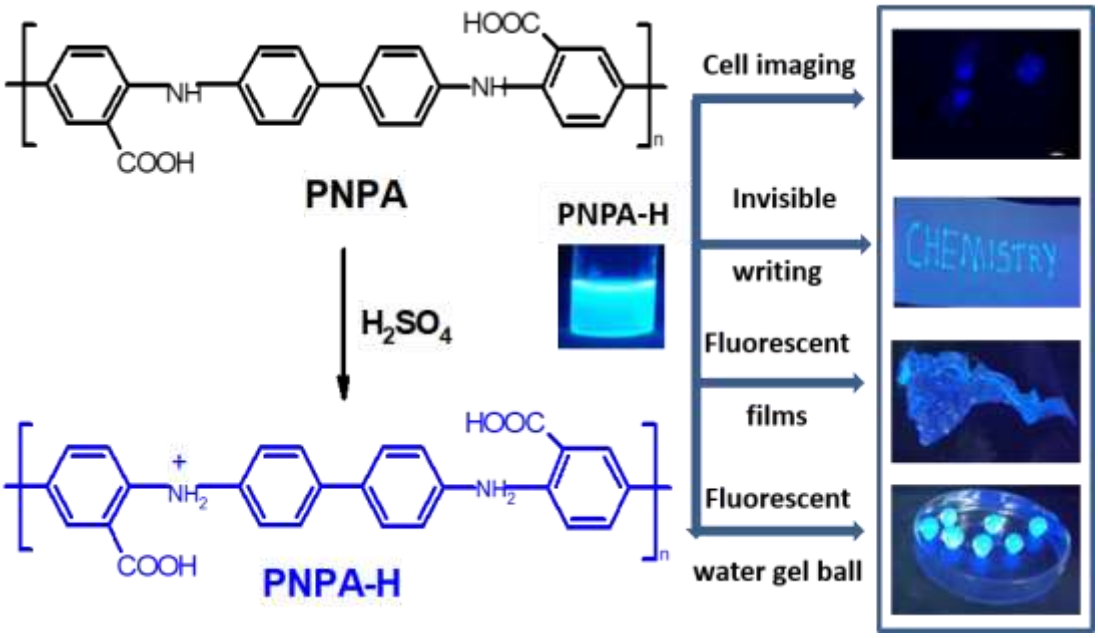

7.1. Introduction

Fluorescent dyes or fluorophores exhibit characteristic fluorescence emission by absorption of UV or visible radiation. The structure of the fluorescent organic dye plays a crucial role in the fluorescence emission of the molecule, which often involves the conjugated structure of fluorophore in the form of hetero atom containing rings or aromatic rings or reduced/oxidized rings etc. Xanthene, coumarin, and perylene dyes exhibit fluorescence in the daylight [1] (see **Figure 7.1.**). Other fluorescent materials include lanthanide complexes, inorganic quantum dots, carbon dots, BODIPY compounds, and conjugated polymers [2-5]. BODIPY compounds have wide applications, including chemosensing, bio-imaging, and biomolecular labeling, because of sharp absorption and intense fluorescence emission [6-7].

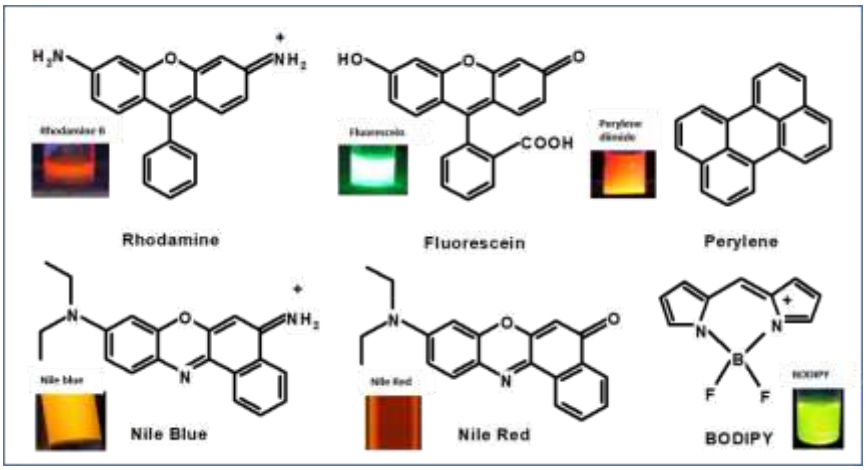

Figure 7.1. *Structure of fluorescent organic dyes.*

Due to their attractive fluorescence glow, fluorescent dyes have many commercial, technological, and diagnostic applications in various fields [8]. They were helpful in lasers for microsurgery and communication technologies and applicable to detecting defects in components of heavy instruments [9]. Highly fluorescent materials were suitable for detecting water currents in hydrogeology [10]. Fluorescent dyes have been widely used in quantitative microanalysis as fluorescent indicators due to their high sensitivity [11, 12]. The potential uses of fluorescent dyes in solar cells as solar collectors and LEDs as electroluminescent materials were also reported [13, 14]. Fluorescent materials, especially invisible fluorescent dyes, were explored as anti-counterfeiting labels and to ensure document security [15]. Security fibers, security inks, security films and various security materials have been developed for anti-counterfeiting applications

using fluorescent dyes [16, 17]. Invisible fluorescent dyes have much more advantages in data protection since the letters are invisible in daylight and visible only under UV light. Swapnil et al. used ethanol dispersions of fluorophore-incorporated polystyrene microbeads as fluorescent invisible security ink, which became visible only under UV light [18]. Mondal et al. synthesized pH-sensitive luminescent carbon quantum dots and used them as an invisible dye in paper and polymer substrates [19]. Chen et al. synthesized 1,3,6,8 -pyrene sulfonic acid sodium salt (PTSA) to prepare invisible fluorescent inks using hydroxyethylcellulose as a binder due to its pure blue fluorescence and water solubility [20]. Some challenging factors for these invisible inks are photostability, quantum yields, and chemical fastness. Conjugated polymers with narrow emission and high photostability have been rarely reported as fluorescent ink [21-23]. Chang et al. used polyfluorene and its derivatives to design fluorescent ink, as their emission colours could be tuned by introducing narrow band gap monomers into the polymer backbone (see **Figure 7.2.**) [24].

Figure 7.2*. Schematic representation for preparing polyfluorene derivative and its application in water-based invisible ink (Adapted from Chang et al. 2019).*

The chemical and bio-applications of fluorescent dyes have included fluorescent sensing of biomolecules and cell imaging to trace cell components [25]. Optical sensors for oxygen, carbon dioxide, enzymes, metal ions, and cell temperature have also been developed based on fluorescent materials [26, 27]. Fluorescence-based cell imaging allowed the visualization of cell structure to study the biological and dynamic cellular processes, which helped diagnose early disease stages [28]. Fluorescent organic dyes like rhodamine, coumarin, fluorescein, BODIPY, cyanine dyes, and fluorescent proteins have been used as fluorescent probes in cell imaging [29-33]. Fluorescent water-soluble organic dyes and conjugated poly or oligo electrolytes have been developed for cell imaging to monitor

intra and extracellular environments [34-38]. Quantum dots were widely used as fluorescent agents in biomedical applications because of narrow emission and resistance to photobleaching compared to organic dyes and fluorescent proteins [39]. However, heavy metal toxicity is a major concern in inorganic quantum dots and lanthanide materials, which limit their *in vivo* bio-applications [40]. Hydrophobic organic dyes like rhodamines lack cell permeability and can cause problems in cellular imaging [41]. Rapid photobleaching of organic dyes and fluorescent proteins may also limit their use in clinical diagnostics [42, 43]. In the present scenario, the development of water-soluble conjugated polymers functioning as efficient fluorophores with good photostability, intense emission, high quantum yield, easy signal amplification for detection or imaging, and easy functionalization on polymer structure is advantageous [43-47]. The water-soluble nanoparticles of conjugated polymers like poly (fluorene-co-phenylene) (PFP), poly (p-phenylenevinylene) (PPV), poly (p-phenyleneethynylene) (PPE), polydiacetylene (PDA), and polythiophene (PT) derivatives were used in cell imaging as fluorescent probes via allowing it to accumulate on the living cells [48].

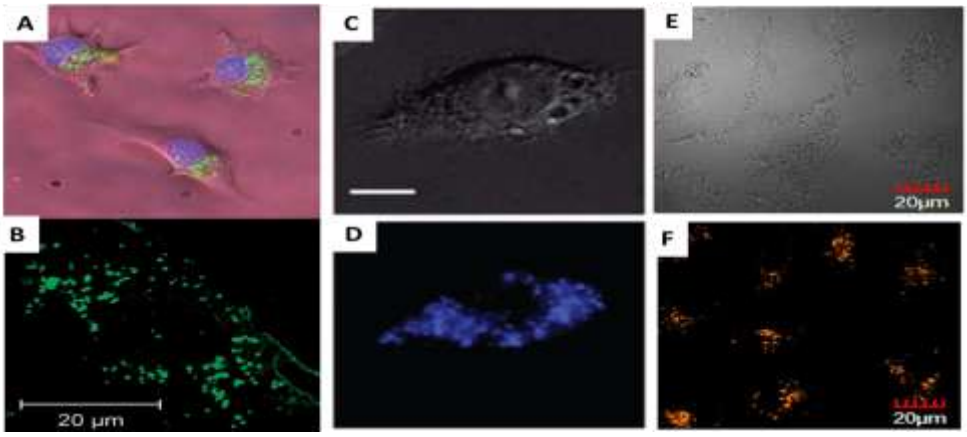

Figure 7.3. *Fluorescence images of A) BALB/C3T3 cells incubated sequentially with poly (p-phenylene ethynylene nanoparticles (green) and Hoechst dye (blue) and B) Live BALB/C3T3 cells incubated with poly (p-phenyleneethynylene) nanoparticles. C) Differential interference contrast images and D) fluorescence images of macrophage cell J774 incubated with poly (p-phenylene ethylene). E) Phase contrast images and F) Fluorescence images of A549 cells incubated with polythiophene derivative (Adapted from Moon et al. 2007 (A&D) Zhu et al. 2012 (B&C) and Wang et al. 2015 (C&F).*

The fluorescence images of cells incubated with fluorescent conjugated polymer materials were reported in the literature (see **Figure 7.3.**). Moon et al. used poly (para-

phenyleneethynylene) based conjugated polymer nanoparticles for the live and fixed cell imaging of BALB/CT3T cells, and staining in cytosol around the perinuclear region was obtained [49]. Wang et al. synthesized water-soluble polythiophene derivatives with different pendent moieties via oxidative copolymerization and used them as a fluorescent lysosome-specific imaging material [47]. Brunz et al. have synthesized folate-substituted poly (para-phenyleneethynylene) with water solubility, photostability, and low cytotoxicity and used it to stain KB cancer cells in vitro, especially in the cytoplasm [50]. Cells generally uptake small nanoparticles by endocytosis and any biological entities associated with these nanoparticles may be directly exposed to the environment containing endosomes and lysosomes [51]. These lysosomes and endosomes can cause degradation to the biological entities, so nanoparticle-based drug deliveries are sometimes ineffectual. But the drug deliveries using microspherical particles prevented the direct exposure of biological entities into the degradable environment so that larger particles of conjugated polymers, other than nanoparticles, were also developed for cell imaging and drug deliveries. The cellular uptake of polymeric materials was mostly based on energy-dependent endocytic uptake. The major concern in conjugated polymer-based bioimaging is their hydrophobic nature. Thus, conjugate polymers containing water-soluble fragments, which provide hydrophilicity apart from their hydrophobic backbones, were effectively used for cell imaging. Behrendt et al. developed polymer micro-spheres for in vitro cell imaging and biomolecule delivery [51]. Alexander et al. prepared amine functionalised crosslinked polystyrene microspheres that can enter B16F10 cells via passive and rapid mechanisms [52].

Nuclear staining is an important process in bioimaging to allow the visualization of cell growth and development, DNA quantification, and cancer biology [53]. The abnormal behavior of the nucleic acids and enzymes in the nucleus is responsible for cellular carcinogenesis. Thus, the development of nuclear-targeted therapy can detect the malfunctioning of such cellular compounds and be effective in cancer treatments [54]. Therefore, developing highly selective and sensitive fluorescent molecules for nuclear staining was necessary. Some of the organic dyes like DAPI, Hoechst, and transition metal complexes of Ru(II) and Ir(III) were commonly used as nuclear stains in cell imaging[55-60]. DAPI and Hoechst contain short hydrophobic chains and planar aromatic cationic structures. Hydrophilic cations in the molecules could easily combine with the negatively charged DNA molecules in the nucleus through electrostatic interactions; thus,

nuclear staining was easily achieved (see **Figure 7.4**) [61]. Conjugated polymer-based systems for cell membrane lysosome and mitochondrial staining were available but rarely reported for nuclear staining [62-65]. Liu et al. used red emissive quinoxaline-based polymer dot-folate conjugate for nuclear staining of SKOV-3 [66].

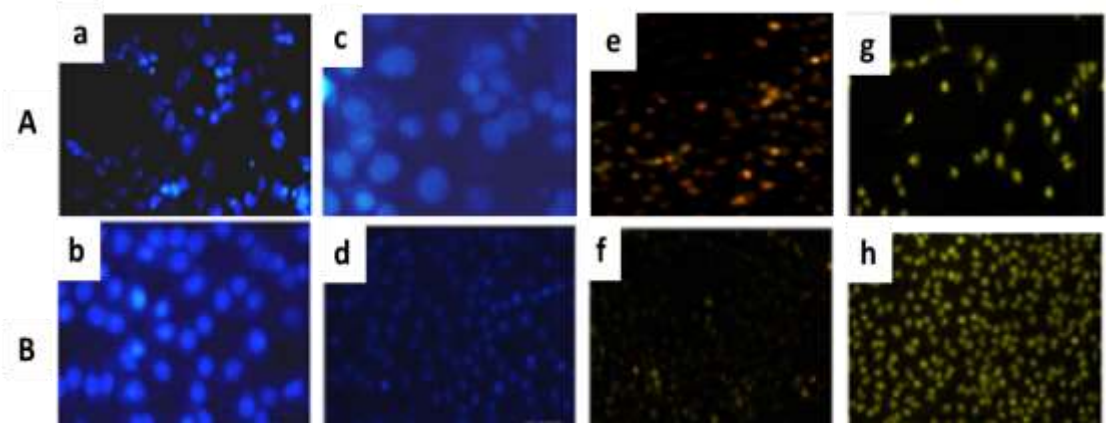

Figure 7.4. *Fluorescence microscopy images of A) H522 cells and B) A549 cells incubated with DAPI (a&b), Hoechst 33258 (c&d), Acridine orange-ethidium bromide (e&f) and Dichlorodihydrofluorecein diacetate (g&h).(Adapted from Sikdar et al. 2013).*

The fluorescent materials were suitable for fluorescent ink and cell staining action was reported in the literature. Atchuthan et al. used nitrogen-doped quantum dots as a staining agent for HCT-116 human colon cancer cells and as fluorescent ink [4]. Zhou et al. used photo-responsive supramolecular assembly of cyclodextrin/anthracene/Eu^{3+} as tunable fluorescent ink and white fluorescent tags for cell imaging, which are present in the cytoplasm [75]. Nandi et al. developed nitrogen-doped carbon dots as security inks, and cell imaging showed preferential localization of quantum dots into the cytoplasm and the nucleus of HeLa cells [67]. Fluorescent materials reported for both cell imaging and invisible ink, along with different parameters such as their cell viability and concentrations used for staining and stained part, were summarized in **Table 7.1**.

Table 7.1. *Fluorescent materials reported for cell imaging and other applications with cell viability, concentrations of fluorophore used for staining, and stained part of cell adapted from literature.*

Sl. No	Material	Cells	Cell viability	Conc. used for staining	Stained part of the cell	Other applications	Ref.
1	N-doped carbon dot from L-aspartic acid and 3,6-diamino acridine hydrochloride	*In vitro* HeLa cell	80% for 500 µg/mL	200 µg/mL	Cytoplasm and nucleus	Vitamine B_{12} and bilirubin detection and invisible fluorescent ink	67
2	N-doped quantum dots from Phyllanthus embilica	*In vitro* HCT-116 and *In vivo* Caenorhabditis elegans (C. elegans)	98% for 100 µg/mL for C.elegans	25-200 µg/mL for HCT-116 and 50 µg/mL for C.elegans	Whole-cell	invisible fluorescent ink	4
3	Guar gum grafted acrylic acid-co-3-(N-isopropylacryl amido) propanoic acid-co-N-isopropylacryl amide	*In vitro* MDCK and *in vitro* HOS	95% for 200 µg/mL for MDCK and 68% for 0.5 µg/µL for HOS.	200 µg/mL	Cell or nuclear membrane	Pb(II) sensor and invisible fluorescent ink	68
4	N-doped carbon dots from Magnolia liliiflora	*In vivo* clone-9-hepatocytes	97% for 100 µg/mL	-	Whole-cell	Fe(III) sensor and invisible fluorescent ink	69
5	Carbon dots	*In vitro* HepG2	90% for 500	350	Cytoplas	Fe(III)	70

	from Prunus cerasifera	cell	µg/mL	µg/mL	m and nuclei	sensor and invisible fluorescent ink	
6	N-doped carbon dots from phyllanthus acidus	*In vitro* Clone 9 hepatocytes	98% for 100 µg/mL for Clone 9 hepatocytes	-	Whole-cell	Fe(III) sensor and invisible fluorescent ink	71
7	N-doped graphene quantum dots from Passiflora Edulia Sims	*In vitro* fibroblast cell	90% for 300 µg/mL	100 µg/mL	Whole-cell	Ag^{+} sensor and security ink	72
8	Carbon dots from plant petals	*In vivo* A193	85 % for 0.6 mg/mL	0.6 mg/mL	Whole-cell	invisible fluorescent ink	73
9	Nitrogen-sulphur-co doped carbon dots from cigarette butts	*In vitro* HeLa cells	85% for µg/mL	200 µg/mL	Cell membrane and cytoplasmic area	Fe^{3+} sensor and security ink	74

In this chapter, we have developed a poly-N-phenyl anthranilic acid-based multifunctional fluorescent dye. The improved hydrophilicity of PNPA-H upon protonation effectively provided fluorescence emission to non-emissive hydrophilic materials. The stability of fluorescence emission of PNPA-H in an acidic, neutral, basic medium made them suitable for various applications. The invisible character of PNPA-H was utilized for secret writing as an anti-counterfeiting tool. A fluorescent conjugated polymer, suitable for both nucleus-targeted staining and invisible ink applications, was not yet reported. The biocompatibility and staining ability of protonated N-phenyl anthranilic acid monomer and poly-N-phenyl anthranilic acid polymer enabled us to perform cell imaging studies. Cell uptake of monomer NPA-H and polymer PNPA-H was compared using normal cell line L929 and papillary thyroid cancer cell line MDA-T32. The nuclear staining ability of NPA-H and PNPA-H was evident from the bright blue fluorescence from the nucleus of the cells. The nuclear staining of NPA-H and PNPA-H

toward cancer cells was more effective compared to normal cells, which indicates the selectivity of NPA-H and PNPA-H toward cancer cells. In short, the bright bluish-white emission of PNPA-H was suitable for secret writing and cell imaging.

7.2. Experimental

7.2.1. Materials and Reagents: N-phenyl anthranilic acid and polyvinyl alcohol (number with an average molecular weight of 1,15000) were purchased from Loba Chemie. Concentrated sulphuric acid was purchased from Merck Chemicals. Roswell Park Memorial Institute (RPMI) medium was purchased from Sigma Aldrich. Human thyroid cancer cell line MDA-T32 was purchased from Americal type culture collection (ATCC). Phosphate buffer saline (PBS), 3-(4,5-dimethylthiazol-2-yl)-2,5-diphenyltetrazolium bromide (MTT), Fetal bovine serum (FBS), paraformaldehyde (PFA), Trypsin-EDTA solution and Dulbecco's Modified Eagle Medium and high glucose (DMEM+HG) were purchased from high media chemicals. Eagle's minimum essential medium supplemented with nonessential amino acids (NEAA) 100x were purchased from GIBCO chemicals.

7.2.2. Measurements and Instruments: UV-Visible absorption spectra of the samples were recorded by Shimadzu UV-Visible spectrometer 1800 series in the 200-800 nm range with deionised water. The pH of solutions were measured using a portable pH meter of Hanna instruments. The absorbance of MTT assays was recorded using a Tecan multimode plate reader to determine cell viability. Fluorescence images of the samples were photographed on a NikonTi2 epifluorescent microscope to quantify cells. Image analysis was done using ImageJ software v1.53i

7.2.3. Preparation of PNPA-H solution (4.6×10^{-4} M): Poly-N-phenyl anthranilic acid (0.0098 g, 0.0046 moles) was dissolved in 10 mL concentrated H_2SO_4 (18M) in a 30 mL vial by sonicating for 15-20 minutes till dark blue colored solution obtained. From the above solution, 1 mL was diluted to 10 mL using double deionized water to get a colorless solution (4.6×10^{-4} M) with bright bluish-white light fluorescence emission under long wavelength UV light (365 nm).

7.2.4. Preparation of fluorescent polyvinyl alcohol hydrogels and films: Polyvinyl alcohol (0.2 g) was dissolved in 10 mL water by heating. Ultrasonic probe sonication (750 W) was required for 15 minutes for the complete dissolution. To the clear viscous

solution of PVA, PNPA-H (0.2 mL, 4.6×10^{-4} M) was added and stirred well. A colourles hydrogel was obtained, and a thin colorless film was obtained on subsequent slow evaporation of water.

7.2.5. Preparation of NPA-H and PNPA-H solutions for cell imaging and cytotoxicity studies: The recrystallized NPA (0.10 g, 4.7×10^{-4} moles) was accurately weighed and dissolved in 2 mL concentrated H_2SO_4 (18 M) by sonication. A colourless NPA-H solution was obtained. The above solution (2 mL) was diluted to 3 mL in water to obtain NPA-H stock solution (1.57×10^{-1} M). For the cytotoxicity and cell imaging studies, NPA-H solutions with different concentrations (100 nM, 500 nM, 1 µM, and 10 µM) was prepared by diluting stock solution using phosphate-buffered saline (PBS).

The polymer PNPA-H (0.050 g, 2.4×10^{-4} moles) was accurately weighed and dissolved in 2 mL concentrated H_2SO_4 (18 M) using a sonicator. A dark blue colour PNPA-H solution was obtained. The solution was diluted to 3 mL to obtain colourless PNPA-H solution (7.89×10^{-2} M). For the cytotoxicity and cell imaging studies, PNPA-H solutions with different concentrations (100 nM, 500 nM, 1 µM, and 10 µM) was prepared by diluting stock solution using phosphate buffered saline (PBS).

7.2.6. Procedure for incorporating fluorescent PNPA-H into different hydrophilic substrates like filter paper, water gel balls, glass fiber, and silica gel: The protonated PNPA-H solution having a concentration of 4.6×10^{-4} M (10 mL) was taken in a 100 mL beaker. A Whatman number 42 filter paper and glass fiber was dipped into the solution separately in order to absorb PNPA-H solution and dried using an air drier. The colourless water gel balls were soaked in the PNPA-H solution for two hours to absorb the dye. A silica gel slurry was prepared using 4.6×10^{-4} M PNPA-H solution and coated on a dried glass plate. The glass plate was dried at 80°C in hot air oven. The fluorescence of these materials was checked by irradiating UV light of wavelength 365 nm.

7.2.7. Procedure for cell culture and cytotoxicity Experiment: MDA-T32 cells are cultured in RPMI media. The complete Roswell Park Memorial Institute (RPMI) medium supplemented with 10% Fetal bovine serum, 100µg/mL Penicillin, 100 µg/mL streptomycine, and 1% non-essential amino acids. These cells were incubated at 37°C in a 5% CO_2 humidified atmosphere and passages on reaching 70%-80% confluency. L929 cells were cultured in DMEM + 2mM Glutamine + 10% Fetal Bovine Serum (FBS)

medium and were incubated at 37°C in a 5% CO_2 humidified atmosphere and passages on reaching 70-80% confluency.

To evaluate the cytotoxicity of PNPA-H and NPA-H having different concentrations like 100nM, 500nM, 1µM, and 10 µM in RPMI medium with 2% FBS and 1% NEAA, 3000 MDA-T32 cells were cultured per well in 96 well plate containing 100µL of RPMI culture medium. The vehicle in which PNPA-H and NPA-H main stock were prepared, was also seeded as a control in MTT assay. Incubated overnight and the culture medium was removed after 24 hours of cell culture, and the cells were treated with each concentration of PNPA-H and NPA-H freshly in each day for 16 hours and the cells were harvested for MTT after 16 hours. A time period of 16 hours of treatment was selected after standardizing the MTT assay at different time intervals of 4 hours, 16 hours and 24 hours. MTT assay was done to determine cell viability after the experimental period. Similarly, cell viability was also analysed for L929 cells, to evaluate the cytotoxicity of PNPA-H and NPA-H (100nM, 500nM, 1uM, and 10 µM) in DMEM medium with 2% FBS and 1% NEAA. Cell viability was calculated using the formula.

$$\text{Viability (\%)} = \frac{A_s - A_b}{A_c - A_b}\ x\ 100$$

Where A_s is the absorbance of the sample, A_b is the absorbance of the blank, and A_c is the absorbance of the control at 570 nm.

7.2.8. Procedure for Immunocytochemistry analysis: For Immunocytochemistry studies, 10,000 MDA-T32 cells and L929 cells were cultured on coverslips. The cells were then fixed with ice cold 4% paraformaldehyde solution for 20 minutes and washed with 1x PBS (1x PBS contains 137 mM NaCl, 10 mM phosphate and 2.7 mM KCl) thrice. These fixed cells were treated with PNPA-H and NPA-H having concentrations like 100nM, 500nM, 1µM, and 10µM for 16 hours and kept at room temperature. The cells were washed thrice with 1x PBS. The samples were then mounted onto slides with Fluoroshield mounting media. The coverslips were sealed with clear nail polish to prevent drying. A minimum of five randomly selected fields per sample were photographed on NikonTi2 epifluorescent microscope to quantify cells.

7.3. Results and Discussion

7.3.1. Synthesis of PNPA-H as fluorescent dye

Poly-N-phenyl anthranilic acid (PNPA) was synthesised from N-phenyl anhranilic acid (NPA) by oxidative chemical polymerisation using $FeCl_3$ as an oxidising agent in ethanol medium. The blue-coloured polymer powder was soluble in polar solvents like ethanol, dimethyl sulfoxide, and acetone and in non-polar solvents like chloroform and ether. The polymer PNPA was insoluble in water but became soluble in concentrated H_2SO_4 due to the partial protonation of aromatic secondary amines. The hydrophilic character of PNPA was attributed to polar –COOH functional groups in the polymer chains. The hydrophobic character was due to conjugated aromatic rings in the polymer backbone. The polymer PNPA was denoted as PNPA-H due to its protonation. The polymer has shown blue colour and strong bluish-white fluorescence emission in concentrated H_2SO_4 (see **Figure 7.5.**).

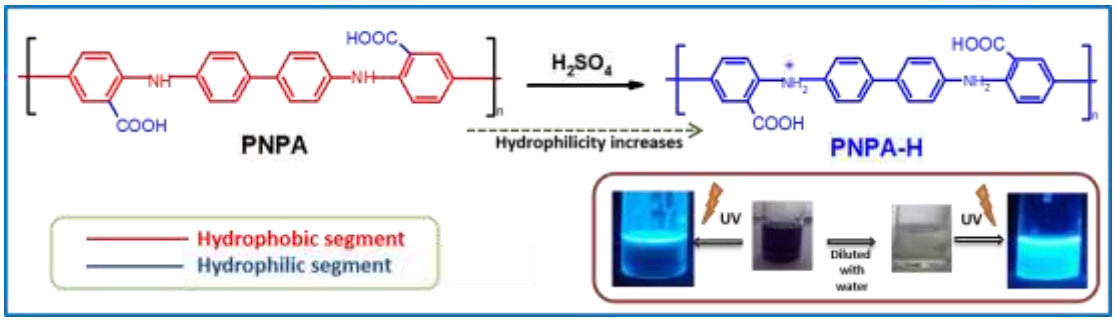

Figure 7.5. *The schematic representation of protonation in poly-N-phenyl anthranilic acid (PNPA-H) and the photographs of protonated PNPA-H in concentrated H_2SO_4 under UV light and visible light.*

PNPA-H prepared in concentrated H_2SO_4 was diluted using water. Dilution of the protonated PNPA-H to a higher pH (neutral and basic) did not reduce the solubility of the polymer. The solution became colourless, and the fluorescence intensity was enhanced on dilution (see **Figure 7.6.**). The effect of concentrated H_2SO_4 on the protonation of PNPA was studied by dissolving 1 mg of PNPA in different volumes of concentrated H_2SO_4 like 0.5 mL, 1 mL, 1.5 mL, 2 mL, and 2.5 mL. The photographs of PNPA dissolved in different volumes of concentrated H_2SO_4 were given in **Figure 7.6**. PNPA-H solutions dissolved in concentrated H_2SO_4 have shown blue colour in visible light and blue emission in UV light. All the concentrated PNPA-H solution prepared in 0.5 mL, 1 mL,

1.5 mL, 2 mL, and 2.5 mL was further diluted to 10 mL using deionised water. The photographs of diluted PNPA-H solutions under UV light were also given in **Figure 7.6.** The PNPA-H solution prepared by dissolving 1 mg in 0.5 mL concentrated H_2SO_4 solution was found to be turbid and could be due to insufficient protonation. The hydrophilicity of the polymer fragments can be improved through protonation. Once the protonation in the chains was sufficient, their hydrophilic nature increased and gave them water solubility. Clear solutions were obtained by diluting 1 mg of PNPA dissolved in 2 mL and 2.5 mL in concentrated H_2SO_4. Thus, 2 mL or 2.5 mL concentrated H_2SO_4 was sufficiently needed to protonate 1 mg of PNPA. Strong, bright, bluish-white fluorescence was observed for all solutions under UV light.

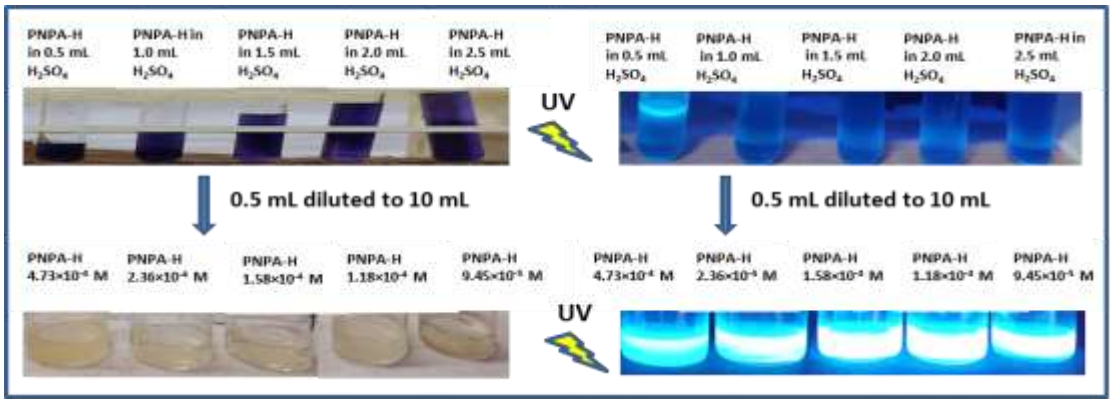

Figure 7.6. *Photographs of 1 mg PNPA dissolved in different volumes in concentrated H_2SO_4 under UV light and visible light before and after dilution with deionised water (10 mL).*

7.3.2. UV-Visible absorption studies

The solubility, hydrophilicity, and fluorescence of PNPA-H in the neutral medium were also important by considering their applications in security inks and cell imaging. PNPA was protonated using sulphuric acid. Protonated PNPA-H was diluted and then neutralised to pH=7 by adding 4 M NaOH (~ 10 mL) by checking pH. The solubility of PNPA-H continues to remain stable in a neutral medium. UV-visible absorption spectra of protonated PNPA-H after dilution and after neutralization with concentrations 7.9×10^{-5} M, 5.9×10^{-5} M, and 4.71×10^{-5} M were shown in **Figure 7.7.A and B,** respectively. A blank was also prepared, in which 0.5 mL concentrated H_2SO_4 was diluted to 10 mL without adding PNPA. The absence of any absorption peaks in the UV-visible absorption spectra of blank shows less interference of solvent medium on the absorption. The

absorbance spectra of PNPA-H have shown two absorption maxima at 252 nm and 398 nm. Among them, a narrow absorption was observed at 252 nm, corresponding to π to π* transition and broad absorption was observed at 398 nm, which corresponded to an extended π to π* transition. UV-visible absorption spectra of neutralised PNPA-H were given in **Figure 7.7.B**. The absorption at 252 nm was observed in neutralised PNPA-H similar to diluted PNPA-H and the broadness of the peak at 398 nm was increased on neutralisation. The presence of an additional peak at 287 nm could be due to the presence of HSO_4^- ions, which were formed during neutralisation [76]. The photographs of neutralised PNPA-H solution under visible and UV light were given in the inset of **Figure 7.7.B**. The neutralised PNPA-H solutions were also colourless and showed bright fluorescence emissions under UV light. Thus, PNPA-H was effective for applications in acidic and neutral mediums.

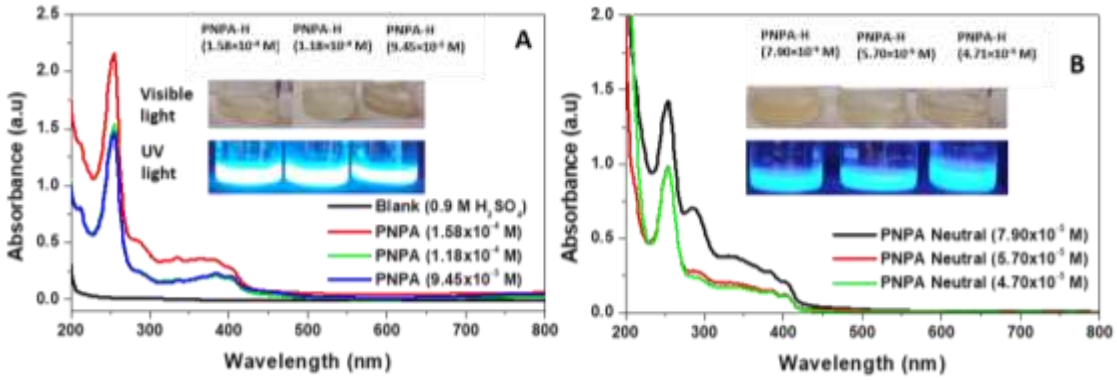

Figure 7.7. *UV-visible absorption spectra of PNPA-H with concentrations 1.58×10^{-4} M, 1.18×10^{-4} M, and 9.45×10^{-5} M A) before neutralisation and B) after neutralisation. Photographs of PNPA-H under visible light and UV light before and after neutralisation is given in the inset.*

7.3.3. Fluorescence stability studies of PNPA-H

The invisible colourless character of PNPA-H solutions was retained even after neutralisation. The stability of fluorescence emission of PNPA-H was checked by keeping PNPA-H solutions with different concentrations like 9.45×10^{-5} M, 1.18×10^{-4} M, 1.58×10^{-4} M, and 2.36×10^{-4} M for ten days. The highly acidic pH of the solutions was changed to pH=3.0, pH=5.0, and pH=7.0, respectively, to observe the changes in the fluorescence intensity with pH during a period of ten days. The photographs of PNPA-H solutions having different concentrations in UV light at pH=3.0, 5.0, and 7.0 in day 1, day 2, day 5,

and day 10 were given in **Figure 7.8**. The fluorescence intensity of the solutions was not affected by the pH and time. The appearance of the same bright bluish-white fluorescence emission of PNPA-H at different pH and time period indicated the stability of PNPA-H.

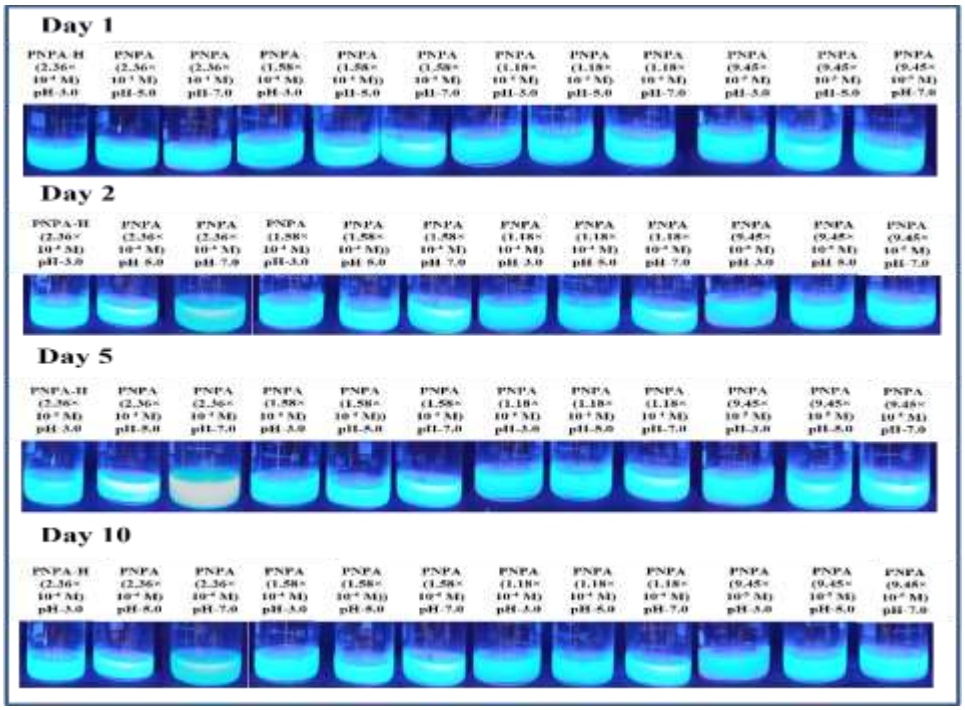

Figure 7.8. *Photographs of PNPA-H with different concentrations like 2.36×10^{-4} M, 1.58×10^{-4} M, 1.18×10^{-4} M, and 9.45×10^{-5} M at pH 3.0, 5.0 and 7.0 under UV light in day 1, day 3, day 5, and day 10.*

7.3.4. Application of PNPA-H on hydrophilic substrates

The PNPA-H solution was colourless in visible light and bright bluish-white light emissive in UV light at acidic and neutral pH. Invisible luminescent materials have potential applications in the anti-counterfeiting field to secure the safety of data and objects [70]. Here, non-fluorescent hydrophilic substrates were changed to fluorescent substrates by simple blending with a very low quantity of PNPA-H. The strong binding of PNPA-H was observed with hydrophilic substrates like filter paper, silica gel and water gel balls to produce bright bluish-white fluorescence emission (see **Figure 7.9**). A piece of ordinary filter paper dipped in acidic PNPA-H solution with a concentration 4.6×10^{-4} M was dried and showed fluorescence emission under UV irradiation at 365 nm (see **Figure 7.9.A**). TLC plate coated with silica gel slurry prepared in 4.6×10^{-4} M acidic PNPA-H solution, after drying, have also shown strong fluorescence emission under UV light (see **Figure 7.9.B**). Similarly, glass fiber dipped into PNPA-H solutions has also

shown fluorescence emission under UV light (**Figure 7.9.D).** Polyvinyl alcohol (PVA) films and gels were also prepared in aqueous medium containing PNPA-H (see **Figure 7.9.C and 7.9.E**). The bluish-white fluorescence emission of PNPA-H was observed in films and gels, indicating the affinity of PNPA-H to the substrates to which it is being applied. Water gel balls are non-toxic super absorbent polymeric beads made of acrylic acid, sodium hydroxide and water that can grow to a hundred times their original size when soaked in water. They are originally invented to keep the moisture in soils for plants. But their non-toxic and beautiful nature made them attractive as a home décor. The colourless and transparent water gel balls have expanded to a big size when soaked in a 4.6×10^{-4} M acidic PNPA-H solution. The bright bluish-white light emission was observed from these water jellies on UV irradiation (see **Figure 7.9.F**). The physically expandable and swellable materials like polyacrylate hydrogels were used in expansion microscopy to magnify biological specimens and enable super-resolution microscopy with an ordinary microscope. Thus, PNPA-H may also find applications in expansion microscopy as it can impart fluorescence emission to hydrophilic and physically expandable materials. The fluorescence emission of PNPA-H, which was retained after the blending and drying process, indicated the stability of the optical characteristics of PNPA-H. The property of PNPA-H to provide fluorescence to hydrophilic materials, to which they have an affinity, by simple blending, indicated the dye-like characteristics of the polymer.

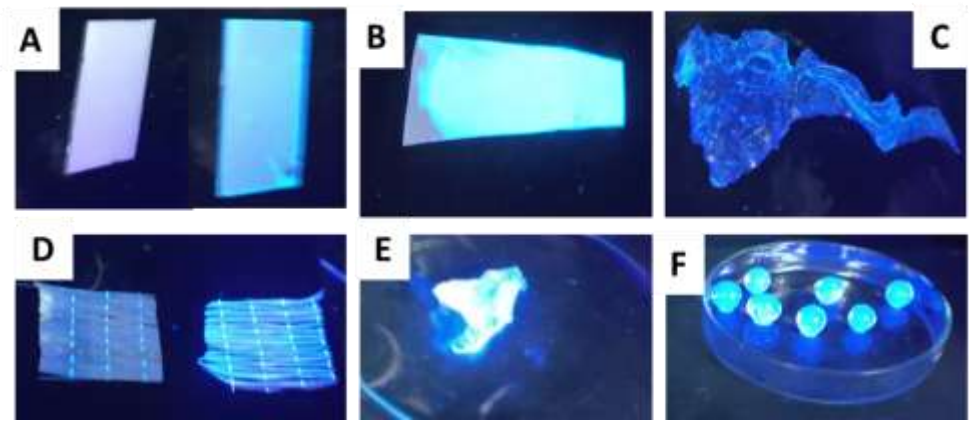

Figure 7.9. *Photographs of different hydrophilic substrates blended with PNPA-H and irradiated under UV light (365 nm). A) Silica TLC plate in the absence and presence of PNPA-H, B) Filter paper coated with PNPA-H, C) PVA film containing PNPA-H, D) Glass fiber in the presence and absence of PNPA-H, E) PVA hydrogel containing PNPA-H and D) PNPA-H incorporated water gel beads.*

7.3.5. Secret writing using PNPA-H

The affinity of fluorescent PNPA-H dye towards hydrophilic substrates was utilized as invisible fluorescent ink to write letters and draw patterns on Whatman filter paper. Initially, the PNPA-H solution with 4.6×10^{-4} M was loaded into an empty pen, which can be used directly as an ink without any coagulations or clogging in the pen. The photographs of handwritten words on the filter paper using acidic PNPA-H solution under UV light and visible light were given in **Figure 7.10**. The invisibility of the letters in visible light and fluorescence emission of the letters in UV light was clear from the photographs. The erasability of fluorescent ink was also explored based on fluorescence quenching of PNPA-H with oxidising analytes, which was mentioned in Chapter 2. The erasibility and re-writability of fluorescent inks are advantageous in the security of the encrypted data. Here we have used Ce (IV) sulphate solution having a concentration of 1×10^{-3} M, which has a pale yellow colour, as an erasing medium. The letter 'M' disappeared by rubbing with cotton dipped in Ce (IV) sulphte solution. The cleared empty space was again utilised to write the letter 'M' with PNPA-H solution (see **Figure 7.10**). The security of the encrypted data could be maintained using erasable and re-writable fluorescent ink. The storage of the data created using acidified PNPA-H solution was difficult due to the acidic nature of PNPA, which could damage documents. The storage issue can be avoided by replacing acidified PNPA-H with neutralised PNPA-H. The stability of fluorescence emission of neutralised PNPA-H on filter paper was checked for one month and the un-faded emission intensity of letters written with PNPA-H indicated their stable emission behaviour.

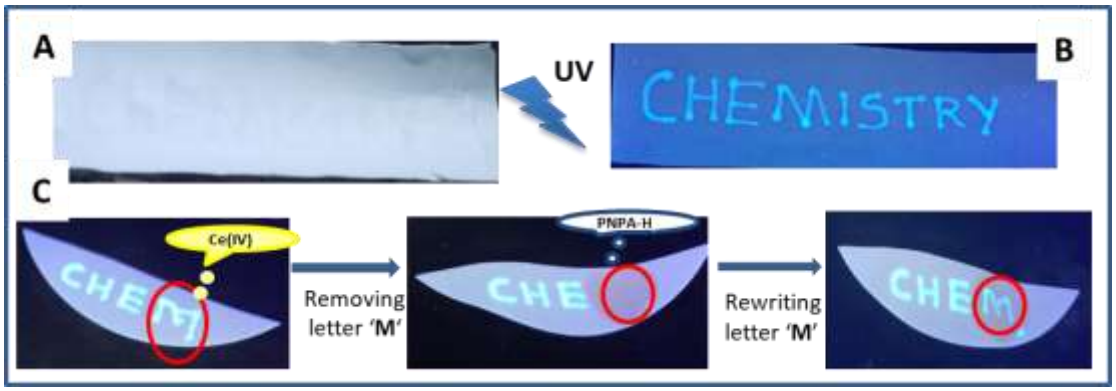

Figure 7.10. *Photographs of letters written using PNPA-H A) in visible light and B) in UV light. C) Removing letter using ce(IV) solution and rewriting letter using PNPA-H under UV light.*

7.3.6. Cytotoxicity and cell imaging using NPA-H and PNPA-H

Cells are the basic unit of all living things, which is made up of cell organelles with specific functions like helping in energy production, growth of organisms, structural support to the body, reproduction etc. The cytological studies using imaging is a fundamental and important analysis to diagnose cell abnormalities [77]. Cancer is developed as a consequence of abnormal cell divisions which destroy body tissues. Therefore, studying cell behavior is important to understand various biological processes and disease conditions. *In vitro* and *in vivo* cell imaging approaches are available, among them, *in vitro* cell imaging is used to study the cell behaviour in precisely controlled conditions and *in vivo* imaging can be used to visualize biological components within living organisms [78]. *In vitro* studies are relatively fast and cost-effective compared to *in vivo* studies. The ethical issues associated with the *in vivo* cell imaging of animal cells can be avoided by *in vitro* imaging. However, the exact cell behaviour in real physiological conditions could not be achieved with in vitro cell imaging studies. Controlled dosing and effective use of chemicals are the advantages of *in vitro* cell imaging [79]. The preliminary studies of chemicals on the cells can be effectively performed by *in vitro* analysis. Here, we have studied the applicability of the polymer PNPA-H and monomer NPA-H as fluorescent probes for imaging normal and cancer cells. The adherent type of mouse fibroblast cell line L929 was chosen as normal cell line and human papillary thyroid cancer cell line MDA-T32 was chosen as cancer cell line. Prior to the cell imaging studies, cytotoxicity of NPA-H and PNPA-H for concentrations 100 nM, 500 nM, 1µM and 10 µM were evaluated using normal cell line L929 and cancer cell line MDA-T32 cells by standard 3-(4,5-dimethylthiazol-2-yl)-2,5- diphenyltetrazolium bromide (MTT) assay over 16 hours incubation time. The plots of cell viability percentage of L929 cells and MDA-T32 cells vs concentrations of NPA-H and PNPA-H were given in **Figure 7.11**. Cell viability of cancer cell MDA-T32 was higher compared to normal cells for both NPA-H and PNPA-H. MDA-T32 cells have shown more than 80% cell viability even with 10µM NPA-H and PNPA-H. Low cytotoxicity differences of NPA-H and PNPA-H towards cancer cells compared to normal cells could be due to the differences between the normal and cancer cell lines in cell proliferation, physiological activities and micro-environments [74 80]. The viability of both cells decreased with increased concentrations of NPA-H and PNPA-H. The cytotoxicity of polymer PNPA-H was less towards normal and cancer cells for every concentration than the monomer NPA-H. Thus, PNPA-H was more

biocompatible with cells compared to NPA-H. Cell viability of 90% and above were obtained for both NPA-H and PNPA-H at 500 nM concentrations, which indicated their low toxicity towards cancer cells and normal cells at 500 nM concentrations. Therefore, both NPA-H and PNPA-H could be safely used for bioimaging and *in vivo* cell imaging as well.

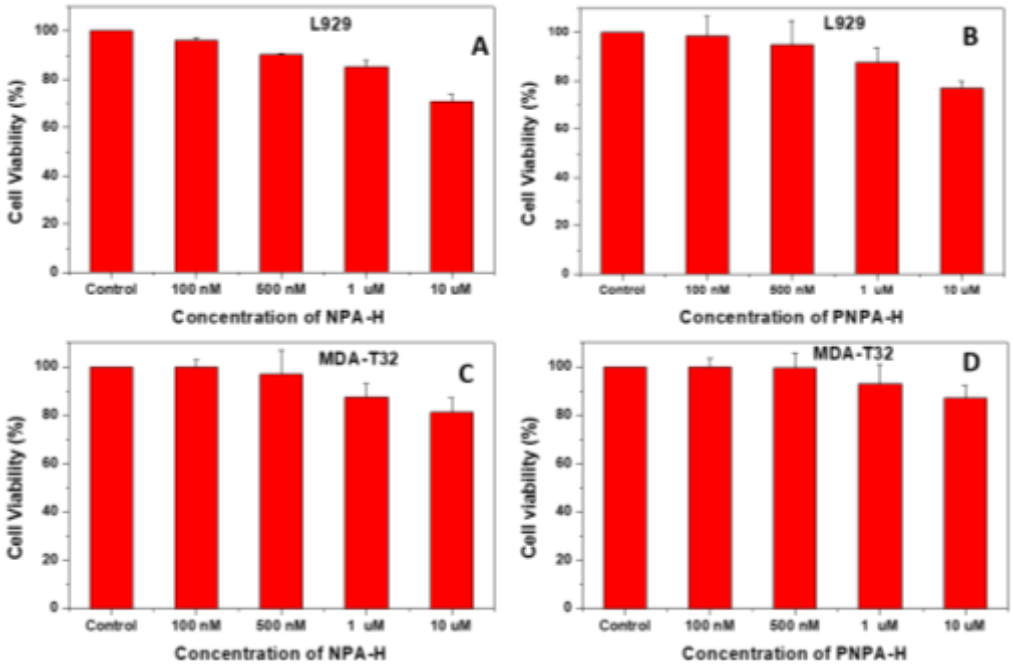

Figure 7.11. *The plot of cell viability percentage of normal cell L929 vs. concentration of A) NPA-H and B) PNPA-H and that of cancer cell MDA-T32 vs. concentration of C) NPA-H and D) PNPA-H, respectively.*

The in-vitro cell imaging and cellular uptake experiments using monomer NPA-H and polymer PNPA-H were performed using normal cell L929 and cancer cell MDA-T32 to study their intracellular behaviours. The normal cells and cancer cells were fixed and incubated with NPA-H and PNPA-H. NPA-H and PNPA-H were slowly internalised into the cells, and fluorescence images were recorded after one week of incubation. The fluorescence microscopy images of L929 cells incubated with NPA-H with 100 nM, 500 nM, 1µM, and 10 µM were excited under the excitation wavelength 365 nm were given in **Figure 7.12**. The blue fluorescence emission observed from the cells in dark field images indicated the good staining of NPA-H towards L929 cells, whereas the cells incubated without NPA-H or PNPA-H (control) did not show any fluorescence in the dark field. The internalisation of NPA-H in L929 cells was clearly observed on merging

dark field and bright field images of L929 cells with 500 nM NPA-H (see **Figure 7.12.B)**. The staining was not very effective for higher concentrations of NPA-H. In order to analyse the staining ability of NPA-H in the cancer cell, MDA-T32 was incubated with different concentrations of NPA-H, and corresponding fluorescence microscopy images were given in **Figure 7.12.C and 7.12.D**. The bright blue fluorescence observed from cancer cells stained with 100 nM NPA-H and higher concentrations of NPA-H indicated the good staining ability of NPA-H towards MDA-T32 at lower and higher concentrations.

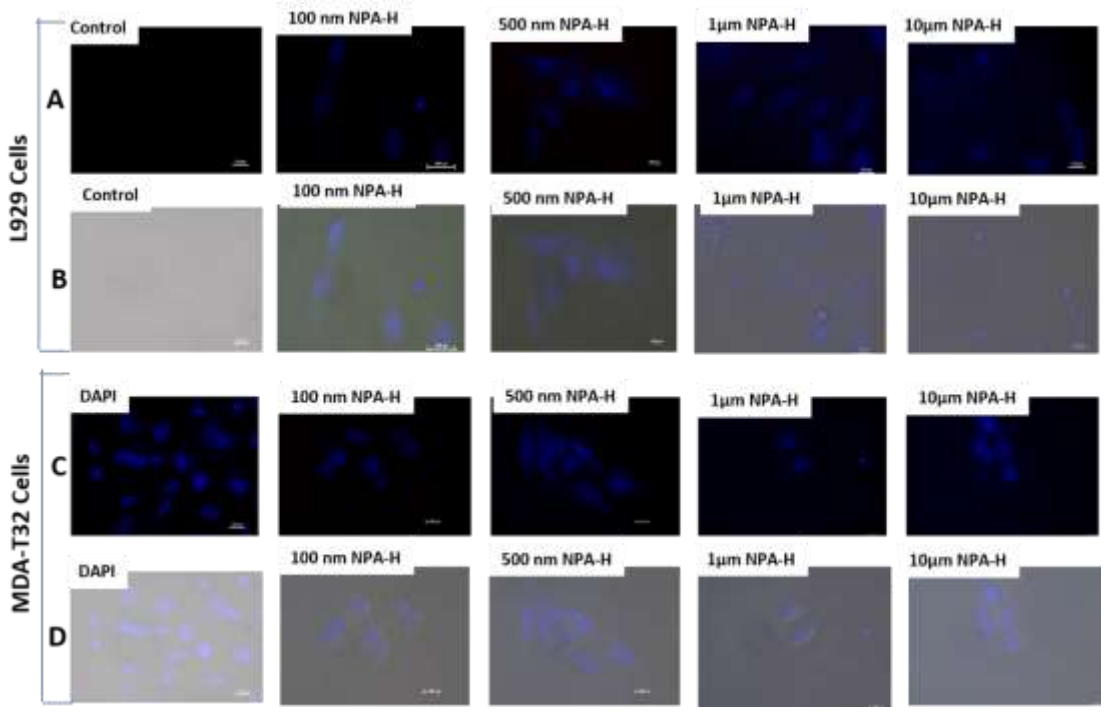

Figure 7.12*. Fluorescence microscopic images of normal cell L929 incubated with control and different concentrations of NPA-H in A) dark field and B) merged dark and bright field. Cancer cell MDA-T32 incubated with DAPI and different concentrations of NPA-H in C) dark field and D) merged dark and bright field under 365 nm excitation.*

The polymer PNPA-H was also subjected to cellular imaging using the same procedure used for NPA-H. The normal cells L929 was incubated with different concentrations of PNPA-H and the fluorescence microscopy images were given in **Figure 7.13.A and 7.13.B**. The blue fluorescence observed from cells under UV excitation indicated the penetration of PNPA-H into the cells. The cell images were more clearly visible on staining with 10µM PNPA-H. The fluorescence microscopy images of cancer cell MDA-T32 stained with PNPA-H was given in **Figure 7.13.C and 7.13.D**. Here also, blue fluorescence was observed on irradiation of UV light of 365 nm. Staining of cancer

cells with low concentrations of PNPA-H, like 100 nM, indicated the affinity of PNPA towards cancer cells. The NPA-H treated cells could emit better fluorescence than PNPA-H, indicating the easier penetration of NPA-H into the cells than PNPA-H. The polymeric structure of PNPA-H may slow down the endocytosis and complete internalisation inside the cell components. The imaging of cancer cell MDA-T32 using NPA-H and PNPA-H was more efficient than normal cells. The cancer cell surface was covered with a layer of negatively charged nine carbon atoms containing sialic acid [81]. The anomalous sialylated glycans can facilitate the cancer cell growth and thereby increasing the negative charge on the cancer cell surface than normal cells [82]. Thus positively charged NPA-H and PNPA-H can easily bind with the negatively charged cancer cells and hence can easily internalise into them than normal cells [83].

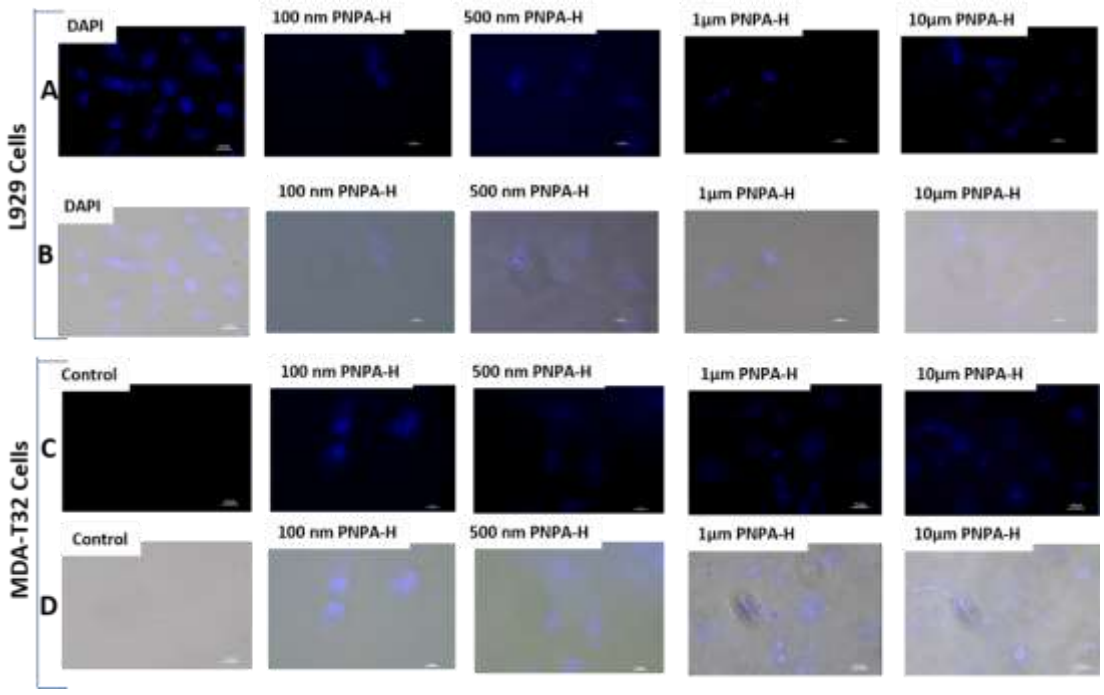

Figure 7.13. *Fluorescence microscopic images of normal cell L929 incubated with DAPI and different concentrations of PNPA-H in A) dark field and B) merged dark and bright field. Cancer cells MDA-T32 incubated with control and different concentrations of PNPA-H in C) dark field and D) merged dark and bright field under 365 nm excitation.*

In this study, we have used 3.5 µM 4', 6 - diamidino-2-phenylindole (DAPI), as a reference to stain the fixed cancer cell. The images of cells under a dark field on UV irradiation were given in **Figure 7.13. A and 7.13.B**. The blue fluorescence was emitted from the nucleus of the cells stained with DAPI, since DAPI was selectively targeted into

the nucleus [53]. The nucleus of the cell is covered with a nuclear membrane, which separates the nucleus from the cytoplasm and small hydrophilic molecules can only diffuse into the nucleus [54]. The NPA-H and PNPA-H were more accumulated into the nucleus, like DAPI, through permeabilization, which was evident from the images of DAPI stained cells and NPA-H or PNPA-H stained cells (see **Figure 7.12 and 7.13**). The hydrophilicity, enhanced through protonation of NPA-H, allowed them to diffuse into the nucleus, whereas the diffusion of PNPA-H was not effective due to their large size. Even though the internalisation of NPA-H and PNPA-H into the nucleus of the cells was slow, the good fluorescence emission from the cells in the dark field under UV light indicated the staining ability of NPA-H and PNPA-H with good biocompatibility. The blue emission from the nucleus of the cells in dark field images and merged images allowed studying the cell properties and nuclear behaviour *in vitro* conditions. The improvements in the hydrophilicity, size, and biocompatibility of NPA-H and PNPA-H would make them suitable for live cell imaging in the future as nuclear-targeted fluoroprobes.

In short, the fluorescent dye-like property of hydrophilic protonated conjugated polymer like PNPA was effectively used to stain different hydrophilic substrates. The invisibility and fluorescence emission of PNPA-H was used to prepare an invisible and erasable fluorescent ink. Further studies on pH optimisation of PNPA-H, incorporating additives to meet the requirement for an ink, and ink properties would lead to the commercial preparation of an invisible fluorescent ink suitable for anticounterfeiting. The nuclear staining ability of monomer NPA-H and polymer PNPA-H in cancer cells opens a platform to develop nuclear stain and nuclear tagged fluorescent probes with further improvements. Thus poly-N-phenyl anthranilic acid is a suitable candidate in both anticounterfieting areas and in bioimaging fields.

7.4. Conclusion

Poly-N-phenyl anthranilic acid was protonated using concentrated H_2SO_4 to improve fluorescence emission, hydrophilicity, and solubility. The suitable conditions for effective protonation was analysed and the stability of fluorescence emission of PNPA-H at different pH was studied. The affinity of PNPA-H towards hydrophilic substrates was used to impart fluorescence to non-fluorescent materials by simple blending with PNPA-H. The invisible, erasable, and rewritable property of PNPA-H was apt for anti-counterfeiting application for secret writing without coagulation. The monomer NPA-H

and polymer PNPA-H exhibited less toxicity towards normal cell L929 and cancer cell MDA-T32. The biocompatible and fluorescent NPA-H and PNPA-H were used to stain L929 and MDA-T32. The bright fluorescence emission from the nucleus of the cells under UV light indicated the successful uptake of PNPA-H and NPA-H. The good fluorescence and hydrophilicity of PNPA-H and NPA-H were effective in nuclear staining. Further studies on optimizing the properties of polymer would explore the potential of PNPA-H in anti-counterfeiting techniques and bio-imaging fields.

Reference

1. Taniguchi, M., & Lindsey, J. S. (2018). Database of Absorption and Fluorescence Spectra of >300 Common Compounds for use in Photochem CAD. *Photochemistry and Photobiology*, *94*(2), 290–327. https://doi.org/10.1111/php.12860.
2. Motson, G. R., Fleming, J. S., & Brooker, S. (2004). *Potential applications for the use of lanthanide complexes as luminescent biolabels* (pp. 361–432). https://doi.org/10.1016/S0898-8838(03)55007-3.
3. Zheng, X. T., Ananthanarayanan, A., Luo, K. Q., & Chen, P. (2015). Glowing Graphene Quantum Dots and Carbon Dots: Properties, Syntheses, and Biological Applications. *Small*, *11*(14), 1620–1636. https://doi.org/10.1002/smll.201402648.
4. Atchudan, R., Jebakumar Immanuel Edison, T. N., Perumal, S., & Lee, Y. R. (2018). Indian Gooseberry-Derived Tunable Fluorescent Carbon Dots as a Promise for In Vitro/In Vivo Multicolor Bioimaging and Fluorescent Ink. *ACS Omega*, *3*(12), 17590–17601. https://doi.org/10.1021/acsomega.8b02463.
5. Tuncel, D., & Demir, H. V. (2010). Conjugated polymer nanoparticles. *Nanoscale*, *2*(4), 484. https://doi.org/10.1039/b9nr00374f.
6. Loudet, A., & Burgess, K. (2007). BODIPY Dyes and Their Derivatives: Syntheses and Spectroscopic Properties. *Chemical Reviews*, *107*(11), 4891–4932. https://doi.org/10.1021/cr078381n.
7. Fan, G., Yang, L., & Chen, Z. (2014). Water-soluble BODIPY and aza-BODIPY dyes: synthetic progress and applications. *Frontiers of Chemical Science and Engineering*, *8*(4), 405–417. https://doi.org/10.1007/s11705-014-1445-7.
8. Clark, M. (2011). *Handbook of textile and industrial dyeing*. Woodhead Publishing Limited. https://doi.org/10.1533/9780857093974.
9. Brackmann, U. (2000). *Lambdachrome ® Laser Dyes*, 2nd ed.; Lambda Physik GmbH, Vol. 3.
10. Magal, E., Weisbrod, N., Yakirevich, A., & Yechieli, Y. (2008). The use of fluorescent dyes as tracers in highly saline groundwater. *Journal of Hydrology*, *358*(1–2), 124–133. https://doi.org/10.1016/j.jhydrol.2008.05.035.
11. Das, K. R., & Antony, M. J. (2022). Microscale Redox Titrations Using Poly- *N* -phenyl Anthranilic Acid Fluorescent Turn-Off Indicator for Undergraduate Analytical Chemistry Lab. *Journal of Chemical Education*, *99*(2), 892–901. https://doi.org/10.1021/acs.jchemed.0c01354.
12. Sagi, S. R., & Rao, G. G. (1962). Titrimetric determination of molybdenum (V) and uranium(IV) with ceric sulphate using rhodamine 6G as a fluorescent indicator. *Fresenius' Zeitschrift Für Analytische Chemie*, *189*(3), 229–243. https://doi.org/10.1007/BF00497570.
13. Goetzberger, A., & Greube, W. (1977). Solar energy conversion with fluorescent collectors. *Applied Physics*, *14*(2), 123–139. https://doi.org/10.1007/BF00883080.

14. Kong, D., Zhang, K., Tian, J., Yin, L., & Sheng, X. (2022). Biocompatible and Biodegradable Light-Emitting Materials and Devices. *Advanced Materials Technologies*, *7*(2). https://doi.org/10.1002/admt.202100006.
15. Baatout, K., Saad, F., Baffoun, A., Mahltig, B., Kreher, D., Jaballah, N., & Majdoub, M. (2019). Luminescent cotton fibers coated with fluorescein dye for anti-counterfeiting applications. *Materials Chemistry and Physics*, *234*, 304–310. https://doi.org/10.1016/j.matchemphys.2019.06.007.
16. Bandi, R., Devulapalli, N. P., Dadigala, R., Gangapuram, B. R., & Guttena, V. (2018). Facile Conversion of Toxic Cigarette Butts to N,S-Codoped Carbon Dots and Their Application in Fluorescent Film, Security Ink, Bioimaging, Sensing and Logic Gate Operation. *ACS Omega*, *3*(10), 13454–13466. https://doi.org/10.1021/acsomega.8b01743.
17. Abdollahi, A., Roghani-Mamaqani, H., Razavi, B., & Salami-Kalajahi, M. (2020). Photoluminescent and Chromic Nanomaterials for Anticounterfeiting Technologies: Recent Advances and Future Challenges. *ACS Nano*, *14*(11), 14417–14492. https://doi.org/10.1021/acsnano.0c07289.
18. Sonawane, S. L., & Asha, S. K. (2016). Fluorescent Polystyrene Microbeads as Invisible Security Ink and Optical Vapor Sensor for 4-Nitrotoluene. *ACS Applied Materials & Interfaces*, *8*(16), 10590–10599. https://doi.org/10.1021/acsami.5b12325.
19. Mondal, T. K., & Saha, S. K. (2019). Facile Approach To Synthesize Nitrogen- and Oxygen-Rich Carbon Quantum Dots for pH Sensor, Fluorescent Indicator, and Invisible Ink Applications. *ACS Sustainable Chemistry & Engineering*, *7*(24), 19669–19678. https://doi.org/10.1021/acssuschemeng.9b04817.
20. Chen, L., Hu, B., Zhang, J., Zhang, J., Huang, S., Ren, P., Zou, Y., Ding, F., Liu, X., & Li, H. (2019). A facile synthesis of 1,3,6,8-pyrenesulfonic acid tetrasodium salt as a hydrosoluble fluorescent ink for anti-counterfeiting applications. *RSC Advances*, *9*(1), 476–481. https://doi.org/10.1039/C8RA09106D.
21. Tsai, W.-K., Lai, Y.-S., Tseng, P.-J., Liao, C.-H., & Chan, Y.-H. (2017). Dual Colorimetric and Fluorescent Authentication Based on Semiconducting Polymer Dots for Anticounterfeiting Applications. *ACS Applied Materials & Interfaces*, *9*(36), 30918–30924. https://doi.org/10.1021/acsami.7b08993.
22. Abdollahi, A., Sahandi-Zangabad, K., & Roghani-Mamaqani, H. (2018). Rewritable Anticounterfeiting Polymer Inks Based on Functionalized Stimuli-Responsive Latex Particles Containing Spiropyran Photoswitches: Reversible Photopatterning and Security Marking. *ACS Applied Materials & Interfaces*, *10*(45), 39279–39292. https://doi.org/10.1021/acsami.8b14865.
23. Abdollahi, A., Alidaei-Sharif, H., Roghani-Mamaqani, H., & Herizchi, A. (2020). Photoswitchable fluorescent polymer nanoparticles as high-security anticounterfeiting materials for authentication and optical patterning. *Journal of Materials Chemistry C*, *8*(16), 5476–5493. https://doi.org/10.1039/D0TC00937G.
24. Chang, K., Liu, Z., Chen, H., Sheng, L., Zhang, S. X.-A., Chiu, D. T., Yin, S., Wu, C., & Qin, W. (2014). Conjugated Polymer Dots for Ultra-Stable Full-Color Fluorescence Patterning. *Small*, n/a-n/a. https://doi.org/10.1002/smll.201401436.
25. Díaz-García, M. E., & Badía-Laíño, R. (2018). Fluorescence: Overview ☆. In *Reference Module in Chemistry, Molecular Sciences and Chemical Engineering*. Elsevier. https://doi.org/10.1016/B978-0-12-409547-2.11182-5.
26. Borisov, S. M., & Wolfbeis, O. S. (2008). Optical Biosensors. *Chemical Reviews*, *108*(2), 423–461. https://doi.org/10.1021/cr068105t.
27. Gota, C., Okabe, K., Funatsu, T., Harada, Y., & Uchiyama, S. (2009). Hydrophilic Fluorescent Nanogel Thermometer for Intracellular Thermometry. *Journal of the American Chemical Society*, *131*(8), 2766–2767. https://doi.org/10.1021/ja807714j.
28. Tu Phan, L. M. (2023). Carbon dot-based microscopic techniques for cell imaging. In *Carbon Dots in Analytical Chemistry* (pp. 271–277). Elsevier. https://doi.org/10.1016/B978-0-323-98350-1.00005-0.

29. Zeng, L., Miller, E. W., Pralle, A., Isacoff, E. Y., & Chang, C. J. (2006). A Selective Turn-On Fluorescent Sensor for Imaging Copper in Living Cells. *Journal of the American Chemical Society*, *128*(1), 10–11. https://doi.org/10.1021/ja055064u.
30. Domaille, D. W., Que, E. L., & Chang, C. J. (2008). Erratum: Corrigendum: Synthetic fluorescent sensors for studying the cell biology of metals. *Nature Chemical Biology*, *4*(8), 507–507. https://doi.org/10.1038/nchembio0808-507.
31. Nienhaus, K., & Ulrich Nienhaus, G. (2014). Fluorescent proteins for live-cell imaging with super-resolution. *Chem. Soc. Rev.*, *43*(4), 1088–1106. https://doi.org/10.1039/C3CS60171D.
32. De, M., Rana, S., Akpinar, H., Miranda, O. R., Arvizo, R. R., Bunz, U. H. F., & Rotello, V. M. (2009). Sensing of proteins in human serum using conjugates of nanoparticles and green fluorescent protein. *Nature Chemistry*, *1*(6), 461–465. https://doi.org/10.1038/nchem.334.
33. Donner, J. S., Thompson, S. A., Kreuzer, M. P., Baffou, G., & Quidant, R. (2012). Mapping Intracellular Temperature Using Green Fluorescent Protein. *Nano Letters*, *12*(4), 2107–2111. https://doi.org/10.1021/nl300389y.
34. Gao, Z., Zhang, X., Zheng, M., & Chen, Y. (2015). Synthesis of a water soluble red fluorescent dye and its application to living cells imaging. *Dyes and Pigments*, *120*, 37–43. https://doi.org/10.1016/j.dyepig.2015.04.010.
35. Gwozdzinska, P., Pawlowska, R., Milczarek, J., Garner, L. E., Thomas, A. W., Bazan, G. C., & Chworos, A. (2014). Phenylenevinylene conjugated oligoelectrolytes as fluorescent dyes for mammalian cell imaging. *Chem. Commun.*, *50*(94), 14859–14861. https://doi.org/10.1039/C4CC06478J.
36. Feng, G., Ding, D., & Liu, B. (2012). Fluorescence bioimaging with conjugated polyelectrolytes. *Nanoscale*, *4*(20), 6150. https://doi.org/10.1039/c2nr31392h.
37. Li, K., & Liu, B. (2012). Polymer encapsulated conjugated polymernanoparticles for fluorescence bioimaging. *J. Mater. Chem.*, *22*(4), 1257–1264. https://doi.org/10.1039/C1JM14397B.
38. Wang, Y., & Liu, B. (2009). Conjugated Polyelectrolyte-Sensitized Fluorescent Detection of Thrombin in Blood Serum Using Aptamer-Immobilized Silica Nanoparticles as the Platform. *Langmuir*, *25*(21), 12787–12793. https://doi.org/10.1021/la901703p.
39. Wang, Y., Hu, R., Lin, G., Roy, I., & Yong, K.-T. (2013). Functionalized Quantum Dots for Biosensing and Bioimaging and Concerns on Toxicity. *ACS Applied Materials & Interfaces*, *5*(8), 2786–2799. https://doi.org/10.1021/am302030a.
40. Huang, X., & Tang, M. (2021). Research advance on cell imaging and cytotoxicity of different types of quantum Dots. *Journal of Applied Toxicology*, *41*(3), 342–361. https://doi.org/10.1002/jat.4083.
41. Kowada, T., Maeda, H., & Kikuchi, K. (2015). BODIPY-based probes for the fluorescence imaging of biomolecules in living cells. *Chemical Society Reviews*, *44*(14), 4953–4972. https://doi.org/10.1039/C5CS00030K.
42. Shaner, N. C., Lin, M. Z., McKeown, M. R., Steinbach, P. A., Hazelwood, K. L., Davidson, M. W., & Tsien, R. Y. (2008). Improving the photostability of bright monomeric orange and red fluorescent proteins. *Nature Methods*, *5*(6), 545–551. https://doi.org/10.1038/nmeth.1209.
43. Yang, J., Zhang, Y., Gautam, S., Liu, L., Dey, J., Chen, W., Mason, R. P., Serrano, C. A., Schug, K. A., & Tang, L. (2009). Development of aliphatic biodegradable photoluminescent polymers. *Proceedings of the National Academy of Sciences*, *106*(25), 10086–10091. https://doi.org/10.1073/pnas.0900004106.
44. McRae, R. L., Phillips, R. L., Kim, I.-B., Bunz, U. H. F., & Fahrni, C. J. (2008). Molecular Recognition Based on Low-Affinity Polyvalent Interactions: Selective Binding of a Carboxylated Polymer to Fibronectin Fibrils of Live Fibroblast Cells. *Journal of the American Chemical Society*, *130*(25), 7851–7853. https://doi.org/10.1021/ja8007402.
45. Zhu, C., Liu, L., Yang, Q., Lv, F., & Wang, S. (2012). Water-Soluble Conjugated Polymers for Imaging, Diagnosis, and Therapy. *Chemical Reviews*, *112*(8), 4687–4735. https://doi.org/10.1021/cr200263w.

46. Traina, C. A., Bakus, R. C., & Bazan, G. C. (2011). Design and Synthesis of Monofunctionalized, Water-Soluble Conjugated Polymers for Biosensing and Imaging Applications. *Journal of the American Chemical Society*, *133*(32), 12600–12607. https://doi.org/10.1021/ja202877q.
47. Wang, F., Li, M., Wang, B., Zhang, J., Cheng, Y., Liu, L., Lv, F., & Wang, S. (2015). Synthesis and Characterization of Water-Soluble Polythiophene Derivatives for Cell Imaging. *Scientific Reports*, *5*(1), 7617. https://doi.org/10.1038/srep07617.
48. Feng, X., Liu, L., Wang, S., & Zhu, D. (2010). Water-soluble fluorescent conjugated polymers and their interactions with biomacromolecules for sensitive biosensors. *Chemical Society Reviews*, *39*(7), 2411. https://doi.org/10.1039/b909065g.
49. Moon, J. H., Mendez, E., Kim, Y., & Kaur, A. (2011). Conjugated polymer nanoparticles for small interfering RNA delivery. *Chemical Communications*, *47*(29), 8370. https://doi.org/10.1039/c1cc10991j.
50. McRae, R. L., Phillips, R. L., Kim, I.-B., Brunz, U. H. F., & Fahrni, C. J. (2008). Molecular Recognition Based on Low-Affinity Polyvalent Interactions: Selective Binding of a Carboxylated Polymer to Fibronectin Fibrils of Live Fibroblast Cells. *Journal of the American Chemical Society*, *130*(25), 7851–7853. https://doi.org/10.1021/ja8007402.
51. Behrendt, J. M., Nagel, D., Chundoo, E., Alexander, L. M., Dupin, D., Hine, A. v., Bradley, M., & Sutherland, A. J. (2013). Synthesis and Characterization of Dual-Functionalized Core-Shell Fluorescent Microspheres for Bioconjugation and Cellular Delivery. *PLoS ONE*, *8*(3), e50713. https://doi.org/10.1371/journal.pone.0050713.
52. Alexander, L. M., Pernagallo, S., Livigni, A., Sánchez-Martín, R. M., Brickman, J. M., & Bradley, M. (2010). Investigation of microsphere-mediated cellular delivery by chemical, microscopic and gene expression analysis. *Mol. BioSyst.*, *6*(2), 399–409. https://doi.org/10.1039/B914428E.
53. Hu, C., Xu, S., Song, Z., Li, H., & Liu, H. (2023). Recent Advance in Nucleus-Targeted Fluorescent Probes for Bioimaging, Detection and Therapy. *Chemosensors*, *11*(2), 125. https://doi.org/10.3390/chemosensors11020125.
54. Long, X., Zhang, X., Chen, Q., Liu, M., Xiang, Y., Yang, Y., Xiao, Z., Huang, J., Wang, X., Liu, C., Nan, Y., & Huang, Q. (2022). Nucleus-Targeting Phototherapy Nanodrugs for High-Effective Anti-Cancer Treatment. *Frontiers in Pharmacology*, *13*. https://doi.org/10.3389/fphar.2022.905375.
55. Sikdar, S., Mukherjee, A., Boujedaini, N., & Khuda-Bukhsh, A. R. (2013). Ethanolic extract of Condurango (Marsdenia condurango) used in traditional systems of medicine including homeopathy against cancer can induce DNA damage and apoptosis in non small lung cancer cells, A549 and H522, in vitro. *Tang [Humanitas Medicine]*, *3*(1), 9.1-9.10. https://doi.org/10.5667/tang.2012.0044.
56. Kaneko, M., Ishihara, K., & Nakanishi, S. (2020). Redox-Active Polymers Connecting Living Microbial Cells to an Extracellular Electrical Circuit. *Small*, *16*(34), 2001849. https://doi.org/10.1002/smll.202001849.
57. Kapuscinski, J. (1995). DAPI: a DNA-Specific Fluorescent Probe. *Biotechnic & Histochemistry*, *70*(5), 220–233. https://doi.org/10.3109/10520299509108199.
58. Chen, T. R. (1977). In situ detection of mycoplasma contamination in cell cultures by fluorescent Hoechst 33258 stain. *Experimental Cell Research*, *104*(2), 255–262. https://doi.org/10.1016/0014-4827(77)90089-1.
59. Gill, M. R., Garcia-Lara, J., Foster, S. J., Smythe, C., Battaglia, G., & Thomas, J. A. (2009). A ruthenium(II) polypyridyl complex for direct imaging of DNA structure in living cells. *Nature Chemistry*, *1*(8), 662–667. https://doi.org/10.1038/nchem.406.
60. Li, C., Yu, M., Sun, Y., Wu, Y., Huang, C., & Li, F. (2011). A Nonemissive Iridium(III) Complex That Specifically Lights-Up the Nuclei of Living Cells. *Journal of the American Chemical Society*, *133*(29), 11231–11239. https://doi.org/10.1021/ja202344c.
61. Horobin, R. W., Stockert, J. C., & Rashid-Doubell, F. (2006). Fluorescent cationic probes for nuclei of living cells: why are they selective? A quantitative structure–activity relations analysis. *Histochemistry and Cell Biology*, *126*(2), 165–175. https://doi.org/10.1007/s00418-006-0156-7.

62. Li, M., Nie, C., Feng, L., Yuan, H., Liu, L., Lv, F., & Wang, S. (2014). Conjugated Polymer Nanoparticles for Cell Membrane Imaging. *Chemistry - An Asian Journal*, *9*(11), 3121–3124. https://doi.org/10.1002/asia.201402711.
63. Zhou, L., Lv, F., Liu, L., & Wang, S. (2017). Polarity Conversion of Conjugated Polymer for Lysosome Escaping. *ACS Applied Materials & Interfaces*, *9*(33), 27427–27432. https://doi.org/10.1021/acsami.7b10105.
64. Ye, F., Wu, C., Jin, Y., Wang, M., Chan, Y.-H., Yu, J., Sun, W., Hayden, S., & Chiu, D. T. (2012). A compact and highly fluorescent orange-emitting polymer dot for specific subcellular imaging. *Chemical Communications*, *48*(12), 1778. https://doi.org/10.1039/c2cc16486h.
65. Twomey, M., Mendez, E., Manian, R. K., Lee, S., & Moon, J. H. (2016). Mitochondria-specific conjugated polymer nanoparticles. *Chemical Communications*, *52*(27), 4910–4913. https://doi.org/10.1039/C6CC00810K.
66. Liu, H.-Y., Wu, P.-J., Kuo, S.-Y., Chen, C.-P., Chang, E.-H., Wu, C.-Y., & Chan, Y.-H. (2015). Quinoxaline-Based Polymer Dots with Ultrabright Red to Near-Infrared Fluorescence for In Vivo Biological Imaging. *Journal of the American Chemical Society*, *137*(32), 10420–10429. https://doi.org/10.1021/jacs.5b06710.
67. Nandi, N., Gaurav, S., Sarkar, P., Kumar, S., & Sahu, K. (2021). Multifunctional N-Doped Carbon Dots for Bimodal Detection of Bilirubin and Vitamin B_{12}, Living Cell Imaging, and Fluorescent Ink. *ACS Applied Bio Materials*, *4*(6), 5201–5211. https://doi.org/10.1021/acsabm.1c00371.
68. Mitra, M., Mahapatra, M., Dutta, A., Deb, M., Dutta, S., Chattopadhyay, P. K., Roy, S., Banerjee, S., Sil, P. C., & Singha, N. R. (2020). Fluorescent Guar Gum- *g* -Terpolymer via In Situ Acrylamido-Acid Fluorophore-Monomer in Cell Imaging, Pb(II) Sensor, and Security Ink. *ACS Applied Bio Materials*, *3*(4), 1995–2006. https://doi.org/10.1021/acsabm.9b01146.
69. Atchudan, R., Edison, T. N. J. I., Aseer, K. R., Perumal, S., & Lee, Y. R. (2018). Hydrothermal conversion of Magnolia liliiflora into nitrogen-doped carbon dots as an effective turn-off fluorescence sensing, multi-colour cell imaging and fluorescent ink. *Colloids and Surfaces B: Biointerfaces*, *169*, 321–328. https://doi.org/10.1016/j.colsurfb.2018.05.032.
70. Ma, H., Sun, C., Xue, G., Wu, G., Zhang, X., Han, X., Qi, X., Lv, X., Sun, H., & Zhang, J. (2019). Facile synthesis of fluorescent carbon dots from Prunus cerasifera fruits for fluorescent ink, Fe^{3+} ion detection and cell imaging. *Spectrochimica Acta Part A: Molecular and Biomolecular Spectroscopy*, *213*, 281–287. https://doi.org/10.1016/j.saa.2019.01.079.
71. Atchudan, R., Edison, T. N. J. I., Aseer, K. R., Perumal, S., Karthik, N., & Lee, Y. R. (2018). Highly fluorescent nitrogen-doped carbon dots derived from Phyllanthus acidus utilized as a fluorescent probe for label-free selective detection of Fe3+ ions, live cell imaging and fluorescent ink. *Biosensors and Bioelectronics*, *99*, 303–311. https://doi.org/10.1016/j.bios.2017.07.076.
72. Wang, Z., Chen, D., Gu, B., Gao, B., Wang, T., Guo, Q., & Wang, G. (2020). Biomass-derived nitrogen doped graphene quantum dots with color-tunable emission for sensing, fluorescence ink and multicolor cell imaging. *Spectrochimica Acta Part A: Molecular and Biomolecular Spectroscopy*, *227*, 117671. https://doi.org/10.1016/j.saa.2019.117671.
73. Shi, L., Li, Y., Li, X., Wen, X., Zhang, G., Yang, J., Dong, C., & Shuang, S. (2015). Facile and eco-friendly synthesis of green fluorescent carbon nanodots for applications in bioimaging, patterning and staining. *Nanoscale*, *7*(16), 7394–7401. https://doi.org/10.1039/C5NR00783F.
74. Bandi, R., Devulapalli, N. P., Dadigala, R., Gangapuram, B. R., & Guttena, V. (2018). Facile Conversion of Toxic Cigarette Butts to N,S-Codoped Carbon Dots and Their Application in Fluorescent Film, Security Ink, Bioimaging, Sensing and Logic Gate Operation. *ACS Omega*, *3*(10), 13454–13466. https://doi.org/10.1021/acsomega.8b01743.
75. Zhou, W., Chen, Y., Yu, Q., Li, P., Chen, X., & Liu, Y. (2019). Photoresponsive cyclodextrin/anthracene/Eu^{3+} supramolecular assembly for a tunable photochromic

multicolor cell label and fluorescent ink. *Chemical Science*, *10*(11), 3346–3352. https://doi.org/10.1039/C9SC00026G.

76. Mujtaba Karim, S., & Samuel, R. (1934). Absorption spectra of the sulphite and sulphate ions. *Proceedings of the Indian Academy of Sciences - Section A*, *1*(6), 398–406. https://doi.org/10.1007/BF03035583.
77. Thomas Dean Pollard. (2017). William C. Earnshaw, Jennifer Lippincott-Schwartz, G. T. J. *Cell Biology*; Elsevier Ltd.
78. Gao, H., & Chen, S. (2019). AIEgen-Based Fluorescent Nanoparticles for Long-Term Cell Tracing. In *Theranostic Bionanomaterials* (pp. 359–375). Elsevier. https://doi.org/10.1016/B978-0-12-815341-3.00016-X.
79. Fröhlich, E., & Salar-Behzadi, S. (2014). Toxicological Assessment of Inhaled Nanoparticles: Role of in Vivo, ex Vivo, in Vitro, and in Silico Studies. *International Journal of Molecular Sciences*, *15*(3), 4795–4822. https://doi.org/10.3390/ijms15034795.
80. Mondal, A., Sen, U., Roy, N., Muthukumar, V., Sahoo, S. K., Bose, B., & Paira, P. (2021). DNA targeting half sandwich Ru(II)- *p* -cymene-N^N complexes as cancer cell imaging and terminating agents: influence of regioisomers in cytotoxicity. *Dalton Transactions*, *50*(3), 979–997. https://doi.org/10.1039/D0DT03107K.
81. Munkley, J., & Scott, E. (2019). Targeting Aberrant Sialylation to Treat Cancer. *Medicines*, *6*(4), 102. https://doi.org/10.3390/medicines6040102.
82. Ghirardello, M., Shyam, R., & Galan, M. C. (2022). Reengineering of cancer cell surface charges can modulate cell migration. *Chemical Communications*, *58*(36), 5522–5525. https://doi.org/10.1039/D2CC00402J.
83. Tansi, F. L., Filatova, M. P., Koroev, D. O., Volpina, O. M., Lange, S., Schumann, C., Teichgräber, U. K., Reissmann, S., & Hilger, I. (2019). New generation CPPs show distinct selectivity for cancer and noncancer cells. *Journal of Cellular Biochemistry*, *120*(4), 6528–6541. https://doi.org/10.1002/jcb.27943.

CHAPTER 8

Summary and Conclusions

Conjugated polymers are highly demanded materials due to their characteristic properties like light absorption, fluorescence emission, conductivity, thermal stability, and eco-friendliness, which have effective applications in different fields. Thus, the synthesis of conjugated polymers and studies on their novel applications utilizing their characteristic properties are highly desired. Poly-N-phenyl aniline derivatives, their optical properties, and their functional applications were less explored. In this work, studies on the synthesis and characterizations of poly-N-phenylaniline derivatives like poly-N-phenyl anthranilic acid, poly-N-phenyl-o-phenylenediamine and copolymers of N-phenyl anthranilic acid and o-phenylenediamine were conducted. The applications of these polymers as fluorescent sensors, colorimetric sensors, fluorescent indicators, and fluorescent dye for cell imaging were also explored. **Chapter 1** includes an introduction on conjugated polymers, types of conjugated polymers, their properties and synthetic methods adopted for their preparations. A literature review on the properties and general applications of conjugated polymers in sensors, electric and electronic fields, and biological areas were also discussed.

In **Chapter 2**, poly-N-phenyl anthranilic acid (PNPA) was synthesized via chemical oxidative polymerization using $FeCl_3$ as oxidizing agent in ethanol medium. The bright bluish-white light fluorescence emission of PNPA in an acidic medium (PNPA-H) was effectively used to sense oxidizing analytes like MnO_4^-, Ce^{4+}, and $Cr_2O_7^{2-}$. The mole ratio of analytes required for the quenching of fluorescence of polymer was determined using naked-eye fluorescence detection, UV-visible absorption spectra, and fluorescence spectra. The fluorescence quenching mechanism was explained by the oxidation of PNPA-H from its fluorescent reduced form to a non-fluorescent oxidized form. The redox reversibility of the polymer was determined from the fluorescence reappearance of oxidized PNPA-H on adding reducing analytes like ascorbic acid and from the electrochemical studies. In **Chapter 3**, the application of poly-N-phenyl anthranilic acid (PNPA-H) and N-phenyl anthranilic acid (NPA-H) as fluorescent indicators in microscale redox titrations were studied. Microscale redox titrations with micromolar concentration and semi-micromolar volumes of analyes were carried out for the estimation of ferrous ion using permanganometry, cerimetry and dichrometry by utilizing fluorescent indicating actions of PNPA-H and NPA-H. The sharp fluorescence quenching at the endpoint was explained based on the

oxidation of PNPA-H and NPA-H, which was confirmed from UV-visible absorption spectra. Method validations using statistical analysis like normal distribution curves, student's t test, and F test suggested good precision and accuracy of estimated masses of ferrous ion using fluorescent indicators. In addition, a microscale redox titration experiment was designed for chemistry students and their feedbacks were evaluated.

Chapter 4 deals with the synthesis and characterization of poly-N-phenyl-o-phenylenediamine (PPOPD) using chemical oxidative polymerization with $FeCl_3$ as oxidizing agent in ethanol medium. The pH-dependent colour changes of PPOPD from an orange-coloured neutral solution to a pink-coloured acidic solution and a yellow-coloured basic solution were evident from the UV-visible absorption spectra. The absorbance of aqueous solution of PPOPD at 518 nm showed a linear increase with a decrease in pH below 1.5, which was used to develop a colorimetric acid content sensor. The battery acid content of lead acid batteries, which was changing on charging and discharging, was determined using the calibration plot of absorbance of PPOPD at 518 nm with known acid percentage. The state of charge (SoC) of 12 V lead acid battery was calculated using an empirical formula by setting upper limit and lower limit of absorbances as absorbance of PPOPD with 40% and 10% sulphuric acid content at 518 nm, respectively. The good agreement between SoC determined from absorbance and open circuit voltage indicated the accuracy of the proposed method.

In Chapter 5, poly-o-phenylenediamine (POPD) was synthesized by chemical oxidative polymerization using $FeCl_3$ as an oxidizing agent in an ethanol medium. POPD has intense yellow fluorescence in aqueous solution and was quenched on oxidation with $AgNO_3$ solutions. The mole ratio of $AgNO_3$ required for fluorescence quenching was determined using naked-eye fluorescence detection and fluorescence spectra. The reversibility of redox states in POPD was evident from the enhanced yellow fluorescence of oxidized POPD on reduction with $NaBH_4$ and electrochemical studies. **Chapter 6** includes the synthesis and characterization of copolymers of N-phenyl anthranilic acid (NPA) and o-phenylenediamine (OPD) via chemical oxidative polymerization using $FeCl_3$ as an oxidizing agent by varying the co-monomer weight percentage. The structure and properties of copolymers were compared with physical blends prepared by mixing PNPA and POPD by grinding. The monomer reactivity ratio calculated by the Finemann-Ross method using FT-IR data indicated the

possibility of block-type copolymerization and higher reactivity of NPA. The combination of the blue fluorescence of PNPA and the yellow fluorescence of POPD produced attractive fluorescence colours in physical blends. A selective fluorescence sensing of the oxidizing power of analytes using copolymer P(NPA-co-OPD) 10:90 was achieved. The copolymer showed a change in fluorescence from yellow to blue on adding $AgNO_3$, indicating the semi-oxidation of POPD and a further change from blue fluorescence to colourless on adding $KMnO_4$, indicating the complete oxidation of PNPA and POPD fragments.

In **Chapter 7**, a fluorescent dye was developed using PNPA-H, and their applications in anticounterfeiting and cell imaging were studied. The hydrophilicity of PNPA-H was utilized to produce fluorescence in non-fluorescent materials. The invisibility and erasability of PNPA-H was effectively used for secret writing. The less cytotoxicity of NPA-H and PNPA-H towards normal cell line L929 and cancer cell line MDA-T32 indicated their good biocompatibility. The cellular imaging studies of L929 and MDA-T32 using NPA-H and PNPA-H indicated their selective nuclear staining ability.

FUTURE SCOPE

The characteristic optical and fluorescent properties of conjugated polymers would make them highly promising materials for optoelectronic and sensing applications. We have studied the optical and fluorescence properties of some poly-N-phenyl aniline derivatives and their copolymers. Some of their applications, like sensing, bio-imaging and anti-counterfeiting were reported. The future scope includes the following.

- The protonation strategy would provide a novel approach to develop fluorescence in conjugated polymers.
- The fluorescence indicating action of PNPA-H would be effective to quantify other biologically relevant redox analytes like ascorbic acid, and calcium oxalate in micromolar quantities.
- The extensive studies on the PNPA-H-based ink would lead to the commercial preparation of invisible secret ink.

- Further studies on cell imaging would explore the potential of PNPA-H in the biomedical field.

Publications and Conference Presentations

Journal Papers-published

1. K. Rohini Das and M Jinish Antony* "Acid content sensitive colorimetry of poly-N-phenyl-o-phenylenediamine for state of charge determination of lead-acid battery". *Journal of Energy Storage*. Vol: 86, year: 2024, page: 111193. *Publisher: Elsevier*. DOI: https://doi.org/10.1016/j.est.2024.111193.

2. K. Rohini Das and M Jinish Antony* "Silver Ion-Induced Reversible Turn-Off Fluorescence in Redox States of Poly-*o*-phenylenediamine". *Industrial & Engineering Chemistry Research*. Vol: 63, year: 2024, page: 2087-2099. *Publisher: ACS*. DOI: https://doi.org/10.1021/acs.iecr.3c03380.
3. K. Rohini Das and M Jinish Antony* "Microscale Redox Titrations using Poly-N-phenyl Anthranilic Acid Fluorescent Turn-Off Indicator for Undergraduate Analytical Chemistry Lab". *Journal of Chemical Education*. Vol: 99, year: 2022, page: 892-901. *Publisher: ACS*. DOI: https://doi.org/10.1021/acs.jchemed.0c01354.
4. K. Rohini Das, M Jinish Antony*, and Shinto Varghese "Highly Bluish White Light Emissive and Redox Active conjugated Poly-N-phenyl anthranilic acid polymer fluoroprobe for analytical sensing". *Polymer*. Vol: 181, year: 2019, page: 121747. *Publisher: Elsevier*. DOI: https://doi.org/10.1016/j.polymer.2019.121747.
5. K. Rohini Das and M Jinish Antony* "Synthesis and characterization of water dispersible copolymer submicron spheres of poly-(phenylenediamine-co-N-sulfopropylaniline) via random copolymerisation". *Polymer*. Vol: 87, year: 2016, page: 215-225. *Publisher: Elsevier*. DOI: https://doi.org/10.1016/j.polymer.2016.01.078.
6. M Jinish Antony*, C Albin Jolly, K Rohini Das, T S Swathy "Normal and reverse AOT micelles assisted interfacial polymerization for polyaniline nanostructures". *Colloids and Surfaces A*. Vol: 578, Year: 2019, Page: 123627. *Publisher: Elsevier* DOI: https://doi.org/10.1016/j.c olsurfa.2019.123627.

Journal Papers-communicated

1. K. Rohini Das, I. Anjana and M Jinish Antony* "Oxidizing analytes triggered selective fluorescence sensing in Poly-N-phenyl anthranilic acid-co-poly-o-phenylenediamine block type copolymers". *Journal of Applied Polymer Materials. Publisher: ACS.*

Conference Presentations

1. K. Rohini Das, and M Jinish Antony*. "Poly-N-Phenyl Anthranilic Acid Fluorescent Polymer Dye for Cell Imaging and Secret Writing Applications". *International Conference on Advanced Materials for Sustainability* (*ICAMS-2023),* Dec 21-23, 2023, *University of Calicut*.

2. K. Rohini Das, M Jinish Antony*, and Anjana I. "Oxidative Metal Ion induced Fluorescent Turn-off in Poly-O-phenylenediamine and colour tuning of yellow emission of Poly-O-phenylenediamine and its Copolymers". *International Conference on Materials for the Millennium (MATCON-2023),* Jan 12-14, 2023, *Cochin University of science and technology*, Cochin.
3. K. Rohini Das, and M Jinish Antony*." Charge-Discharge Determination in Lead Acid Batteries via Sulphuric Acid Content Estimation Using pH Dependent Poly N-phenyl-O-phenylenediamine". *International Conference on Chemistry and Applications of Soft Materials (CASM 2022)*, Jul 25-27, 2022, *CSIR NIIST, Thiruvananthapuram.*
4. K. Rohini Das, and M Jinish Antony*." Poly (N-phenyl anthranilic acid) based efficient redox fluoroprobe for analytical sensing". *International Conference on Science and Technology of Advanced Materials 2020 (STAM 2020)*, Jan 14-16, 2020, *Mar Athanasius College, Kothamangalam*.
5. K. Rohini Das, and M Jinish Antony*." Water soluble phenylenediamine copolymer nanospheres via oxidative polymerisation" *International Conference on Chemistry and Physics of Materials 2018*, Dec 19-21, 2018. St. Thomas' College (autonomous) Thrissur.